Fungal pretreatment of lignocellulosic crop residues as feed for Black Soldier Fly larvae

Alexander T. Setchfield

PhD

University of York

Biology

November 2022

Abstract

Global food security presents an unprecedented challenge in which food supply must meet ever-rising demand, driven by rapid population growth. Sustainable protein sources are urgently required, such as alternatives to soybean and fish meals in livestock feed. Black Soldier Fly larvae (BSFL) are a promising alternative, though they require a sustainable feed source to be reared upon. Agricultural crop residues are abundant, underutilised and of low value. As such, they are excellent candidates as feed for BSFL. However, crop residues possess a complex cell wall structure composed of lignocellulose, which is indigestible by BSFL and prevents their growth.

This thesis describes the development and characterisation of an innovative fungal pretreatment process to convert wheat straw into BSFL feed. The lignocellulolytic ability of *Parascedosporium putredinis* NO1 (soft rot ascomycete fungus) was exploited to improve the digestibility of cell wall lignocellulose, enabling larval growth. Feeding trials were conducted to demonstrate the effect of the biomass pretreatment upon BSFL growth. The pretreatment process was also fundamentally characterised to reveal the changes in cell wall composition and the enzymatic mechanisms underpinning the improvements in its digestibility by BSFL.

Wheat straw pretreated with *P. putredinis* NO1 under submerged fermentation (SmF) and solid-state fermentation (SSF) supported BSFL growth during feeding trials. A solid-state system offers greater commercial viability and was taken forward for further testing, including feed safety analysis which confirmed the compliance of pretreated wheat straw with EU feed regulations around mycotoxins and hazardous heavy metals. Biomass composition analyses revealed the changes to cell wall lignocellulose which likely enabled larval growth on wheat straw.

A proteomic study of *P. putredinis* NO1 growth on wheat straw under SmF and SSF revealed the carbohydrate-active enzymes likely responsible for the changes observed in cell wall composition, and thus, those underpinning the improved digestibility of lignocellulose by BSFL.

Table of contents

List of figures

Acknowledgements

Firstly, I would like to thank my University of York supervisors, Prof. Neil Bruce and the late Prof. Simon McQueen-Mason, as well as my thesis advisory panel (TAP) members, Prof. Gavin Thomas and Prof. James Moir. Your support, expert guidance and advice throughout my PhD has been invaluable. Simon – I will always remember your unique insight and perspective, natural curiosity and infectious passion for science. You are greatly missed by all at CNAP.

I would also like to thank Dr Adrian Charlton, my industrial CASE supervisor at Fera Science, as well as Dr Maureen Wakefield. Your technical expertise on conducting feeding trials and insect related analyses has been greatly appreciated. Without the facilities and resources provided by Fera Science this PhD project would not have been possible.

In addition, I would particularly like to thank Dr Daniel Leadbeater and Dr Nicola Oates. Dan – your input and advice over the years has been invaluable, as was your contribution to the bioinformatic analyses of proteomic data. Nicola – thank you for your valued support early on in my PhD, and for discovering such an interesting fungus on which my project was based. I would also like to thank Rachael Hallam whose support and expert advice during biomass composition analyses was much appreciated, as well as Dave Neale for your excellent technical support. Thank you to all M2 members, past and present, for making this PhD such a great experience.

Finally, I would like to thank my Mum, Dad and partner, Laura. Your love and devoted support over the past four years has truly made the completion of this thesis possible. Thank you.

Author’s declaration

I declare that this thesis is a presentation of original work and I am the sole author. This work has not previously been presented for an award at this, or any other, University. All sources are acknowledged as References.

1) General introduction

1.1 The challenge of global food security

The total human population has risen by over threefold since 1950, yet all inhabited regions on Earth (except for East and South East Asia) are expected to see further population rises between now and 2050 (United Nations, 2022). The most recent projections by the United Nations indicate that the global population could reach 8.5 billion by 2030 and 9.7 billion by 2050, increasing from a current population of 8 billion. It is anticipated that over half of the total population growth (approximately 54%) will occur in Sub-Saharan Africa (+ 942 million people), with Central and Southern Asia expected to see the second most significant rise (+ 500 million people) (Figure 1.1).

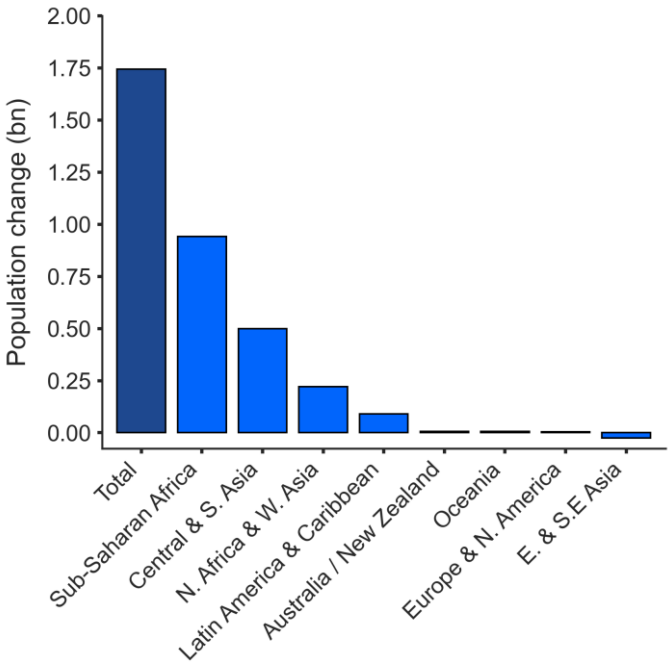

Figure 1.1. Projected population changes between 2022 and 2050. Graph shows the projected population changes (in billions) across all inhabited global regions between 2022 and 2050, according to the United Nations 'medium scenario' for population growth, ranked in descending order. Oceania excludes Australia and New Zealand. Data obtained from United Nations World Population Prospects (United Nations, 2022).

As a consequence of rapid population growth, an additional 1.75 billion people will require sources of high-quality food in less than three decades. Estimates have revealed that over the next 35 years the growing global population will demand more food than that ever produced during human history (Global Food Security, 2022). However, even at current population levels, approximately 795 million people face hunger on a daily basis, while more than two billion people lack vital micronutrients (e.g. iron, vitamin A and zinc) within their diets (IFPRI, 2016). As such, at current trajectories, the world is expected to fall short of its commitment to zero hunger by 2030 (United Nations Sustainable Development Goal 2) and faces an unprecedented food security challenge in which current and future food supply must meet ever-growing demand.

1.2 Rising demand for protein

Rising demand for sources of animal-derived protein (e.g. meat and fish) is an area of particular concern. By 2050, global meat consumption is likely to rise by over 60% relative to current levels, particularly in regions expected to experience high population growth such as Africa, Asia (Central, Southern and Western), Latin America and the Caribbean (Revell, 2015). Fish consumption is expected to double in the same time period (Naylor et al., 2021), with aquaculture now the world's fastest growing food production system (Troell et al., 2014; WWF, 2022). The production of meat and fish products involves the farming of livestock (e.g. pigs, chickens and fish) which rely upon sufficient supplies of protein rich feed for healthy growth and development. Currently, protein within livestock feed formulations is provided primarily by soybean and fish meals; demand for which will continually increase if the demand for meat and fish rises in line with future projections.

1.2.1 Soybean meal

Soybean meal (the by-product of soybean oil extraction) is the most widely used protein source in non-ruminant livestock feeds due to its nutritional performance, including a high protein content (44-48%, as-fed basis) and significant quantities of essential amino acids (e.g. lysine) (Bernard, 2022; Ibáñez et al., 2020). The production of soybean is concentrated largely across regions of North and South America (e.g. Brazil, Argentina), as well as China and India, whose combined output in 2018 contributed 88.1% of total global production (de Maria et al., 2020). Of these countries, Brazil remains the main exporter of soybean worldwide, having increased its land area devoted to soybean production by 21 million hectares between 2000 and 2018. This represents approximately 40% of all land area expansion worldwide (intended for soybean cultivation) during the same period, driven primarily by the increasing demands of pig and poultry export markets in China and Europe (de Maria et al., 2020; Fraanje and Garnett, 2020).

Such rapid soybean expansion has driven significant land use change, involving deforestation of natural habitats across Brazil (e.g. Amazon rainforest) and other countries including Argentina and Paraguay (e.g. Gran Chaco region of savannah and woodland) (Fraanje and Garnett, 2020). This has led to substantial biodiversity loss, as well as the pollution of soil and water bodies due to extensive application of fertilisers and pesticides (Gaitán-Cremaschi et al., 2015). In recent years, however, initiatives to reduce soybean driven deforestation have been established (e.g. Amazon Soy Moratorium and certification schemes) with the support of European livestock industries, though these remain in their early stages with just 0.2-6% of soy production volume covered by certification (Fraanje and Garnett, 2020). Nevertheless, as limitations upon soybean expansion develop further to curb climate change, its rate of production will ultimately slow.

1.2.2 Fish meal

Fish meal (derived from wild marine fish of little to no commercial value) is widely considered the gold standard protein source for various fish species farmed in aquaculture (e.g. Atlantic salmon), due to its high protein content (approximately 60%) and balanced amino acid profile (Ween et al., 2017; Egerton et al., 2020). Its production, however, is environmentally damaging, leading to the depletion of small fish species (particularly within pelagic ocean zones) as well as wider biodiversity loss across marine ecosystems. Despite this, global fish meal production increased by 3.6% in 2021, led by countries such as Peru, Chile and India, driven by the rising demand of export markets (IFFO, 2022). However, as the demand for fish meal rises, the populations of suitable small fish will continue to decline, and it is increasing unlikely that supplies will recover to mitigate this going forward (Habte-Tsion et al., 2022). This, over time, will lead to a decline in production.

1.2.3 The need for alternative protein sources

At current trajectories, the United Nations forecasts a global protein deficit of at least 60 million tonnes by 2050, equivalent to a demand increase of 32-43% (Henchion et al., 2017). In line with this, growing demand for meat and fish products continues to stimulate demand for protein rich feed sources such as soybean and fish meals. However, their supplies are diminishing and their production is increasingly unsustainable, associated with a range of negative environmental impacts (e.g. deforestation and overfishing). Furthermore, recent high demand for increasingly scarce resources has led to significant rises in market prices, with the cost of feed in Europe typically contributing 60-70% of total livestock production costs (Spranghers et al., 2017). Therefore, there are both environmental and economic drivers to pursue alternative protein sources for inclusion in livestock feeds, which must be performative, sustainable and safe.

In addition, alternative protein sources should be abundant and deployable within regions of most need, such as those forecast to experience the greatest population growth. Their production, therefore, should also be simple, cost-effective and offer local availability.

1.3 Insects as food and feed

Throughout regions of Africa and Asia, the human consumption of insects (entomophagy) has been widely practised for over 2000 years, while they remain a valuable source of nutrition for an estimated two billion people worldwide (Hall, Fitches and Smith, 2021). In contrast, across western countries, entomophagy is typically met with issues around public acceptance and is therefore seldom practised. In recent years, however, a number of insect species have gathered significant interest due to their potential to transform the sustainability and economic viability of livestock farming. Edible insects, such as larvae of the common house fly (*Musca domestica*) and yellow mealworm (*Tenebrio molitor*), hold the potential to be farmed at both small and industrial scale, and can be processed into a range of products including protein meals, oils and chitin (Sogari et al., 2019). Interest has been driven largely by the ever-growing demand for protein rich feeds as a consequence of global dietary shifts, as well as improved awareness of the environmental consequences of soybean and fish meal production in relation to climate change. Insect farming enables the production of high-quality feed products using locally sourced low value inputs (e.g. organic wastes), which, therefore, reduces reliance on imports of conventional feeds. This approach aligns with the objectives outlined by the EU's 'Green Deal', specifically to reduce greenhouse gas emission and transition towards locally sourced produce. However, insect farming does not yet offer economic viability at the commercial scale required, which currently constrains production volumes (Hall, Fitches and Smith, 2021).

1.4 The Black Soldier Fly

One of the major insects of interest is the Black Soldier Fly (BSF; *Hermetia illucens*), a Dipteran (two-winged) organism belonging to the Stratiomyidae (soldier fly) family. Native to America, it is now widespread across tropical and warmer climates between the latitudes of 40°S and 45°N (Bjone and Fitches, 2021). Its lifecycle comprises egg, larval (including pre-pupal), pupal and adult stages; the total duration of which is dependent upon the feed substrate available (Figure 1.2).

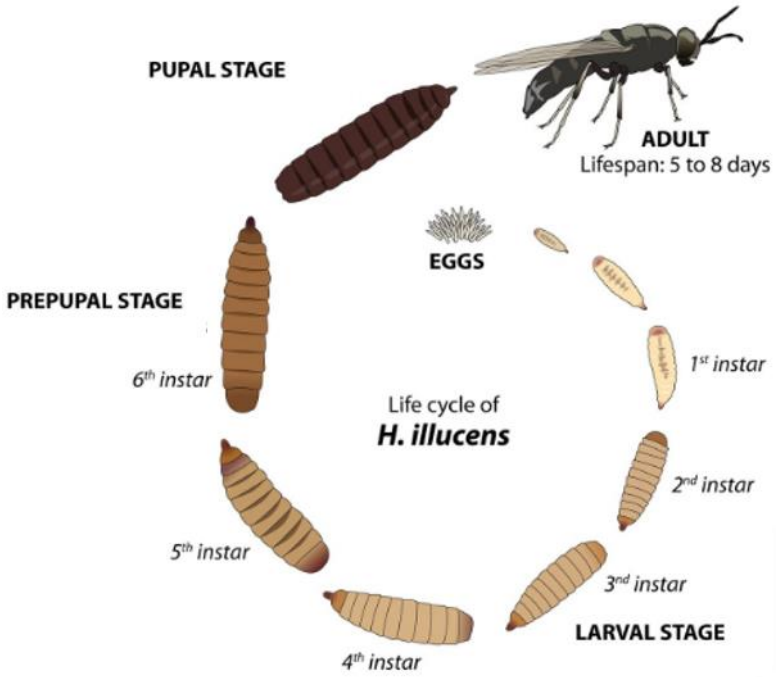

Figure 1.2. Lifecycle of the Black Soldier Fly (*H. illucens*). Diagram shows the BSF lifecycle, including egg, larval, pupal and adult life stages, adapted from de Smet et al. (2018).

The adult BSF has no mouth parts and therefore does not feed, living only for a short duration (five to eight days) on the reserves established during the larval stages (Newton et al., 2005). As a result, the adult fly is not a vector for transmissible oral-borne disease and is considered a non-pest, which is of particular importance for food and feed safety (Bjone and Fitches, 2021). Furthermore, the female BSF confers high fecundity (the ability to produce an abundance of eggs), ovipositing between 206 and 1088 eggs at once (Kaya et al., 2021; Samayoa, Chen and Hwang, 2016; Tomberlin, Sheppard and Joyce, 2002). Females oviposit eggs in close proximity to a moist feed source, to be consumed later by larvae, and are attracted to appropriate substrates by volatile organic compounds released by resident bacteria (Zheng et al., 2013; Hocid et al., 2019). Eggs hatch two to four days later and enter the six larval instar stages (Figure 1.2), which may last between two weeks and four months depending upon conditions such as feed substrate and quantity (Makkar et al., 2014; Bjone and Fitches, 2021). During the sixth and final instar (pre-pupal), BSFL cease feeding, empty their digestive tracts and migrate away from their feed source to pupate into adult flies at a drier site (Diener et al., 2011; Makkar et al., 2014).

1.4.1 Black Soldier Fly larvae as an alternative protein source

BSF larvae (BSFL) are a promising alternative protein source for livestock, typically containing 35-57% crude protein and 35% crude oil (dry weight). Fat content varies significantly with diet, though lauric acid generally contributes a significant proportion of their total fat content (Liu et al., 2017; Veldkamp et al., 2012). In comparison to soybean and fish meals, their protein content and essential amino acid profiles are similar, and unlike their fat content, amino acid profiles do not differ significantly between larvae reared on different substrates (Hawkey et al., 2021; Spranghers et al., 2017). Crucially, BSFL are rich in the essential amino acids that are typically most limiting in monogastric (non-ruminant) livestock feeds, including lysine (first limiting amino acid in swine diets) and methionine (first limiting amino acid in poultry diets) (Farkhoy et al., 2012; Hasan, Crenshaw and Liao, 2020). In general, amino acids derived from BSFL are of comparable digestibility to those from soybean and fish meals, though it has been reported that their amino acids are less digestible than those of other insect species. However, the methodology used to calculate amino acid digestibility influences the values obtained and differs between studies, which limits the validity of such comparisons (Hawkey et al., 2021; Masey O'Neill et al., 2014).

In nature, BSFL are voracious feeders, possessing an innate saprophytic ability which enables them to metabolise a wide range of decaying organic materials. Dense populations are typically found growing within animal manures, as well as various other organic wastes (e.g. distillery and brewery waste, fruit and vegetable waste) (van Huis et al., 2013). This ability, therefore, can be exploited to facilitate the transformation of organic wastes, residues and by-products into high-quality protein sources (insect bioconversion). To this end, BSFL are an ideal species to farm commercially, possessing short life cycles, high feed conversion efficiencies and existing in high population densities (Bjone and Fitches, 2021). They can also be vertically farmed, which enables a more efficient use of space, and their production offers substantial opportunity for automation. Advocates of insect protein production believe its environmental footprint to be lower than that of traditional soybean production, supported by reports of low greenhouse emission and land use by BSFL, though further work is required to enable valid comparisons of their environmental impacts (Booth, O'Neill and Quigley, 2021; Boakye-Yiadom, Ilari and Duca, 2022; Oonincx, 2021). For instance, there currently exists no standardised methodology for BSFL life cycle assessments, leading to significant variation between studies for metrics such as global warming potential, land area and energy use (Boakye-Yiadom, Ilari and Duca, 2022). Nevertheless, BSFL production holds significant potential to reduce global reliance on soybean and fish meals, while valorising organic wastes, residues and by-products, aligned with a circular

economy approach. As the sector progresses and scales, it is likely that the environmental impact of BSFL rearing will reduce as production efficiencies improve (Oonincx, 2021).

1.4.2 UK and European Union insect feed legislation

In July 2017, the EU passed new legislation authorising the use of insect processed animal proteins (PAPs) derived from seven species (including BSFL) as feed for aquaculture, with insect rearing substrates limited to materials of vegetal origin (Rojo, 2021). In September 2021, the EU passed further legislation authorising the use of insect PAPs in poultry and pig feed, with rearing substrates again limited predominantly to those of vegetal origin. Insect PAPs are now also authorised for use in pet food formulations (e.g. cat and dog food) (IPIFF, 2022b). This legislation enables the direct substitution of soybean or fish meals with BSFL PAPs, live or whole BSFL (dried/frozen), depending upon the target species and EU member state (Figure 1.3). Currently, the equivalent UK legislation remains in line with EU controls (McCulloch and Nelson, 2021).

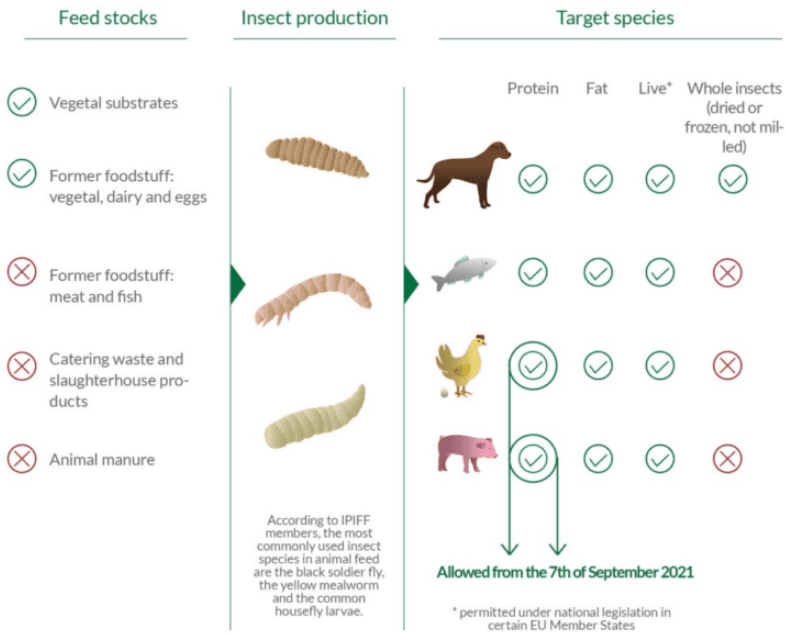

Figure 1.3. Current EU legislation on the use of insect derived feed sources. Diagram shows the current EU legislation outlining the use of BSFL PAPs, live and whole (dried/frozen) BSFL in livestock (aquaculture, poultry, swine) and pet food formulations, sourced from IPIFF (2022).

1.5 Agricultural crop residues as feed for Black Soldier Fly larvae

Life cycle assessments conducted on insect protein production systems have indicated that the rearing feed substrate is a primary driver of their overall environmental impacts; the cultivation of which is associated with land, water and energy use (Oonincx, 2021). Therefore, to enable their environmentally friendly production as livestock feed at the scale required to rival industrial soybean and fish meal production, BSFL must be reared on a sustainably sourced (low value) substrate available in great abundance worldwide. In nature, BSFL feed on a wide range of organic materials. It has been proposed that the utilisation of underused feedstocks (e.g. wastes, residues and by-products) for mass insect rearing could decrease the environmental impact of their production (Oonincx, 2021). To this end, agricultural crop residues are potentially excellent candidates as feed for BSFL and, at present, are heavily underutilised by the insect protein sector. Examples include wheat straw, rice straw and oil palm empty fruit bunch (EFB).

1.5.1 The need for alternative crop residue management strategies

The sustainable management of agricultural crop residues, co-produced during the cultivation of crops such as wheat, rice and oil palm, poses significant challenges worldwide. As food demand rises with population growth, the requirement for cereals and other crops continues to increase, with the demand for rice expected to rise by 116 million tonnes by 2035, driven largely by countries within Africa and Asia (Singh et al., 2021). As crop production grows, the volumes of co-produced residues increase concurrently. However, at current levels, the global capacity to process crop residues sustainably is significantly below the volumes generated. As a result, it remains a common disposal practice to burn freshly generated residues, particularly rice straw in Asia (mainly China and India), in which 90% of the world's rice is produced. This, therefore, leads to the emission of greenhouse gases (e.g. carbon dioxide) which drive climate change and negatively impact human health (Singh et al., 2021). Similarly, the production of palm oil in South East Asia, particularly in Malaysia and Indonesia, generates vast quantities of oil palm EFB (fibrous biomass remaining after removal of oil palm fruits from bunches). In Malaysia alone, up to 23 million tonnes is generated per year (Padzil et al., 2020). Typically, oil palm EFB is left to decompose naturally on plantation fields, or burned if space does not permit this. More recently, conversion to biochar (via pyrolysis) and composting have been explored as valorisation approaches for oil palm EFB, though these technologies remain limited by scale (Adu et al., 2022). Therefore, there exists a pressing need to develop strategies to valorise crop residues efficiently, sustainably and at the global scale required, particularly as their volumes increase.

1.5.2 Wheat straw as feed for Black Soldier Fly larvae

Wheat is the dominant cereal crop cultivated across Europe (NNFCC, 2019). As a result, wheat straw (stalk remaining after wheat grain harvest) is one of the major agricultural crop residues within Europe, with approximately 144 million tonnes generated every year (Gillman, 2017). The UK alone produces more than 12 million tonnes annually, and beyond use as animal bedding or soil conditioner (via incorporation back into land), it has little commercial utility (NNFCC, 2019). As such, wheat straw commands a low market value (£44/tonne ex-farm, week ending 6th Nov 2022) and approximately one third is not valorised (Copeland, 2008; AHDB, 2022). Due to its abundance, lack of industrial application and low value, wheat straw is the focus of this thesis. It is a potentially excellent candidate as feed for BSFL across the UK, Europe and globally.

1.6 Lignocellulose and its indigestibility by Black Soldier Fly larvae

One key challenge with the use of some of the most abundant and cost-effectively sourced agri-food wastes for BSFL bioconversion, such as crop residues, is their typically low process performance as feed substrates. This is commonly associated with their inherently high crude fibre content, containing lignocellulose of poor biodegradability (Peguero et al., 2022). Due to their complex composition and recalcitrance to deconstruction, the components within lignocellulose are considered indigestible by BSFL (Peguero et al., 2022; Himmel et al., 2007).

1.6.1 Plant cell wall composition

Lignocellulose is the major constituent of agricultural crop residues. It is contained within secondary plant cell walls, deposited during the maturation process in tissues that require greater physical strength, having evolved in plants to provide durability, water resistance and protection against pathogens (Harris and DeBolt, 2010). In contrast to the primary plant cell wall, which is synthesised during growth and confers viscoelasticity (liquid and solid-like behaviour), the secondary cell wall is formed in tissues where cell growth has ceased and is characterised predominantly by the presence of lignin (aromatic polymer) which confers rigidity (Cosgrove and Jarvis, 2012; Harris and DeBolt, 2010). The secondary plant cell wall is organised into bundles of microfibrils, comprised of two main polysaccharides (cellulose, hemicellulose) and lignin (Cosgrove and Jarvis, 2012) (Figure 1.4).

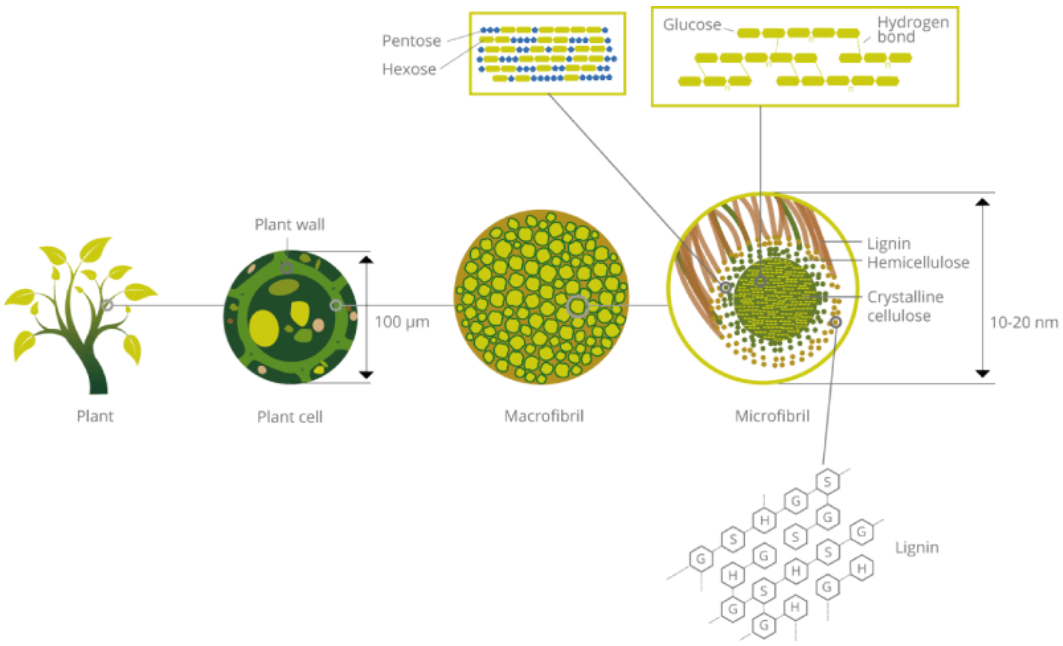

Figure 1.4. Structure of the plant cell wall. Diagram shows the structural organisation of the lignocellulose containing plant cell wall, comprising cellulose, hemicellulose and lignin; sourced from Streffer (2014).

The relative proportions of cellulose, hemicellulose (herein referred to as matrix polysaccharides) and lignin vary across residues of different crop species. Wheat straw typically contains 32-45% cellulose, 20-45% matrix polysaccharides and 11-26% lignin (Zhang et al., 2022). The following sections describe each of these structural components in more detail.

1.6.2 Cellulose

Cellulose is the most abundant polymer within lignocellulose, comprising linear chains of repeating cellobiose (disaccharide) units. Each unit consists of two glucose monomers rotated 180° relative to one other, linked covalently by a β-1,4 glycosidic bond, creating a flat ribbon like structure (Zoghlami and Paës, 2019; McKendry, 2002; Harris and DeBolt, 2010) (Figure 1.5).

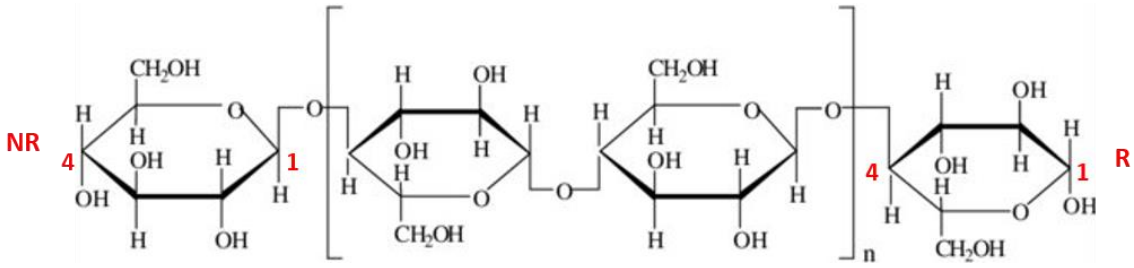

Figure 1.5. Chemical structure of cellulose. Structural diagram shows repeating glucose monomers, oriented 180°C to each other and linked with glycosidic bonds, with pairs forming cellobiose units. One cellobiose unit is outlined within square brackets. NR = non-reducing end (C-4), R = reducing end (C-1, anomeric carbon). Adapted from Al-Mobarak (2010).

The flat structure of cellulose chains enables their tight packaging. Each glucose residue has three hydroxyl groups which participate in inter- and intra-chain hydrogen bonding, coordinating cellulose chains in parallel to form microfibrils of 2-3 nm in diameter (Harris and DeBolt, 2010; Song et al., 2020). This ordered structural arrangement confers crystallinity, which increases the rigidity of cellulose and its recalcitrance to enzymatic deconstruction (Nishiyama, Langan and Chanzy, 2002). In higher plants (e.g. wheat), cellulose chains are also known to form less ordered (amorphous) regions, every 100-150 nm or so depending upon the degree of polymerisation (DP; number of monomers within the chain). Amorphous regions coat the crystalline structure, hindering its accessibility, though are readily digestible in comparison (Himmel et al., 2007; Ruel, Nishiyama and Joseleau, 2012). Recalcitrance is further promoted by the heterogeneity of exposed cellulose chain ends. The C-1 (anomeric carbon) end possesses reducing potential, though 30-40% of those in intact cellulose are buried within chains (involved in glycosidic bonding), while the C-4 end (possessing a free hydroxyl group) is non-reducing (Azadfar, Graham and Wolcott, 2019; Kongruang et al., 2004) (Figure 1.5). Cleavage of glycosidic bonds between glucose monomers, therefore, necessitates the action of different enzymes.

1.6.3 Matrix polysaccharides

The matrix polysaccharides encompass a diverse range of biopolymers within lignocellulose, comprising chains of various pentose (e.g. xylose, arabinose) and hexose (e.g. glucose, galactose) monomers (Zoghlami and Paës, 2019; Tian, Zhao and Chen, 2018). They are amorphous and possess significantly lower DP values (number of monomers) in comparison to cellulose, typically of 100-200 units in length (Mota et al., 2018). Unlike cellulose, matrix polysaccharides are branched, permitting diverse side chain decorations and forming an interwoven short-chain heterogeneous polymer network in which cellulose microfibrils are embedded, binding tightly by hydrogen bonding to their surface (McKendry, 2002).

Despite this, matrix polysaccharides are readily digestible, providing little physical strength due to their amorphous structure, though shield cellulose which limits its accessibility (Zoghlami and Paës, 2019; Himmel et al., 2007). Matrix polysaccharides can also be heavily acetylated, further increasing cell wall recalcitrance to deconstruction whereby acetyl groups inhibit the action of cellulases by interfering with substrate recognition and binding (Pan, Gilkes and Saddler, 2006). However, biomass studies have shown that the removal of acetyl groups (deacetylation) more significantly improves the digestibility of matrix polysaccharides, as opposed to that of cellulose, indicating that the impact of acetylation on cell wall recalcitrance to deconstruction may depend more upon the degree of cellulose crystallinity (Zoghlami and Paës, 2019; Zhu et al., 2008).

In grasses (e.g. wheat), xylan is the most abundant matrix polysaccharide, composed of a β-1,4 linked xylose backbone exhibiting side chain branching with arabinose at the C-2 or C-3 positions (arabinoxylan), and sometimes with glucuronic acid at the C-2 position to form glucuronoarabinoxylan (Rodríguez-Sanz et al., 2022). Glucuronoarabinoxylan may also present hydroxycinnamic acids (e.g. ferulic acid) ester linked to arabinose residues, which can become oxidatively coupled to form diferulate cross-links (bridges) between xylan chains (Tabuchi, Li and Cosgrove, 2011; de O. Buanafina, 2009; de Oliveira et al., 2015) (Figure 1.6).

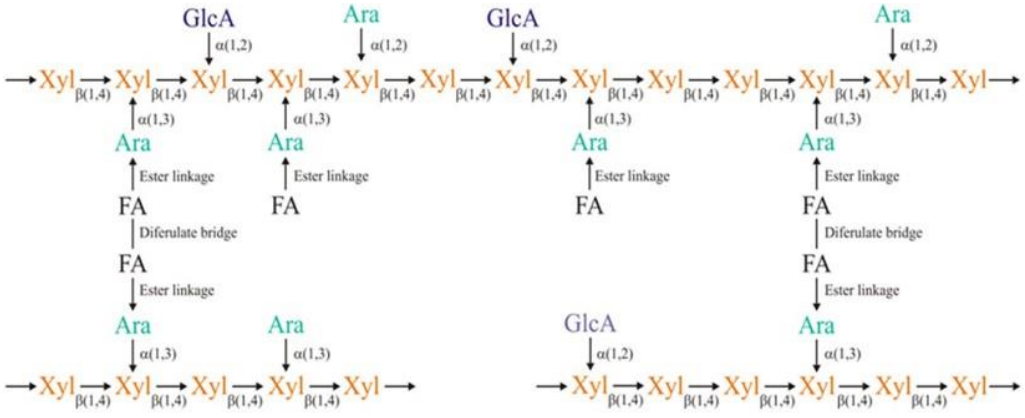

Figure 1.6. Structure of feruloylated glucuronoarabinoxylan. Diagram shows β-1,4 linked xylose repeating monomers (Xyl), with arabinose (Ara) and glucuronic acid (GlcA) side chain branches at C-2 and C-3 positions, ester linked to diferulate bridges of ferulic acid (FA) moieties. Sourced from Mota et al. (2018).

1.6.4 Lignin

Lignin is the most abundant non-polysaccharide component within lignocellulose, composed of three main phenylpropanoid units (guaiacyl, G; *p*-hydroxyphenyl, H; syringyl, S) derived from various hydroxycinnamic alcohols (coniferyl, *p*-coumaryl and sinapyl alcohols, respectively) (Figure 1.7). The phenylpropanoid units form a highly complex amorphous heteropolymer linked primarily by the β-O-4 (β-aryl ether) linkage, as well as others including the 5-O-4, β-β and β-5 linkages (Boerjan, Ralph and Baucher, 2003; Mota et al., 2018; Zoghlami and Paës, 2019).

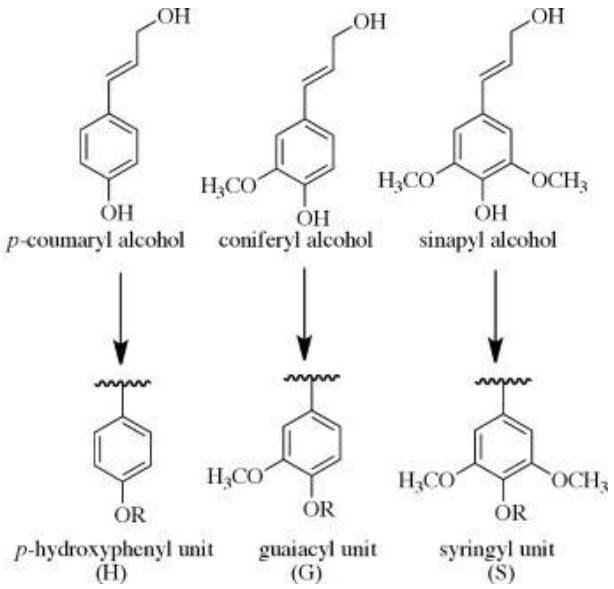

Figure 1.7. Chemical structure of lignin phenylpropanoid units and their hydroxycinnamic alcohol precursors. Structural diagram shows the three main phenylpropanoid units (guaiacyl, G; *p*-hydroxyphenyl, H; syringyl, S) and their hydroxycinnamic alcohol precursors (coniferyl, *p*-coumaryl and sinapyl alcohols, respectively). Adapted from Sangha et al. (2012).

Lignin is responsible for hydrophobicity and structural rigidity of the cell wall. It is bound to matrix polysaccharides (e.g. arabinoxylans) via covalent cross-links (e.g. ether-linked ferulate bridges) which form lignin-carbohydrate complexes (LCCs) (Terrett and Dupree, 2019; Zoghlami and Paës, 2019). LCCs confer lignocellulose with mechanical strength and reduce enzyme accessibility to cellulose; thus, increasing the recalcitrance of the cell wall to deconstruction (Giummarella et al., 2019; Min et al., 2014). To this end, the cleavage of linkages within LCCs has been reported to improve cellulose accessibility, while lignin content is negatively correlated with the digestibility of wheat straw (Herbaut et al., 2018; Tarasov, Leitch and Fatehi, 2018).

Furthermore, the degradation of lignin during hydrolysis can hinder the activity of cellulases. For instance, cleavage of the β-O-4 linkage within lignin leads to the generation of free phenolic hydroxyl groups which can irreversibly adsorb cellulases via hydrogen bonding. This, therefore, interferes with cellulose binding (Yoo et al., 2017; Yuan et al., 2021). In support of this, the blocking of free phenolic hydroxyl groups (by hydroxypropylation with propylene oxide) significantly reduces the inhibitory effect of lignin breakdown (Yang and Pan, 2016).

1.7 Enzymes involved in the deconstruction of lignocellulose

Lignocellulolytic enzymes have been discovered in organisms from across the tree of life (Cragg et al., 2015). Microorganisms, such as bacteria and fungi, often secrete a diverse range of carbohydrate-active enzymes (CAZymes) during growth on lignocellulose which catalyse the deconstruction of cellulose, matrix polysaccharides and lignin. CAZymes are categorised by amino acid sequence similarity within the CAZyme database using methodology originally established by Bernard Henrissat (Henrissat, 1991; Lombard et al., 2014). They are broken down into enzyme classes which include glycoside hydrolases (GHs), carbohydrate esterases (CEs), auxiliary activities (AAs) and polysaccharide lyases (PLs). Although not catalytic, carbohydrate binding modules (CBMs) are also categorised by the CAZyme database, frequently found attached to GH class enzymes and of short amino acid chain length (typically 30-200 amino acids). CBMs instead confer a substrate binding function and increase the proximity of their linked enzyme to its substrate; hence improving the ability of the enzyme to disrupt the crystallinity of insoluble substrates, such as crystalline cellulose (Sidar et al., 2020; Bernardes et al., 2019). CAZyme classes are further subdivided into families based on amino acid sequence similarity, with at least one biochemically characterised member (Lombard et al., 2014). Currently, the GH, CE and AA classes are subdivided into 173, 20 and 17 families, respectively.

Cellulose degradation is catalysed by the action of various GH class enzymes. These include the classical endo-β-1,4 glucanases (e.g. GH5) which cleave at internal sites within the cellulose chain, exo-β-1,4 glucanases or cellobiohydrolases (e.g. GH7, GH6) which cleave cellobiose (two linked glucose monomers) from the reducing end (GH7) or non-reducing end (GH6) of the cellulose chain, and β-glucosidases (e.g. GH3) which hydrolyse cellobiose into two separate glucose molecules (Glass et al., 2013) (Figure 1.8). The degradation of xylan (the most abundant matrix polysaccharide within wheat straw) is enabled by the collective action of various GH and CE class enzymes. These include endo-β-1,4 xylanases (e.g. GH10, GH11), β-xylosidases (e.g. GH43, GH3), α-L-arabinofuranosidases (e.g. GH3, GH10, GH43), acetylxylan esterases (e.g. CE1-CE7), and ferulic acid esterases (e.g. CE1) (Glass et al., 2013) (Figure 1.8).

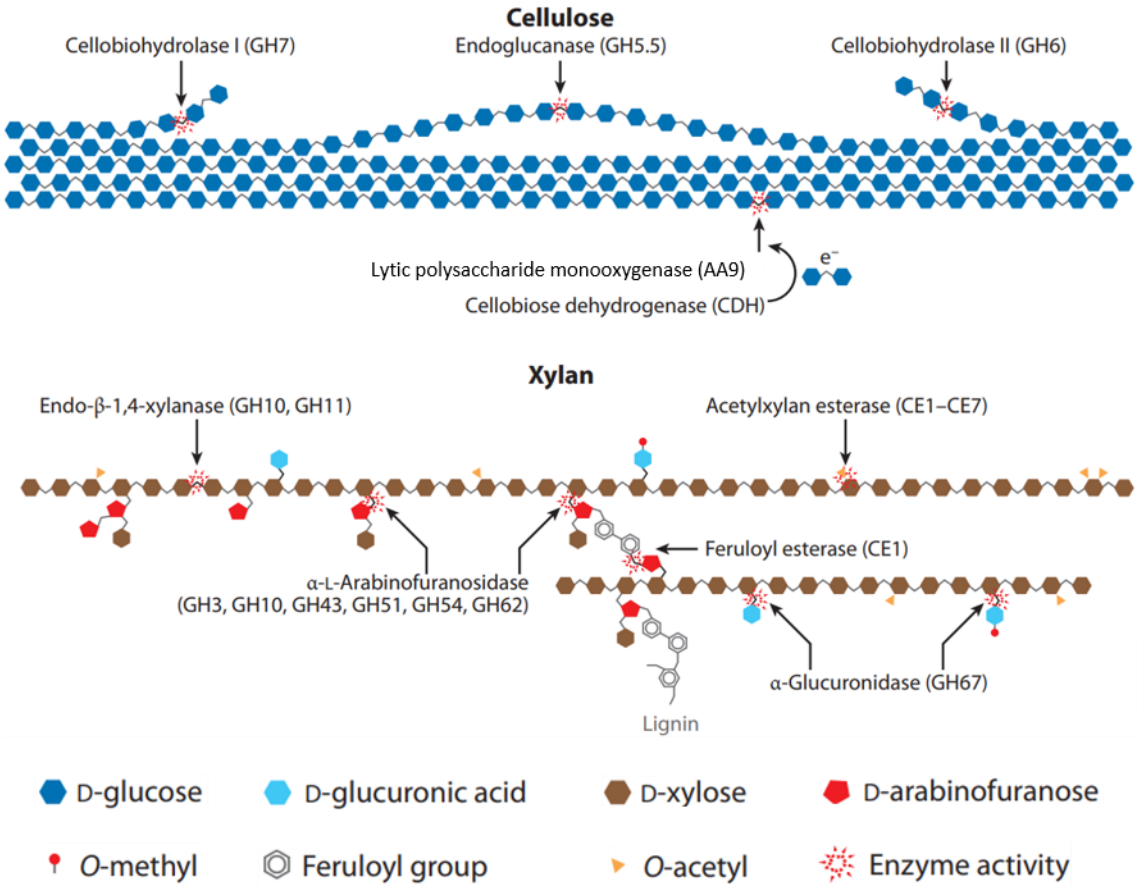

Figure 1.8. Enzymatic deconstruction of cellulose and xylan. Diagram shows the degradation of cellulose and xylan (glucuronoarabinoxylan) within lignocellulose by the action of various extracellular CAZymes. GH = glycoside hydrolase; CE = carbohydrate esterase; AA = auxiliary activity. Adapted from Glass et al. (2013).

Enzymes within the AA class play an auxiliary role during the deconstruction of lignocellulose, aiding the ability of GH and CE enzymes to access their target substrates. For instance, proteins within the AA9 family contain copper-dependent lytic polysaccharide monooxygenases (LPMOs) which weaken the architecture of cellulose fibres by creating 'nicking' points via the oxidative cleavage of glycosidic bonds (Figure 1.8). These nicks in the cellulose chain create new initiation sites for hydrolytic cellulases, thereby boosting saccharification (Chorozian et al., 2022; Villares et al., 2017). Other copper-dependent LPMOs include AA10, AA11 and AA13 family proteins.

Lignin-degrading activities are also categorised within the AA class. These include a range of enzymes which can be split into two main groups: lignin-oxidising enzymes and lignin-degrading auxiliary enzymes (Sista Kameshwar and Qin, 2018). Lignin-oxidising enzymes include proteins belonging to the AA1 (laccase) and AA2 (lignin peroxidase) families, while lignin-degrading auxiliary enzymes include proteins belonging to the AA4 (vanillyl-alcohol oxidase) and AA5 (copper radical oxidase) families (Challacombe et al., 2019; Sista Kameshwar and Qin, 2018).

1.8 Fungal degradation of lignocellulose

In nature, wood-decaying fungi have evolved the ability to degrade lignocellulose. These can be categorised into three classical groupings based on the mechanisms by which they deconstruct the cell wall – white rot, brown rot and soft rot (Cragg et al., 2015).

1.8.1 White rot fungi

White rot fungi are named due to their ability to selectively mineralise lignin (of dark colour), leaving behind cellulose (of pale colour), forming ultimately carbon dioxide and water as reaction products (Miyauchi et al., 2020). To degrade lignin, white rot fungi secrete a range of oxidative AA class enzymes including manganese peroxidases (whose activities rely on the oxidation of Mn^{2+} to Mn^{3+}), lignin peroxidases (whose activities rely on the production of hydrogen peroxide) and multi-copper containing laccases; induced often by limited nutrient levels (typically of carbon and/or nitrogen) (Wesenberg, Kyriakides and Agathos, 2003). In addition to the selective decay of lignin observed by species such as *Phellinus pini* and *Grifola frondosa*, other species of white rot fungi (e.g. *Trametes versicolor*) can elicit the simultaneous decay of all cell wall components (cellulose, matrix polysaccharides and lignin), while some species (e.g. *Pleurotus ostreatus*) exhibit dual modes of degradation dependent upon environmental growth conditions (Bari et al., 2020). Species capable of this secrete a wide range of cellulases (e.g. GH enzymes) in addition to their oxidative enzyme suite (Cragg et al., 2015).

1.8.2 Brown rot fungi

Brown rot fungi have evolved from their white rot ancestors, though over evolutionary time have lost many lignocellulose degrading enzyme systems including all possessing ligninolytic activities, as well as key cellulase activities (Floudas et al., 2012). In at least three orders of brown rot fungi (Gloeophyllales, Polyporales and Boletales) an alternative biomass depolymerisation system has evolved, known as the chelator-mediated Fenton (CMF) system, which replaces much of the ancestral cellulolytic machinery from white rot fungi. This unique system is based on oxygen radical chemistry, enabling non-enzymatic deconstruction of substrates at significant distance (microns) away from the fungus (Cragg et al., 2015).

In comparison to cellulolytic enzyme-based degradation which requires a suite of extracellular proteins, the CMF system is of lower molecular weight, though shares the capacity to efficiently deconstruct the plant cell wall. Brown rot fungi are generally considered to possess an evolutionary advantage in certain ecological niches, as their low molecular weight metabolites are able to diffuse deep into the cell wall to catalyse depolymerisation at internal sites, whereas white rot fungal enzymes are too large and only able to attack at exposed surfaces (Zhu et al., 2020). Brown rot fungi have exploited this for the degradation of woody biomasses such as conifer wood, having displaced their white rot ancestors (Cragg et al., 2015; Langer et al., 2021).

1.8.3 Soft rot fungi

Soft rot fungi, such as filamentous ascomycetes, are named after their ability to elicit a distinctive softening of the plant cell wall. Well characterised soft rot ascomycete species include *Aspergillus niger*, *Neurospora crassa* and *Trichoderma reesei* (Glass et al., 2013). Their action is enabled by specialist branching filaments (hyphae) which collectively constitute the mycelium; an intricate branching network of hyphae. Fungal hyphae physically penetrate the cell wall and secrete large quantities of CAZymes from their tips in close proximity to the target substrate, leading to the formation of small cavities in the biomass (Langer et al., 2021). Although soft rot ascomycetes can degrade a wide range of polysaccharides, their lignin-degrading ability is more limited in comparison to white rot fungi, and their genomes typically lack the majority of traditional lignin oxidase activities (Cragg et al., 2015; Challacombe et al., 2019). However, some ascomycetes (e.g. *Podospora anserina*) can degrade lignin, whose genomes encode laccases (AA1s) and a range of other lignin oxidative enzymes (Challacombe et al., 2019). Recent reports have also demonstrated the ability of soft rot ascomycetes to catalyse lignin degradation via the modification of linkages between monolignols, such as hydrolysis of the β-O-4 linkage by *P. anserina* (Dicko et al., 2020; van Erven et al., 2020).

1.8.4 *Parascedosporium putredinis* NO1

Multi-‘omics technologies (e.g. genomics, transcriptomics and proteomics) have been used extensively for the investigation of lignocellulose processing systems within mixed microbial communities. Sequence analysis of prokaryotic 16S ribosomal genes and eukaryotic internal transcribed spacer regions enables temporal tracking of microbial community dynamics. Recent multi-‘omics profiling of a wheat straw enriched composting community identified a soft rot ascomycete fungus – *Parascedosporium putredinis* NO1 (Oates, 2016). This fungus dominated the community during the latter growth stages once the majority of digestible sugars (e.g. cellulose and xylose) had likely been depleted by other microbial members, indicating its ability to metabolise highly lignified biomass (Figure 1.9).

To this end, recent work discovered a new oxidase capable of breaking the β-O-4 linkage between monolignols within lignin (Oates et al., 2021).

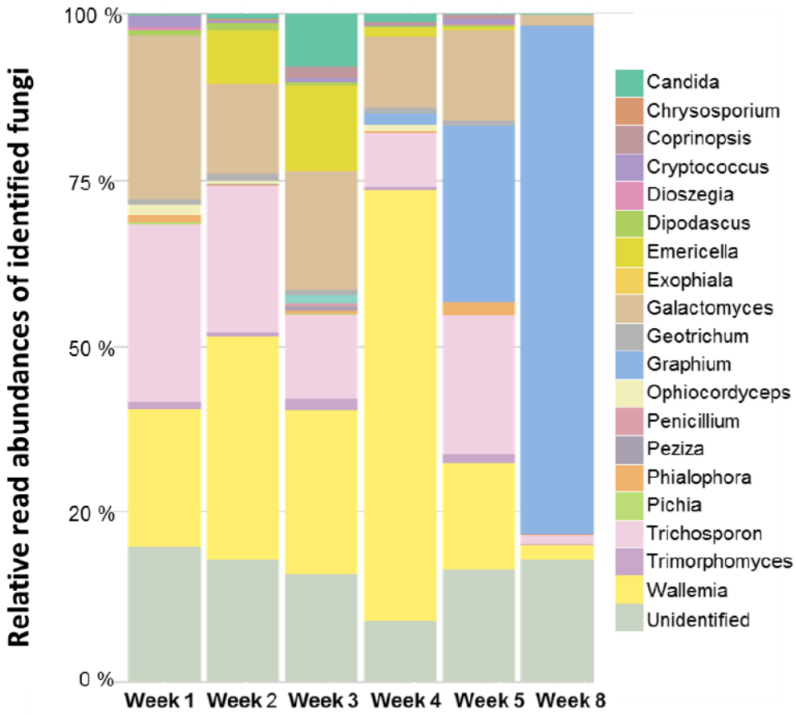

Figure 1.9. Composition of the fungal composting community in which *P. putredinis* NO1 was discovered. Community members were identified using their internal transcribed spacer regions. *P. putredinis* NO1 (blue bars, known formerly as *Graphium* sp.) dominated the latter stages of growth. Adapted from Oates (2016).

P. putredinis NO1 secretes a wide range of CAZymes when grown on wheat straw, including GH, CE and AA class enzymes (Oates, 2016). Previous work partially characterised a selection of these, including a protein belonging to the GH7 family (ID: c7203_g1_i1_2) and a protein belonging to the AA9 family (ID: c19570_g1_i1). The GH7 family protein was the most abundant of all proteins detected within the culture supernatant and sequence analysis indicated a reducing-end acting cellobiohydrolase role, with activity against cellulose demonstrated by *para*-nitrophenol based assays (Oates, 2016). The AA9 family protein was revealed by sequence analysis to be an LPMO which had one of the least conserved amino acid sequences compared to those in the non-redundant NCBI database, sharing just 40% of its amino acids with its closest match. It also had a particularly interesting proteomic profile, present only in the latter growth stages, and its activity was demonstrated on both chitin and cellulose (Oates, 2016).

1.9 Pretreatment of crop residues as feed for Black Soldier Fly larvae

There is currently no commercially employed technology to transform agricultural crop residues (e.g. wheat straw) into feed for BSFL. However, solutions to enable their conversion are urgently needed to ensure the affordability and sustainability of BSFL production going forward (Peguero et al., 2022). The pretreatment of crop residues with *P. putredinis* NO1 may be a promising solution. By exploiting its exceptional ability to deconstruct lignocellulose, it may be possible to use *P. putredinis* NO1 to break open the structure of the plant cell wall and improve the availability of sugars (e.g. cellulose, xylose) for BSFL to feed upon. In addition, the fungus itself is likely to act as a protein source for the larvae during rearing. This bioconversion process can be considered as part of a novel six-stage circular concept (Figure 1.10).

Figure 1.10. Circular concept in which agricultural crop residues are pretreated with *P. putredinis* NO1 as BSFL feed. The circular bioconversion concept to convert crop residues (wheat straw) into BSFL feed has six stages. (**1**) cultivation of wheat crops, (**2**) wheat harvest and production of wheat straw as an unavoidable residue, (**3**) pretreatment of wheat straw with *P. putredinis* NO1 to produce an edible BSFL feed, (**4**) BSFL rearing on pretreated wheat straw, (**5**) BSFL are harvested, processed and fed to livestock, (**6**) organic by-product ('frass') generated by BSFL rearing applied back to land as a natural nutrient rich biofertiliser. N.B. scanning electron microscopy image (stage 3) was obtained from Oates (2016).

This thesis focusses on stages three and four of the concept, in which *P. putredinis* NO1 is used to pretreat crop residues to enable their conversion into BSFL feed. During BSFL rearing, a by-product known as 'frass' is also generated, comprising rearing residues (e.g. leftover feed substrate) and faeces. Although only preliminary studies have been conducted thus far, early findings have indicated that the application of insect frass as biofertiliser is beneficial to soil and plant health (Bloukounon-Goubalan et al., 2021). Therefore, in the proposed concept, BSFL frass could be applied back to the land from which the wheat straw originated (stage six), closing the nutrient loop and enabling a circular approach in which rearing by-products are also utilised.

This has the potential to reduce reliance on chemical fertilisers, which would further improve the sustainability and cost-effectiveness of BSFL protein production going forward.

1.10 Aims and objectives

Biotechnologies that enable the conversion of low value wastes and residues into feed for BSFL are urgently required. The aim of this thesis is to develop an innovative pretreatment process using *P. putredinis* NO1 to transform wheat straw into an edible BSFL feed.

The project has two main objectives:

1. Pretreat wheat straw with *P. putredinis* NO1 under submerged fermentation (SmF) and solid-state fermentation (SSF), and assess its feed performance in BSFL feeding trials. Feed safety testing will also be conducted to assess its compliance with safety legislation.
2. Characterise wheat straw degradation by *P. putredinis* NO1 under SmF and SSF using a range of techniques such as cell wall composition analyses (cellulose, matrix polysaccharides and lignin), solid-state NMR and scanning electron microscopy. An exo-proteomic analysis of *P. putredinis* NO1 secretomes during growth on wheat straw will also be undertaken to establish the enzymatic mechanisms responsible for the changes in cell wall composition.

2) Materials and methods

2.1 Substrates

A small conventional bale of wheat straw (20 kg) was sourced from Rowland Hill Farm (Yapham Mill, York) and milled to a particle size of 2 mm using an SM 300 cutting mill (1900 rpm; Retsch) at the Biorenewables Development Centre (York). Oil palm empty fruit bunch (EFB) was provided pre-milled (2 mm) by Dr Chong Chun Shiong (Universiti Teknologi Malaysia).

2.2 Reagents and chemicals

Reagents and chemicals were purchased from a range of suppliers: Abcam (Cambridge, UK); Avantor (PA, USA); BioLegend (CA, USA); GE Healthcare (IL, USA); Honeywell Research Chemicals (NC, USA); Invitrogen (MA, US); Life Technologies (CA, USA); Merck (Darmstadt, Germany); NBS Biologicals (Huntingdon, UK); New England Biolabs (MA, USA); Sigma-Aldrich (MO, USA) and Thermo Scientific (MA, USA). All water was obtained from an ultra-pure water dispenser (dH_2O).

Phosphate buffered saline was prepared by combining 8 g/L NaCl, 0.20 g/L KCl, 1.44 g/L Na_2HPO_4 and 0.24 g/L KH_2PO_4 in dH_2O, either at 1X or 10X concentration. The solution was adjusted to pH 7.4 using HCl, autoclaved (121°C for 15 minutes) and stored at room temperature.

2.3 Microbial culture of *P. putredinis* NO1

2.3.1 Spore preparation and harvesting

For the culture of fresh fungal spores, slants were prepared in 30 mL universal tubes using 10 mL potato glucose agar prepared according to manufacturer recipe (39 g/L dH_2O). Once the agar had solidified, slants were inoculated with *P. putredinis* NO1 by streaking from an existing glycerol stock (spore suspension, 30% v/v glycerol, stored at -20°C) and incubated at 30°C until sporulation. After approximately 14 days, spores from each slant were harvested under sterile conditions into sterile saline solution (0.5% NaCl w/v, 0.2% Tween 20 v/v). To do so, 500 µL saline solution was pipetted onto the surface of each slant and a sterile loop used to gently separate fungal spores from mycelia. All spore containing solutions were combined into a single suspension, mixed by vortex to break up any mycelia harvested and stored at 4°C. Glycerol stocks (30% v/v) were taken routinely and stored at -20°C for future fresh culture.

2.3.2 Spore quantification

For spore quantification, a 1:10 and/or 1:100 dilution of spore suspension was made up (using sterile saline solution as diluent) and 10 µL applied to both counting chambers of a clean haemocytometer (Improved Neubauer 1/400 mm^2, Hawksley). Under x40 magnification, spores in each square of both haemocytometer counting chambers were counted (Figure 2.1).

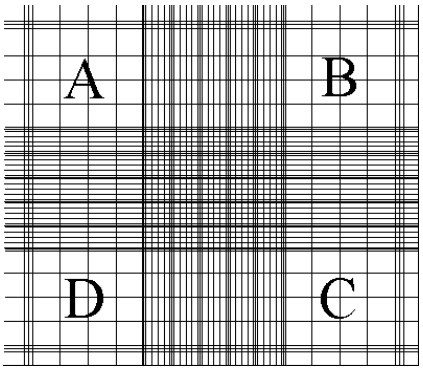

Figure 2.1. Layout of a haemocytometer counting chamber. Each square (A-D) has a surface area of 1 mm^2 and a volume of 0.1 mm^3, in which *P. putredinis* NO1 spores were counted.

Equation 2.1 was used to determine the concentration of the original undiluted suspension.

Equation 2.1. Calculation to determine the concentration of the original undiluted spore suspension. N = total number of spores counted within all eight haemocytometer squares.

$$Spores/mL\ of\ \boldsymbol{original}\ suspension\ =\ \left(\frac{N}{8}\times 10^4\right)\times dilution\ factor$$

2.3.3 Composition of Hutner's trace elements

Hutner's trace elements were stored at 4°C (in darkness) and consisted of: 50 g/L $Na_2EDTA \cdot 2H_2O$; 22 g/L $ZnSO_4 \cdot 7H_2O$; 11.40 g/L H_3BO_3; 0.51 g/L $MnCl_2 \cdot 4H_2O$; 0.45 g/L $FeSO_4 \cdot 7H_2O$; 0.16 g/L $CoCl_2 \cdot 6H_2O$; 0.16 g/L $CuSO_4 \cdot 5H_2O$ and 0.11 g/L $(NH_4)_6Mo_7O_{24} \cdot 4H_2O$.

2.3.4 Preparation of optimised growth media

In all experiments, *P. putredinis* NO1 was cultured in optimised growth media consisting of: 8.55 g/L yeast extract; 0.52 g/L KCl; 0.82 g/L KH_2PO_4; 1.05 g/L K_2HPO_4; 1.35 g/L $MgSO_4$ and 1.75 g/L $NaNO_3$ (Oates, 2016). Unless otherwise stated, Hutner's trace elements were added routinely to the growth media at a 1:1000 (v/v) dilution on the day of culture preparation.

2.3.5 Culture under submerged fermentation

For culture of *P. putredinis* NO1 under submerged fermentation, growth media was supplemented with milled wheat straw at 8.4% (w/v) in shake flasks, unless otherwise stated. Flasks were sterilised by autoclaving (121°C for 15 minutes) prior to the addition of *P. putredinis* NO1 spores (10^5 spores/mL) at 1% (v/v). For negative control flasks, sterile saline solution was added at 1% (v/v) in place of spores. Cultures were incubated at 30°C and 140 rpm, following which biomass was filtered from the growth media using Miracloth. Afterwards and unless otherwise stated, biomass was lyophilised (a method in which a material is frozen and ice is removed by sublimation) using a Heto PowerDry LL3000 (Thermo Scientific).

2.3.6 Culture under solid-state fermentation

For culture of *P. putredinis* NO1 under solid-state fermentation, growth media was supplemented with milled wheat straw at 35% (w/v) in shake flasks according to a protocol obtained from Dr Chong Chun Shiong (Universiti Teknologi Malaysia). Flasks were sterilised by autoclaving (121°C for 15 minutes) prior to the addition of *P. putredinis* NO1 spores (10^5 spores/mL) at 1% (v/v). For negative control flasks, sterile saline solution was added at 1% (v/v) in place of spores. Cultures were incubated at 30°C and mixed by manual agitation (shaking by hand) once per week. Afterwards, biomass was either lyophilised or stored at -20°C.

2.4 Black Soldier Fly larvae feeding trials

All Black Soldier Fly larvae (BSFL) feeding trials were conducted at Fera Science (York) using their in-house insect rearing facilities. Growth room conditions were set at 27°C, 60% relative humidity and 16/8 lighting (daylight hours/night hours).

2.4.1 Preparation of positive control feed

Positive control feed fed to BSFL was chick starter crumb (R950C; Thompsons of York feed supplier). To prepare feed for trials, dH_2O was added to feed crumbs to achieve a dry matter content of 31.6%, mixed and left to combine at room temperature for 30 minutes.

2.4.2 Black Soldier Fly larvae

All BSFL used in this thesis were provided by Fera Science, either as neonate (egg-hatched) or four-day-old larvae (reared initially for four days on a 'nursery' diet of chick starter crumb).

2.4.3 Feeding trial setup

All feeding trials were set up in 16 oz. containers in biological triplicate using 50 larvae per replicate (neonate or four days old). Trial containers were prepared according to Figure 2.2.

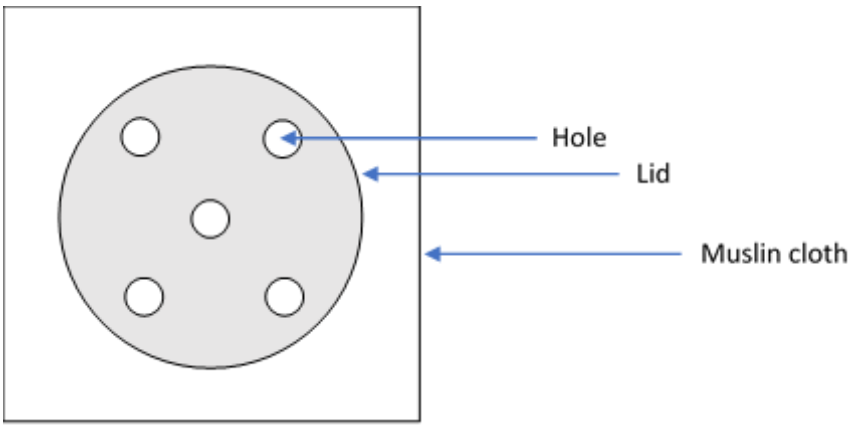

Figure 2.2. Preparation of trial containers for BSFL feeding trials. As indicated, container lids were punctured with five evenly sized holes (for larval respiration). A layer of muslin cloth was trapped between the lid and container, preventing the escape of larvae through the holes.

Once the starting feed portion had been added, BSFL were counted into trial containers under a microscope (day 0), and fed every three to four days thereafter with the same quantity. Those fed *P. putredinis* NO1 pretreated wheat straw received feed at 100 mg/day/larva (wet weight) in accordance with previous research in which a 100 mg daily feeding rate resulted in an optimum trade-off between substrate reduction efficiency and larval biomass production (Diener, Zurbrügg and Tockner, 2009). Positive control BSFL, fed chick starter crumb, received feed at either 100 mg/day/larva or 37.26 mg/day/larva, depending upon the experimental setup.

2.4.4 Assessment of larval growth performance

To monitor BSFL growth rates, groups of ten larvae were selected randomly at various time points during feeding trials (days 7, 14 and 21), weighed using a fine analytical balance and then returned. At the end of each trial, all remaining larvae were weighed for calculation of total wet yield (representative of the combined wet mass of those that survived the entire length of the trial). The number of pre-pupal larvae was also noted, as indicated by a darkened body colour.

2.5 Proteomic methods

2.5.1 Protein quantification by Bradford assay

To measure the protein concentration of solutions, Bradford assays were performed using a Coomassie protein assay kit (Thermo Scientific) according to manufacturer's protocol in 96-well plate format. Briefly, 5 µL samples were combined with 250 µL Coomassie reagent, incubated for ten minutes at room temperature and absorbance measured at 595 nm using a Tecan Sunrise microplate reader. Protein concentrations were calculated by comparison against a standard curve of bovine serum albumin at known concentrations (0-2000 µg/mL).

2.5.2 Sodium dodecyl sulfate polyacrylamide gel electrophoresis

Proteins were separated by size using sodium dodecyl sulfate polyacrylamide gel electrophoresis (SDS-PAGE), run on either 4-20% Mini-PROTEAN TGX precast (Bio-Rad) or self-made gels. To prepare gels, the separating layer was made first by combining 4 mL dH_2O, 3.3 mL acrylamide (30% w/w), 2.5 mL Tris-HCl (1.5 M, pH 8.8), 100 µL ammonium persulfate (10% w/v), 100 µL SDS (10% w/v), and 15 µL tetramethylethylenediamine (TEMED). This layer was immediately pipetted into a 0.75 mm thick gel cast and left to set, and an isopropanol (50% v/v) covering added. The isopropanol layer was then poured off and the gel surface rinsed with dH_2O, before the stacking layer was pipetted over the top and the well comb added. The stacking layer was prepared by combining 7.35 mL dH_2O, 1.3 mL acrylamide (30% w/w), 1.25 mL Tris-HCl (1 M, pH 6.8), 100 µL ammonium persulfate (10% w/v), 100 µL SDS (10% w/v) and 10 µL TEMED. Once the stacking layer had solidified, gels were assembled into electrophoresis apparatus and the tank filled with running buffer (25 mM Tris, 192 mM glycine, 0.1% SDS w/v, pH 8.3). Samples (10-15 µL) were combined with 2.5-5 µL 4X SDS sample buffer and incubated at 98°C for ten minutes to denature. Samples were loaded into gels alongside 5 µL protein ladder and ran for approximately five minutes at 140 V through the stacking layer, then for 30-45 minutes at 200 V through the separating layer (PowerPac Basic 300V 400mA 75W, Bio-Rad). Gels were stained for approximately four hours using InstantBlue Coomassie protein stain and de-stained with dH_2O. Gel photographs were captured using a gel documentation system (Genesys).

2.6 Data analysis

All data was manipulated, statistically analysed and graphically presented using computer scripts written in either Python or R programming languages.

2.6.1 Python

Python (v3.6-3.9) was used inside Spyder, an integrated development environment (IDE). All packages were downloaded through Anaconda Navigator.

2.6.2 R

R (v3.4-3.6) was used inside R Studio (IDE) via which all packages were downloaded.

2.7 Ethical considerations

2.7.1 Nagoya Protocol

The Nagoya Protocol was entered into force on 12th October 2014 to ensure fair access to genetic resources obtained from party countries, and the fair sharing of benefits obtained from their use. An ethics due-diligence report was conducted for all genetic resources used in this thesis (e.g. wheat straw, oil palm EFB, BSFL). Although no resources fell within scope of the Nagoya Protocol, all were sourced and handled in accordance with local domestic regulation.

2.7.2 Black Soldier Fly larvae

Invertebrates, like BSFL, are not covered by research ethics guidelines. Despite this, the '3R' principles were applied (e.g. reduction and refinement) (Tannenbaum and Bennett, 2015).

3) Fungal pretreated wheat straw as Black Soldier Fly larvae feed

3.1 Introduction

The insect protein sector is largely in its infancy, with an emerging market composed mainly of small to medium-sized European and North American Black Soldier Fly larvae (BSFL) production companies – e.g. Better Origin (UK), InnovaFeed (France), Protix (Netherlands), Enterra (Canada) and EnviroFlight (USA). In general, BSFL and other industrial insect producers use food waste to rear their larvae, though under current EU legislation controlling feed safety, BSFL may only be reared on pre-consumer food waste of predominantly vegetal origin (e.g. fruit and vegetable processing by-products) (IPIFF, 2022a). This approach is deemed unsustainable, as it is widely recognised by the sector that the volumes available for conversion are insufficient to fuel the growing market demand for BSFL. For instance, pre-consumer food waste in the UK represents only a fraction (approximately 17%) of total annual food waste production (WRAP, 2017). In addition, it is highly geographically dispersed which hinders its collection and dictates significant transport costs between its origin and BSFL production sites. Furthermore, the physical and nutritional characteristics of pre-consumer food waste limit its performance as BSFL feed. Typically, it possesses a high moisture content (e.g. vegetable wastes = 88-94%) which greatly reduces the relative proportion of solid fraction containing proteins, carbohydrates and other nutrients available for insect growth (Jain, Daga and Kalamdhad, 2019). This, therefore, restricts BSFL yields and feed conversion ratios (input feedstock dry mass to output BSFL dry mass).

One of the primary flaws of pre-consumer food waste, however, is that it exhibits inconsistent and heterogeneous composition due to seasonal and annual variation, as well as variation between loads (e.g. different origin facilities) (Prescott et al., 2019). This presents significant problems in maintaining feed consistency and ultimately leads to poor reproducibility in BSFL yield and nutritional quality. To combat this, pre-consumer food waste requires significant pre-processing to create a consistent feed formulation with a reproducible nutritional profile, though this significantly increases overall production costs and consequently BSFL market price. Therefore, for the global BSFL sector to become cost competitive (relative to soybean and fish meal industries) and sustainable in the long term, these costs must decrease while production scale must increase. This will require implementation of alternative feedstocks which ideally should be available in high localised abundances, highly defined/reproducible, of identifiable origin (to improve supply chain transparency) and possess a lower moisture content.

In addition to their sheer abundance, the physical characteristics of lignocellulosic crop residues, such as wheat straw, mitigate many of the shortfalls of pre-consumer food waste. Crucially, for instance, wheat straw represents a single homogenous feed substrate with a lower moisture content (5-8%), likely leading to greater reproducibility in BSFL yield and quality (Zhang, Ghaly and Li, 2012). Furthermore, its availability in localised abundances (e.g. in fields) would likely reduce transportation costs, especially for companies employing a decentralised business model in which BSFL are produced in smaller quantities on-farm using locally-sourced wastes and residues as feed (e.g. Better Origin). Although the chemical characteristics of wheat straw (e.g. relative quantities of sugars and lignin) can vary between cultivars, the majority of variation reflects the differences in tissue ratio (e.g. between ear, leaf, node and internode) as opposed to the composition of the tissues themselves (Collins et al., 2014). Therefore, wheat straw, composed of a single species, is subject to less overall variation in its physical, chemical and nutritional profiles in comparison to pre-consumer food waste. However, despite these characteristic benefits, cell wall lignocellulose is considered indigestible by BSFL and hence a pretreatment is required to make it suitable for their digestion (Peguero et al., 2022).

Here, wheat straw was subjected to a microbial pretreatment with *P. putredinis* NO1 under submerged fermentation (SmF), involving its direct inoculation and growth in liquid medium under constant shaking conditions, in line with previous work (Oates, 2016; Oates et al., 2021). To do so, *P. putredinis* NO1 was used in monoculture as opposed to being a member of a mixed microbial community. Given the importance of maintaining feed consistency, *P. putredinis* NO1 monoculture was deemed a more controllable system to pretreat wheat straw, in which the inoculum is more easily standardised and growth parameters can be manipulated, optimised and reproduced in ways not possible using a mixed community (Oates, 2016). Therefore, fungal monoculture should offer greater feed reproducibility, and consequently more consistent larval growth and composition on an otherwise inedible feedstock; thus, overcoming the issues and limitations associated with the use of pre-consumer food waste. However, few studies have investigated the effects of biological pretreatments upon BSFL conversion (Peguero et al., 2022).

In this chapter, *P. putredinis* NO1 was grown on wheat straw and oil palm empty fruit bunch (EFB) to validate its fundamental ability to degrade lignocellulosic biomass under SmF. Pretreated wheat straw was then fed to BSFL for the first time and its performance as feed was assessed in various exploratory feeding trials.

3.2 Methods

3.2.1 Quantification of biomass loss under submerged fermentation

Mass loss experiments were performed on wheat straw and oil palm EFB to assess the degradative ability of *P. putredinis* NO1. Cultures (25 mL) were set up in biological triplicate. Biomass was harvested from SmF at various time points (days 0, 3, 7, 10, 14, 17 and 21) into pre-weighed 50 mL falcon tubes using 15 mL phosphate buffered saline to collect any residual biomass. Biomass was lyophilised and falcon tubes were re-weighed, then empty falcon tube masses subtracted to obtain the dry mass of wheat straw/oil palm EFB.

3.2.2 Biomass processing for production of Black Soldier Fly larvae feed

To process wheat straw in preparation for BSFL feeding trials, a range of SmF cultures (500 mL) were set up in two litre shake flasks and subjected to various conditions. These included presence/absence of:

- **Wheat straw**. Substrate material to provide a carbon source for *P. putredinis* NO1 growth and a partially digested feed source for BSFL. Included at 8.4% (w/v).
- **Growth media**. Where present, 500 mL added.
- **Hutner's trace elements**. Where present, stock solution diluted in growth media (1:1000).
- ***P. putredinis* NO1**. Fungal species selected to perform biomass degradation and to provide a protein source for BSFL. Where present, included at 10^5 spores/mL.

Cultures were incubated as described (chapter section 2.3.5) for 3-14 days. To improve storage longevity, processed biomass was lyophilised (unless otherwise stated). Biomass moisture contents were calculated routinely using the oven dry method, in which wet samples were heated at 105°C for 24 hours and weighed to obtain their dry weight (technical triplicate). This enabled BSFL feed dry matter content to be standardised and controlled across all feeding trials.

3.2.3 Feed preparation and Black Soldier Fly larvae feeding trials

To prepare BSFL feed, pretreated wheat straw was supplemented with dH_2O (variable volumes) to achieve a dry matter content of approximately 11.2%, and mixed thoroughly. Where applicable, the diluent (dH_2O) was supplemented with either zero, medium (12.51 g/L) or high (40.69 g/L) concentrations of peptone (trial dependent) to test the effect of feed supplementation with an additional nitrogen source upon BSFL growth. All feeding trials were set up and conducted at Fera Science alongside positive controls (BSFL fed on chick starter crumb) using established laboratory practices as described (chapter sections 2.4.1-2.4.4).

3.3 Results

3.3.1 Biomass degradation under submerged fermentation

Mass loss was used as a proxy for biomass degradation to demonstrate the ability of *P. putredinis* NO1 to degrade lignocellulose under SmF (Figure 3.1).

A

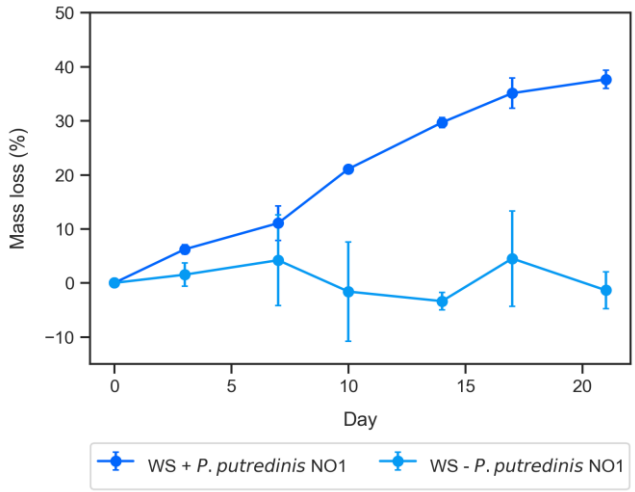

B

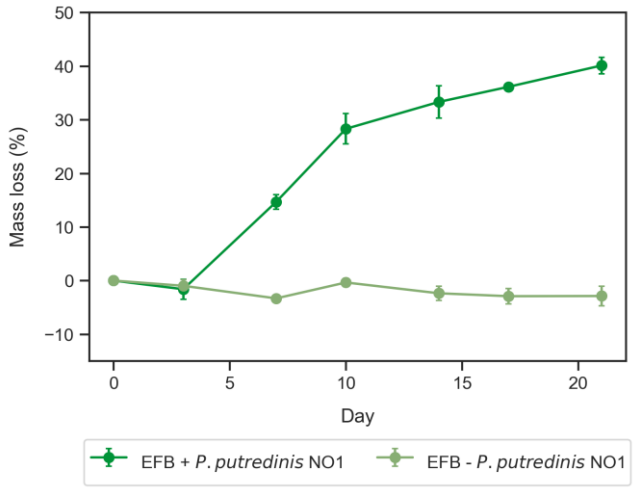

Figure 3.1. Mass loss during *P. putredinis* NO1 growth on wheat straw and oil palm EFB under SmF. Graphs show percentage mass loss of wheat straw (**A**) and oil palm EFB (**B**) over three week cultures with and without *P. putredinis* NO1 under SmF. Data are means ± SD (n = 3).

P. putredinis NO1 growth on wheat straw and oil palm EFB under SmF led to a 37.7% and 40.1% reduction in total mass by day 21, respectively. For both substrates, negative controls (lacking *P. putredinis* NO1) showed no reduction in mass, and thus, no observable degradation. Interestingly, *P. putredinis* NO1 showed similar temporal degradation patterns on wheat straw and oil palm EFB (Figure 3.2).

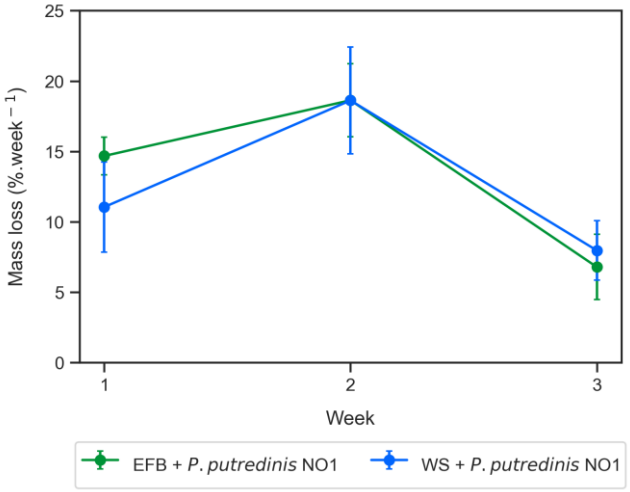

Figure 3.2. Weekly mass loss during *P. putredinis* NO1 growth on wheat straw and oil palm EFB under SmF. Graph shows weekly percentage mass loss of wheat straw and oil palm EFB over three week cultures with *P. putredinis* NO1 under SmF. Data are means ± SD (n = 3).

For both substrates, the majority of degradation occurred during the second week, with an 18.6% reduction in mass. In the first week, oil palm EFB degradation was higher (14.7% mass loss) relative to wheat straw (11.1% mass loss), while during the third week similar degradation levels were observed (8.0% and 6.8% reduction in wheat straw and oil palm EFB mass, respectively). Based on these data, it was expected that the duration of fungal fermentation during biomass processing would directly affect final composition, and likely BSFL growth during rearing. However, due to various COVID-19 related issues, feeding trials did not include oil palm EFB and focussed solely on wheat straw. As a result, ten-day pretreated wheat straw was selected as BSFL feed for initial experimentation, representing an approximate mid-point in biomass degradation (day 10 = 56% of the total mass loss observed over 21 days) (Figure 3.1).

3.3.2 Black Soldier Fly larvae growth on pretreated wheat straw

The initial proof of concept feeding trial showed for the first time that BSFL can survive and grow on wheat straw pretreated with *P. putredinis* NO1 (Figure 3.3). In contrast, BSFL fed untreated wheat straw failed to grow significantly, showing only negligible increases in mass over 28 days. This initial experiment used egg-hatched (neonate) and four-day-old BSFL (pre-reared on a nursery chick starter crumb diet) to ascertain any differences in growth performance derived from larval starting age. On fungal pretreated wheat straw, neonate larvae showed higher growth rates and achieved a greater total yield in comparison to four-day-old larvae (by day 28: neonate = 3.26 g; four-day-old = 3.20 g). Interestingly, on chick starter crumb, neonate positive control larvae achieved a lower total yield in comparison to four-day-old larvae (by day 14: neonate = 10.19 g; 4-day-old = 12.24 g). However, it should be noted that by day 14, 64% of the starting population (32 BSFL) had reached the pre-pupal stage (darkened body colour), in which larvae reduce in mass as they begin to use stored energy reserves (Tomberlin, Adler and Myers, 2009). Neonate larvae fed chick starter crumb were the only group observed to reach this stage.

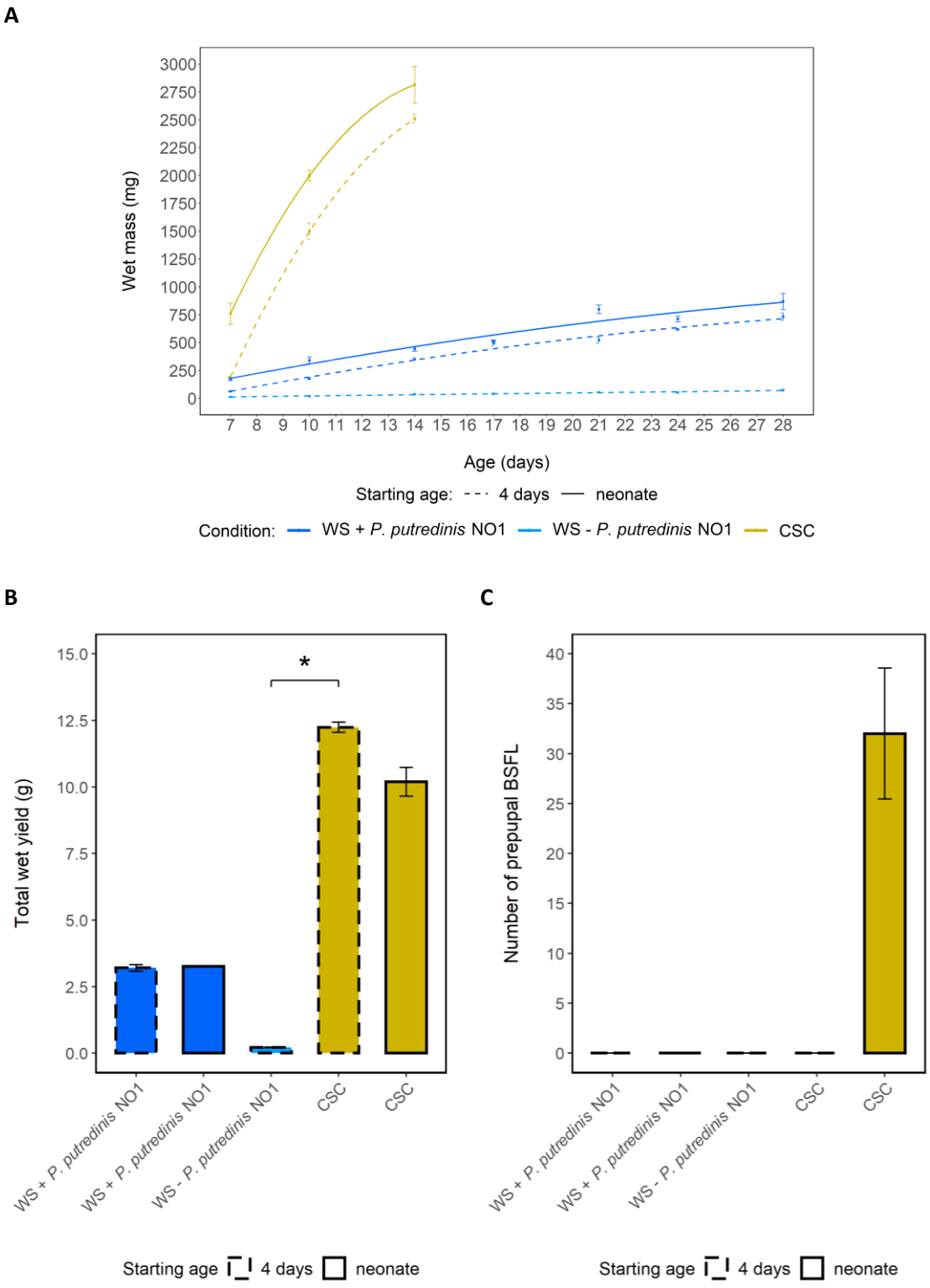

Figure 3.3. Proof of concept BSFL growth study on wheat straw pretreated with *P. putredinis* NO1 under SmF. Data shows change in wet mass (**A**), total wet yield (**B**) and total pre-pupal (**C**) of BSFL fed wheat straw over 28 days, pretreated with and without *P. putredinis* NO1 under SmF, or with positive control feed (chick starter crumb; CSC) over 14 days. All larvae received 100 mg feed/larva/day regardless of starting age.

(**A**) BSFL growth rates (change in wet mass) on wheat straw pretreated with and without *P. putredinis* NO1, and on CSC. Data are means ± SD (n = 3) of ten randomly selected larvae. (**B**) Total wet yields of BSFL fed the same feed conditions as in A. Data are means ± SD (n = 3) of all remaining larvae at the end of the trial. Significant difference ($\alpha = 0.05$) as determined by the Kruskal-Wallis one-way ANOVA is indicated by *****. (**C**) Number of BSFL that reached the pre-pupal stage by the end of the trial. Data are means ± SD (n = 3).

Trace element mixtures are commonly added to growth media formulations, providing essential micronutrients (e.g. copper, iron and sodium) for effective microbial growth during culture. *P. putredinis* NO1 media includes Hutner's trace elements at 0.1% (v/v). To ascertain whether the inclusion of trace elements affects BSFL growth, larvae were fed ten-day pretreated wheat straw produced under either the presence or absence of Hutner's trace elements (Figure 3.4).

A

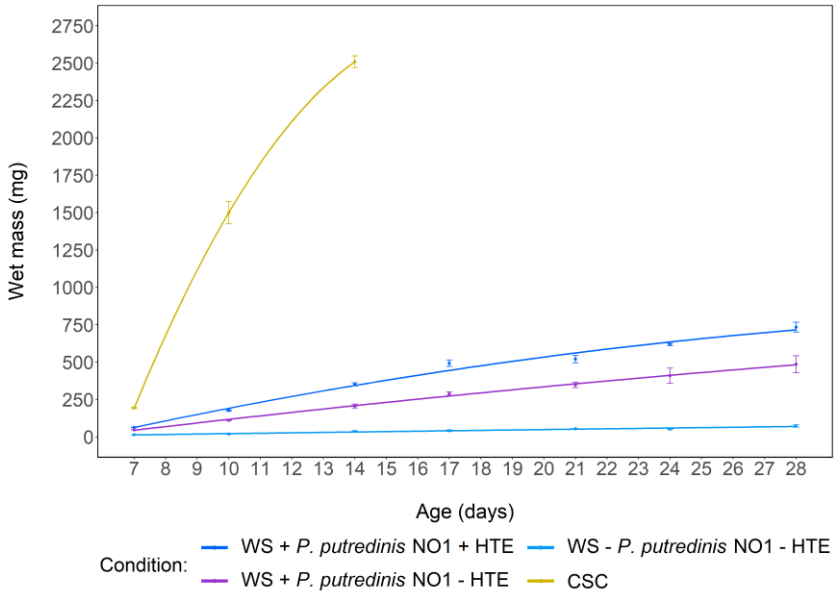

B

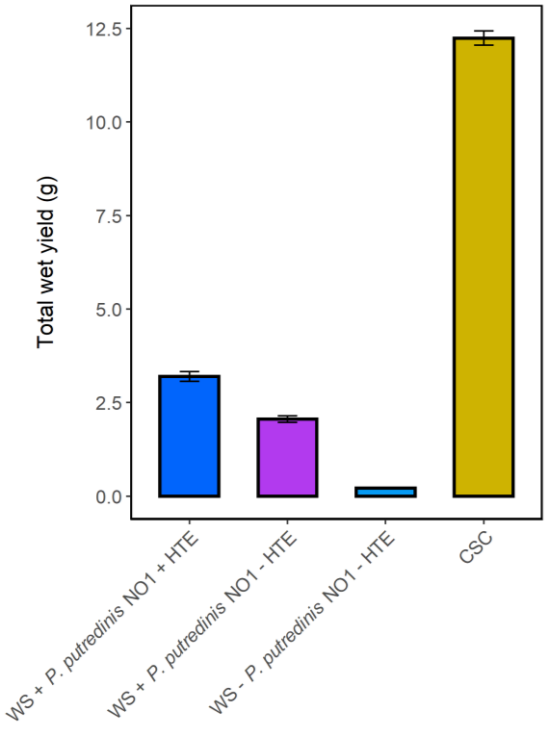

Figure 3.4. BSFL growth study (effect of Hutner's trace elements) on wheat straw pretreated with *P. putredinis* NO1 under SmF. Data shows change in wet mass (**A**) and total wet yield (**B**) of BSFL fed wheat straw over 28 days, pretreated with and without *P. putredinis* NO1 under various conditions, or with positive control feed (chick starter crumb; CSC) over 14 days. All larvae were four days old at the beginning of the trial and received 100 mg feed/larva/day.

(**A**) BSFL growth rates (change in wet mass) on wheat straw pretreated with and without *P. putredinis* NO1 in the presence or absence of Hutner's trace elements, and on CSC. Data are means ± SD (n = 3) of ten randomly selected larvae. (**B**) Total wet yields of BSFL fed the same feed conditions as in A. Data are means ± SD (n = 3) of all remaining larvae at the end of the trial. HTE = Hutner's trace elements.

Larvae fed wheat straw pretreated with *P. putredinis* NO1 in the presence of Hutner's trace elements showed higher growth rates and total yields (3.20 g with trace elements; 2.06 g without trace elements). Based on these results, it was decided that future feeding trials would use neonate larvae, and that Hutner's trace elements would be routinely added to the media.

3.3.3 Supplementation of pretreated wheat straw feed

It was anticipated that BSFL growth performance would be affected by the total nitrogen content within their feed. To test this, a feeding trial was conducted in which ten-day pretreated wheat straw was supplemented with various concentrations of peptone (nitrogen source) to increase feed nitrogen content (Figure 3.5). Unfortunately, due to COVID-19 related issues at the time, it was not possible to measure total carbon and nitrogen for calculation of carbon to nitrogen (C:N) ratio; a critical feed parameter known to affect BSFL growth performance. Therefore, an estimation was made in which the C:N ratio of untreated wheat straw was assumed to be 80:1 (USDA, 2011), and that a *P. putredinis* NO1 pretreatment would improve the C:N ratio to approximately 60:1. Based on this, ten-day pretreated wheat straw was supplemented with peptone to increase feed C:N ratios to an estimated 30:1 and 10:1, then fed to BSFL alongside negative and positive controls. In addition, the effect of biomass lyophilisation following SmF treatment was investigated, whereby BSFL feed was either lyophilised or not lyophilised, then amended with a water/peptone mixture to the desired dry matter content.

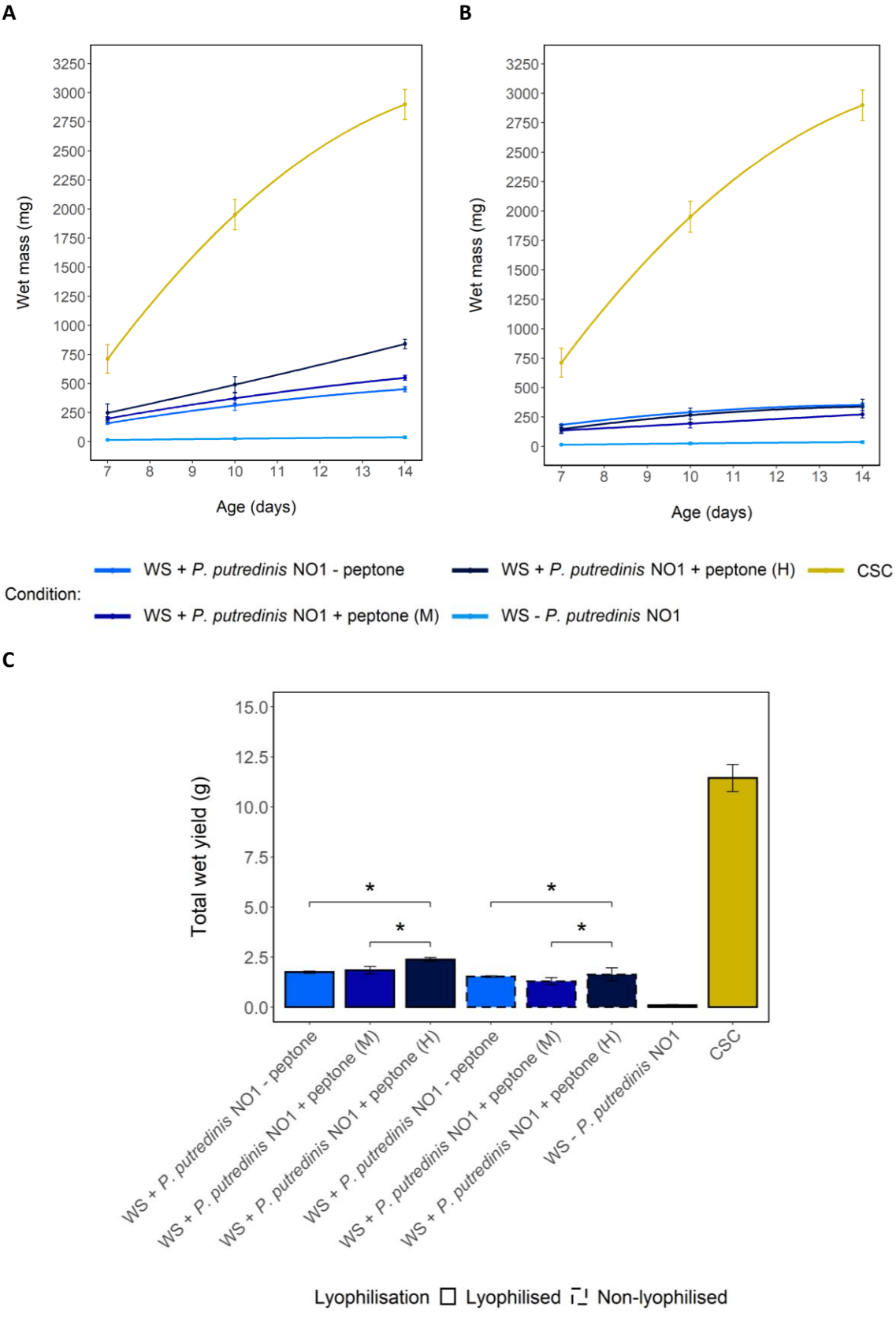

Figure 3.5. BSFL growth study (effect of peptone supplementation and lyophilisation) on wheat straw pretreated with *P. putredinis* NO1 under SmF.

Data shows change in wet mass (**A**, **B**) and total wet yield (**C**) of BSFL fed wheat straw pretreated with and without *P. putredinis* NO1 under various conditions or with positive control feed (chick starter crumb; CSC), over 14 days. All larvae were neonates at the beginning of the trial and received 100 mg feed/larva/day. Prior to BSFL feeding, pretreated wheat straw was supplemented with dH_2O containing zero, medium (M; 12.51 g/L) or high (H; 40.69 g/L) concentrations of peptone. (**A**) BSFL growth rates (change in wet mass) on wheat straw pretreated with and without *P. putredinis* NO1, lyophilised and supplemented with/without peptone, and on CSC. Data are means ± SD (n = 3) of ten randomly selected larvae. (**B**) Conditions as in A, but pretreated wheat straw was not lyophilised prior to peptone supplementation and feeding. (**C**) Total wet yields of BSFL fed the same feed conditions as in A/B. Data are means ± SD (n = 3) of all remaining larvae at the end of the trial. Significant differences ($\alpha = 0.05$), as determined by a two-way parametric ANOVA (excl. control groups) followed by post-hoc testing (Tukey's Honest Significant Difference), are indicated by *****.

Peptone supplementation of ten-day pretreated wheat straw subjected to lyophilisation improved BSFL growth rates, with peptone concentration correlating positively with growth. Interestingly, peptone supplementation of non-lyophilised pretreated wheat straw showed little correlation between peptone concentration and growth. BSFL fed non-lyophilised feed showed lower growth rates relative to those fed lyophilised feed at all peptone concentrations. The same trend was observed with total yields, ranging between 1.75 g (zero peptone) and 2.38 g (high peptone) for BSFL fed pre-lyophilised feed, while larvae fed non-lyophilised feed reached yields of just 1.63 g (high peptone), approximately 1.5 times lower in comparison. Statistically significant differences in total yield were found between zero and high peptone feed conditions, as well as medium and high peptone feed conditions, within both lyophilisation groups.

3.3.4 Effect of pretreatment duration on Black Soldier Fly larvae growth

It was expected that the duration of fungal pretreatment during BSFL feed production would affect larval growth performance during rearing. Therefore, a feeding trial was conducted in which wheat straw was subjected to SmF pretreatment for a range of durations (3-14 days), then fed to BSFL (Figure 3.6). Here, positive control larvae received a reduced feeding rate (37.26 mg feed/larva/day) in comparison to previous feeding trials (100 mg feed/larva/day). This accounted for the differences in dry matter content between pretreated wheat straw feed (11.2%) and chick starter crumb (31.6%), and ensured that positive control larvae received the same amount of feed on a dry matter basis as those fed pretreated wheat straw.

A

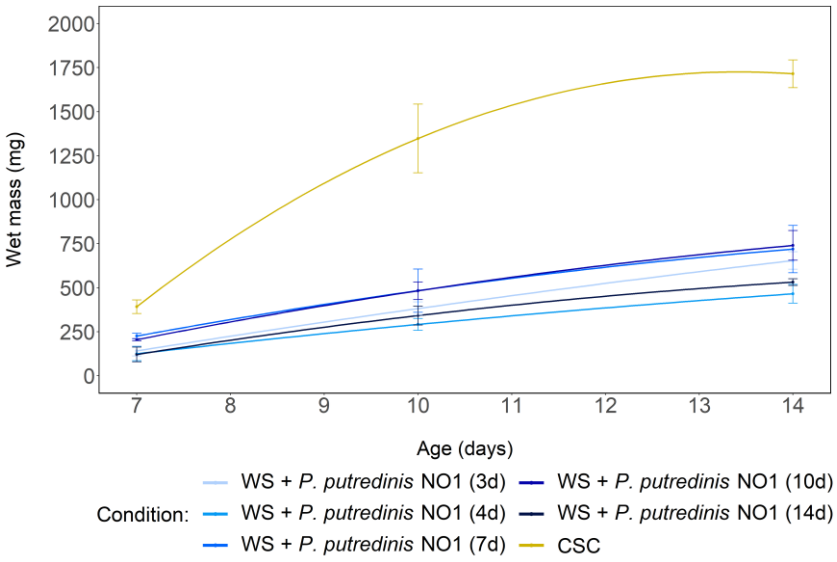

B

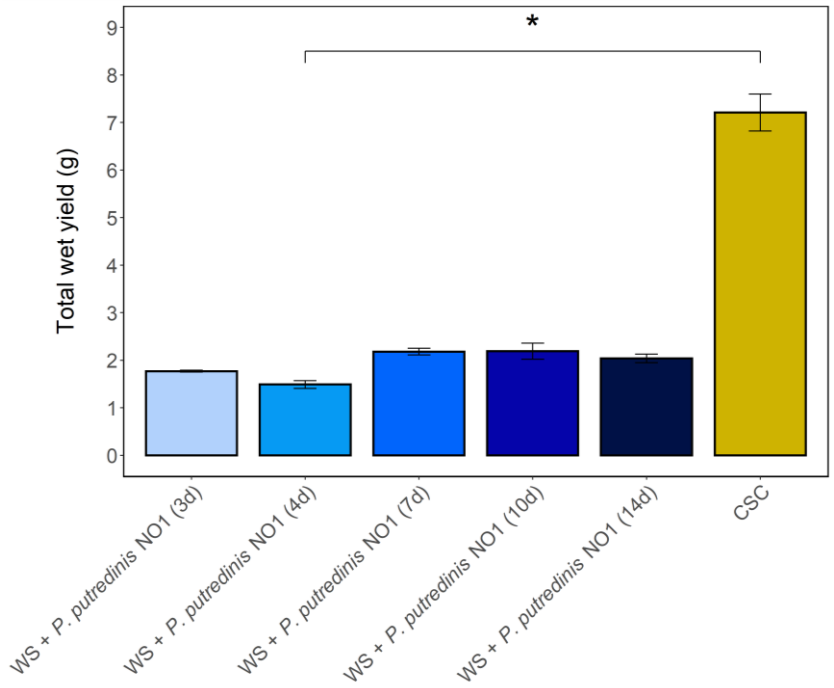

Figure 3.6. BSFL growth study (effect of pretreatment duration) on wheat straw pretreated with *P. putredinis* NO1 under SmF. Data shows change in wet mass (**A**) and total wet yield (**B**) of BSFL fed wheat straw pretreated with *P. putredinis* NO1 for various durations or with positive control feed (chick starter crumb; CSC), over 14 days. All larvae were neonates at the beginning of the trial and received 100 mg feed/larva/day, except for positive control larvae which received a reduced rate (37.26 mg feed/larva/day). (**A**) BSFL growth rates (change in wet mass) on wheat straw pretreated with *P. putredinis* NO1 for various durations (3-14 days), and on CSC. Data are means ± SD (n = 3) of ten randomly selected larvae.

(**B**) Total wet yields of BSFL fed the same feed conditions as in A. Data are means ± SD (n = 3) of all remaining larvae at the end of the trial. Significant difference ($\alpha = 0.05$) as determined by the Kruskal-Wallis one-way ANOVA is indicated by *****.

Interestingly, ten-day pretreated wheat straw enabled the greatest larval growth rates and the highest total yield (2.19 g), closely followed by seven-day pretreated wheat straw. Although significant differences in total yield were found only between BSFL fed four-day pretreated wheat straw and chick starter crumb, there was nevertheless observable differences in total yield between fermentation durations (e.g. four days/lowest = 1.49 g; ten days/highest = 2.19 g; approximately 47% increase in mass). Positive control larvae that received a reduced feeding rate showed a reduction in growth rates and total yield (7.21 g), relative to those observed in previous feeding trials. However, due to the unavoidable differences in experimental conditions between feeding trials (e.g. fluctuations in BSFL stock quality and room temperature/humidity), it is difficult to make between-trial comparisons without consideration of confounding variables.

3.4 Discussion

3.4.1 *P. putredinis* NO1 degrades lignocellulose under submerged fermentation

The ability of *P. putredinis* NO1 to grow on and degrade lignocellulose was validated by mass loss experiments in which wheat straw and oil palm EFB showed reductions in total mass during pretreatment under SmF. These data support previous work that first demonstrated the degradative capacity of *P. putredinis* NO1 towards wheat straw (Oates, 2016). Wheat straw and oil palm EFB showed similar degradation patterns over time, which were non-linear and showed that the majority of degradation occurred during the second week. However, unexpectedly, oil palm EFB showed comparatively greater mass loss after three weeks, as well as during the first week of culture. Due to its fibrous nature, oil palm EFB is considered a more recalcitrant biomass in comparison to wheat straw. Although biomass composition analyses vary in the literature due to a range of factors (e.g. crop variety, seasonal variation, different analytical methods), oil palm EFB has been reported to contain 32-35% lignin (Coral Medina et al., 2018; Karunakaran, Abd-Talib and Kelly Yong, 2020) while wheat straw is typically reported as containing 15-19% lignin (Tufail et al., 2018; Yu et al., 2021). Despite this, *P. putredinis* NO1 elicited significant mass loss on oil palm EFB, supporting previous work in which its presence was shown to dominate a wheat straw enriched composting community during its latter, more heavily lignified stages (Oates, 2016). This, therefore, provides promising evidence that *P. putredinis* NO1 could be used to pretreat a variety of biomasses with differing cell wall compositions, with the aim of breaking open and partially degrading the lignocellulose complex to improve its digestibility by BSFL.

3.4.2 Pretreated wheat straw supports Black Soldier Fly larvae growth

Feeding trials showed for the first time that BSFL can survive and grow on wheat straw pretreated with *P. putredinis* NO1 under SmF. In contrast, larvae reared on untreated wheat straw showed negligible growth. This provided proof of concept, in which a pretreatment using *P. putredinis* NO1 improved the digestibility of wheat straw by BSFL and enabled growth on an otherwise inedible feedstock. Although there is limited literature available for comparison of BSFL growth performance on lignocellulosic biomass, maize straw fermented with *Aspergillus oryzae* also supported BSFL growth, though larvae wet masses were a little over ten-fold lower than those fed wheat straw pretreated with *P. putredinis* NO1 (Gao et al., 2019). However, direct comparisons between larval parameters (e.g. growth rates and yields) are hindered by differences in methodological approach (e.g. culture moisture content, inoculum concentration, pretreatment time and BSFL feeding rate). Nevertheless, early trials provided a promising indication that *P. putredinis* NO1 may be particularly effective in improving biomass digestibility by BSFL, though at this stage the underlying mechanisms responsible remained unclear.

Prior to feeding, it is typical for BSFL to be added to their feed substrate as either neonates (egg-hatched) or as young larvae (e.g. four days old) reared initially on a nursery diet. However, the effect of larval starting age upon growth performance is poorly understood, and thus was investigated. Interestingly, neonate larvae fed pretreated wheat straw from the outset achieved higher growth rates in comparison to four-day-old larvae reared initially on a nursery diet of chick starter crumb, then switched to the same wheat straw feed. Therefore, this suggests that the diet switch early in the larval life cycle was detrimental to overall growth, despite larvae having been raised on an optimal diet (chick starter crumb) for their first four days. Neonate larvae fed pretreated wheat straw also achieved a greater total yield than those reared initially on chick starter crumb, although the same was not observed for positive control larvae fed chick starter crumb throughout, on which neonates achieved a comparatively lower yield. However, almost two-thirds of the neonate population reared on chick starter crumb reached the pre-pupal stage (sixth larval instar), indicated by a darkened body colour, upon which larvae vacate their feed source to later metamorphose into an adult fly (Barros-Cordeiro, Báo and Pujol-Luz, 2014; Fischer et al., 2022). During the pre-pupal and pupal stages, BSF decrease in mass, typically by 50%, as they use energy reserves stored during the larval stages (Georgescu et al., 2020; Tomberlin, Adler and Myers, 2009). This may explain the reduced yield observed for positive control neonate larvae fed chick starter crumb, of which the majority had reached the sixth instar and were pre-pupae when harvested. As a result, neonate larvae were selected for use in all future feeding trials due to their comparatively superior growth performance.

Feeding rate is an important parameter requiring optimisation and generally correlates positively with BSFL yield (Diener, Zurbrügg and Tockner, 2009; Dzepe et al., 2021). In line with this, positive control larvae that received a reduced feeding rate of chick starter crumb showed a reduction in growth rates and yields, indicating larval growth is in-part limited by the quantity of feed available. Although the effect of feeding rate was not assessed on wheat straw, it would be expected to have a similar effect upon BSFL growth. As such, it may be possible to improve larval growth on pretreated wheat straw by increasing feeding rates, as observed when BSFL were fed increasing quantities of dairy manures (Myers et al., 2008). However, it should be noted that the degree of correlation between feeding rate and larval yield varies significantly between substrates, as well as feeding regimes (e.g. single batch or continuous) (Dzepe et al., 2021).

3.4.3 Peptone supplementation of feed improves Black Soldier Fly larvae growth

Lignocellulosic biomasses typically possess high carbon to nitrogen (C:N) ratios, and are therefore inherently low in nitrogen. Untreated wheat straw, for example, has been reported to have a C:N ratio of between 50:1 and 100:1 (Reichel et al., 2018), and enabled negligible BSFL growth during feeding trials. In line with this, BSFL are only versatile with respect to their feed preferences if substrate nitrogen content is sufficient to enable their growth (Lalander et al., 2019). Therefore, the negligible growth observed on untreated wheat straw may be attributed to its inherently poor nitrogen content. In comparison, poultry feed possesses a C:N ratio of 18.1:1, while food waste has been reported at a C:N ratio of 14:1-21:1, both of which support larval growth (Lalander et al., 2019; Lu et al., 2021). It should be noted, however, that C:N ratios vary considerably depending upon substrate composition, particularly for heterogeneous substrates such as food waste. Nevertheless, the manipulation of substrate C:N ratio significantly affects a range of BSFL growth parameters (e.g. mass, protein and lipid yield) (Lu et al., 2021; Pang et al., 2020). In accordance with this, feeding trials indicated that BSFL growth rates and yields on pretreated wheat straw can be improved by supplementation with an additional nitrogen source (peptone). Although it was not possible to quantify absolute C:N ratio at the time, peptone supplementation provided a method by which to increase the nitrogen content of pretreated wheat straw, in a similar way as described using urea, thereby decreasing its C:N ratio (Palma et al., 2019). These results correlate with recent work in which stepwise reductions in feed C:N ratio (almond hull based feedstocks and brewers spent grain/sawdust) led to increases in BSFL dry weight, growth and yield (Beesigamukama et al., 2021; Palma et al., 2019). Furthermore, in line with this, BSFL fed various blends of chicken feed and cellulose showed improved yield with reductions in cellulose content, and hence reductions in C:N ratio (Barragan-Fonseca, Dicke and van Loon, 2018). However, in contrast, reductions in the C:N ratio of food waste and pig manure/corncob showed poor correlation with BSFL yield, instead fluctuating with reductions in their C:N ratio (Lu et al., 2021; Pang et al., 2020). These results suggest the existence of substrate specificity, in which there may be an optimum C:N ratio depending upon substrate composition.

Methionine is of particular importance in livestock feed and is generally one of the first limiting amino acids (Liland et al., 2017). Although BSFL are generally considered to possess an amino acid profile favourable to their target livestock (e.g. growing pigs), it has been suggested that they may be deficient in methionine and cysteine (Makkar et al., 2014), with larvae containing low levels of methionine in comparison to fish meal (Liland et al., 2017).

However, this deficiency has also been disputed, with BSFL reared on a range of organic waste substrates (anaerobic digestion digestate, vegetable and restaurant waste) shown to comply with the required levels of all essential amino acids within livestock feeds, including methionine (Spranghers et al., 2017). Interestingly, BSFL showed similar amino acid profiles regardless of feed substrate, indicating little influence of substrate. However, in contrast, as well as improving larval growth, reductions in feed C:N ratio led to reductions in the methionine and cysteine contents of BSFL (Palma et al., 2019; Miner et al., 2022). Given their importance, reduced quantities of essential amino acids such as these are undesirable and reduce feed performance. Therefore, any changes made to feed C:N ratio with the aim of improving larval growth should be carefully balanced alongside the potentially detrimental changes to amino acid profiles.

3.4.4 Duration of fermentation affects Black Soldier Fly larvae growth on wheat straw

Feeding trials indicated that the duration of SmF affects BSFL growth on wheat straw, in line with previous work showing pretreatment time to be the third most highly ranked factor affecting BSFL growth on a range of straw types (Gao et al., 2019). Interestingly, ten-day pretreated wheat straw (representing an approximate mid-point in biomass degradation) showed the greatest larval growth. Wheat straw pretreated for shorter durations (three, four and seven days) and 14 days showed lower larval growth in comparison. This suggests that there is an optimum fermentation duration, in which *P. putredinis* NO1 likely increases the accessibility of cell wall sugars within wheat straw, while simultaneously providing a protein source (e.g. hyphae and spores) for BSFL to feed upon. Given that BSFL growth (and quality) vary with substrate (Gao et al., 2019; Miner et al., 2022), it is likely that the optimum fermentation duration of *P. putredinis* NO1 will also differ across substrates. Therefore, fermentation duration should be optimised for specific substrates to enable optimal larval growth.

4) Development of a solid-state fermentation pretreatment process for the production of Black Soldier Fly larvae feed

4.1 Introduction

Early experiments (chapter 3) demonstrated the initial proof of concept in which wheat straw pretreated with *P. putredinis* NO1 under submerged fermentation (SmF) enabled Black Soldier Fly larvae (BSFL) growth, in contrast to untreated wheat straw. Under SmF, predominantly liquid cultures require significant quantities of water, as well as constant agitation (by shaking) to provide sufficient mixing, mass/heat transfer and dissolved oxygen levels for fungal respiration and activity (Ibrahim, Weloosamy and Lim, 2015). As such, SmF can be cost intensive due to high energy demand, while also complex to operate at scale (Doriya et al., 2016). Furthermore, solid (biomass) loadings are heavily restricted to maintain fluidity of the culture. This increases the space required by the process as the amount of biomass which can be pretreated in a given volume is limited, which therefore has scale-up implications. As such, an alternative *P. putredinis* NO1 culture system was pursued which largely mitigates the shortfalls of SmF, potentially enabling a more cost-effective process to convert wheat straw into feed for BSFL.

Filamentous fungi, such as *P. putredinis* NO1, are typically found living in Nature on solid organic substrates. Solid-state fermentation (SSF), in contrast to SmF, is conducted in the absence or near absence of free water. Under SSF, the substrate (e.g. wheat straw) acts as a solid scaffold for fungal growth which better emulates the natural habitat of filamentous fungi (Verduzco-Oliva and Gutierrez-Uribe, 2020; Abu Yazid et al., 2017; Pandey, Larroche and Soccol, 2017). Crucially, SSF is less energy intensive than SmF, with a significantly lesser need for agitation during culture (Soccol et al., 2017; Viniegra-González et al., 2003). However, SSF cultures should still be agitated, albeit infrequently, to maintain aeration for sufficient oxygen supply and carbon dioxide removal, as well as to facilitate various other culture parameters (e.g. mass/heat transfer, distribution of inoculum and nutrients within the growth media) (Gassara et al., 2013). Furthermore, SSF enables higher biomass loadings in a given pretreatment volume which reduces its overall space requirements and increases process efficiency (Meng, Yin and Yu, 2019). Therefore, SSF is generally considered a more cost-effective system in comparison to SmF (Zhao et al., 2019), with comparative economic analyses showing SSF could significantly reduce the cost to produce cellulose for bioethanol production (Zhuang et al., 2007).

In line with this, SSF holds strong economic feasibility at scale, validated by modern-day industrial scale enzyme production (Lizardi-Jiménez and Hernández-Martínez, 2017). Furthermore, with particular importance for the production of BSFL feed, an SSF system is less susceptible to bacterial contamination (Soccol et al., 2017; Meng, Yin and Yu, 2019) and, therefore, may better ensure fungal monoculture during *P. putredinis* NO1 pretreatment. This should enhance the reproducibility of the pretreatment process in line with comparative studies showing SSF to be a more reproducible system relative to SmF (Gupta, Lee and Chen, 2018). Consequently, this should improve the consistency of output BSFL upon rearing, which currently presents a significant challenge using existing feed sources (e.g. pre-consumer food waste).

Previous studies have demonstrated the role of SSF in the nutritional enrichment of organic wastes and residues as livestock feed (e.g. pigs), typically in which filamentous fungi increase their protein content and overall digestibility (Pandey, Larroche and Soccol, 2017). For instance, a *Rhizopus* sp. (filamentous fungus) cultured under SSF improved the characteristics of fruit and vegetable waste as feed (e.g. enriched protein content and amino acid profile), while SSF of *Trichoderma reesei* increased the digestibility of banana peel by monogastric animals (Katongole et al., 2017; Ibarruri, Cebrián and Hernández, 2021). These results, in conjunction with reports suggesting fermentation leads to an increased ability of animals to digest structural carbohydrates such as cellulose and hemicellulose (Kerr and Shurson, 2013), indicate that SSF holds significant potential to convert wheat straw into feed for BSFL. SSF may enable this in an efficient, reproducible, scalable and cost-effective pretreatment process not feasible using SmF.

In this chapter, *P. putredinis* NO1 was grown on wheat straw and oil palm empty fruit bunch (EFB) under SSF. Its ability to degrade lignocellulose was monitored by mass loss experiments and the performance of pretreated wheat straw as BSFL feed was assessed during various feeding trials, in accordance with chapter 3. Pretreated wheat straw was also tested for feed safety (mycotoxins and heavy metals) to ensure its compliance with the relevant legislation.

4.2 Methods

4.2.1 Quantification of biomass loss under solid-state fermentation

Mass loss experiments were performed on wheat straw and oil palm EFB to assess the degradative ability of *P. putredinis* NO1. Cultures (25 mL) were set up in biological triplicate. Biomass was harvested from SSF at various time points (days 0, 3, 7, 10, 14, 17 and 21) into pre-weighed 50 mL falcon tubes using 15 mL phosphate buffered saline to collect any residual biomass. Biomass was lyophilised and falcon tubes were re-weighed, then empty falcon tube masses subtracted to obtain the dry mass of wheat straw/oil palm EFB.

4.2.2 Biomass processing for production of Black Soldier Fly larvae feed

To process wheat straw in preparation for BSFL feeding trials, a range of SSF cultures (500 mL) were set up in two litre shake flasks and subjected to various conditions. These included presence/absence of:

- **Wheat straw**. Included at 35% (w/v).
- **Growth media**. Where present, 500 mL added.
- **Hutner's trace elements**. Where present, stock solution diluted in growth media (1:1000).
- ***P. putredinis* NO1**. Where present, included at 10^3-10^6 spores/mL (trial dependent).

Cultures were incubated as described (chapter section 2.3.6) for 3-28 days. Moisture contents of pretreated biomass were calculated routinely using the oven dry method, in which wet samples were heated at 105°C for 24 hours and weighed to obtain their dry weight (technical triplicate). This enabled BSFL feed dry matter content to be standardised and controlled across all feeding trials.

4.2.3 Feed preparation and Black Soldier Fly larvae feeding trials

To prepare BSFL feed, pretreated wheat straw was supplemented with dH_2O (variable volumes) to achieve a dry matter content of approximately 11.2%, and mixed thoroughly. Where applicable, the diluent (dH_2O) was supplemented with either zero, medium (12.51 g/L) or high (40.69 g/L) concentrations of peptone (trial dependent) to test the effect of feed supplementation with an additional nitrogen source upon BSFL growth. All feeding trials were set up and conducted at Fera Science alongside positive controls (BSFL fed on chick starter crumb) using established laboratory practices as described (chapter sections 2.4.1-2.4.4). Brewers' spent grain (BSG) was provided in ground lyophilised form by Entofood (Malaysia).

4.2.4 Determination of carbon to nitrogen ratios

To calculate carbon to nitrogen (C:N) ratios of SSF pretreated wheat straw (3, 7, 14, 21, 28-day pretreated), chick starter crumb and BSG, total carbon and nitrogen contents were measured using a Flash 1112 NC analyser fitted with an MAS200R autosampler (Thermo Scientific), courtesy of Dr Matt Pickering (Department of Environment & Geography, UoY). Instrument control and data acquisition were controlled by Eager Smart software (Thermo Scientific). For elemental analysis, 4-5 mg samples and 2-3 mg aspartic acid standards were prepared in 8 x 5 mm tin foil capsules. Helium was used as the carrier and reference gas (flow rate = 140 mL/min and 100 mL/min, respectively). Sample introduction coincided with a 250 mL pulse of oxygen for ten seconds. The oxidation reactor was a quartz tube packed with copper oxide wires and silvered cobaltous oxide, held at 940°C during analysis, while the reduction reactor was a quartz tube packed with copper wires and held at 840°C. Moisture removal was conducted by a magnesium perchlorate filter. Combustion gases (carbon dioxide and N_2) were separated on a packed chromatographic column and detected using a thermal conductivity detector held at 50°C. These values were used to calculate percentage carbon/nitrogen, and thus C:N ratios.

4.2.5 Mycotoxin screening

Liquid chromatography with tandem mass spectrometry (LC-MS/MS) was used to determine the presence of 68 mycotoxins in SSF pretreated wheat straw (3, 7, 14, 21 and 28-day pretreated), courtesy of Susan MacDonald and Stephen Chapman (Fera Science) using in-house validated methodology. Samples were extracted by shaking using a mixture of acetonitrile, dH_2O and acetic acid, then centrifuged and the supernatant decanted. An aliquot of the supernatant was diluted with an equal volume of acetonitrile, dH_2O and acetic acid to give a final solvent ratio of 1:1 (acetonitrile/dH_2O). Mycotoxin determination was performed by LC-MS/MS using solvent calibration standards for analyte identity and quantification. Reporting limits (µg/kg) were raised as a result of the dilution required due to the absorbent nature of the wheat straw samples.

4.2.6 Standard preparation for multi-elemental analysis

In preparation for multi-elemental analysis using inductively coupled plasma-optical emission spectrometry (ICP-OES), a range of calibration standards were prepared. Calibration standards enable conversion of the data obtained (light intensity emitted at various wavelengths) into elemental concentration (e.g. in ppm or ppb). The following six standard solutions were prepared: (1) ICP multi-element standard solution IV, 0-10 mg/L; (2) ICP multi-element standard solution IV, 0-1 mg/L; (3) ICP multi-element standard solution XVI, 0-1 mg/L; (4) P single standard, 0-10 mg/L; (5) S single standard, 0-1 mg/L; (6) Sn single standard, 0-1 mg/L.

Initially, 100 mg/L solutions were prepared, from which 0-10 mg/L (e.g. for alkali metals) and 0-1 mg/L (e.g. for trace elements) dilutions were made in 100 mL volumetric flasks. All standards (including 0 mg/L) were matrix-matched with nitric acid (TraceSELECT, ≥ 69%) and hydrogen peroxide (ULTREX II, 30%) in a 2.67:1 ratio, respectively. The 0-10 mg/L range included 0, 2.5, 5, 7.5 and 10 mg/L, while the 0-1 mg/L range included 0, 0.25, 0.5, 0.75 and 1 mg/L.

4.2.7 Acid digestions for multi-elemental analysis

Prior to analysis by ICP-OES, samples were acid digested using an adapted protocol (Rahman and Hopke, 2017). SSF pretreated wheat straw (3, 7, 14, 21, 28-day pretreated) and chick starter crumb were first ground into fine powders using a cyclone mill (Retsch TWISTER), and 50 mg samples weighed into 40 mL glass vials (five biological replicates). For acid digestion, 800 µL nitric acid (TraceSELECT, ≥ 69%) and 300 µL hydrogen peroxide (ULTREX II, 30%) were added, and the vials placed in a heat block (DB200/2, Techne) at 110°C for 16 hours. Afterwards, vials were allowed to cool, and the samples were diluted with 2.2 mL dH_2O. Diluted samples were then poured into 5 mL volumetric flasks and the vials washed three times with 500 µL dH_2O. All washings were added to the volumetric flasks. Samples were then made up to 5 mL with dH_2O to achieve a concentration of 22% (v/v) and decanted into 15 mL falcon tubes. Tubes were centrifuged at 4495 rpm (5 minutes, 20°C) and the supernatants transferred to fresh 15 mL falcon tubes. Samples were stored at 4°C (in darkness) until final preparation and analysis.

4.2.8 Multi-elemental analysis

Prior to analysis, 1.5 mL samples were transferred to fresh 15 mL falcon tubes and further diluted with 5.1 mL dH_2O to achieve a final concentration of 5% (v/v). Analyte elements (As, B, Ca, Cd, Co, Cr, Cu, Fe, Mg, Mn, Mo, Na, Ni, P, Pb, K, S, Se, Sn and Zn) were quantified using an iCAP 7000 Series ICP spectrometer (Thermo Scientific) coupled to an ASX-520 autosampler (CETAC), and analysed using Qtegra software (Thermo Scientific).

4.3 Results

4.3.1 Biomass degradation under solid-state fermentation

Mass loss was used as a proxy for biomass degradation to demonstrate the ability of *P. putredinis* NO1 to degrade lignocellulose under SSF (Figure 4.1).

A

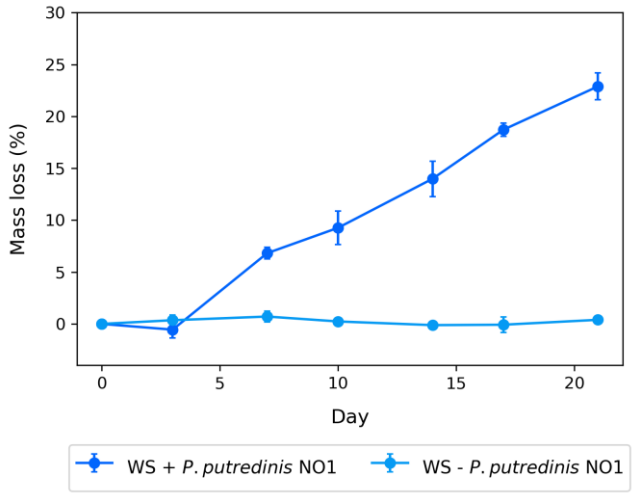

B

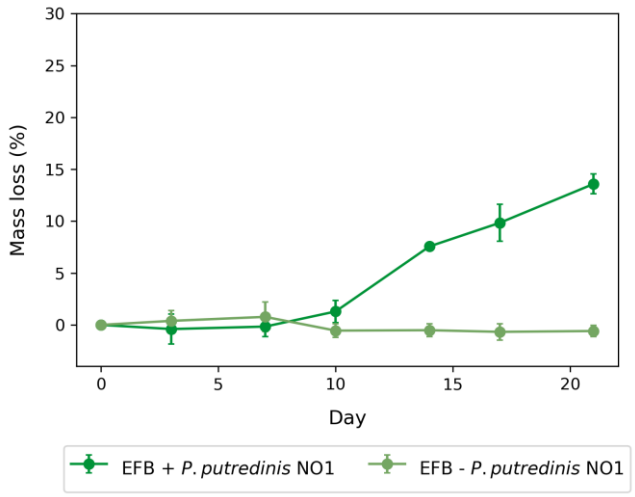

Figure 4.1. Mass loss during *P. putredinis* NO1 growth on wheat straw and oil palm EFB under SSF. Graphs show percentage mass loss of wheat straw (**A**) and oil palm EFB (**B**) over three-week cultures with and without *P. putredinis* NO1 under SSF. Data are means ± SD (n = 3).

P. putredinis NO1 growth on wheat straw and oil palm EFB led to a 22.9% and 13.6% reduction in total mass by day 21, respectively. For both substrates, negative controls (lacking *P. putredinis* NO1) showed no reduction in mass, and thus, no observable degradation. In contrast to observations under SmF (chapter 3), *P. putredinis* NO1 showed different temporal degradation patterns on wheat straw and oil palm EFB (Figure 4.2).

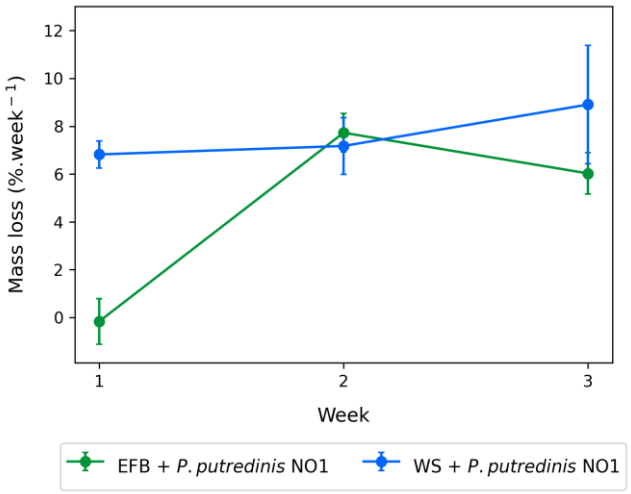

Figure 4.2. Weekly mass loss during *P. putredinis* NO1 growth on wheat straw and oil palm EFB under SSF. Graph shows weekly percentage mass loss of wheat straw and oil palm EFB over three-week cultures with *P. putredinis* NO1 under SSF. Data are means ± SD (n = 3).

Wheat straw degradation showed a gradually increasing pattern, with a mass loss of 6.8% by the first week, rising to 7.2% in the second week and 8.9% during the third week. In contrast, for oil palm EFB, no mass loss was observed during the first week, while the majority of degradation occurred during the second week (7.7%) and was higher than that observed on wheat straw. During the third week degradation tailed off, with a mass loss of 6.0%, in contrast to the gradual increase in degradation observed over time for wheat straw. Based on these data and the results from proof of concept trials (chapter 3), the duration of the pretreatment was deemed the first processing parameter that should be established, providing a baseline for future experimentation to be compared against. To test whether biomass pretreated under SSF could support BSFL growth, feeding trials were conducted. As in chapter 3, due to various COVID-19 related issues, wheat straw was again the sole focus of experimentation.

4.3.2 Effect of pretreatment duration on Black Soldier Fly larvae growth

To identify an optimal pretreatment duration, a feeding trial was performed in which wheat straw was subjected to SSF for a range of time periods (3-28 days), then fed to BSFL (Figure 4.3).

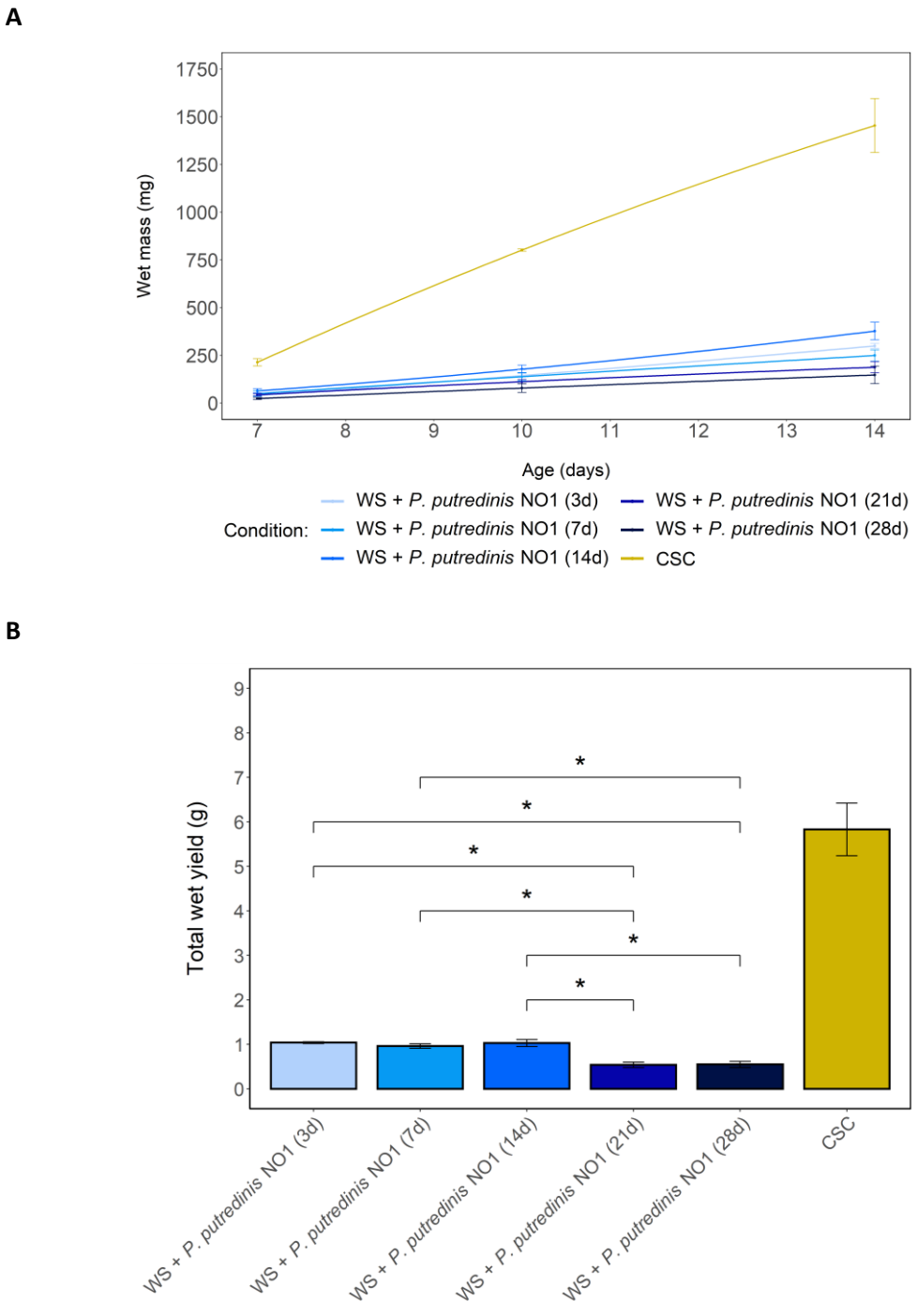

Figure 4.3. BSFL growth study (effect of pretreatment duration) on wheat straw pretreated with *P. putredinis* NO1 under SSF.

Data shows change in wet mass (**A**) and total wet yield (**B**) of BSFL fed wheat straw pretreated with *P. putredinis* NO1 for various durations or with positive control feed (chick starter crumb; CSC), over 14 days. All larvae were neonates at the beginning of the trial and received 100 mg feed/larva/day, except for positive control larvae which received a reduced rate (37.26 mg feed/larva/day). (**A**) BSFL growth rates (change in wet mass) on wheat straw pretreated with *P. putredinis* NO1 for various durations (3-28 days), and on CSC. Data are means ± SD (n = 3) of ten randomly selected larvae. (**B**) Total wet yields of BSFL fed the same feed conditions as in A. Data are means ± SD (n = 3) of all remaining larvae at the end of the trial. Significant differences ($\alpha = 0.05$), as determined by a one-way parametric ANOVA (excl. positive control group) followed by post-hoc testing (Tukey's Honest Significant Difference), are indicated by *****.

The 14-day pretreated wheat straw enabled the greatest larval growth rates, with a total yield of 1.03 g. As observed during proof of concept studies using SmF (chapter 3), the most effective pretreatment duration represented an approximate midpoint in biomass degradation during the 21-day processing period (Figure 4.1; by day 14, 61% of total mass loss). Statistically significant differences in total yield were found between multiple pretreatment durations, with larvae fed on 21-day or 28-day pretreated wheat straw reaching yields approximately half those relative to larvae fed wheat straw pretreated for 3-14 days (0.54 g and 0.55 g respectively). Positive control larvae that received a reduced feeding rate again showed a reduction in growth rate and total yield (5.83 g), in line with the results of previous feeding trials (chapter 3). Based on these data, 14-day pretreated wheat straw was selected as the baseline SSF duration for future testing.

4.3.3 Effect of feed carbon to nitrogen ratio on Black Soldier Fly larvae growth

Due to COVID-19 related issues at the time, it was not possible to measure total carbon and nitrogen for calculation of C:N ratios. However, samples of pretreated wheat straw (3-28 days) were retained and lyophilised in preparation for future elemental analysis. Fortunately, it was possible later in the project to conduct analyses of carbon and nitrogen (Figure 4.4).

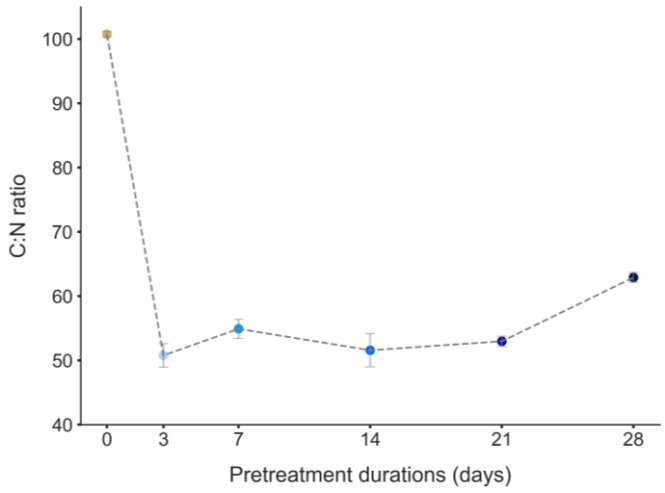

Figure 4.4. Carbon to nitrogen ratio of wheat straw pretreated under SSF. Graph shows change in C:N ratio of wheat straw pretreated with *P. putredinis* NO1 over 28 days under SSF. Data are means ± SD (n = 3).

Untreated wheat straw (day 0) was found to have a C:N ratio of 101:1. In comparison, chick starter crumb and BSG were calculated as having C:N ratios of 9:1 and 12:1, respectively. During pretreatment with *P. putredinis* NO1, the C:N ratio of wheat straw showed a sharp initial reduction (by approximately half at day 3), followed by a relatively stable profile up to day 21, before increasing again by day 28. Wheat straw C:N ratios were lower at all time points during pretreatment (relative to day 0), ranging from 51:1 at day 3 to 63:1 by day 28. At day 14, the C:N ratio was 52:1. Despite only small fluctuations between day 3 and day 21, plotting C:N ratio against total BSFL yield showed that C:N ratio influences larval growth performance (Figure 4.5).

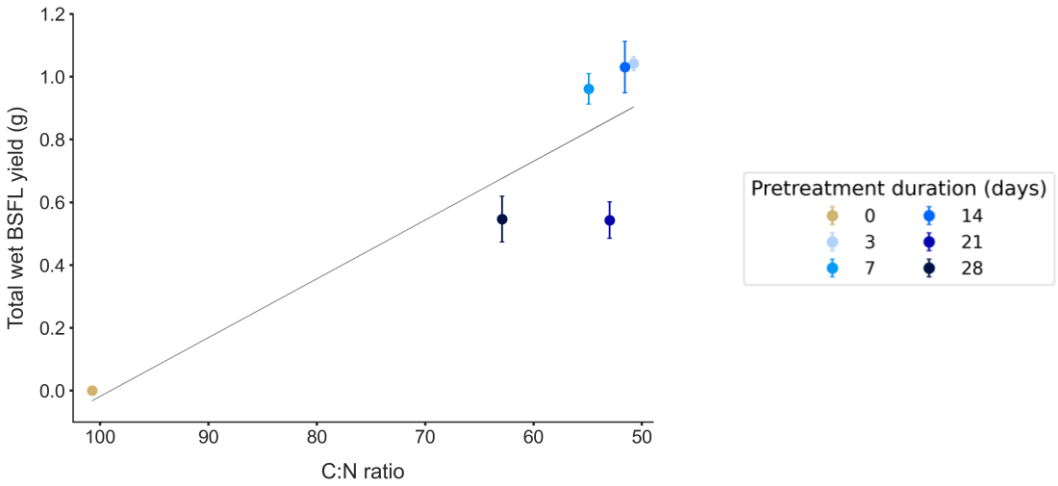

Figure 4.5. Relationship between feed carbon to nitrogen ratio and BSFL yield. Graph shows the relationship between the C:N ratio of wheat straw pretreated with *P. putredinis* NO1 under SSF and total wet BSFL yield achieved following a 14-day feeding trial. Data points are colour coded by pretreatment duration (number of days). Data are means ± SD (n = 3).

Untreated (day 0) wheat straw possesses a poor C:N ratio and showed negligible BSFL growth performance, while pretreated wheat straw with a reduced C:N ratio showed improved growth. Despite generally poor correlation between fermentation duration and BSFL yield, it is interesting to note 21-day pretreated wheat straw, which possessed a similar C:N ratio to biomass pretreated for 3-14 days, yet showed markedly lower larval yields. Larval yield was similarly low on 28-day pretreated wheat straw, which had an increased C:N ratio, relatively.

4.3.4 Supplementation of pretreated wheat straw feed

Having demonstrated the relationship between feed C:N ratio and BSFL yield, 14-day pretreated wheat straw was supplemented with various concentrations of peptone in the same manner as described during proof of concept trials; thus, further decreasing its C:N ratio (Figure 4.6).

A

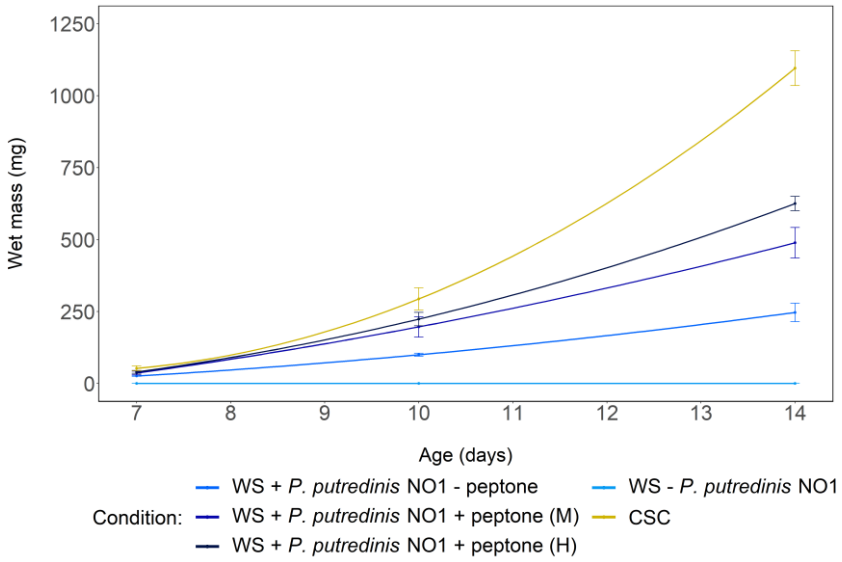

B

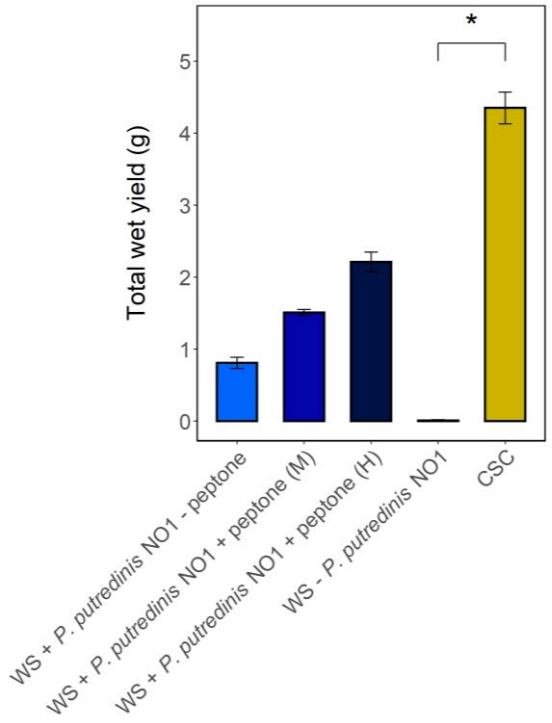

Figure 4.6. BSFL growth study (effect of peptone supplementation) on wheat straw pretreated with *P. putredinis* NO1 under SSF. Data shows change in wet mass (**A**) and total wet yield (**B**) of BSFL fed wheat straw pretreated with and without *P. putredinis* NO1 under various conditions or with positive control feed (chick starter crumb; CSC), over 14 days. All larvae were neonates at the beginning of the trial and received 100 mg feed/larva/day, except for positive control larvae which received a reduced rate (37.26 mg feed/larva/day). Prior to BSFL feeding, pretreated wheat straw was supplemented with dH_2O containing either zero, medium (M; 12.51 g/L) or high (H; 40.69 g/L) concentrations of peptone.

(**A**) BSFL growth rates (change in wet mass) on wheat straw pretreated with and without *P. putredinis* NO1 and supplemented with/without peptone, and on CSC. Data are means ± SD (n = 3) of ten randomly selected larvae that were then returned. (**B**) Total wet yields of BSFL fed the same feed conditions as in A. Data are means ± SD (n = 3) of all remaining larvae at the end of the trial. Significant difference ($\alpha = 0.05$) as determined by the Kruskal-Wallis one-way ANOVA test is indicated by *****.

Peptone supplementation of 14-day pretreated wheat straw improved BSFL growth rates, with peptone concentration correlating positively with growth as previously observed (chapter 3). The same trend was observed with total yields, ranging between 0.81 g (zero peptone) and 2.21 g (high peptone). Once again, where *P. putredinis* NO1 was absent from the pretreatment, negligible BSFL growth was observed during rearing, with a total yield of just 0.0094 g.

4.3.5 Effect of fungal inoculum concentration on Black Soldier Fly larvae growth

In addition to peptone supplementation, it may be possible to improve the nitrogen content of pretreated wheat straw by manipulating the starting fungal inoculum concentration. To this end, wheat straw was inoculated with various *P. putredinis* NO1 spore concentrations (10^3-10^6 spores/mL), pretreated for seven and 14 days under SSF, and fed to BSFL (Figure 4.7).

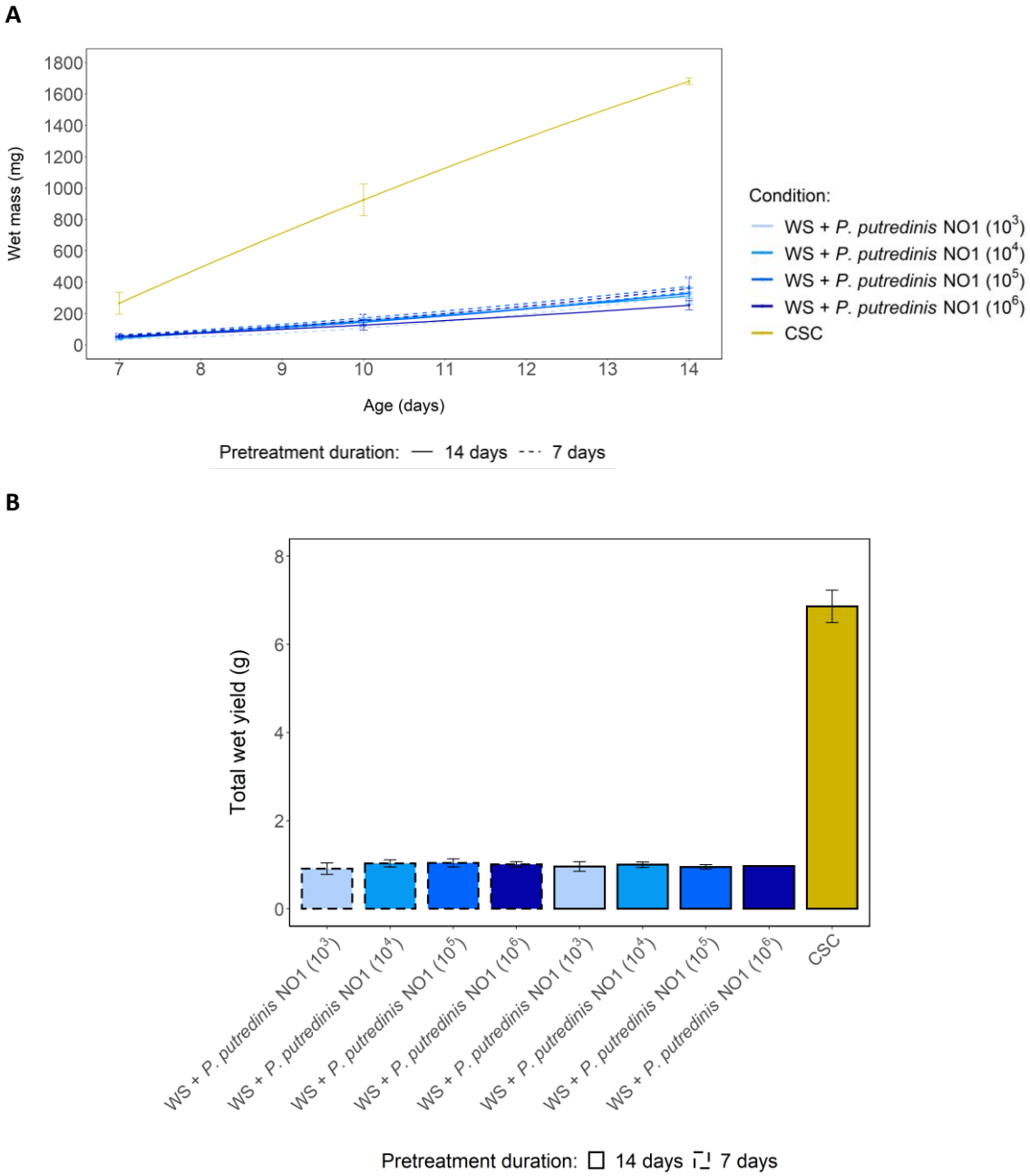

Figure 4.7. BSFL growth study (effect of fungal inoculum concentration) on wheat straw pretreated with *P. putredinis* NO1 under SSF. Data shows change in wet mass (**A**) and total wet yield (**B**) of BSFL fed wheat straw pretreated with *P. putredinis* NO1 under various conditions, or with positive control feed (chick starter crumb; CSC), over 14 days. All larvae were neonates at the beginning of the trial and received 100 mg feed/larva/day, except for positive control larvae which received a reduced rate (37.26 mg feed/larva/day). (**A**) BSFL growth rates (change in wet mass) on wheat straw pretreated with *P. putredinis* NO1 at various starting inoculum concentrations (10^3-10^6 spores/mL) for either seven or 14 days, and on CSC. Data are means ± SD (n = 3) of ten randomly selected larvae.

(**B**) Total wet yields of BSFL fed the same feed conditions as in A. Data are means ± SD (n = 3) of all remaining larvae at the end of the trial.

Interestingly, changes in the inoculum concentration of *P. putredinis* NO1 added at initiation of the pretreatment showed only small effects on BSFL growth during rearing. For BSFL fed wheat straw pretreated for seven days, inoculum concentration correlated positively with total yield, whereby yield increased subtly in line with increasing spore concentration between 10^3 and 10^5 spores/mL (0.91 g, 1.03 g, 1.05 g). For BSFL fed wheat straw pretreated for 14 days, total yield fluctuated with changes in inoculum concentration (0.95 - 1 g), showing no pattern or trend.

4.3.6 Effect of nitrogen rich feedstock blending on Black Soldier Fly larvae growth

Approaches thus far aimed at directly enriching pretreated wheat straw with additional nitrogen to improve BSFL growth performance on wheat straw alone. However, in industry, a range of different feedstocks are typically blended to create a feed formulation with desirable composition. Therefore, a more industrially relevant method by which to improve the nitrogen content of pretreated wheat straw would be to blend it with nitrogen rich feedstocks. To test the effect of this on BSFL growth, 14-day pretreated wheat straw was blended with brewers' spent grain (BSG) at various different ratios and fed to BSFL (Figure 4.8).

A

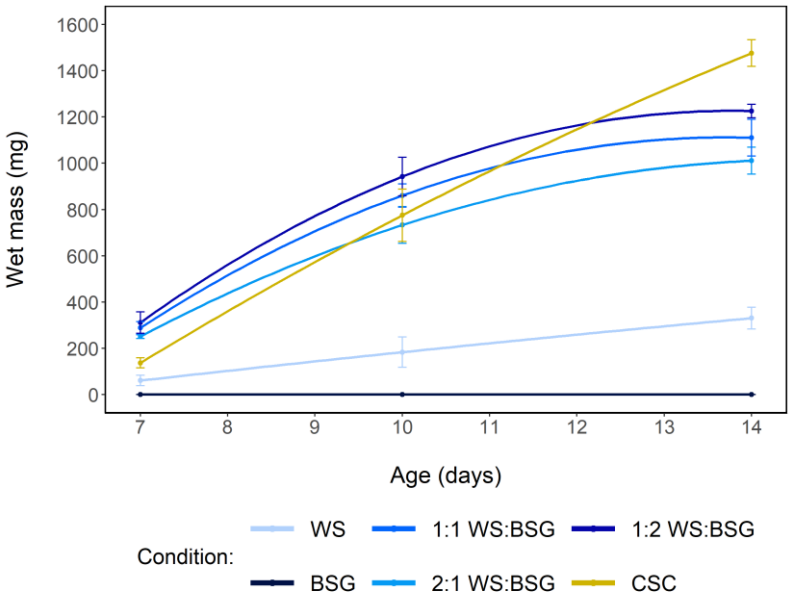

B

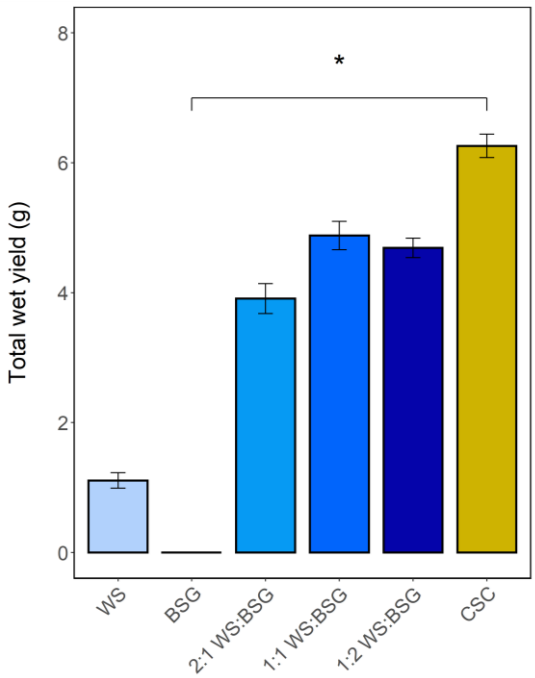

Figure 4.8. BSFL growth study (effect of nitrogen rich feedstock blending) on wheat straw pretreated with *P. putredinis* NO1 under SSF. Data shows change in wet mass (**A**) and total wet yield (**B**) of BSFL fed wheat straw pretreated with *P. putredinis* NO1 under various conditions, or with positive control feed (chick starter crumb; CSC), over 14 days. All larvae were neonates at the beginning of the trial and received 100 mg feed/larva/day, except for positive control larvae which received a reduced rate (37.26 mg feed/larva/day).

(**A**) BSFL growth rates (change in wet mass) on wheat straw pretreated with *P. putredinis* NO1 and blended with BSG at various ratios (2:1, 1:1, 1:2), and on CSC. Data are means ± SD (n = 3) of ten randomly selected larvae. (**B**) Total wet yields of BSFL fed the same feed conditions as in A. Data are means ± SD (n = 3) of all remaining larvae at the end of the trial. Significant difference ($\alpha = 0.05$) as determined by the Kruskal-Wallis one-way ANOVA test is indicated by *****.

In line with previous observations, pretreated wheat straw supported larval growth, with BSFL reaching a total yield of 1.11 g. However, in contrast, BSFL fed BSG (supplemented with water) failed to survive, with zero living larvae found at all sampling time points. Intriguingly though, where BSG was blended with pretreated wheat straw at various ratios and fed to BSFL, larvae survived and showed substantial growth relative to positive controls, despite the presence of BSG which when fed to BSFL in isolation was fatal. Furthermore, growth curve data showed positive correlation between feed BSG content and BSFL growth. In comparison to those of BSFL fed chick starter crumb, growth rates had plateaued by day 14, though total yields were high for all ratio blends (2:1 WS:BSG = 3.91 g; 1:1 WS:BSG = 4.88 g; 1:2 WS:BSG = 4.69 g).

In accordance with previous trials, fungal growth morphology of *P. putredinis* NO1 was not visible to the naked eye (e.g. no visible mycelial growth) during BSFL feeding on pretreated wheat straw (Figure 4.9). However, by day 3, BSG and BSG-containing feed blends (e.g. 1:1 WS:BSG) were heavily contaminated with what appeared to be fungal mycelial growth on the surface of the feed. By day 7, where BSG was present in isolation, contamination was reduced but still present, with no surviving larvae. Interestingly, in contrast, where BSG was blended with pretreated wheat straw at various ratios, all visible contamination had disappeared by day 7 and larvae were on average heavier than those fed on chick starter crumb. This may suggest that *P. putredinis* NO1 has the potential to decontaminate other feedstocks with high microbial loads.

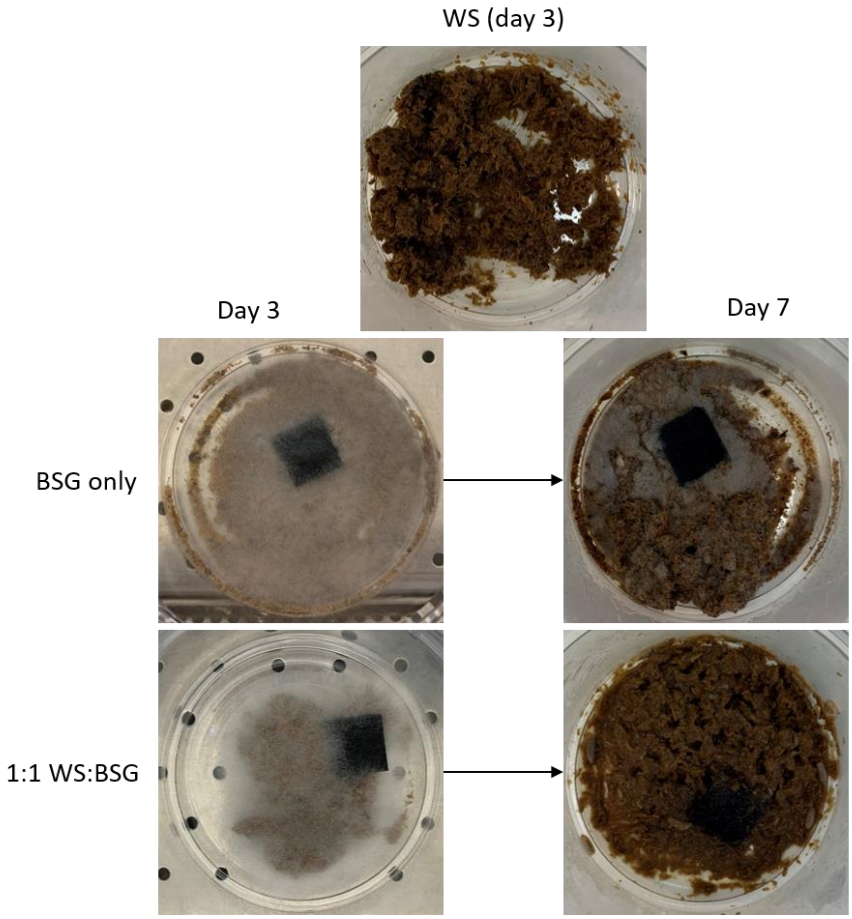

Figure 4.9. BSFL growth on pretreated wheat straw and BSG. Photographs show BSFL feeding on pretreated wheat straw at day 3, BSG (only) and a 1:1 WS:BSG blend at days 3 and 7.

These results indicated the importance of maintaining feed safety and hygiene controls, showing contaminated feedstocks can be lethal to BSFL, or may result in larvae bio-accumulating toxins.

4.3.7 Feed safety testing on pretreated wheat straw

To ensure its feed safety, wheat straw pretreated with *P. putredinis* NO1 for 3-28 days was screened for a range of 68 mycotoxins (toxic secondary metabolites produced exclusively by fungi), including all those regulated under EU feed safety legislation (Figure 4.10).

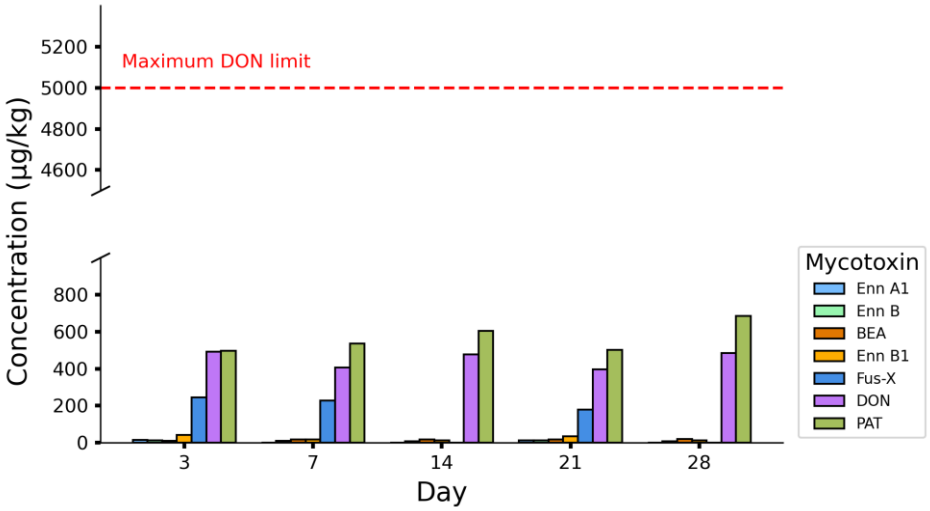

Figure 4.10. Mycotoxin testing on wheat straw pretreated with *P. putredinis* NO1 under SSF. Data shows all mycotoxins detected on wheat straw pretreated with *P. putredinis* NO1 for 3-28 days under SSF, from a total of 68 screened for using LC-MS/MS. BEA = beauvericin, DON = deoxynivalenol, Enn A1/B/B1 = enniatin A1/B/B1, Fus-X = fusarenon-X, PAT = patulin.

Of the 68 mycotoxins screened for, seven were detected across all samples – beauvericin, deoxynivalenol, enniatin (A1, B and B1), fusarenon-X and patulin. Of these, deoxynivalenol is regulated under EU legislation, with the maximum limit permitted in feed set at 5 mg/kg (Commission Recommendation 2006/576/EC). Wheat straw pretreated with *P. putredinis* NO1 for all durations (3-28 days) contained deoxynivalenol at levels greater than ten-fold below this limit, with a temporal minimum of 398 µg/kg (day 21) and maximum of 493 µg/kg (day 3). Patulin was also detected in all samples, increasing over time from 497 µg/kg (day 3) to 685 µg/kg (day 28), though is not regulated under EU legislation. Beauvericin, enniatin A1, B and B1 were detected at very low levels across the profile (below 42 µg/kg), while fusarenon-X was detected in three samples (3, 7 and 21-day pretreated wheat straw).

In addition to mycotoxins, the same EU legislation outlines the maximum permissible limits on a range of hazardous heavy metals (e.g. arsenic, cadmium, lead and mercury) whose excess levels can cause severe toxicity in livestock. Therefore, elemental analysis using ICP-OES was conducted on pretreated wheat straw to quantify the levels of arsenic, cadmium and lead (Figure 4.11). In addition, untreated wheat straw and chick starter crumb were assessed for the same metals. Unfortunately, due to limitations of the instrument used (which had no facility for hydride generation), it was not possible to assess the levels of mercury.

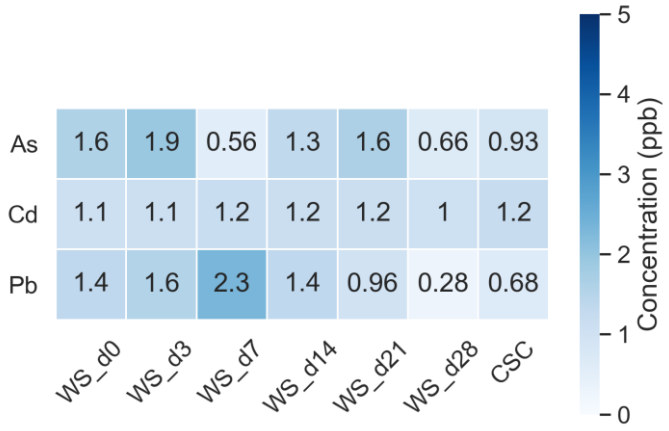

Figure 4.11. Elemental analysis of hazardous heavy metals within pretreated wheat straw. Data shows a heat map of arsenic, cadmium and lead concentrations (ppb) measured by ICP-OES in untreated wheat straw (day 0), wheat straw pretreated with *P. putredinis* NO1 under SSF for 3-28 days, and chick starter crumb (CSC).

Arsenic, cadmium and lead were detected in all wheat straw samples and chick starter crumb at extremely low levels (≤ 2.3 ppb), significantly below their permitted regulatory limits.

4.3.8 Multi-element profiling of pretreated wheat straw

Elemental analysis also elucidated the levels of various other elements within pretreated wheat straw, untreated wheat straw and chick starter crumb, including a range of trace elements (Figure 4.12), alkali metals and other elements (Figure 4.13). These elements may influence BSFL growth performance and, therefore, be potential targets for future process optimisation.

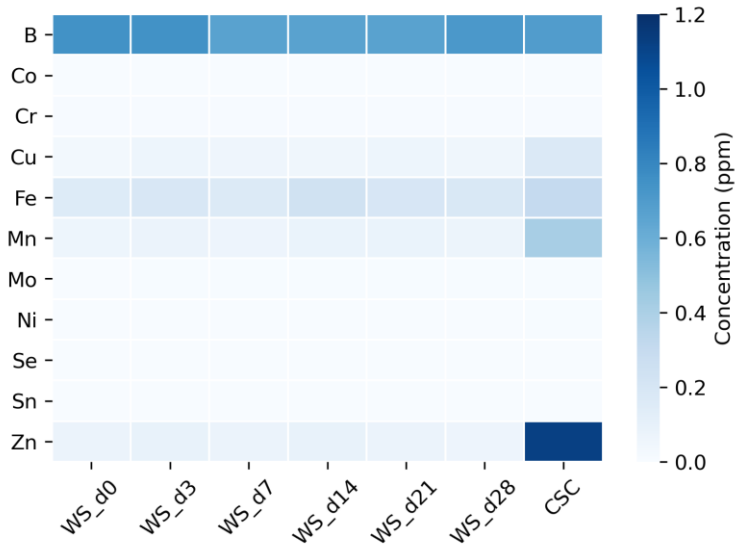

Figure 4.12. Analysis of trace elements within pretreated wheat straw. Data shows a heat map of various trace elements and their concentrations (ppm) measured by ICP-OES in untreated straw (day 0), wheat straw pretreated with *P. putredinis* NO1 for 3-28 days, and chick starter crumb (CSC).

Chick starter crumb showed a substantially higher concentration of zinc (1.12 ppm) in comparison to pretreated wheat straw (0.067-0.093 ppm) and untreated wheat straw (0.076 ppm), and was higher in manganese (0.42 ppm), iron (0.31 ppm) and copper (0.17 ppm). Boron, however, showed similar levels across all samples, with a concentration range of between 0.66 and 0.75 ppm. Elemental analysis also assessed the levels of various alkali metals (e.g. sodium, potassium) and a range of other elements expected at higher concentrations (Figure 4.13).

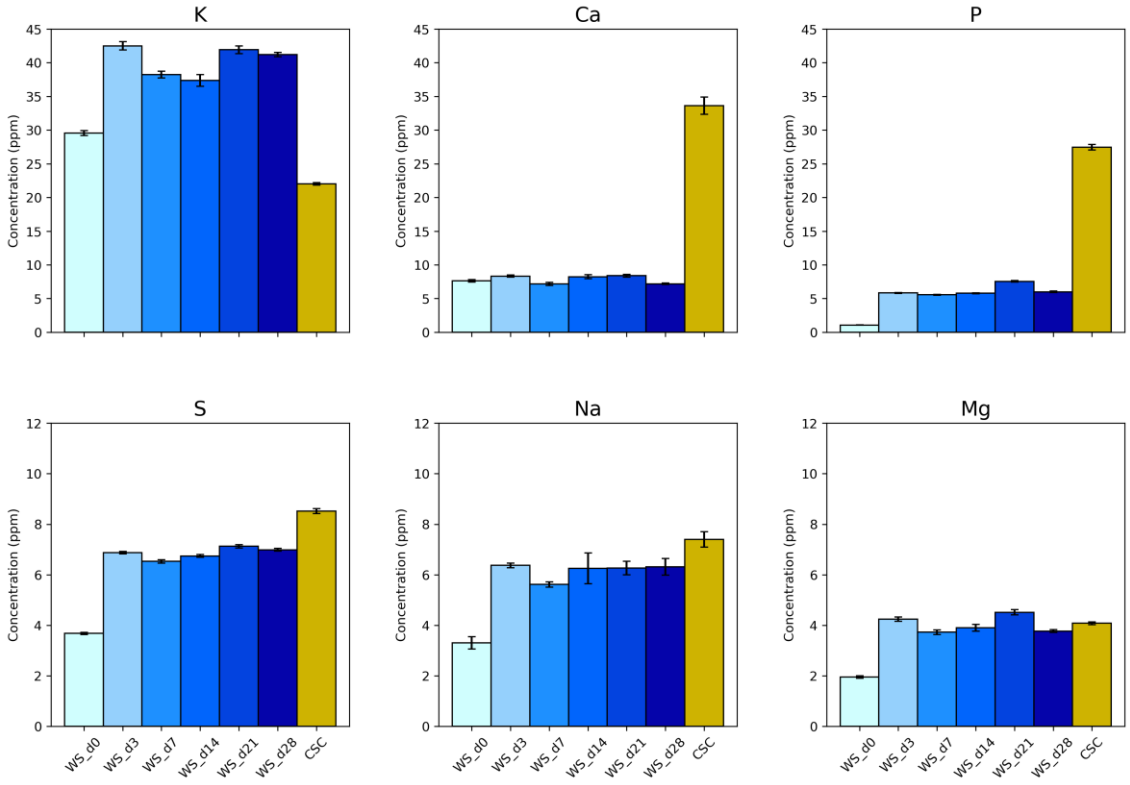

Figure 4.13. Analysis of abundant elements within pretreated wheat straw. Data shows various elements and their concentrations (ppm) measured by ICP-OES in untreated wheat straw (day 0), wheat straw pretreated with *P. putredinis* NO1 for 3-28 days, and chick starter crumb (CSC).

Chick starter crumb showed much higher concentrations of calcium (33.61 ppm) and phosphorus (27.46 ppm) in comparison to pretreated wheat straw (calcium = 7.18-8.40 ppm; phosphorus = 5.55-7.55 ppm) and untreated wheat straw (calcium = 7.62 ppm; phosphorus = 1.06 ppm). Chick starter crumb also showed higher levels of sulphur (8.52 ppm) and sodium (7.39 ppm) in comparison to pretreated wheat straw (sulphur = 6.53-7.13 ppm; sodium = 5.61-6.37 ppm) and untreated wheat straw (sulphur = 3.68 ppm; sodium = 3.30 ppm). Potassium, in contrast, was detected at higher levels in pretreated wheat straw (37.38-42.50 ppm), in comparison to untreated wheat straw (29.54 ppm) and chick starter crumb (22.02 ppm). The concentration of magnesium was similar between chick starter crumb (4.01 ppm) and pretreated wheat straw (3.73-4.51 ppm), though lower in untreated wheat straw (1.95 ppm). All elements (except calcium) showed sharp initial increases in pretreated wheat straw between days 0 and 3, likely reflecting the composition of Hutner's trace elements included in the media.

4.4 Discussion

4.4.1 *P. putredinis* NO1 degrades lignocellulose under solid-state fermentation

Previously, *P. putredinis* NO1 had been cultured under SmF, though given the benefits of a solid-state system, SSF was deemed a more desirable pretreatment method for the production of BSFL feed. However, the ability of *P. putredinis* NO1 to grow on lignocellulose under SSF was unknown. Here, mass loss experiments showed the ability of *P. putredinis* NO1 to degrade lignocellulosic biomass under SSF. After 21 days, wheat straw had lost almost a quarter of its mass (22.9%), in line with studies showing comparable degradation (5.5-30% mass loss) by the white rot basidiomycetes *Polyporus brumalis* and *Irpex lacteus* (Zhou et al., 2017; Pallín et al., 2022). Mass loss on oil palm EFB was comparatively lower (13.6%) though still significant.

In contrast to observations under SmF, wheat straw and oil palm EFB showed different degradation patterns over time under SSF. Wheat straw degradation showed a gradually increasing pattern, following an initial three-day lag phase in which mass remained relatively constant. For oil palm EFB, however, mass remained constant for the entire first week, after which the majority of degradation occurred during the second week and tailed off in the third. The initial lag phase observed on both substrates, though shorter for wheat straw, is a known drawback associated with the use of fungal spore suspensions to inoculate SSF cultures. This may be due to slow spore germination (for hyphal formation) and subsequently delayed secretion of extracellular enzymes for the deconstruction of lignocellulose (Tengerdy and Szakacs, 2003). Spore germination is a vital developmental process in the life cycle of filamentous fungi in which dormant spores develop into vegetative hyphae, from which carbohydrate-active enzymes are secreted. Under favourable conditions this morphological transition can occur in just 6 hours (Sephton-Clark et al., 2018). The factors triggering spore germination are various and diverse, and differ among fungal species as they are based on evolutionary adaptations (Turgeman et al., 2016). However, culture moisture content is a key factor known to affect the germination rate of various filamentous fungi, including *Aspergillus niger*, whereby a lower initial moisture content correlates with a reduced germination rate (Hassouni et al., 2007). Therefore, during *P. putredinis* NO1 growth on wheat straw and oil palm EFB under SSF in which spores were used as inoculum, the initial moisture content may have been too low, leading to a reduced spore germination rate and subsequently a reduction in the rate of hyphal formation, enzyme secretion and biomass degradation; thus causing the observed lag phases. This may be overcome by increasing culture moisture content or by inoculating cultures with pre-germinated spores (Tengerdy and Szakacs, 2003), or fungal mycelia.

Spore germination is also affected by substrate (Hassouni et al., 2007). This, therefore, supports the comparatively longer delay observed in oil palm EFB degradation, and further validates oil palm EFB as a more recalcitrant substrate, reflected by its lesser degradation over 21 days.

4.4.2 Solid-state pretreated wheat straw supports Black Soldier Fly larvae growth

Feeding trials showed that wheat straw pretreated with *P. putredinis* NO1 under SSF can support BSFL growth, in line with previous results obtained using SmF pretreated wheat straw (chapter 3). In contrast, larvae fed untreated wheat straw showed no increase in mass, demonstrating the role of the pretreatment in improving biomass digestibility by BSFL. In accordance with this, wheat straw pretreated under SSF by basidiomycete fungi (*Ganoderma* and *Crinipellis* sp.) showed improved nutrient composition and digestibility as animal feed (Shrivastava et al., 2012, 2014). Fungi partially degraded the key components of lignocellulose (lignin, matrix polysaccharides and cellulose) within wheat straw, which after SSF showed a significant enrichment in fungal protein and various essential amino acids (e.g. threonine and arginine). Interestingly, wheat straw treated for ten days (out of 15 in total; *Ganoderma* sp.) and five days (out of nine in total; *Crinipellis* sp.) showed the greatest organic matter digestibility and metabolisable energy (Shrivastava et al., 2012, 2014). As a result, calves fed on five-day pretreated wheat straw showed significantly higher dry matter intake and gained greater daily body weight (Shrivastava et al., 2014). In line with this, wheat straw pretreated with *P. putredinis* NO1 under SSF for 14 days (out of 28 in total) showed the greatest BSFL growth performance, which represented an approximate mid-point in biomass degradation as similarly observed in chapter 3. By day 14, 61% of the total mass loss observed over 21 days had occurred, in comparison to 56% at day 10 under SmF. This, therefore, supports the indication of an optimal fermentation duration which improves the digestibility of lignocellulose by balancing the accessibility of sugars via partial digestion of the cell wall and the production of fungal protein. Wheat straw pretreated for 21 and 28 days showed yields approximately half those relative to larvae fed wheat straw pretreated for 3-14 days. This may have been because *P. putredinis* NO1 had metabolised the sugars required by larvae for their growth, in line with observations of BSFL fed banana peel pretreated with *Trichoderma reesei* for 21 days (Isibika et al., 2019). Interestingly, wheat straw pretreated with *P. putredinis* NO1 for three days also supported BSFL growth, despite no evidence of biomass degradation (mass loss) and little time for the fungal culture to establish during the pretreatment. Larvae, therefore, may have been able to feed upon the nitrogen rich yeast extract added as part of the growth media, in line with results showing their ability to feed on peptone (a similar nitrogen source). After a short three-day pretreatment, *P. putredinis* NO1 had likely not yet fully depleted the yeast extract within the growth media and, thus, it would have been present on the pretreated wheat straw.

Therefore, the effect of yeast extract upon BSFL growth performance should be further investigated and if its presence is deemed beneficial, an alternative (cheaper) nitrogen source should be pursued for commercial application (e.g. of waste origin). The optimal fermentation duration and processing parameters, however, are likely to be substrate and fungal species specific, and will therefore require targeted optimisation efforts.

4.4.3 Solid-state fermentation improves the carbon to nitrogen ratio of wheat straw

Previous results (chapter 3) showed that an increase in feed nitrogen content improves BSFL growth on wheat straw. However, at the time, it was not possible to quantify C:N ratios. Here, elemental analysis showed that the pretreatment of wheat straw by *P. putredinis* NO1 under SSF significantly decreases its C:N ratio, thereby enabling BSFL growth in line with previous work (Palma et al., 2019; Beesigamukama et al., 2021). Initially, between days 0 and 3, wheat straw C:N ratio showed a sharp reduction (101:1 to 51:1), likely the result of an influx of nitrogen added in the form of yeast extract as part of the growth media, as well as fungal inoculum (spores). However, between days 3 and 21, C:N ratio remained relatively constant (51:1-55:1), indicating that the quantities of carbon and nitrogen remained in near equilibrium. In contrast, the C:N ratio of rice straw treated under SSF with *Penicillium purpurogenum* (ascomycete fungus) declined consistently between day 3 (69:1) and day 9 (21:1), indicating a net gain of nitrogen (El-Metwally, El-Hersh and Saber, 2017). In this study, *P. purpurogenum* was selected based upon its enzyme activity, in similar justification used here for *P. putredinis* NO1. However, *P. purpurogenum* was co-cultured in synergy with the nitrogen-fixing bacterium *Azotobacter chroococcum*, which fixes gaseous atmospheric nitrogen into ammonia via its nitrogenase complex (Wang et al., 2018). As a result, this approach enabled a gradual reduction in rice straw C:N ratio in which *P. purpurogenum* elicited lignocellulose degradation and consequent mass loss as carbon dioxide, while *A. chroococcum* simultaneously fixed gaseous nitrogen. Therefore, it may be possible to improve BSFL growth on wheat straw if *P. putredinis* was used in co-culture with a nitrogen-fixing bacterium (e.g. *Azotobacter* sp.) to further decrease feed C:N ratio.

In the same study, rice straw was inoculated with *P. purpurogenum* at 10^7 spores/mL. Here, wheat straw was inoculated with *P. putredinis* NO1 at 10^5 spores/mL. Given the positive correlation between spore concentration and germination rate (Nol and Henis, 1987), an increase in *P. putredinis* NO1 inoculum concentration may lead to faster and more extensive hyphal formation. This, therefore, may lead to an increase in fungal protein for consumption by BSFL, and thus improve their growth. However, the inoculum concentration of *P. putredinis* NO1 showed only small effects upon BSFL growth, with no significance, contrary to expectation.

As discussed, an insufficient culture moisture content (i.e. lower than optimal) can restrict the germination rate of fungal spores (Hassouni et al., 2007). Moisture content, therefore, may have limited the rate of fungal biomass production, despite changes to the inoculum concentration. In addition, spore viability can affect germination rate, which itself is influenced by various factors such as temperature and length of storage (Bohorquez et al., 2021). Therefore, spore viability may also have limited germination rate and consequent fungal growth on wheat straw. Alternatively, the lack of improvement in larval growth may be related to nitrogen accessibility which differs between sources (Miner et al., 2022). In line with prior results (chapter 3), peptone supplementation of pretreated wheat straw improved BSFL growth, indicating its high nitrogen accessibility as observed for urea (Palma et al., 2019; Miner et al., 2022). In contrast, the accessibility of nitrogen within *P. putredinis* NO1 mycelia may be more limited. This, therefore, should be tested. To do so, ergosterol (a membrane lipid found almost exclusively in fungi) could be used to quantify living fungal biomass (Nurika et al., 2018), with any reduction observed during BSFL feeding indicating consumption of *P. putredinis* NO1 by larvae.

Peptone supplementation of pretreated wheat straw, although effective at improving BSFL growth, would not be a viable method by which to reduce feed C:N ratio at commercial scale due to its cost. Therefore, alternative supplementary nitrogen sources should be explored which are less costly (e.g. organic wastes) and provide adequate feed performance. For example, BSG, which represents 85% of the total waste generated by the beer brewing process and contains roughly 16% crude protein (Rocha et al., 2014; Bava et al., 2019), has been widely shown to support BSFL growth (Bava et al., 2019; Jucker et al., 2020; Chia et al., 2020). Here, BSG (C:N ratio = 12:1) was blended with pretreated wheat straw at various ratios and fed to BSFL. Larval growth correlated positively with BSG content, in line with previous work showing increased BSFL growth on blended feedstocks (Jucker et al., 2020). This approach is commonly adopted by industrial insect producers, in which a range of ingredients are combined to produce a reproducible (defined) feed formulation. However, the addition of any external nitrogen source, unless free to acquire and transport, increases overall process cost. As such, a more desirable method by which to increase feed nitrogen content would involve an in-situ microbial approach, such as co-culture with a nitrogen-fixing bacterium (El-Metwally, El-Hersh and Saber, 2017).

4.4.4 Mycotoxin testing and multi-elemental analysis demonstrate feed safety

Although BSG content showed positive correlation with BSFL growth, feeding trials with BSG also indicated the importance of ensuring feed safety. Interestingly, BSG fed in isolation to BSFL was lethal, likely the result of detrimental contamination, though this was not proven. Nevertheless, these experiments demonstrated the need to carefully control insect feed hygiene.

For instance, mycotoxins are commonly found in agricultural crops and can have detrimental impacts upon the agricultural industry, livestock and human health (Niermans et al., 2021). As a result, particularly dangerous mycotoxins (e.g. aflatoxins, deoxynivalenol, fumonisin B1/B2, ochratoxin A, T-2 toxin and zearalenone) are regulated by the EU under various directives (e.g. Directive 2002/32/EC and Recommendation 2006/576/EC) which outline maximum permissible limits on mycotoxins in animal and pet feed. Therefore, untreated and pretreated wheat straw were tested for a wide range of mycotoxins to ensure their safety as animal feed. Testing detected only a fraction of analytes across all samples, all of which were present at low levels. Profiles were dominated by deoxynivalenol, patulin and fusarenon-X, though deoxynivalenol was found significantly below permitted limits, thereby satisfying the relevant EU regulatory requirements. This, therefore, indicated feed safety of the input feedstock (untreated wheat straw) as well as *P. putredinis* NO1 itself, used during the SSF pretreatment. However, despite low abundance levels, mycotoxins were still present, yet BSFL survived. These results are in line with previous work in which BSFL fed poultry feed spiked with aflatoxin B1 (the most toxic and frequently occurring aflatoxin) showed it to have no significant effect upon larval survival and body weight, indicating a high tolerance (Bosch et al., 2017; Meijer et al., 2019). Furthermore, aflatoxin B1 and aflatoxin M1 were found to be below the detection limit (0.1 µg/kg) in BSFL, regardless of the spiking concentration, indicating a lack of bio-accumulation and instead suggesting an ability to metabolise such contaminants. A similar study in which BSFL were fed a corn-based substrate spiked with a range of mycotoxins (aflatoxins B1/B2/G2, deoxynivalenol, ochratoxin A and zearalenone) showed no significant effects upon BSFL growth, and showed no bio-accumulation in larval tissue (Purschke et al., 2017). Despite this, feed mycotoxin profiles should always be assessed to prevent their possible transmission through the food chain.

The same study fed BSFL a diet spiked with various heavy metals (arsenic, cadmium, chromium, mercury, nickel and lead) often found in organic wastes and residues; some of which are regulated under EU safety legislation (arsenic, cadmium and lead) (Purschke et al., 2017). Various studies have demonstrated that BSFL can bio-accumulate heavy metals, particularly cadmium and to a lesser extent lead (Charlton et al., 2015; Diener, Zurbrügg and Tockner, 2015; Purschke et al., 2017; Wu et al., 2020). As a result, elemental analysis tested untreated and pretreated wheat straw for cadmium, lead and arsenic levels, and showed similarly low concentrations for all three metals across all samples. This, therefore, confirmed feed safety of the input feedstock, and confirmed no further accumulation during the pretreatment. However, the effects of heavy metals upon larval growth are contested, with some evidence suggesting cadmium and lead to significantly reduce BSFL yields and feed conversion ratios (Purschke et al., 2017), while refuting evidence shows no significant effect upon BSFL growth and instead reveals shifts in larval gut microbiota (Diener, Zurbrügg and Tockner, 2015; Wu et al., 2020).

Similar to mycotoxins, therefore, feed elemental profiles should always be assessed to prevent the possible transmission of potentially toxic heavy metals through the food chain.

4.4.5 Elemental analysis suggests Black Soldier Fly larvae growth is multi-element limited

Elemental analysis also elucidated the levels of various other trace and macro elements, in addition to those of particular importance for feed safety. In comparison to chick starter crumb, pretreated wheat straw was particularly low in calcium and phosphorus, and to a lesser extent sulphur, sodium and zinc. Although the specific mineral requirements of BSFL are largely unknown, the five most abundant minerals in their bodies are potassium, calcium, phosphorus, magnesium and sodium (in order of abundance) (Seyedalmoosavi et al., 2022). In contrast to most insects, their chitin-rich 'mineralised' cuticle (main component of the insect exoskeleton) contains significant quantities of calcium (Finke, 2007, 2013). Previous work has demonstrated correlation between the abundance of calcium in the larval diet and its bio-accumulation during rearing (Liland et al., 2017), while the same has been observed for phosphorus and sodium (Schmitt et al., 2019; Shumo et al., 2019). Therefore, given their key roles in larval development and their low levels in comparison to chick starter crumb, BSFL growth on pretreated wheat straw may have been limited by calcium and phosphorus in particular. In support of this, BSFL development rate has been reported as proportional to the percentage of dietary phosphorus (Oonincx et al., 2015). However, it should be noted that the investigation of mineral nutrition and metabolism in heterogeneous feeds (e.g. food waste) is complex due to the difficulties in isolating the effects of a single dietary variable (Seyedalmoosavi et al., 2022). This may be overcome by spiking a single control feed (e.g. chick starter crumb) with elemental sources (e.g. $CaCO_3$ as calcium) and monitoring the effects upon larval growth performance using a 'Design of Experiment' approach, thereby building a novel and valuable understanding of BSFL mineral requirements. This could inform future process optimisation, in which elemental analyses would facilitate the optimisation of feed element profiles; thus, improving BSFL growth performance.

5) Characterisation of wheat straw degradation by *P. putredinis* NO1 under submerged and solid-state fermentation

5.1 Introduction

Chapters 3 and 4 demonstrated that wheat straw pretreated with *P. putredinis* NO1 under submerged fermentation (SmF) and solid-state fermentation (SSF) supports the growth of Black Soldier Fly larvae (BSFL), in contrast to untreated wheat straw, indicating that a pretreatment improves its digestibility by larvae. Although pretreatment under both culture conditions enabled larval growth on wheat straw, filamentous fungi (such as *P. putredinis* NO1) exist typically in environments more akin to solid-state conditions in nature, particularly in terrestrial ecosystems (Clemmensen et al., 2013; Stuart and Plett, 2020). As such, they are morphologically adapted to growth on solid substrates (e.g. lignocellulosic biomass). Therefore, their growth under SSF should induce behaviours and metabolism aligned with their evolutionary optima.

During growth on solid substrates, filamentous fungal cells form elongating tubular hyphae which predominantly exhibit apex directed growth, in which elongation and carbohydrate-active enzyme secretion occur at the tips (Valkonen et al., 2007; Commer and Shaw, 2021) and branching at subapical sites (e.g. intercalary) (Read, 2011; Harris, 2019). Growth under solid-state conditions (either in nature or under SSF) increases the proximity of these cells to the substrate via an extensive hyphal network, collectively known as the mycelium, which creates a large surface area for various physiological processes (e.g. gas exchange and oxygenation, bidirectional transport and distribution of nutrients (Schmieder et al., 2019; Viniegra-González et al., 2003). Secretion of cell wall degrading enzymes, triggered by the presence of complex carbohydrates (e.g. within lignocellulose), enables penetration of the substrate via hyphal appressoria located at the hyphal tips (Lübeck and Lübeck, 2022). In addition, some fungal species develop high turgor (hydrostatic) pressure at the appressoria due to an accumulation of glycerol, which enables mechanical penetration in tandem with enzymatic penetration of the substrate cell wall (Riquelme et al., 2018; Agrios, 2005; Fricke, 2017). Delivery of extracellular enzymes facilitates deconstruction of lignocellulose into metabolisable sugars, enabling access and subsequent absorption of otherwise inaccessible nutrients across a wide surface area.

In contrast, filamentous fungal growth under SmF, involving constant culture agitation, leads to the formation of 'pellets' (quasi-spherical agglomerates of hyphal elements) with a small surface area for gas exchange and other processes (e.g. nutrient absorption). These, therefore, limit the cell-substrate interface (Viniegra-González et al., 2003; Veiter, Rajamanickam and Herwig, 2018). In addition, analysis of non-enzyme proteins produced under SmF and SSF showed those related to stress tolerance as more prevalent under SmF, whereas proteins involved in mycelial growth and conidiation (asexual reproduction from spores) were more prevalent under SSF; thus, indicating SmF may impose stress upon filamentous fungal growth (Li, Peng and Chen, 2013).

The differences in fungal growth morphology under SmF and SSF are reflected in the productivity of the culture systems. Comparative studies have grown filamentous fungi on a range of substrates (including wheat straw) and demonstrated greater enzyme productivity under SSF (e.g. of cellulases and xylanases), accompanied by greater fungal biomass and protein production, and a lower rate of protein breakdown (Soccol et al., 2017; Li, Peng and Chen, 2013; Viniegra-González et al., 2003). However, the structural and chemical alterations elicited upon substrates during fungal growth are seldom investigated. These are crucial to aid understanding of the compositional changes within cell wall lignocellulose which enable its digestion by BSFL following *P. putredinis* NO1 pretreatment, and may also inform future process optimisation.

In this chapter, comparative characterisations of wheat straw degradation by *P. putredinis* NO1 under SmF and SSF were conducted using a range of analytical techniques, investigating the structural and chemical changes elicited upon the major cell wall lignocellulose components (lignin, matrix polysaccharides and crystalline cellulose) during pretreatment.

5.2 Methods

5.2.1 Degradation efficiency under submerged and solid-state fermentation

Mass loss data (from chapter sections 3.3.1 and 4.3.1) were normalised against the ratio between fungal inoculum and wheat straw biomass under SmF and SSF. To do so, mass loss values were divided by the values derived from Equation 5.1 (used to establish the total number of spores per gram of biomass at culture inoculation, day 0). Normalised profiles were then used to infer the degradation efficiency of *P. putredinis* NO1 under SmF and SSF, with higher values indicating greater mass loss on a per spore/gram basis and, thus, greater per unit efficiency.

Equation 5.1. Calculation for the number of spores per gram of biomass at culture inoculation.

$$Number\ of\ spores\ g^{-1} = \frac{(concentration\ of\ spore\ suspension \times\ volume\ of\ spore\ suspension)}{mass\ of\ biomass\ (g)}$$

5.2.2 Biomass preparation for composition analyses

Lyophilised biomass samples were obtained from mass loss experiments in which *P. putredinis* NO1 was grown on wheat straw under SmF and SSF over three-week time courses in biological triplicate (chapter sections 3.3.1 and 4.3.1). Composition analyses were performed on samples from each time point (days 0, 3, 7, 10, 14, 17, 21) to determine and quantify the main lignocellulose fractions (lignin, matrix polysaccharides and crystalline cellulose). To do so, lyophilised biomass samples were first milled to fine powders using a cyclone mill (Retsch Twister). Lignin was analysed by an independent assay of the acetyl bromide soluble fraction using 4 mg samples. For analysis of other components, separate 4 mg samples were first analysed for their matrix polysaccharide composition, then analysed downstream for their crystalline cellulose composition (same biomass aliquots). The non-carbon fraction (ash) was also determined, using 1 g (lyophilised) biomass samples harvested from the same cultures.

5.2.3 Analysis of non-carbon fraction (ash)

Wheat straw samples (1 g) from each time point were weighed into pre-weighed crucibles (W_C) to obtain W_{C+S}, then heated at 600°C in a furnace (Carbolite AAF 1100 Type 301, Barloworld Scientific) for 24 hours. Cooled samples were weighed (W_A) and used for ash determination.

5.2.4 Analysis of acetyl bromide soluble lignin

Samples (4 mg) from each time point were assessed for their lignin content using the acetyl bromide assay (Moreira-Vilar et al., 2014). Phenol bonds were broken by adding 250 µL freshly prepared acetyl bromide solution (25% v/v acetyl bromide, 75% v/v glacial acetic acid) to samples, including a blank (acetyl bromide solution only), prior to incubation at 50°C for three hours. Samples were mixed by vortexing every 15 minutes during the final hour. Samples were then cooled to room temperature and transferred to 5 mL volumetric flasks, to which 1 mL NaOH (2 M) and 175 µL hydroxylamine HCl (0.5 M) were added and mixed thoroughly by vortexing. Following this, samples were taken immediately for analysis, being prepared individually to prevent precipitation. Samples were made up to 5 mL with glacial acetic acid, mixed thoroughly by inversion, then 100 µL diluted with 900 µL glacial acetic acid (1:10).

Diluted samples were measured at 280 nm in quartz cuvettes using a Cary 50 UV-visible spectrophotometer (Agilent Technologies), blanked with glacial acetic acid. Percentage acetyl bromide soluble lignin (ABSL) was determined using Equation 5.2.

Equation 5.2. Calculation of percentage ABSL. Parameters used: absorbance measured at 280 nm; extinction coefficient = 17.75, as cited for grasses (Foster, Martin and Pauly, 2010); path length = 1; total volume = 5 mL; aliquot volume = 0.1 mL; dilution factor = 10; biomass weight variable between samples (approximately 0.004 g).

$$\%\ ABSL = \left(\frac{absorbance}{coefficient\ \times\ pathlength}\right) \times \left(\frac{total\ vol\ (mL) \times\ aliquot\ (mL) \times\ dilution\ factor}{biomass\ weight\ (g)}\right)$$

5.2.5 Analysis of matrix polysaccharides

Separate 4 mg samples from each time point were hydrolysed by 500 µL trifluoroacetic acid (TFA) (2 M) under a dry argon atmosphere during a four-hour incubation at 100°C, with mixing every 30 minutes by vortexing. Samples were cooled to room temperature and evaporated completely under vacuum using a Savant SpeedVac concentrator SPD131DDA linked to a Savant refrigerated vapour trap RVT4104 (Thermo Scientific). Samples were washed twice using 500 µL propanol to remove residual TFA, with complete evaporation under vacuum following each wash. Samples were re-suspended in 200 µL dH_2O, mixed thoroughly, centrifuged at 12,760 x g (five minutes, 20°C) and supernatants filtered through 0.45 µM PTFE filters.

These were then transferred into fresh high-performance liquid chromatography vials for analysis using an ICS-3000 ion chromatography system with AS loading units (Dionex, Thermo Scientific). The residual pellets were used for assessment of crystalline cellulose (section 5.2.6).

Samples were quantified against a standard curve containing various concentrations of each expected monosaccharide – arabinose, fucose, galactose, galacturonic acid, glucose, glucuronic acid, mannose, rhamnose and xylose. Monosaccharide standards were prepared by taking 250 µL, 500 µL and 700 µL from a monosaccharide stock mix (100 µM) and drying them completely prior to TFA hydrolysis. Absolute quantification of each monosaccharide present within sample matrix polysaccharide fractions was permitted by injecting known volumes of hydrolysate (1 µL) and standard (5 µL) onto the column. Peak area integration was used to facilitate quantification using the Chromeleon software package (v6.8 SR16 build 5387, Thermo Scientific).

5.2.6 Analysis of crystalline cellulose

Pellets obtained from section 5.2.5 were washed with 1.5 mL dH_2O, centrifuged at 12,760 x g (five minutes, 20°C) and supernatants discarded. Three additional washes were performed in the same manner using 1.5 mL acetone. Cellulose pellets were dried gently under snorkel extraction, then subjected to a Saeman hydrolysis (to completely hydrolyse cellulose into glucose) using 90 µL H_2SO_4 (72% w/v) during a four-hour incubation at room temperature (Saeman, 1945). Following this, samples were diluted to 3.2% H_2SO_4 by the addition of 1.89 mL dH_2O, incubated at 120°C for four hours and centrifuged at 10,000 x g (five minutes, 20°C) to pellet any residual impurities (e.g. insoluble lignin).

Glucose contents within sample supernatants were measured using the colorimetric anthrone assay with quantification against a glucose standard curve (0 - 6.67 µg). To do so, 800 µL freshly prepared anthrone reagent (2 mg/mL conc. H_2SO_4) was added to dilute sample hydrolysates (40 µL sample, 360 µL dH_2O) prior to incubation at 80°C for 30 minutes. Samples were cooled to room temperature and mixed thoroughly, then 200 µL aliquots transferred to an optical microplate (along with standards in triplicate) and absorbance measured at 620 nm using a Sunrise microplate spectrophotometer (Tecan).

5.2.7 Extrapolation to absolute mass composition

Biomass composition analyses were used in conjunction with mass loss data (chapter sections 3.3.1 and 4.3.1) to extrapolate absolute mass values of the lignocellulose fractions over time.

5.2.8 Scanning electron microscopy

Samples taken from SmF and SSF cultures at days 0, 10 and 21 were analysed by scanning electron microscopy (SEM) at the University of York Technology Facility (Dr Clare Steele-King). To do so, lyophilised samples were mounted on aluminium SEM stubs using conductive carbon tabs, sputter coated with gold/palladium and imaged using a 6490 SE microscope (Jeol) at 5 kV.

5.2.9 Biomass preparation for nuclear magnetic resonance

To further assess chemical changes in cell wall lignocellulose components (lignin and matrix polysaccharides), whole cell heteronuclear single quantum coherence spectroscopy (HSQC) solid-state nuclear magnetic resonance (NMR) was conducted by Dr Christopher Lancefield (formerly University of St. Andrews, UK) on lyophilised samples of untreated wheat straw and wheat straw pretreated with *P. putredinis* NO1 (3, 7, 14 and 21-day pretreated). Wheat straw samples were prepared based on published methodology (Kim and Ralph, 2010; Mansfield et al., 2012). Briefly, samples (250 mg) were milled finely using a Pulverisette 7 planetary micro mill (Fritsch) spinning at 600 rpm with 45 mL nylon vessels containing zirconium dioxide ball bearings (2 x 14 mm and 9 x 10 mm). The total grinding time was one hour and 55 minutes, consisting of 15-minute intervals with five-minute interval breaks to avoid excessive heating.

5.2.10 Sample preparation for nuclear magnetic resonance

NMR samples were prepared based on published methodology (Kim and Ralph, 2010; Mansfield et al., 2012). Briefly, milled samples were transferred to 5 mm NMR tubes (75 mg) and roughly distributed up the sides. Pre-mixed DMSO-d_6/pyridine-d_5 (4:1) was added and samples shaken vigorously (few seconds) to achieve even mixing, then placed in a sonicator bath for one hour. Control (day 0) samples used '100%' d_5-pyrdine, while all other samples used 99.5% d_5-pyridine.

5.2.11 Acquisition and processing of nuclear magnetic resonance data

NMR (2D $_1$H–$_{13}$C HSQC) spectra were acquired on a 600 MHz Avance III HD spectrometer (Bruker) with TCI cryoprobe using a standard pulse program (hsqcetgpsisp2.2, Bruker). NMR spectra were acquired from 12 to -2 ppm in F2 ($_1$H) and from 47 to 137 ppm in F1 ($_{13}$C) using 2048 data points for an acquisition time of 122 ms and an interscan delay of one second, using 144 increments of 16 scans. Spectra were processed using squared cosine bell in both dimensions, and LPfc linear prediction (18 coefficients) in F1. Interactive integrations of contours in 2D-HSQC plots were carried out using TopSpin 3.6 Windows software (Bruker), as was all data processing. Semi-quantitative analysis of lignin units (guaiacyl, G; *p*-hydroxyphenyl, H; syringyl, S) was achieved by integration and comparison of the $S_{2/6}$ and G_2 resonances in the aromatic region and the α signals for each structural unit in the oxygenated alkyl region.

Abundance of the β-O-4 linkage was expressed as the number of linkages detected per 100 C_9 units. Relative amounts of p-coumarates and ferulates were expressed as simple percentages relative to the lignin aromatics, while the relative amounts of reducing sugars (monosaccharides) and acetate groups were expressed as simple percentages relative to the anomeric carbons. Assignments of NMR spectra were made by comparison to published data (Lam et al., 2017, 2019; Takeda et al., 2019; Kim and Ralph, 2010; Mansfield et al., 2012).

5.3 Results

5.3.1 Biomass degradation under submerged and solid-state fermentation

To compare the extent of biomass degradation under SmF and SSF, mass loss profiles (from chapter sections 3.3.1 and 4.3.1) for wheat straw were mapped onto each other (Figure 5.1). Pretreatment under SmF led to greater relative degradation when compared with pretreatment under SSF (37.7% and 22.9% reduction in mass by day 21, respectively). Interestingly, weekly mass loss profiles differed greatly (Figure 5.1). Pretreatment under SSF showed a gradually increasing mass loss pattern, while pretreatment under SmF showed a highly non-linear pattern with the majority of degradation occurring in the second week, then tailing off in the third week.

A

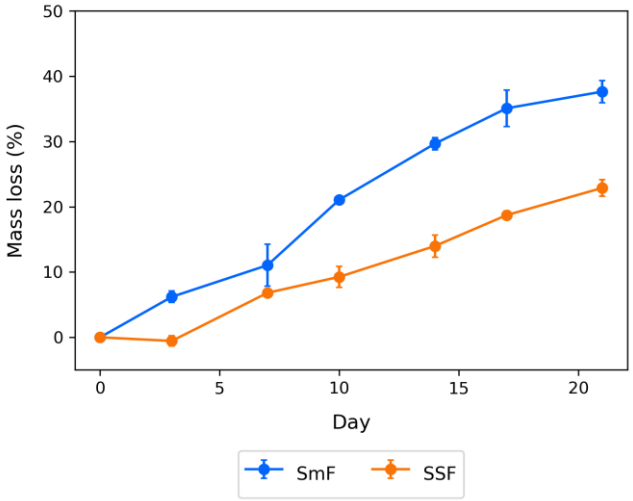

B

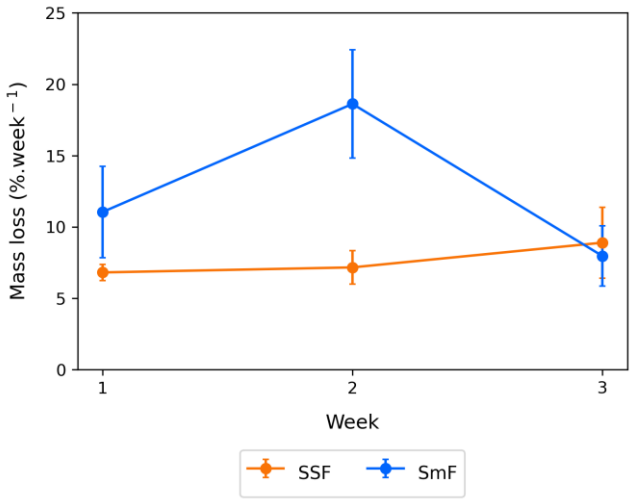

Figure 5.1. Mass loss data of *P. putredinis* NO1 growth on wheat straw under SmF and SSF. Graphs show percentage mass loss (**A**) and weekly percentage mass loss (**B**) of wheat straw over three-week cultures with *P. putredinis* NO1 under SmF and SSF. Data are means ± SD (n = 3).

5.3.2 Degradation efficiency under submerged and solid-state fermentation

Under SmF and SSF, the same volume of fungal inoculum (spores) at the same concentration was added to initiate culture. However, under SSF, 4.2-fold more biomass (wheat straw) was added at the beginning of the pretreatment. Therefore, the ratio between the quantity of spores and mass of wheat straw differed from the onset under SmF and SSF, which should be considered when comparing relative biomass degradation. To this end, mass loss values were normalised against the ratio between fungal inoculum and wheat straw, whose profiles were used to infer the degradation efficiency of *P. putredinis* NO1 under SmF and SSF (Figure 5.2).

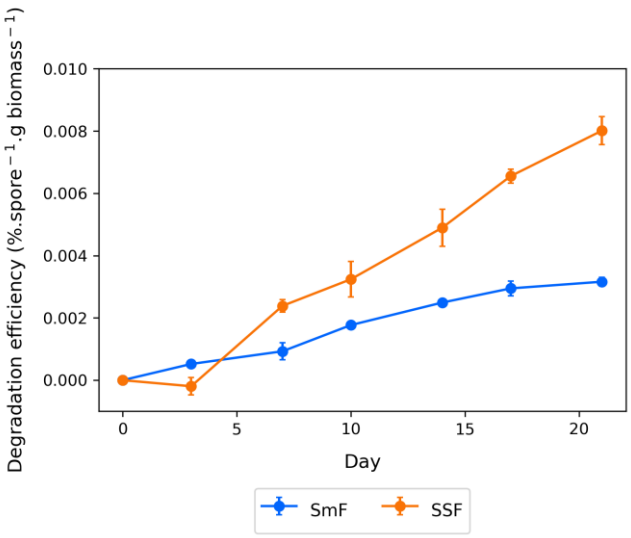

Figure 5.2. Degradation efficiency of *P. putredinis* NO1 growth on wheat straw under SmF and SSF. Graph shows percentage mass loss per spore per gram of biomass (proxy for degradation efficiency) over three-week cultures with *P. putredinis* NO1 under SmF and SSF. Data are means ± SD (n = 3).

Interestingly, *P. putredinis* NO1 showed greater normalised mass loss on wheat straw under SSF from day 7 onwards, indicating greater degradation efficiency. The profile increased over time, beginning with a sharp rise between days 3 and 7, whereas the SmF profile increased steadily and began to plateau at day 14; both in line with their weekly mass loss trajectories (Figure 5.1).

5.3.3 Scanning electron microscopy of *P. putredinis* NO1 growth morphology

To investigate fungal morphology during growth on wheat straw, and to provide visual evidence of wheat straw degradation, SEM was conducted on samples obtained from various time points during the three-week cultures (Figure 5.3). Analysis showed fungal morphologies to differ starkly between pretreatments under SmF and SSF. By day 10, under SmF, *P. putredinis* NO1 showed a greater propensity towards pellet formation, with numerous pellets observed on the biomass. In contrast, under SSF, *P. putredinis* NO1 showed a greater propensity towards hyphal formation with the presence of an intricate hyphal network and little to no evidence of pellets.

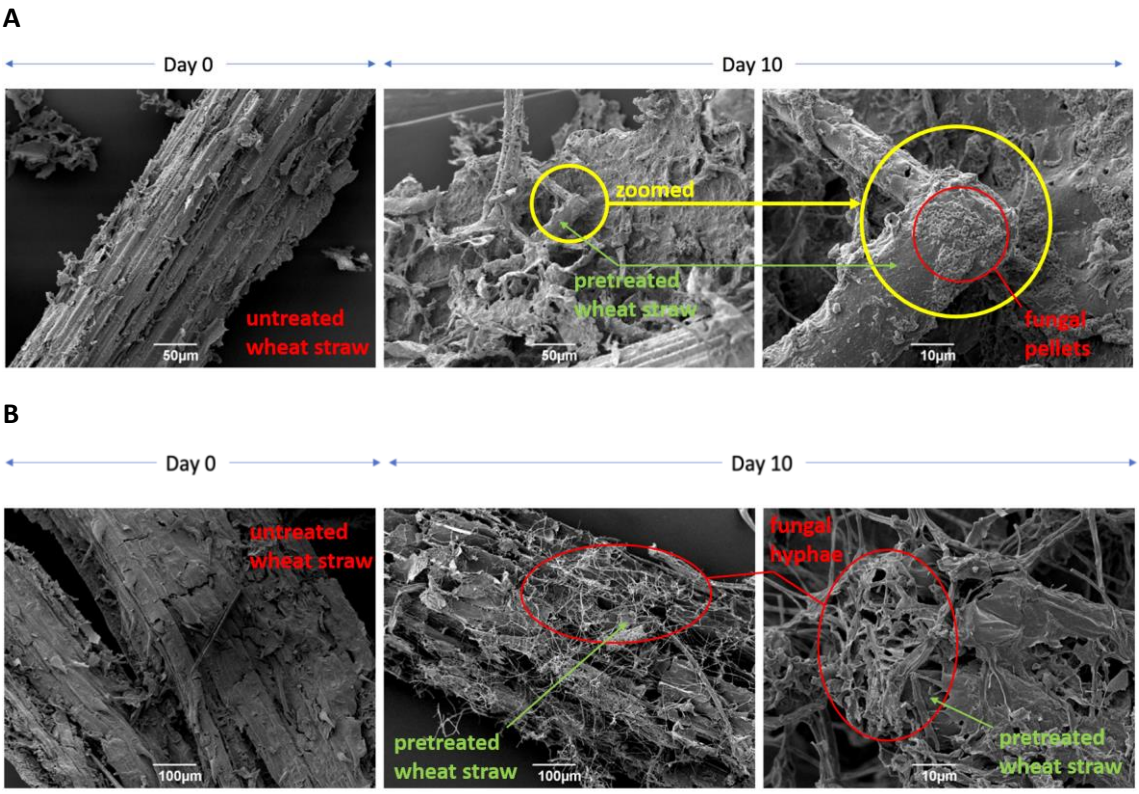

Figure 5.3. Scanning electron microscopy of wheat straw pretreated with *P. putredinis* NO1 under SmF and SSF. SEM images show wheat straw pretreated with *P. putredinis* NO1 under SmF (**A**) and SSF (**B**) at days 0 and 10, with key features annotated.

As the cultures progressed through time, these differences became more visually evident (Figure 5.4). By day 21, under SSF, *P. putredinis* NO1 showed a now expansive hyphal network, while under SmF, the biomass appeared heavily degraded, but there was little evidence of any remaining fungal structures.

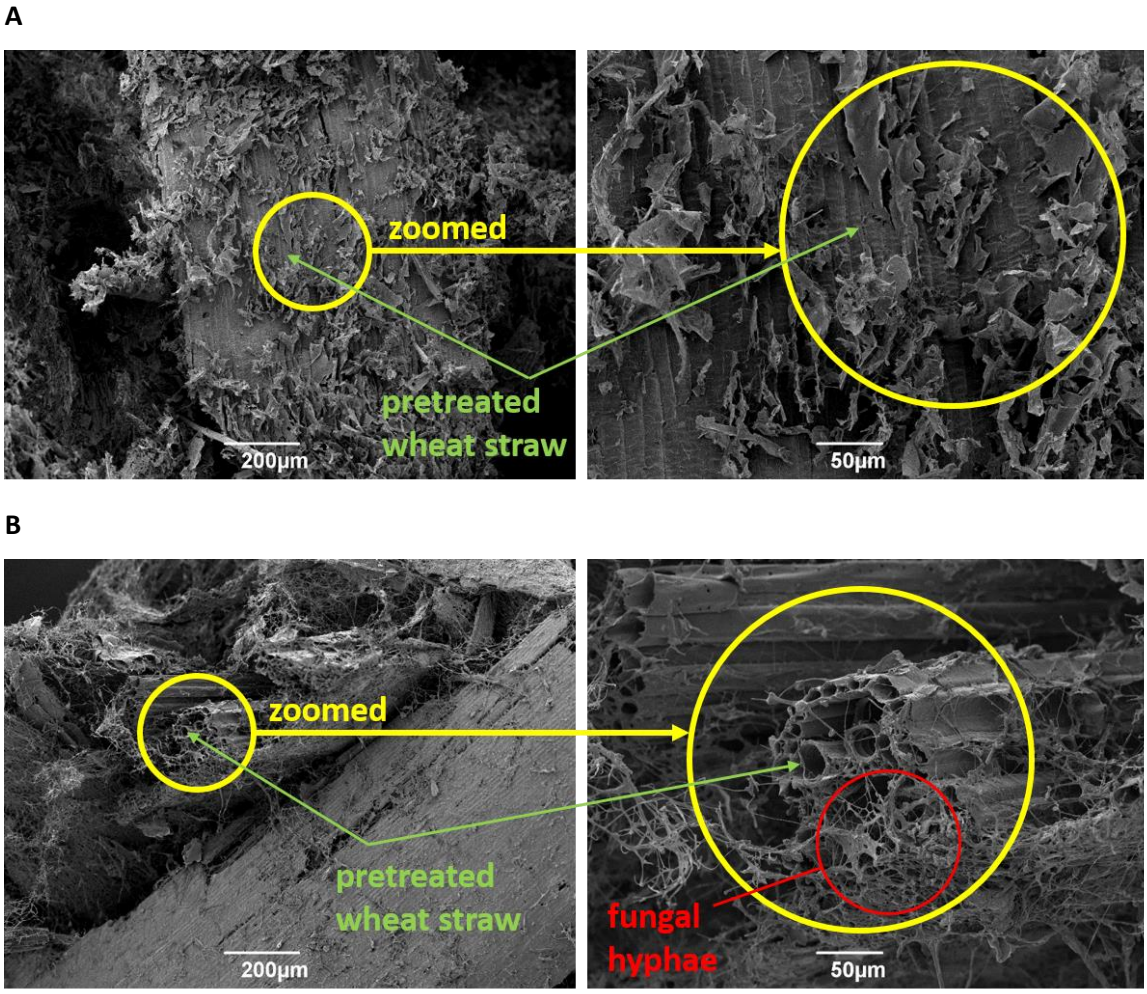

Figure 5.4. Scanning electron microscopy of wheat straw pretreated with *P. putredinis* NO1 under SmF and SSF for three weeks. SEM images show wheat straw pretreated with *P. putredinis* NO1 under SmF (**A**) and SSF (**B**) at day 21, with key features annotated.

Following SEM, a range of composition analyses were conducted on wheat straw pretreated with *P. putredinis* NO1 under SmF and SSF for three weeks, as well as untreated wheat straw (day 0). These targeted the three main components of lignocellulose (lignin, matrix polysaccharides, crystalline cellulose) and ash (non-carbon fraction).

5.3.4 Composition analysis – untreated wheat straw

To construct a baseline composition profile for untreated wheat straw (day 0), all data (from SmF and SSF) were combined and mean values calculated (Figure 5.5). Lignin (measured as acetyl bromide soluble lignin; ABSL) and crystalline cellulose were the predominant fractions captured by the analyses (208 µg/mg and 182.6 µg/mg, respectively). The matrix polysaccharide fraction totalled 110 µg/mg, with xylose the predominant monosaccharide (40.7 µg/mg), followed by arabinose (24.3 µg/mg), glucose (17.2 µg/mg) and galactose (14.3 µg/mg).

The remaining monosaccharides (mannose, rhamnose, galacturonic acid, glucuronic acid and fucose) were detected at levels lower than 5 µg/mg. The non-carbon fraction (ash) showed the smallest overall contribution (63.6 µg/mg).

A

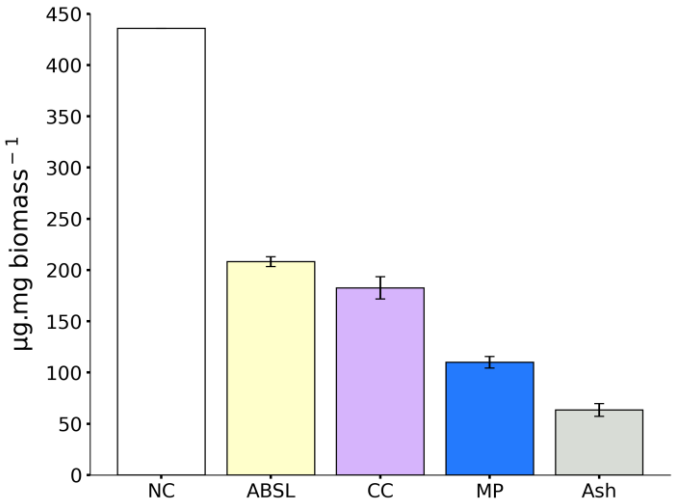

B

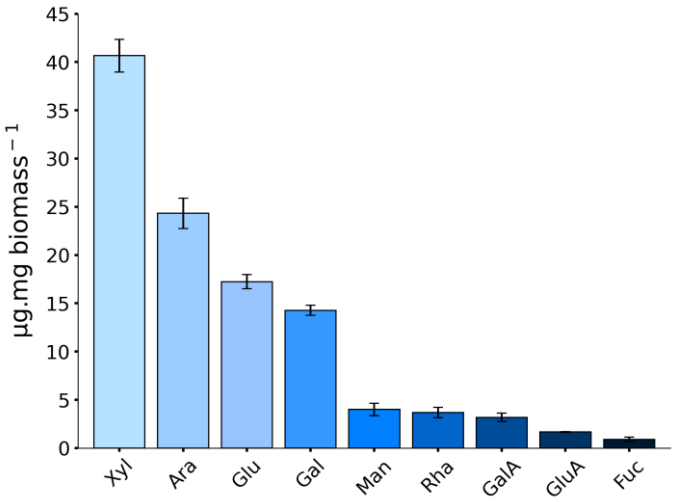

Figure 5.5. Baseline composition profiles of untreated wheat straw. (**A**) Graph shows relative quantities of acetyl bromide soluble lignin (ABSL; n = 12), crystalline cellulose (CC; n = 12), matrix polysaccharides (MP; n = 6) and ash (n = 6) within untreated wheat straw. 'NC' represents the fraction of biomass not captured by the composition analyses undertaken (e.g. amorphous cellulose), defined as 1 mg (1000 µg) minus the sum total of all components measured. Data are means ± SE. (**B**) Graph shows the matrix polysaccharide fraction broken down into its constituent monosaccharides (xylose, arabinose, glucose, galactose, mannose, rhamnose, galacturonic acid, glucuronic acid and fucose). Data are means ± SE (n = 6).

With a baseline composition profile established for untreated wheat straw, temporal analyses explored how the main components of lignocellulose (and ash) changed over three week pretreatments with *P. putredinis* NO1 under SmF and SSF.

5.3.5 Composition analysis – lignin

Lignin is composed of three main phenylpropanoid units (guaiacyl, *p*-hydroxyphenyl and syringyl) linked together predominantly by β-O-4 ether linkages. Solid-state NMR conducted on untreated wheat straw and wheat straw pretreated with *P. putredinis* NO1 under SSF elucidated the temporal abundance profile of these ether linkages, detected between lignin monomers over three weeks (Figure 5.6). Unfortunately, due to COVID-19 related issues, it was not possible to conduct the same NMR analysis on wheat straw pretreated under SmF.

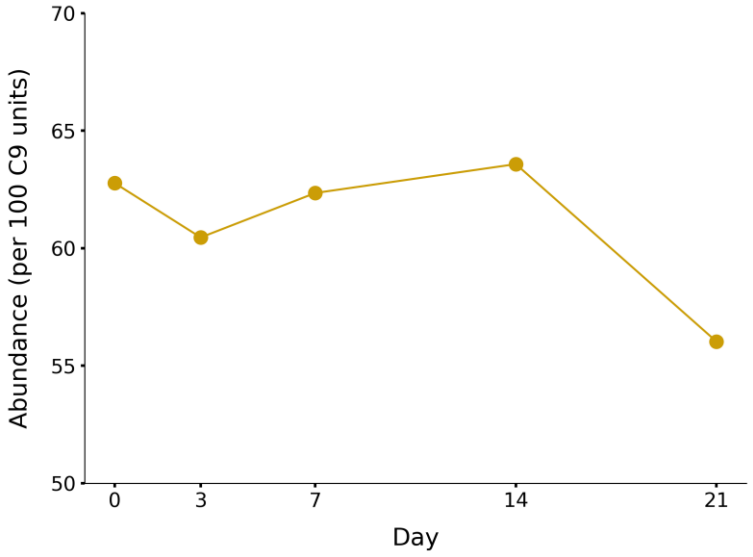

Figure 5.6. Temporal profile of the β-O-4 ether linkage during *P. putredinis* NO1 growth on wheat straw under SSF. Graph shows NMR semi-quantitative abundance data of the β-O-4 linkage (per 100 C_9 units) within wheat straw pretreated with *P. putredinis* NO1 under SSF over three weeks.

During the first two weeks, the relative abundance of the β-O-4 linkage detected within wheat straw fluctuated (60-64 per 100 C_9 units). However, by day 21, its relative abundance had declined to 56 linkages, showing a 12.5% reduction during the third week. This indicated cleavage of the β-O-4 linkage between lignin monomers during the latter growth stages.

To investigate the temporal abundance of lignin, ABSL was quantified and profiled over the three-week time courses (Figure 5.7). Under both SmF and SSF, ABSL increased in relative mass over the 21 days. This indicated a lack of preferential degradation by *P. putredinis* NO1, despite NMR data revealing the cleavage of β-O-4 ether linkages within wheat straw pretreated under SSF. Under SmF, untreated (day 0) wheat straw showed an ABSL content of 19.2%, rising to a temporal maximum of 28% by day 21, while under SSF, untreated wheat straw showed an ABSL content of 21.3%, rising to a maximum of 34.8% in the same time period.

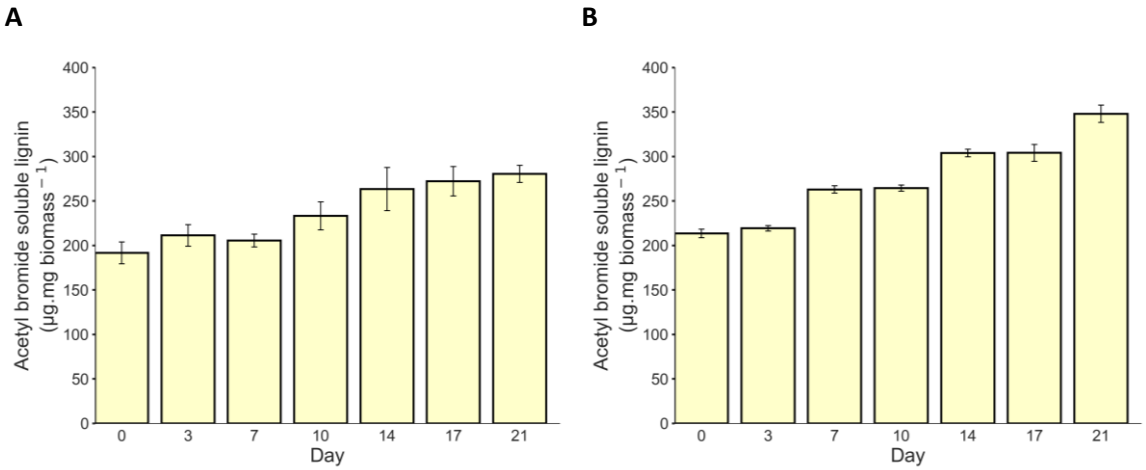

Figure 5.7. Temporal ABSL profiles of wheat straw pretreated with *P. putredinis* NO1 under SmF and SSF. Graphs show lignin content as µg acetyl bromide soluble fraction/mg biomass for wheat straw pretreated with *P. putredinis* NO1 under SmF (**A**) and SSF (**B**) over three weeks. For SmF, data are means ± SD (n = 3). For SSF, data are means ± SE (n = 9).

Solid-state NMR conducted on untreated wheat straw and wheat straw pretreated with *P. putredinis* NO1 under SSF elucidated the temporal changes in lignin composition in greater depth; revealing the relative abundances of guaiacyl, *p*-hydroxyphenyl and syringyl (Figure 5.8).

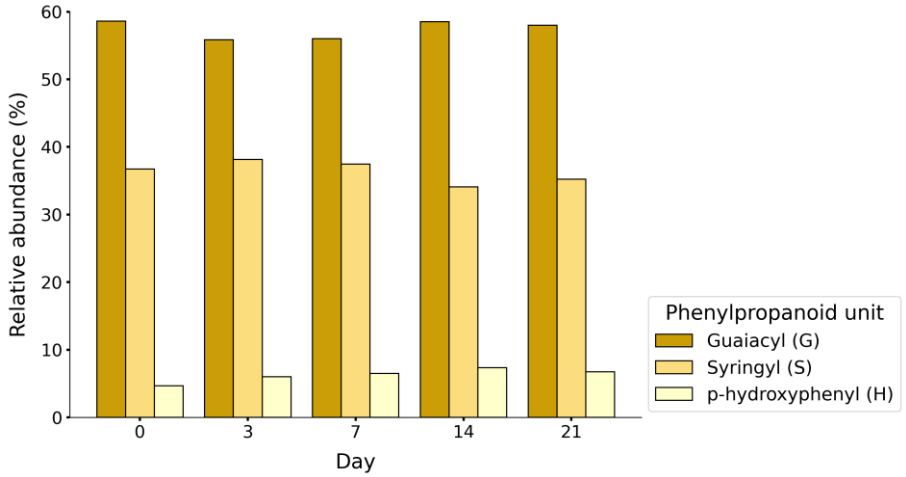

Figure 5.8. Temporal profiles of guaiacyl, *p*-hydroxyphenyl and syringyl within wheat straw pretreated with *P. putredinis* NO1 under SSF. Graph shows NMR semi-quantitative abundance data of guaiacyl, *p*-hydroxyphenyl and syringyl within wheat straw pretreated with *P. putredinis* NO1 under SSF over three weeks.

Solid-state NMR showed guaiacyl to be the predominant phenylpropanoid unit within lignin, followed by syringyl and *p*-hydroxyphenyl. In line with ABSL analysis, NMR showed no evidence for the preferential degradation of lignin monomers. The relative abundances of guaiacyl and syringyl fluctuated over time (guaiacyl = 55.9-58.6%, syringyl = 34.1-38.1%), while the relative abundance of *p*-hydroxyphenyl increased from 4.7% (day 0) to 6.8% by day 21.

5.3.6 Composition analysis – cell wall bound hydroxycinnamic acids

Cell wall bound hydroxycinnamic acids (e.g. ferulic and p-coumaric acids) are involved in cross linking between lignin and matrix polysaccharides. Solid-state NMR conducted on untreated wheat straw and wheat straw pretreated with *P. putredinis* NO1 under SSF yielded the relative abundances of ferulates and p-coumarates over the three-week time course (Figure 5.9).

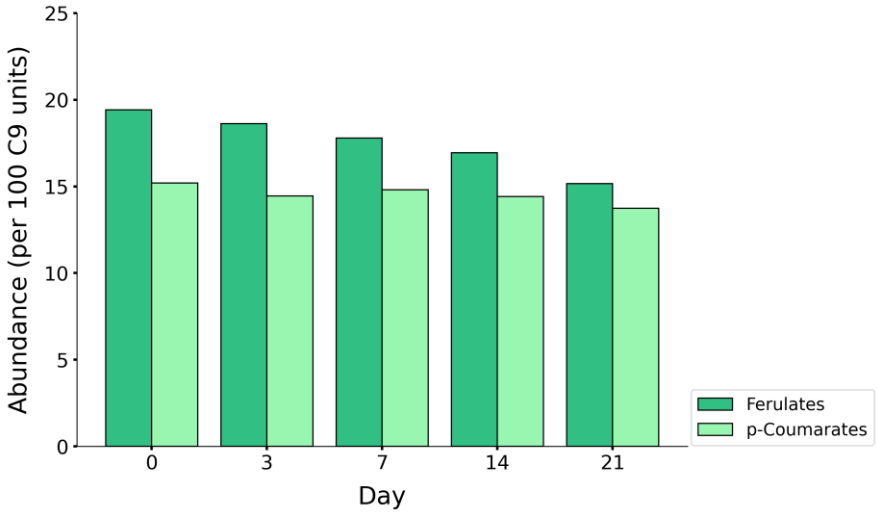

Figure 5.9. Temporal profiles of ferulates and p-coumarates within wheat straw pretreated with *P. putredinis* NO1 under SSF. Graph shows NMR semi-quantitative abundance data of ferulates and p-coumarates, per 100 C_9 units, within wheat straw pretreated with *P. putredinis* NO1 under SSF over three weeks.

Solid-state NMR showed ferulates were more abundant in wheat straw than p-coumarates throughout the time course. Under SSF, NMR showed a slight reduction in p-coumarates, starting at a relative abundance of 15.2% and declining to a temporal minimum of 13.7% by day 21. Ferulates also declined over time but showed a more substantial reduction, beginning at a relative abundance of 19.4% and decreasing to a temporal minimum of 15.2% (day 21).

5.3.7 Composition analysis – matrix polysaccharides

Composition analyses also profiled the abundance of matrix polysaccharides (Figure 5.10). Under SmF, the total hydrolysed fraction decreased gradually in relative mass over the 21 days, declining from 12.2% (untreated wheat straw) to a temporal minimum of 10.3% by day 21; thus, indicating its preferential degradation. However, in contrast, under SSF, the total hydrolysed fraction increased gradually in relative mass. Untreated wheat straw showed a total matrix polysaccharide composition of 9.8% which increased to a temporal maximum of 11% by day 21.

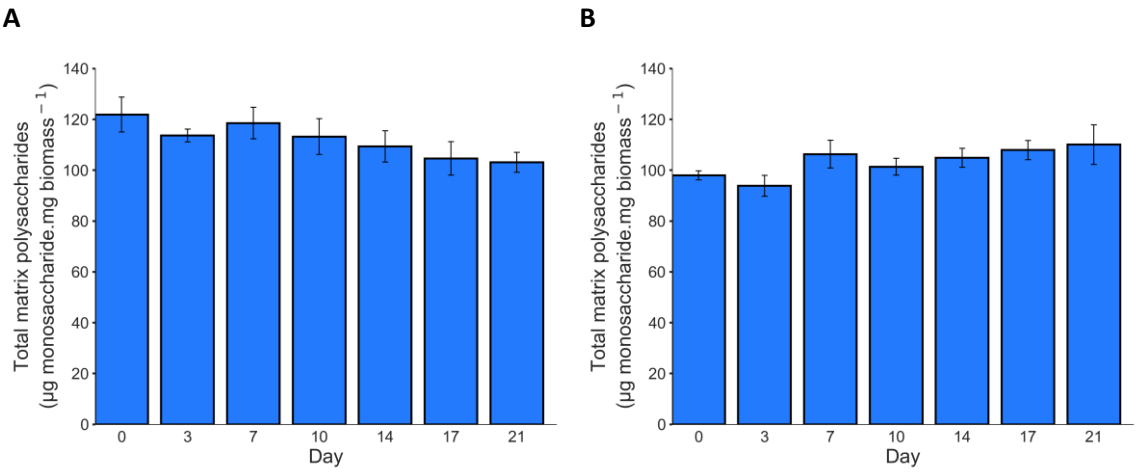

Figure 5.10. Temporal matrix polysaccharide profiles of wheat straw pretreated with *P. putredinis* NO1 under SmF and SSF. Graphs show total matrix polysaccharide content as µg monosaccharide/mg biomass for wheat straw pretreated with *P. putredinis* NO1 under SmF (**A**) and SSF (**B**) over three weeks. Data are means ± SD (n = 3).

The matrix polysaccharide fraction is composed of various monosaccharides, all of which are reducing sugars (those with free aldehyde or ketone functional groups, able to act as reducing agents). As such, reducing sugars contain -OH groups at their anomeric carbons, and this characteristic can be used to interpret their relative abundance using techniques such as solid-state NMR. In addition, by referencing against the anomeric carbons of reducing sugars, the relative abundance of acetate groups can be assessed. Therefore, NMR conducted on untreated wheat straw and wheat straw pretreated under SSF also investigated the temporal profiles of reducing sugars and acetate groups within the matrix polysaccharide fraction (Figure 5.11).

A

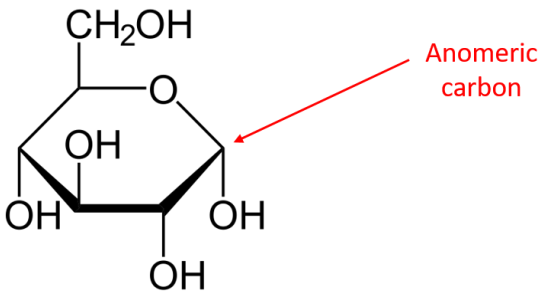

B

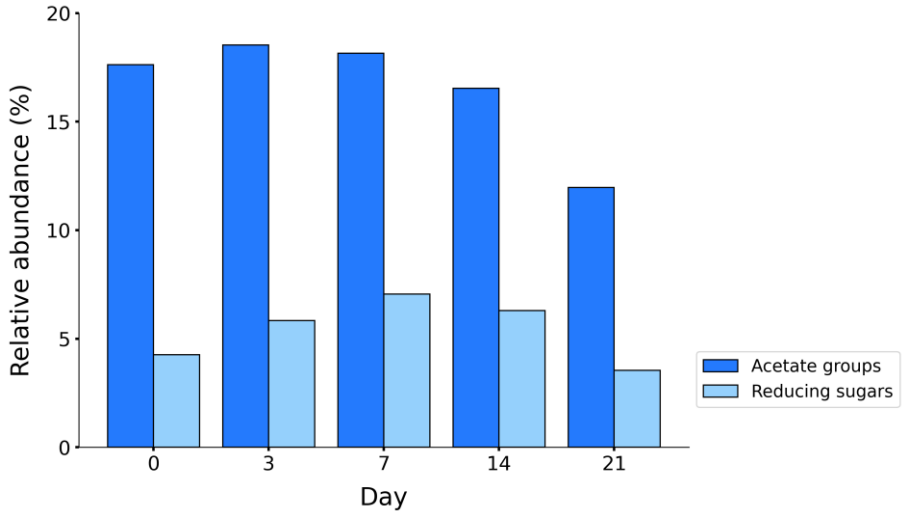

Figure 5.11. Temporal profiles of reducing sugars and acetate groups within wheat straw pretreated with *P. putredinis* NO1 under SSF. (**A**) Molecular structure of glucose (α-D-glucopyranose) and its anomeric carbon. (**B**) Graph shows NMR semi-quantitative abundance data of reducing sugars and acetate groups, relative to the anomeric carbons, within wheat straw pretreated with *P. putredinis* NO1 under SSF over three weeks.

The relative abundance of reducing sugars increased during the first week, starting at 4.3% and rising to 7.1% by day 7. Between days 7 and 21, however, during the middle and latter growth stages, the proportion of reducing sugars declined (day 14 = 6.3%, day 21 = 3.5%). This temporal profile correlated positively with the relative abundance of acetate groups, which increased initially in the first week (day 0 = 17.6%, day 7 = 18.2%), then declined in line with reducing sugars during the second and third weeks (day 14 = 16.5%, day 21 = 12%). Interestingly, for reducing sugars and acetate groups, the decline observed during the third week was steeper than that observed during the second week, indicating an increasing rate of degradation.

To substantiate these results, solid-state NMR spectra for untreated wheat straw and wheat straw pretreated with *P. putredinis* NO1 under SSF for 21 days were overlaid and their differences highlighted (Figure 5.12).

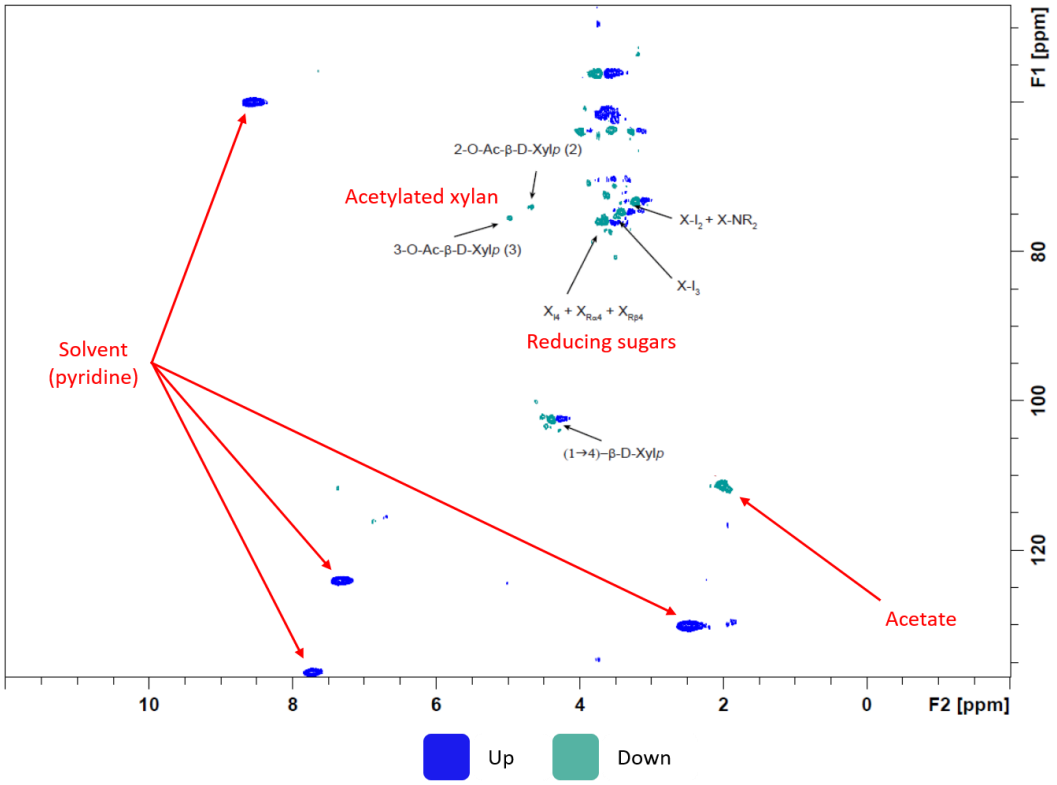

Figure 5.12. Comparative nuclear magnetic resonance spectrum of untreated wheat straw and wheat straw pretreated with *P. putredinis* NO1 under SSF for three weeks. NMR spectra for untreated wheat straw and 21-day pretreated wheat straw (SSF) were overlaid and their differences highlighted. Blue shading represents an increase in relative abundance between untreated wheat straw and 21-day pretreated wheat straw, while turquoise shading represents a decrease in relative abundance. Pyridine was used as a solvent for NMR analysis and its presence is highlighted on the spectrum.

The comparative NMR spectrum validated the observed reduction in reducing sugars and acetate groups over the 21-day pretreatment. Interestingly, the spectrum also showed a reduction in acetylated xylan between untreated and 21-day pretreated wheat straw; indicative of matrix polysaccharide deconstruction not observed under prior analysis of the total fraction.

To investigate temporal changes to matrix polysaccharides in greater depth, results from composition analyses conducted on the total fraction were broken down into constituent monosaccharides (arabinose, fucose, galactose, galacturonic acid, glucose, glucuronic acid, mannose, rhamnose, xylose), and their inter-week change profiles elucidated (Figure 5.13).

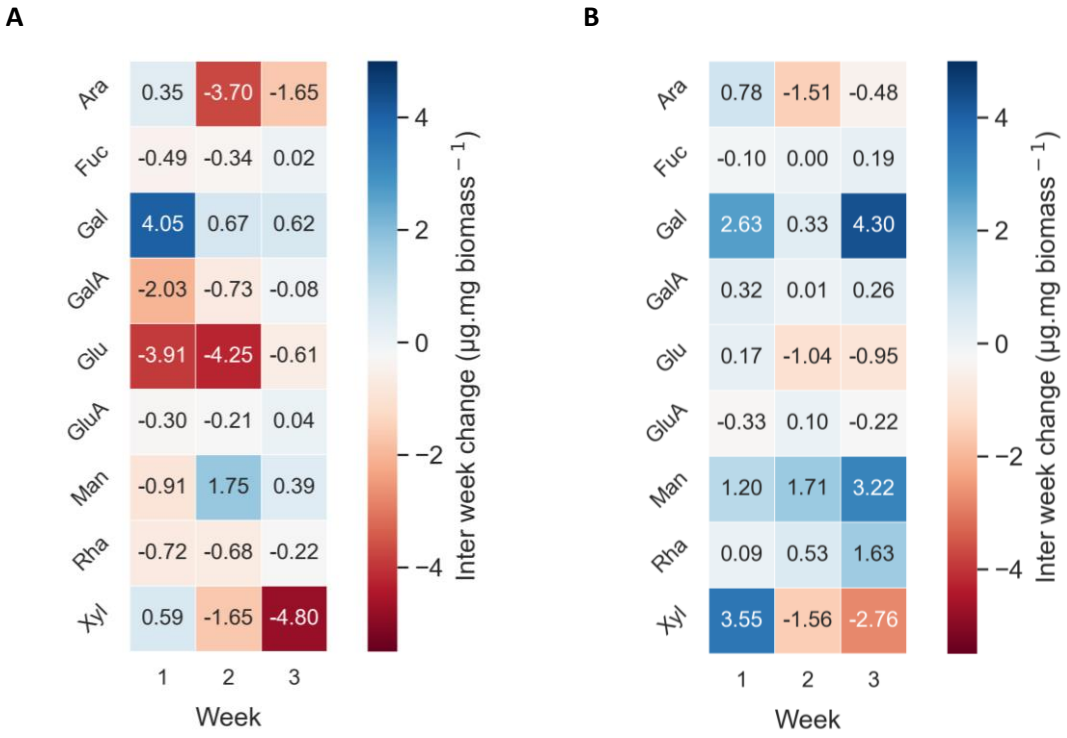

Figure 5.13. Inter-week change profiles of monosaccharides within the matrix polysaccharide fraction of wheat straw pretreated with *P. putredinis* NO1 under SmF and SSF. Heat maps show inter-week change (as µg monosaccharide/mg biomass) of monosaccharides within the matrix polysaccharide fraction of wheat straw pretreated with *P. putredinis* NO1 under SmF (**A**) and SSF (**B**) over three weeks. Negative (red) values represent a relative reduction in mass, whereas positive (blue) values represent a relative increase in mass. Data are means (n = 3).

Under SmF, a range of monosaccharides showed degradation during the first week, predominantly glucose (-3.91 µg/mg), then galacturonic acid (-2.03 µg/mg), mannose (-0.91 µg/mg), rhamnose (-0.72 µg/mg), fucose (-0.49 µg/mg) and glucuronic acid (-0.3 µg/mg). In contrast, under SSF, glucuronic acid and fucose showed degradation during the first week, though with only slight reductions of 0.33 µg/mg and 0.1 µg/mg, respectively.

During the second week under SmF, glucose showed further preferential degradation (-4.25 µg/mg), while arabinose and xylose showed degradation for the first time in the time course (-3.7 µg/mg and -1.65 µg/mg, respectively). Galacturonic acid also showed further degradation (-0.73 µg/mg), as well as fucose (-0.34 µg/mg) and glucuronic acid (-0.21 µg/mg) to lesser extents. Interestingly, under SSF, xylose (-1.56 µg/mg), arabinose (-1.51 µg/mg) and glucose (-1.04 µg/mg) degradation was evident, as observed under SmF, though xylose showed preferential degradation under SSF as opposed to glucose. During the third week, temporal profiles converged with xylose showing preferential degradation under SmF and SSF (-4.8 µg/mg and -2.76 µg/mg, respectively) to the greatest extent observed throughout the time courses. While xylose degradation predominated, arabinose (-1.65 µg/mg) and glucose (-0.61 µg/mg) showed degradation under SmF, as well as under SSF (glucose: -0.95 µg/mg; arabinose: -0.48 µg/mg). In contrast to xylose, under both SmF and SSF, the degradation of glucose and arabinose during the third week was lower than that observed during the second week. Interestingly, galactose showed no degradation under SmF and SSF at all points throughout the three-week time courses, while rhamnose and galacturonic acid degradation was observed under SmF only, showing gradual reductions in their weekly degradation over time. Mannose degradation was also observed exclusively under SmF, though during the first week only (-0.91 µg/mg).

5.3.8 Composition analysis – crystalline cellulose

In addition to ABSL and matrix polysaccharides, biomass composition analyses profiled the abundance of crystalline cellulose over the three-week time courses (Figure 5.14).

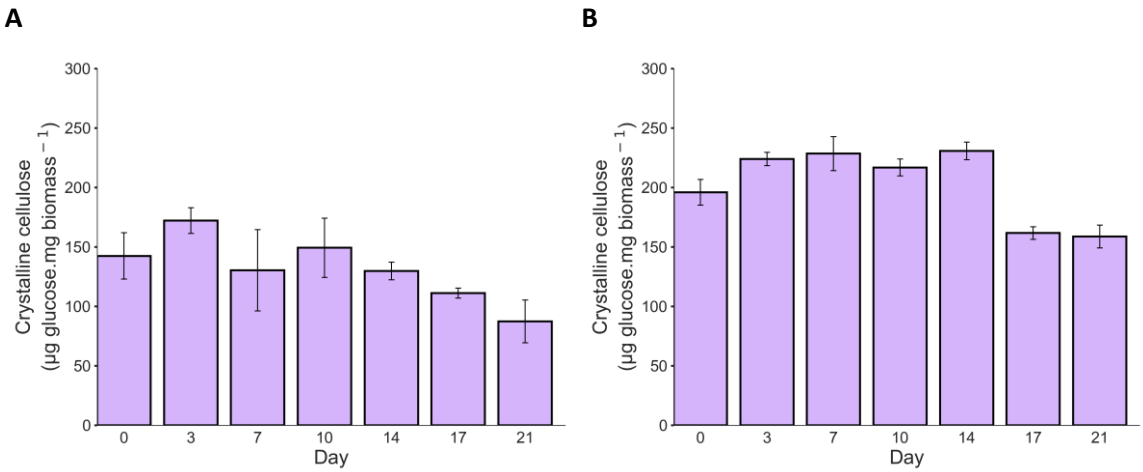

Figure 5.14. Temporal crystalline cellulose profiles of wheat straw pretreated with *P. putredinis* NO1 under SmF and SSF. Graphs show crystalline cellulose as µg glucose/mg biomass for wheat straw pretreated with *P. putredinis* NO1 under SmF (**A**) and SSF (**B**) over three weeks. For SmF, data are means ± SD (n = 3). For SSF, data are means ± SE (n = 9).

Under SmF and SSF, *P. putredinis* NO1 showed preferential degradation of crystalline cellulose, though temporal profiles differed. Under SmF, from day 3 onwards, the crystalline cellulose fraction showed a gradual linear decline in relative mass, following an initial increase. Untreated wheat straw showed a crystalline cellulose content of 14.2%, decreasing to a minimum of 8.7% by day 21. In contrast, under SSF, the crystalline cellulose fraction showed no degradation until the third week, in which (from day 14 onwards) saw a sharp reduction in relative mass (16.2% by day 17 and 15.9% by day 21), relative to 19.6% in untreated wheat straw.

5.3.9 Integration of composition analyses

Integration of inter-week change profiles for all lignocellulose fractions provided holistic views of cell wall degradation within wheat straw under SmF and SSF over three weeks (Figure 5.15).

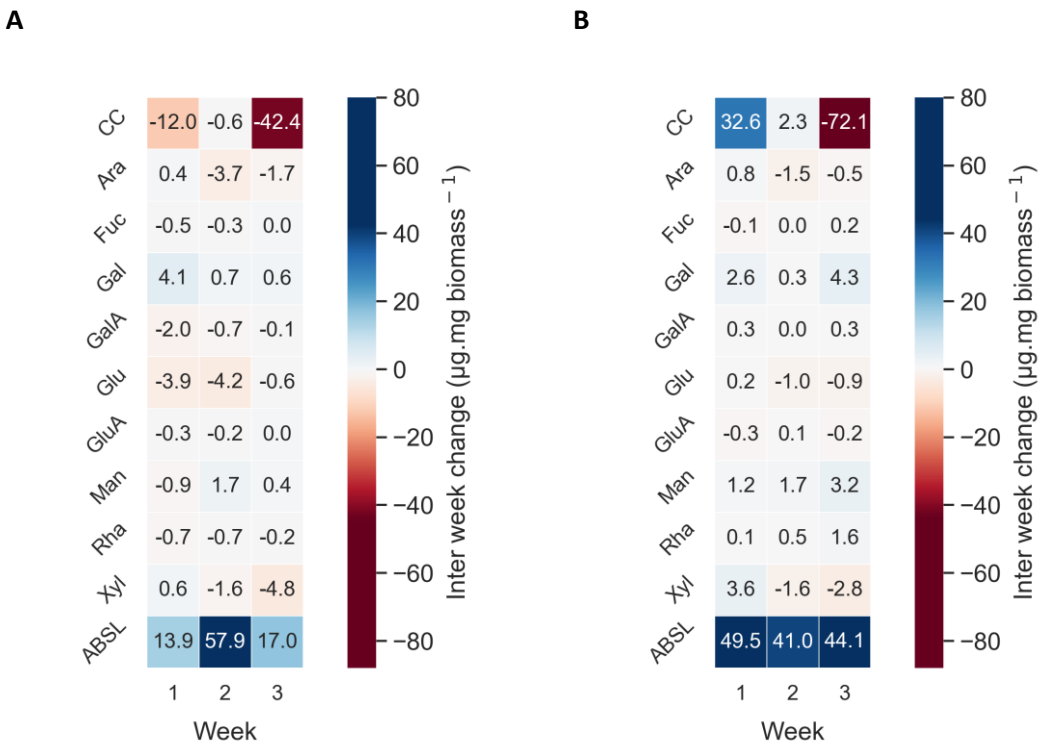

Figure 5.15. Inter-week change profiles of the major lignocellulosic components within wheat straw pretreated with *P. putredinis* NO1 under SmF and SSF. Heat maps show mean inter-week change (as µg/mg biomass) of crystalline cellulose (CC), monosaccharides within the matrix polysaccharide complex (arabinose, fucose, galactose, galacturonic acid, glucose, glucuronic acid, mannose, rhamnose, xylose) and ABSL within wheat straw pretreated with *P. putredinis* NO1 under SmF (**A**) and SSF (**B**) over three weeks. Negative (red) values represent a relative reduction in mass, whereas positive (blue) values represent a relative increase in mass.

Under SmF and SSF, *P. putredinis* NO1 showed preferential degradation of crystalline cellulose over all other lignocellulose components, showing greater relative degradation of this fraction than any other. Under SmF, crystalline cellulose degradation was observed each week, with the majority occurring in the third (week 1 = -12 µg/mg, week 2 = -0.6 µg/mg, week 3 = -42.4 µg/mg). However, under SSF, crystalline cellulose degradation was observed during only the third week (-72.1 µg/mg), though to a greater extent in comparison to that observed under SmF (-42.4 µg/mg). During the first week under SmF, crystalline cellulose degradation coincided with the degradation of glucose (-3.9 µg/mg) and galacturonic acid (-2 µg/mg), as well as various other monosaccharides to lesser degrees (e.g. mannose = -0.9 µg/mg, rhamnose = -0.7 µg/mg, fucose = -0.5 µg/mg). In the second week, crystalline cellulose degradation slowed (-0.6 µg/mg), while glucose (-4.2 µg/mg), arabinose (-3.7 µg/mg) and xylose (-1.6 µg/mg) showed predominant degradation.

During the third week under SmF, crystalline cellulose degradation reached a temporal maximum (-42.4 µg/mg), while xylose degradation increased (-4.8 µg/mg), and arabinose (-1.7 µg/mg) and glucose (-0.6 µg/mg) degradation slowed. Under SSF, very little degradation was observed during the first week, while in the second week, xylose (-1.6 µg/mg), arabinose (-1.5 µg/mg) and glucose (-1 µg/mg) showed predominant degradation. During the third week, crystalline cellulose degradation reached a temporal maximum (-72.1 µg/mg), accompanied by a further increase in xylose degradation (-2.8 µg/mg), while glucose (-0.9 µg/mg) and arabinose (-0.5 µg/mg) degradation slowed. Therefore, under both SmF and SSF, components of the matrix polysaccharide fraction (particularly glucose, arabinose and xylose) appeared rate limiting for crystalline cellulose degradation, while no lignin degradation was observed during either of the time courses. Interestingly, under SSF, crystalline cellulose degradation was higher than that observed under SmF, despite less overall degradation of components within the matrix polysaccharide fraction.

5.3.10 Composition analysis – ash

In addition to the main structural components of lignocellulose, composition analyses profiled the abundance of the non-carbon (ash) fraction over the three-week time courses (Figure 5.16).

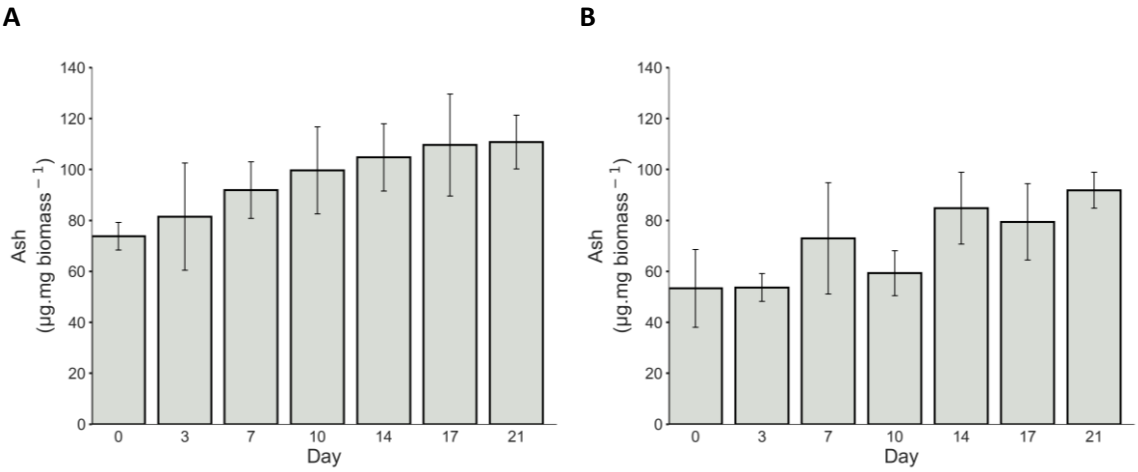

Figure 5.16. Temporal ash profiles of wheat straw pretreated with *P. putredinis* NO1 under SmF and SSF. Graphs show non-carbon content as µg ash/mg biomass for wheat straw pretreated with *P. putredinis* NO1 under SmF (**A**) and SSF (**B**) over three weeks. Data are means ± SD (n = 3).

Under SmF and SSF, the non-carbon fraction (measured as ash) increased gradually in relative mass over the three-week time courses, indicating a lack of degradation. Under SmF, untreated wheat straw showed an ash content of 7.4%, increasing to a maximum of 11.1% by day 21. Under SSF, untreated wheat straw showed an ash content of 5.3% and the same increasing trend was observed, with ash content reaching a maximum of 9.2% by day 21. Interestingly, under SSF, greater fluctuations in ash abundance were observed between time points.

5.3.11 Extrapolation of composition analyses

Relative composition values (µg/mg biomass) were extrapolated to mass remaining data (g biomass; derived from mass loss experiments), revealing complete temporal change profiles for crystalline cellulose, matrix polysaccharides, ABSL and ash, under SmF and SSF (Figure 5.17).

A

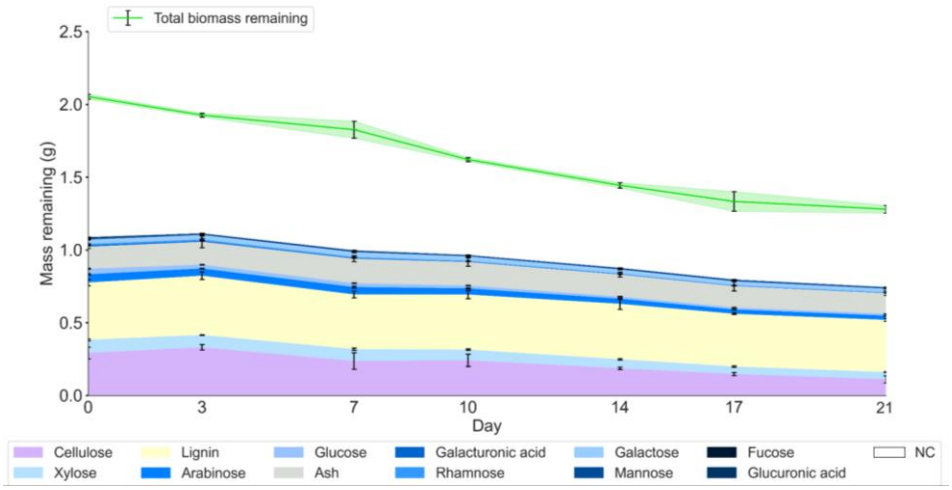

B

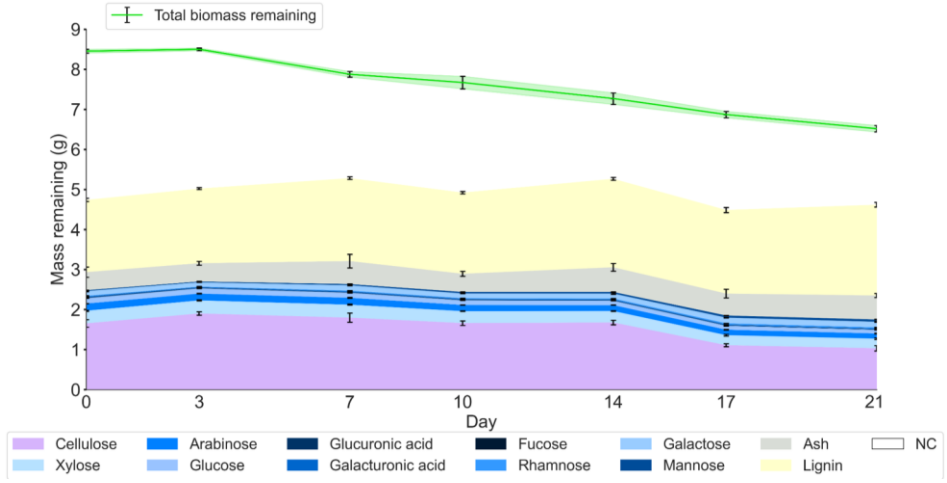

Figure 5.17. Extrapolated temporal composition profiles of wheat straw pretreated with *P. putredinis* NO1 under SmF and SSF. Graphs show temporal fraction content as mean mass remaining (g) for wheat straw pretreated with *P. putredinis* NO1 under SmF (**A**) and SSF (**B**) over three weeks, with stack bars ordered from highest to lowest change in mass between days 0 and 21. 'NC' represents the fraction of biomass not captured by the analyses.

Extrapolated profiles validated the preferential degradation of crystalline cellulose under both SmF and SSF, though with different temporal patterns. In addition, profiles substantiated the degradation of various monosaccharides within the matrix polysaccharide fraction, with degradation under SSF appearing more targeted towards those most abundant (xylose, arabinose, glucose). Degradation of ABSL and ash remained negligible, particularly under SSF.

5.4 Discussion

5.4.1 *P. putredinis* NO1 degrades wheat straw with greater efficiency under solid-state fermentation

Comparative mass loss data of *P. putredinis* NO1 growth on wheat straw showed greater relative mass loss under SmF at every time point. In these experiments, the spore concentration and inoculating volume were standardised to control the amount of fungal inoculum used to initiate each culture system. However, as a result, under SmF (in which the relative proportion of wheat straw was lower), the ratio between the starting fungal inoculum and the biomass was approximately four-fold higher in comparison to SSF. This, therefore, limits the validity of comparison. As such, mass loss profiles were normalised to account for this limitation and instead used to infer degradation efficiency. Interestingly, *P. putredinis* NO1 exhibited greater normalised mass loss under SSF, and thus degradation efficiency, at all but one time point (day 3). This followed a short initial lag phase as observed previously (chapter 4) which may be the result of slow spore germination under low moisture conditions (Hassouni et al., 2007). However, from day 3 onwards, degradation efficiency under SSF showed an increasing trend, corroborated by its increasing weekly mass loss trajectory. This may be a fundamental reflection of the morphological strategies employed by filamentous fungi during growth under SSF, typically characterised by an expansive hyphal network (mycelium) that creates a large surface area for various physiological processes.

To investigate the morphology of *P. putredinis* NO1 during growth on wheat straw under SmF and SSF, SEM was conducted at various time points. As expected, *P. putredinis* NO1 developed a complex hyphal network under SSF that expanded over time. In stark contrast, under SmF and particularly at day 10, an abundance of compact individual fungal pellets was observed. These were likely generated by the non-coagulative agglomeration mode of pellet formation, in which fungal spores germinate into hyphae and branch, but as a consequence of constant agitation experienced during culture (by shaking), then agglomerate to form pellets (Pazouki and Panda, 2000; Veiter, Rajamanickam and Herwig, 2018). These observations have been recorded in various other filamentous fungi, including *Aspergillus ochraceus* (Abd-Elsalam, 2009), with pellets significantly limiting the cell-substrate interface in comparison to growth under SSF. As such, SmF is widely reported to be of inferior culture productivity, which may explain the lower degradation efficiency observed by *P. putredinis* NO1 under such conditions.

The normalised mass loss profiles provided a way in which to infer degradation efficiency in relation to the initial inoculum/biomass ratio. However, they failed to account for the differential growth morphologies of *P. putredinis* NO1 under SmF and SSF, as observed by SEM, and the consequent differences in fungal biomass quantity over time. To overcome this limitation, it may be possible to use ergosterol (an extractable membrane lipid found almost exclusively in fungi) as a direct quantitative measure of living fungal biomass during culture, as is widely practised to determine the extent of mold growth in soils (Nurika et al., 2018; Parkinson, Warren and Pawliszyn, 2010). This would enable mass loss profiles to be considered against the quantity of fungal biomass present at each time point, providing a deeper understanding of the correlation between *P. putredinis* NO1 growth on wheat straw and its relative degradation efficiency under SmF and SSF. Unfortunately, due to the constraints imposed by COVID-19, it was not possible to develop a methodology to routinely assay ergosterol at the throughput required (e.g. by solid phase microextraction-GC/MS) (Parkinson, Warren and Pawliszyn, 2010), though this should be pursued in future work. An assay technique such as this may also be used to quantify the fungal biomass load present on pretreated wheat straw during feeding trials and, thus, provide a robust way in which to assess whether BSFL feed upon *P. putredinis* NO1 during rearing (using reduction in ergosterol over time as an indicator of fungal consumption).

5.4.2 *P. putredinis* NO1 preferentially targets crystalline cellulose

Composition analyses on wheat straw pretreated with *P. putredinis* NO1 under SmF and SSF showed preferential targeting (and subsequent degradation) of the crystalline cellulose fraction, in line with the traditionally reported action of soft rot ascomycetes (Langer et al., 2021). However, analyses also indicated the use of different strategies to do so under these conditions, which are likely influenced by the differential morphologies observed by SEM during culture.

Lignin monomers (guaiacyl, *p*-hydroxyphenyl and syringyl) are linked predominantly by β-O-4 ether linkages, which represent approximately 50% of all inter-monomer bonds within soft and hardwood lignin (Chatel and Rogers, 2014). Therefore, solid-state NMR was undertaken to investigate the cleavage of β-O-4 linkages by *P. putredinis* NO1 during growth on wheat straw, though unfortunately due to COVID-19 related issues, this was only possible for biomass pretreated under SSF. Interestingly, the relative abundance of the β-O-4 linkage declined over time, most notably during the third week, indicating cleavage between lignin monomers during the latter growth stages. In accordance with this, a recent study described the identification of a new extracellular oxidase, secreted by *P. putredinis* NO1, with the ability to release tricin (a pharmaceutically relevant flavonoid) from monocot lignin via the cleavage of β-O-4 linkages. Pretreatment with the oxidase significantly boosted saccharification of wheat straw when used in conjunction with a commercially available cellulase cocktail (Oates et al., 2021).

Therefore, it is likely that the cleavage of β-O-4 linkages observed under SSF was catalysed (at least in part) by the action of this new oxidase activity. In addition, solid-state NMR quantified the relative abundances of the lignin monomers themselves, though showed no degradation of guaiacyl (the predominant unit), *p*-hydroxyphenyl or syringyl under SSF. This was corroborated by temporal analysis of the ABSL fraction which showed no degradation under either SmF or SSF. In line with this, ascomycete fungi are not well known for their ability to solubilise lignin, which instead is an ability more typically associated with white rot basidiomycete fungi (e.g. *Pleurotus eryngii* and *Pleurotus ostreatus*) (Sista Kameshwar and Qin, 2018). Despite this, recent work has demonstrated the ability of an ascomycete fungus (*Podospora anserina*) to degrade lignin (isolated from wheat straw), in which lignin abundance declined during culture along with the abundance of β-O-4 ether linkages (van Erven et al., 2020). Although the mechanisms underpinning the degradation of lignin by ascomycetes remain unclear, the cleavage of β-O-4 linkages is a potential route of ligninolysis used by some fungi, including *P. putredinis* NO1, and likely plays a role in improving accessibility to preferential components (e.g. cellulose). Any subsequent degradation of lignin is likely employed only where more preferential substrates are absent (van Erven et al., 2020) or have been depleted earlier in the time course (Oates et al., 2021). It is also possible that lignin is opened up by *P. putredinis* NO1 and then remodelled, supported by the lack of degradation observed by compositional analyses.

In addition, solid-state NMR conducted on SSF pretreated wheat straw quantified the relative temporal abundance of two major cell wall bound hydroxycinnamic acid derivatives (ferulates and p-coumarates) involved in the cross linking between lignin and matrix polysaccharides (mainly arabinoxylans). Within wheat straw, ferulic acid is bound covalently by ether bonds to lignin (and structural proteins) and by ester bonds to polysaccharides, typically in approximately equal abundance, restricting the accessibility of polysaccharides by plant pathogens (de Oliveira et al., 2015; Pan, Bolton and Leary, 1998). Performing a similar role, p-coumaric acid is most frequently (> 80%) bound by ester bonds to both lignin and polysaccharides (Pan, Bolton and Leary, 1998). As such, their presence increases cell wall rigidity and overall matrix recalcitrance (Cocero et al., 2018). Under SSF by *P. putredinis* NO1, the abundance of ferulates and p-coumarates within wheat straw declined over time, with ferulates showing a more substantial reduction in comparison. In line with this, previous research has shown reductions in the abundance of ferulic and p-coumaric acids during culture with various white rot fungi under SSF (van Erven et al., 2018; Dinis et al., 2009), in addition to their decline under SmF during *P. anserina* growth on wheat straw derived lignin (van Erven et al., 2020). This is indicative of reduced cross linking between lignin and matrix polysaccharides (e.g. by the action of feruloyl/p-coumaroyl esterases), which likely improves the accessibility to crystalline cellulose.

However, it should be noted that the cleavage and subsequent release of cell wall bound phenolic acids during culture can also be inhibitory to fungal and yeast based fermentation (e.g. enzyme inhibition, reduced growth and metabolism); though the mechanisms responsible are not yet fully understood (Schmidt et al., 2014; Gu, Zhang and Bao, 2014; Gu et al., 2019).

Composition analyses also assessed the matrix polysaccharide fraction within wheat straw pretreated with *P. putredinis* NO1 under SmF and SSF. Analysis of the total fraction (sum of all constituent monosaccharides) showed a gradual reduction over time, indicating its degradation, though under SmF only. In contrast, under SSF, the total fraction showed a steady upward trend, with a particular increase during the first week. Due to the relative nature of these measurements (µg/mg biomass), this may indicate the preferential degradation of another cell wall component, or instead the production and/or accumulation of monosaccharides via saccharification of polysaccharides. To explore this in greater depth, solid-state NMR conducted on wheat straw pretreated under SSF quantified the temporal abundance of reducing sugars, which were used as an alternative measure of monosaccharides. NMR also enabled the quantification of acetate groups whose temporal profiles can be used to infer the degree of acetylation (e.g. of xylan). Interestingly, in line with analysis of the total fraction, relative reducing sugar content increased during the first week, which may be indicative of polysaccharide depolymerisation via endoglucanases (e.g. xylan conversion into xylose monomers). In accordance with these observations, previous research has shown an increase in the reducing sugar content of sweet sorghum bagasse and oil palm fronds following SSF based treatments with the ascomycete fungi *Trichoderma harzianum* and *Aspergillus niger*, respectively (Thanapimmetha et al., 2012; Hong et al., 2012). In addition, the relative abundance of acetate groups increased during the first week of *P. putredinis* NO1 growth on wheat straw under SSF, which likely suggests simultaneous acetylesterase activity as the accessibility to crystalline cellulose is further improved via the cleavage of acetate groups from polysaccharide chains (predominantly xylan). During the second and third weeks, however, the relative abundances of reducing sugars declined, particularly in the third week. This may indicate their metabolism by *P. putredinis* NO1, having initially increased their availability as a digestible carbon source during the first week. The relative abundance of acetate groups followed the same trend, with a decline during the second and third weeks, which may indicate their metabolism alongside reducing sugars. In accordance with this, recent work has demonstrated the ability of *Aspergillus oryzae* (ascomycete fungus) to use acetate as a substrate (Kövilein, Umpfenbach and Ochsenreither, 2021); although acetate has also been shown to provoke mitochondrial stress and cell death in the basidiomycete plant pathogen *Ustilago maydis* (Kretschmer et al., 2018).

This indicates that *P. putredinis* NO1 possesses a certain level of tolerance towards some of the potentially inhibitory breakdown products of lignocellulose, or may be adept at metabolising acetate. In addition, further, more detailed analysis of the total matrix polysaccharide fraction into its constituent monosaccharides corroborated the temporal trends observed in reducing sugars, showing the targeted degradation under SSF of the most abundant monosaccharides detected within wheat straw (xylose, arabinose and glucose) during the second and third weeks. Interestingly, the order of preference for these monosaccharides mirrored their order of abundance, suggesting that *P. putredinis* NO1 mounts a coordinated and processive degradative response under SSF towards the major components of the matrix polysaccharide fraction. In contrast, under SmF, a wider diversity of monosaccharides were degraded from the first week onwards, including those of lower abundance such as galacturonic acid, mannose and rhamnose; the degradation rate of which reduced quickly over time through depletion. Degradation of xylose (the most abundant monosaccharide detected within wheat straw) began during the second week, though remained at a lower level relative to the degradation of glucose and arabinose, both of lower abundance. This, therefore, suggests that *P. putredinis* NO1 mounts a seemingly sporadic and non-targeted degradative response towards the matrix polysaccharide fraction under SmF, in contrast to that observed under SSF.

Composition analyses also assessed the crystalline cellulose fraction within wheat straw pretreated with *P. putredinis* NO1 under SmF and SSF. In both culture systems, degradation of this fraction appeared preferential overall, showing the greatest relative reduction in mass across all components measured. This, therefore, is in line with the traditionally reported action of soft rot ascomycetes as well as a recent genome level comparative study elucidating their high cellulolytic (and hemicellulolytic) activity (Sista Kameshwar and Qin, 2018; Langer et al., 2021). Degradation of crystalline cellulose by *P. putredinis* NO1 was evident under SmF throughout the time course, particularly during the third week, likely the result of rapid (yet sporadic) degradation of matrix polysaccharides and the consequent increase in accessibility of cellulose for metabolism. In contrast, under SSF, crystalline cellulose degradation was observed during the third week only, though the relative weekly reduction was significantly higher in comparison, despite less overall degradation of the matrix polysaccharide fraction.

5.4.3 Solid-state fermentation as a beneficial system for Black Soldier Fly larvae feed production

Under SmF, wheat straw degradation appeared sporadic and non-targeted, particularly towards the matrix polysaccharide fraction whose monosaccharides were degraded from an early stage in the time course. Fungal morphology represented pellets, likely due to the constant agitation and mixing experienced during culture, whose limited nutrient supply (e.g. oxygen) can ultimately lead to cell lysis within the pellet core (Kövilein, Umpfenbach and Ochsenreither, 2021). In line with this, SEM showed little evidence of any remaining fungal structures by day 21, indicating rapid decline of the culture, likely due to the harsh conditions experienced. In contrast, under SSF, wheat straw degradation appeared more coordinated via an expansive (and growing) hyphal network. Degradation was targeted towards crystalline cellulose and the most abundant monosaccharides within the matrix polysaccharide fraction. Reducing sugars increased during the first week prior to the degradation of those most abundant during the second and third weeks; thus, indicating a shortened pretreatment (to less than or equal to seven days) may be beneficial for BSFL feeding, in which the sugars are likely more available but not yet depleted by *P. putredinis* NO1. This would also be desirable from a commercial perspective. In addition, it is likely that the processive and targeted approach observed under SSF would provide greater control over biomass degradation, which may lead to greater process reproducibility (once optimised) in line with previous work (Gupta, Lee and Chen, 2018).

6) Exo-proteomics of *P. putredinis* NO1 growth on wheat straw under submerged and solid-state fermentation

6.1 Introduction

Chapter 5 explored the compositional changes to the major components of cell wall lignocellulose within wheat straw, elicited by *P. putredinis* NO1 growth under submerged fermentation (SmF) and solid-state fermentation (SSF). Results revealed those changes most likely responsible for the improvements observed in biomass digestibility by Black Soldier Fly larvae (BSFL) in chapters 3 and 4; in particular, an increase in the accessibility of cell wall sugars (predominantly cellulose and xylose) for larvae to feed upon. However, the enzymatic mechanisms employed by *P. putredinis* NO1 (underpinning these compositional changes) remained unknown, and as such, are the subject of this chapter.

Proteomic approaches enable the high-throughput identification and quantification of all proteins detected in a given system (the proteome), which facilitates downstream elucidation of their functional roles using a range of bioinformatic tools. Unlike transcriptomics (sequencing of mRNA transcripts by microarray or RNA-Seq) where data shows only modest correlation with protein levels (Parkes and Niranjan, 2019), proteomic data includes all modifications made to all proteins (e.g. post-transcriptional and post-translational modifications). Therefore, proteomic techniques offer greater robustness for the interrogation of lignocellulose processing systems at the functional level, with liquid chromatography and tandem mass spectrometry (LC-MS/MS) one of those most widely used. Briefly, protein containing samples are enzymatically digested into smaller peptides, commonly using trypsin (serine protease), which are size separated by liquid chromatography and mass identified by mass spectrometry. Following this, the resultant peptide spectra are searched against a known sequence library (e.g. species-specific protein database) to yield significant matches, which are then used for downstream protein identification. In addition, relative protein abundance (semi-quantitative) can be determined from the number of peptide matches returned per peptide.

Recent advances in proteomic technologies have enabled the mechanistic understanding of a diverse range of complex lignocellulose processing systems. As a result, the secretomes (comprising proteins actively secreted into the extracellular space) of various filamentous fungi have been well characterised on lignocellulosic substrates, typically containing a high proportion of carbohydrate-active enzymes (CAZymes).

For instance, LC-MS/MS based approaches have shown filamentous ascomycete fungi (e.g. *Aspergillus niger*, *Trichoderma reesei*) to secrete large quantities of cellulolytic and hemicellulolytic enzymes during growth on lignocellulose, enabling deconstruction of insoluble cell wall components (e.g. cellulose, matrix polysaccharides) and their consequent metabolism (Adav et al., 2012; Borin et al., 2015). The vast majority of such secretome studies interrogate soluble proteins only, typically those found in the culture supernatant during SmF (Brandt et al., 2021; Grandmontagne et al., 2021). The same approach is also adopted by functional studies comparing fungal secretomes detected during growth on lignocellulose under SmF and SSF, such as those of the filamentous fungus *Thermomyces lanuginosus* (Shi et al., 2020). However, many of the secreted extracellular proteins remain tightly bound to the substrate during culture by specialised carbohydrate-binding modules (CBMs) (Alessi et al., 2017). Therefore, analysis of only the soluble protein fraction fails to reveal the bound (and therefore insoluble) proteins, leading to an incomplete assessment of functional biomass degradation. To overcome this, a recent study recovered bound fraction protein from *T. reesei* cultures on a range of softwood substrates by washing the solid biomass with Tween (non-ionic detergent used for protein extraction), prior to LC-MS/MS analysis (Novy et al., 2021). However, this approach relied solely on the use of a mild detergent (Tween) to break enzyme-substrate interactions and was unlikely sufficient to robustly capture proteins particularly tightly bound; a limitation addressed by a previously described biotin tagging approach in which sulfo-NHS-SS-biotin (water soluble but cell membrane impermeable) is used to non-specifically tag lysine residues and terminal amino groups of bound fraction proteins (Alessi et al., 2017). Biotin-tagged protein is then extracted, precipitated and affinity enriched by streptavidin purification (‘pull down’), leveraging the high binding affinity of avidin for biotin. Bound fraction proteins are then analysed by LC-MS/MS alongside the soluble fraction, enabling a more robust and complete analysis of the total secretome (soluble and insoluble) at a given time point.

Functional (protein-level) characterisation of fungal growth on lignocellulose is essential to gain an understanding of the enzymatic mechanisms via which *P. putredinis* NO1 improves the digestibility of wheat straw by BSFL, as observed in chapters 3 and 4. In this chapter, a comparative exo-proteomic study of *P. putredinis* NO1 growth on wheat straw under SmF and SSF was conducted using a biotin-tagging approach, in which both the soluble and insoluble secretomes were elucidated and interrogated. The analyses of *P. putredinis* NO1 secretomes described in this chapter reveal the extracellular CAZymes most likely responsible for the changes in cell wall composition observed in chapter 5 and, thus, those underpinning the improved digestibility of lignocellulose by BSFL.

6.2 Methods

6.2.1 Quantification of total soluble protein

Cultures (500 mL) were set up in two litre shake flasks in which *P. putredinis* NO1 was grown on wheat straw under SmF (1.5% w/v) and SSF over 21.5 days. Soluble protein was harvested in triplicate at various time points (days 3.5, 7, 14 and 21.5) from culture supernatants (50 mL) under SmF, or biomass aliquots (12.5 g, wet weight) under SSF. Biomass samples harvested under SSF were mixed with 21.5 mL dH_2O and mixed on a rotator (SB3, Stuart) for 20 minutes (4°C). All samples (SmF and SSF) were then centrifuged at 45,000 x g (20 minutes, 4°C) and the supernatants filter sterilised through 0.22 µm syringe-driven PES filter units. For quantification of total soluble protein within the cultures, soluble protein samples were analysed by Bradford assay and their concentrations (µg/mL) extrapolated using either the total culture volume (SmF; mL) or dry mass (SSF; g).

6.2.2 Acquisition of the submerged fermentation proteomic dataset

The SmF proteomic dataset was obtained from an experiment conducted by Dr Nicola Oates in which *P. putredinis* NO1 was grown on wheat straw under SmF (1.5% w/v). Proteins were extracted from the soluble supernatant and insoluble bound fraction at days 2, 3.5, 10, 14 and 21.5, then analysed by LC-MS/MS using the methodology described herein for the SSF cultures.

6.2.3 Biomass processing for protein extractions

To process biomass under SSF for protein extractions, cultures (500 mL) were set up in two litre shake flasks in which *P. putredinis* NO1 was grown on wheat straw over a 28-day time course. Biomass was harvested in biological triplicate at various time points (days 3.5, 7, 14, 21.5, 28) and homogenised by manual mixing under sterile conditions. Aliquots of homogenised biomass (2 g per biological replicate, wet weight) were taken forward for protein extractions.

6.2.4 Protein extractions for LC-MS/MS

At each time point, the soluble and insoluble protein fractions were extracted simultaneously. For extraction of the soluble fractions, biomass aliquots (2 g) were washed twice with ice-cold 0.5X phosphate buffered saline (PBS; 25 mL), with centrifuge spins at 4500 rpm (five minutes, 4°C) between washes (Multifuge 3S-R, Heraeus). Supernatants from the first washes were centrifuged at 12,000 x g (20 minutes, 4°C) using a Sorvall SS-34 rotor (Evolution RC centrifuge, Sorvall), filter sterilised through 0.22 µm syringe-driven PES filter units and aliquoted (2 x 7.5 mL). Protein was then precipitated with five volumes of ice-cold 100% acetone (pre-chilled at -20°C) and incubated at -20°C for approximately 22 hours.

Precipitated proteins were centrifuged at 4500 rpm (20 minutes, 4°C) and the pellets washed twice with ice-cold 80% acetone (pre-chilled at -20°C), with vortexing and centrifuge spins at 4500 rpm (ten minutes, 4°C) between washes. Protein pellets were then air-dried under snorkel extraction, re-suspended in 0.5X PBS (1 mL), transferred to Eppendorf tubes (1.5 mL), snap-frozen and stored at -80°C.

For extraction of the insoluble (biomass bound) fractions, following the initial two PBS washes, solid biomass samples were resuspended in ice-cold 0.5X PBS (19 mL) and proteins labelled with EZ-link-sulfo-NHS-SS-biotin (10 mM). Biomass samples were incubated on a rotator (SB3, Stuart) at 4°C for one hour, then centrifuged at 4500 rpm (ten minutes, 4°C) and the supernatant discarded. The biotinylation reaction was quenched with Tris-HCl (pH 8, 25 mL) and incubated on a rotator at 4°C for 30 minutes. Biomass samples were then centrifuged at 4500 rpm (ten minutes, 4°C) and excess Tris-HCl and biotin removed by two washes with ice-cold 0.5X PBS (20 mL), with centrifuge spins at 4500 rpm (five minutes, 4°C) between washes. Protein was extracted with 2% (w/v) SDS (10 mL, pre-heated to 60°C) and incubated on a rotator at room temperature for one hour. Biomass samples were centrifuged at 4500 rpm (ten minutes, 4°C) and the supernatant (containing biotin-labelled protein) aliquoted (2 x 5 mL). Protein was then precipitated with five volumes of ice-cold 100% acetone (pre-chilled at -20°C) and incubated at -20°C for approximately 19 hours. Precipitated proteins were centrifuged at 4500 rpm (20 minutes, 4°C) and the pellets washed twice with ice-cold 80% acetone (pre-chilled at -20°C), with vortexing (to remove residual SDS) and centrifuge spins at 4500 rpm (10 minutes, 4°C) between washes. Protein pellets were then air-dried under snorkel extraction, resuspended in 0.1% SDS/1X PBS (1 mL) and filter sterilised through 0.22 µm syringe-driven PES filter units.

6.2.5 Clean-up of the insoluble protein fractions

HiTrap Streptavidin HP columns (1 mL, GE Healthcare #17-5112-01) were washed and equilibrated with 0.1% SDS/1X PBS (10 mL) using a peristaltic pump at a flow rate of 1 mL min^{-1} (Econo Pump, Bio-Rad). Protein aliquots (insoluble fractions) were pooled (2 mL per biological replicate), manually loaded onto equilibrated columns using a syringe (1 mL) and incubated at 4°C for one hour to aid sample binding. The columns were washed again with 0.1% SDS/1X PBS (10 mL) using a peristaltic pump at a flow rate of 1 mL min^{-1}, then a syringe (1 mL) used to load 50 mM 1,4-dithiothreitol (DTT)/0.5X PBS (1 mL). Columns were sealed with stoppers and incubated at 4°C for approximately 19 hours, then proteins eluted in 50 mM DTT/0.5X PBS (1 mL). Columns were incubated at 4°C for a further hour, after which proteins were eluted again in 50 mM DTT/0.5X PBS (1 mL). Throughout the purification, various samples (pre-column, start of SDS/PBS wash, end of SDS/PBS wash, DTT flow-through, elution 1 and elution 2) were taken for sodium dodecyl sulfate-polyacrylamide gel electrophoresis (SDS-PAGE) analysis.

6.2.6 Protein preparation for LC-MS/MS

For label-free LC-MS/MS, proteins (soluble and insoluble fractions) were desalted by buffer exchange into dH_2O using Zeba Spin columns (5 mL, 7k MWCO, Thermo Scientific) according to manufacturer's protocol, with an additional elution step using dH_2O (2 mL) to flush out any residual protein bound to the columns. Buffer exchanged proteins were then snap-frozen, lyophilised, resuspended in dH_2O (70 µL) and stored at -80°C. To prepare samples for LC-MS/MS, proteins (26 µL) were solubilised in NuPAGE sample buffer (10 µL) and NuPAGE sample reducing agent (4 µL), then incubated at 70°C for ten minutes to denature. Samples (40 µL) were loaded in duplicate into NuPAGE 10% Bis-Tris gels (Life Technologies) and ran for six minutes at 200 V. Gels were washed three times with dH_2O, stained with SafeBLUE protein stain overnight (18 hours), then de-stained with dH_2O for four hours. Stained gels were sliced into 2 mm^2 fragments and submitted to Dr Adam Dowle (University of York Technology Facility) for LC-MS/MS analysis.

6.2.7 Proteomic analysis by LC-MS/MS

Protein samples were subjected to reduction and alkylation with iodoacetamide, then in-gel digested with trypsin. After peptide extraction, samples were acquired over three-hour acquisitions on an Orbitrap Fusion mass spectrometer (Thermo Scientific). Briefly, peptides were eluted from a 50 cm PepMap column (Thermo Scientific) driven by a UPLC M-Class system (Waters Corporation), onto the Orbitrap Fusion (data dependent acquisition mode). LC-MS chromatograms were imported, peak-picked and aligned within Progenesis QI software (Waters Corporation), before exporting a concatenated MS2 peak list for database searching through Mascot against *P. putredinis* NO1's unique protein database (79,943 sequences) and a database of common proteomic contaminates (118 sequences). Peptide spectra matches were adjusted to a 5% false discovery rate as assessed empirically against a reverse database search. Peptide identifications were imported into Progenesis QI software, associated with mass spectrometry precursor ion areas and mapped between samples. A 'Top3' approach was used for quantification, in which the three best responding peptides were used as a proxy for relative quantification between proteins and samples. Data were not normalised as different amounts of protein were expected between samples. Following ID mapping, data were further filtered to require a minimum of two peptides per protein, and contaminant matches removed. This yielded 986 quantified proteins (soluble and insoluble fractions, combined; constituting the SSF proteome) on which a multi-way ANOVA was applied in Progenesis QI (H_0 = any given protein is of equal abundance between all sample groups). Results were then exported, and the Benjamini-Hochberg multiple test correction applied to generate q-values. The SmF proteomic dataset contained 996 quantified proteins (soluble and insoluble fractions, combined).

6.2.8 Secretome identification and annotation

To identify proteins actively secreted into the extracellular matrix (constituting the secretome), all proteins within the proteomic datasets (SSF and SmF; 1287 unique proteins, combined) were submitted to DeepLoc (Almagro Armenteros et al., 2017) and BUSCA (Savojardo et al., 2018) to predict their subcellular localisations. Following this, proteins predicted to be localised in the plasma membrane or extracellular matrix were submitted to TargetP (Almagro Armenteros et al., 2019a) and SignalP (Almagro Armenteros et al., 2019b) for the prediction of signal peptides (short N-terminus amino acid sequences that target proteins into or across membranes). Those predicted to contain a signal peptide were designated as classically secreted proteins. Plasma membrane or extracellular proteins lacking detectable signal peptides were then submitted to SecretomeP (Bendtsen et al., 2004) to predict additional signal peptides. Proteins predicted not to contain a signal peptide by SecretomeP but with neural network scores ≥ 0.5 were designated as non-classically secreted (i.e. via an alternative secretory pathway) and combined with proteins identified as classically secreted. These were then submitted to TMHMM (Krogh et al., 2001) to predict transmembrane helices (and therefore non-target transmembrane proteins). Proteins with greater than one transmembrane helix were removed which yielded a secretome dataset containing 328 unique proteins (SSF and SmF, combined). All proteins within the secretome dataset were annotated using the CAZyme database via dbCAN (Huang et al., 2018). Annotations with an *E*-value threshold of ≤ 1e−5 were accepted, and proteins annotated as glycosyl transferase (GT) families were filtered. This then yielded two filtered secretome datasets, with one containing 267 annotated proteins identified within SSF cultures and the other containing 266 annotated proteins identified within SmF cultures. Proteins were then re-associated with their relative mol% values, creating temporal abundance profiles.

6.2.9 Statistical analysis

A range of analyses were conducted on SmF and SSF secretomes to explore their diversity, composition and temporal profiles. Non-parametric beta diversity analysis (Bray-Curtis dissimilarity, between communities) was conducted to compute dissimilarity indices for the secretomes, which were analysed within principal coordinate analysis (PCoA). One-way analysis of similarities (ANOSIM) was conducted with 999 permutations on Bray-Curtis indices to determine the strength of the groupings. Alpha diversity analysis (within a single community) was conducted using the dominance index. Diversity in the number of CAZyme families between the secretomes was assessed by the non-parametric Kruskal-Wallis test using the SciPy package (Virtanen et al., 2020). Euclidean clustering of annotated CAZyme proteins, as well as protein abundance distributions, were constructed using the seaborn package (Waskom, 2021), and all normality assessments were made by the Shapiro-Wilk test using SciPy.

6.3 Results

6.3.1 Total soluble protein production

Bradford assays were performed on soluble protein samples harvested from *P. putredinis* NO1 cultures on wheat straw under SmF and SSF. Protein concentrations (derived from samples in triplicate) were then extrapolated using either the total culture volume (SmF) or dry mass (SSF) for quantification of total soluble protein production within the cultures over time (Figure 6.1).

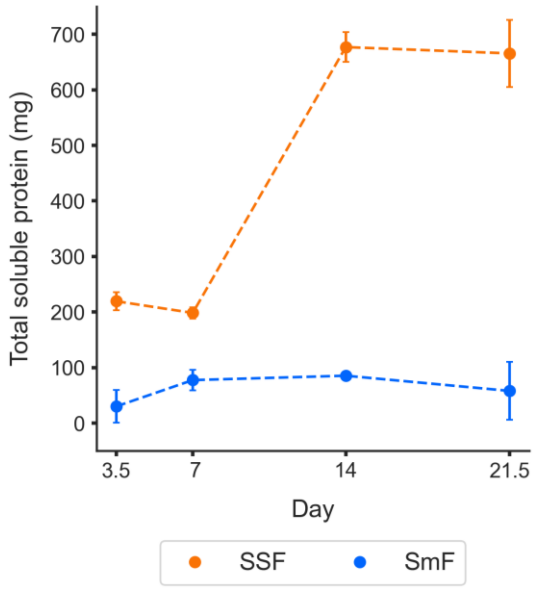

Figure 6.1. Total soluble protein production by *P. putredinis* NO1 during growth on wheat straw under SmF and SSF. Graph shows the total amount of soluble protein (mg) recoverable from *P. putredinis* NO1 cultures on wheat straw under SmF and SSF over 21.5 days. For SmF, protein was recovered from 50 mL samples of culture supernatant, while under SSF, protein was recovered from 12.5 g samples of biomass (wet weight). Data are means ± SD (n = 3).

Total soluble protein production by *P. putredinis* NO1 on wheat straw was markedly greater under SSF at all time points. After an initial lag phase during the first week (198.4-219.5 mg), total soluble protein increased sharply during the second week with a peak at day 14 (676.9 mg). In contrast, under SmF, soluble protein showed a small increase between days 3.5 (30.2 mg) and 7 (77.6 mg), before plateauing at day 14 (85.4 mg) and falling again by day 21.5 (58.1 mg).

6.3.2 Protein extraction and preparation for LC-MS/MS

Proteins (soluble and insoluble fractions) were extracted from *P. putredinis* NO1 cultures on wheat straw under SSF. Following affinity enrichment by streptavidin purification of the insoluble biotin-labelled fractions, protein presence was confirmed by SDS-PAGE (Figure 6.2).

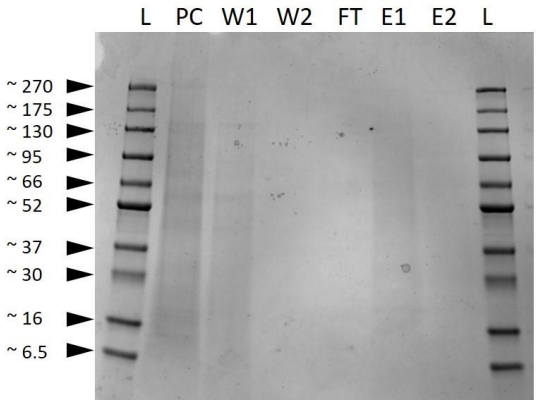

Figure 6.2. SDS-PAGE of protein extraction. Exemplar SDS-PAGE of samples taken throughout affinity enrichment of the biotin-labelled insoluble protein fraction (day 28, SSF). The exemplar replicate shows protein present prior to its application on the column (PC), with the majority recovered in the first elution fraction (E1) and a little lost at the beginning of the SDS/PBS wash (W1). L = ladder, PC = pre-column, W1 = start of SDS/PBS wash, W2 = end of SDS/PBS wash, FT = DTT flow-through, E1 = elution 1, E2 = elution 2.

Following buffer exchange, all protein fractions (soluble and insoluble) were run into NuPAGE Bis-Tris gels (Figure 6.3) prior to in-gel digestion, peptide extraction and analysis by LC-MS/MS.

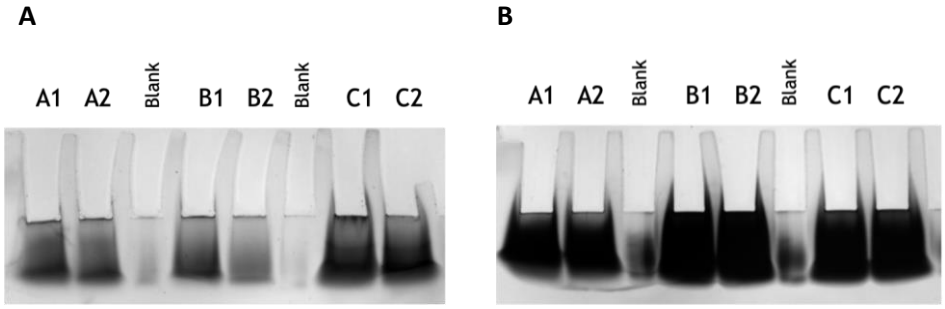

Figure 6.3. Short run SDS-PAGE of protein extractions in preparation for LC-MS/MS. Exemplar SDS-PAGE of proteins extracted from insoluble fractions at day 21 (**A**) and soluble fractions at day 28 (**B**) of SSF cultures. Biological replicates (A-C) were run in duplicate, each separated by a blank lane.

6.3.3 Proteomic analysis by LC-MS/MS

LC-MS/MS analysis of *P. putredinis* NO1 cultures on wheat straw yielded proteomes containing 986 quantified proteins under SSF and 996 quantified proteins under SmF (soluble and insoluble fractions). All unique proteins were passed through a bioinformatic pipeline to identify those actively secreted into the extracellular matrix, yielding 328 unique proteins. These were then passed through a second bioinformatic pipeline (using dbCAN) to annotate proteins with homology to known CAZyme domains and filtered to remove those annotated as GTs. Of the 986 proteins identified and quantified under SSF, 267 (27.1%) were predicted to be extracellular (SSF secretome, both fractions), of which 122 (45.7%) contained at least one identifiable CAZyme or CBM domain. Of the 996 proteins identified and quantified under SmF, 266 (26.7%) were predicted to be extracellular (SmF secretome, both fractions), of which 121 (45.5%) contained at least one identifiable CAZyme or CBM domain. All extracellular proteins within SSF and SmF secretomes were then reassociated with their relative abundance values (molar %), creating temporal CAZyme profiles for comparative analyses.

6.3.4 Bray-Curtis dissimilarity

The degree of dissimilarity between CAZyme profiles within SSF and SmF secretomes derived from *P. putredinis* NO1 cultures on wheat straw was first investigated. Bray-Curtis dissimilarities were calculated via a matrix of vertices containing the sum molar abundance for each CAZyme family identified within each technical replicate. The Bray-Curtis dissimilarity is primarily used within ecology to quantify the differences in species populations between sites of equal size.

Here, it was used to quantify the differences in CAZyme family abundance between the soluble and insoluble fractions of SmF and SSF secretomes, with values explored within PCoA (Figure 6.4); an ordination technique used to summarise multidimensional datasets (e.g. Bray-Curtis dissimilarity matrices) in low dimensional space, revealing intrinsic patterns (Pielou, 1984).

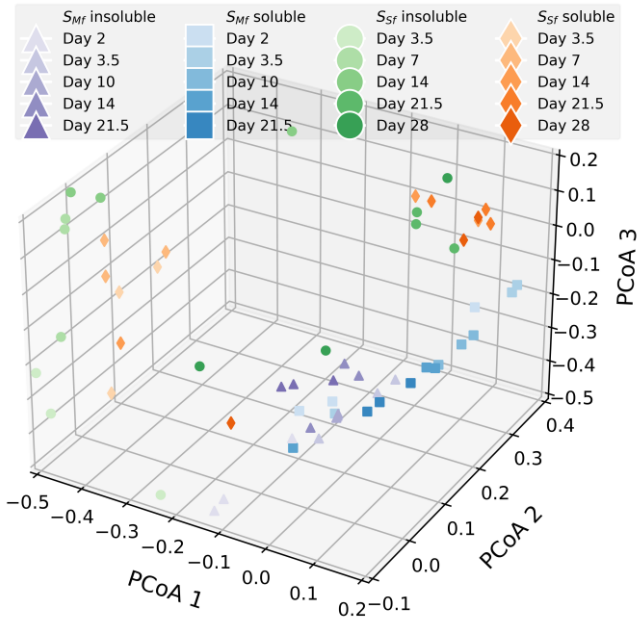

Figure 6.4. PCoA with Bray-Curtis dissimilarity matrix. Data includes all proteins with homology to CAZyme domains within soluble and insoluble secretomes (SmF and SSF). Protein fraction (soluble and insoluble) is colour coded and time point is shaded by colour hue (n = 3).

PCoA with Bray-Curtis dissimilarity showed distinct separation of CAZyme profiles between SmF and SSF secretomes, indicating their comparative dissimilarity in both family composition and relative abundance. The first, second and third axes captured 27.8%, 21.5% and 8% of the total variation within the dissimilarity matrix, respectively. Temporal changes were observed in all independent fractions, though these were greater and showed a more unidirectional shift within SSF secretomes. Particularly for the soluble fractions, CAZyme profiles within SSF secretomes appeared relatively similar to one another early in the time course (e.g. days 3.5 and 7) as well as later (e.g. days 21.5 and 28), while the greatest dissimilarity was observed between mid-stage time points (e.g. days 7 and 14/21.5). In comparison, CAZyme profiles within the SmF secretomes showed less divergence over time, and as such directional temporal shifts were less apparent. Instead, secretome fractions clustered together, particularly the insoluble fractions, yet distantly from the SSF secretome fractions.

To determine the statistical strength of the groupings, ANOSIM was performed on the Bray-Curtis dissimilarity matrix; the results of which verified fermentation state (SmF/SSF) and time to reveal significant dissimilarity between CAZyme profiles (state – $R = 0.48$, $p < 0.001$; time – $R = 0.33$, $p < 0.001$). In contrast, CAZyme profiles within the soluble and insoluble fractions showed no significant dissimilarity under both SmF and SSF, instead indicating their relative similarity (fraction – $R = 0.06$, $p = 0.102$).

6.3.5 Carbohydrate-active and carbohydrate-binding classes

Having established dissimilarities between CAZyme profiles within SmF and SSF secretomes over time, extracellular proteins with homology to known CAZyme or CBM domains were grouped according to their class annotation and temporal changes in their relative molar abundances were explored in heat maps (Figure 6.5).

A

B

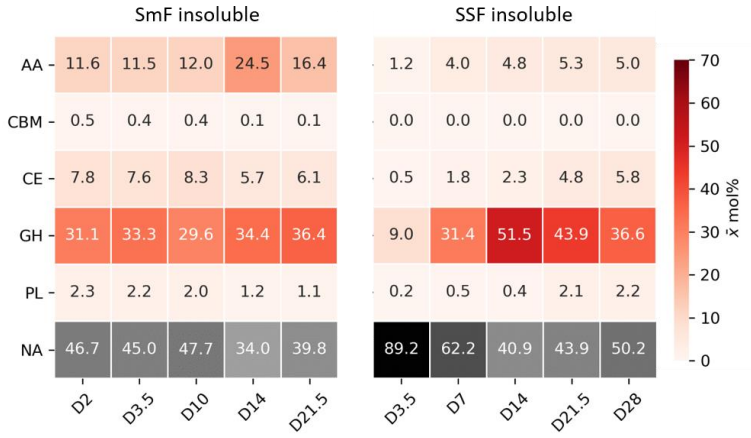

Figure 6.5. Temporal profiles of the carbohydrate-active and carbohydrate-binding classes within SmF and SSF secretomes. Heat maps show relative molar abundance of CAZyme and CBM classes detected within soluble (**A**) and insoluble (**B**) fractions of SmF and SSF secretomes. AA = auxiliary activity; CE = carbohydrate esterase; GH = glycoside hydrolase; PL = polysaccharide lyase; NA = proteins predicted to be extracellular with no homology to known CAZyme or CBM domains. Data are means (n = 3).

Proteins that contained at least one identifiable CAZyme or CBM domain contributed significant proportions of all fractions (soluble and insoluble) over time, typically between 37.8% and 66.9%, with an overall minimum of 10.8% (day 3.5, SSF insoluble fraction) and maximum of 81.1% (day 21.5, SSF soluble fraction). Under SmF, the contribution of CAZyme or CBM proteins within the soluble fraction showed a gradual decline from 66.9% (day 3.5) to 55.3% (day 21.5). In contrast, under SSF, the reverse trend was observed, in which the proportion of CAZyme or CBM proteins increased gradually from 43.4% to a maximum of 81.1% over the same duration.

The glycoside hydrolase (GH) class was the most abundant CAZyme class identified at all time points and across all fractions, though showed different temporal trends under SmF and SSF. This was particularly evident within the soluble fraction, in which under SmF, abundance of the GH class peaked at day 3.5 (49.8%) and declined thereafter, whereas under SSF, its abundance increased over time and peaked at day 21.5 (67.7%). Similarly, under SSF, abundance of the carbohydrate esterase (CE) class increased gradually over time and peaked at day 28 in both fractions (soluble = 9.7%, insoluble = 5.8%), while under SmF, CE abundance increased initially but peaked earlier in the time course at day 10 (soluble = 9.5%, insoluble = 8.3%), then declined. The auxiliary activity (AA) class, however showed the reverse trend, in which its abundance under SmF (soluble and insoluble fractions) remained relatively constant between days 2 and 10, then increased, particularly within the insoluble fraction (day 10 = 12%, day 14 = 24.5%, day 21 = 16.4%). Abundance of the AA class under SSF showed different temporal trends between soluble and insoluble fractions, with its abundance in the soluble fraction increasing initially (day 3.5 = 9.3%, day 7 = 10.3%), then declining, in contrast to that observed under SmF. Temporal AA profiles under SSF were also in stark contrast to those observed for the GH and CE classes.

Excluding the CBM class which contributed a negligible proportion of the SmF and SSF secretomes (≤ 0.5% at all time points), the polysaccharide lyase (PL) class was the least abundant CAZyme class detected but showed different temporal trends in all fractions. Under SmF, its abundance within the soluble fraction remained relatively constant over time (2.1-2.7%), while in the insoluble fraction its abundance declined gradually (temporal minimum = 1.1%, day 21.5). In contrast, under SSF, abundance of the PL class within the insoluble fraction increased over time, with a particularly sharp rise between day 14 (0.4%) and day 21.5 (2.1%), while in the soluble fraction its abundance increased early on, peaking at day 14 (4.0%), but then decreased sharply between day 21.5 (3%) and day 28 (0.6%).

6.3.6 Carbohydrate-active enzyme family level diversity

Bioinformatic analysis enabled protein annotation to both CAZyme class and family levels. Under SmF, secretome fractions contained a significantly greater number of CAZyme families (n = 48 ± 0) in comparison to those under SSF (n = 45.6 ± 2.49), corroborated by the results of a Kruskal-Wallis non-parametric test (H = 51.79, DF = 1, $p < 6.15 \times 10^{-13}$).

6.3.7 Glycoside hydrolase class

To explore the temporal profiles of the 12 most abundant families within the GH class (the most abundant CAZyme class detected within all secretome fractions under SmF and SSF), heat maps were plotted to explore the changes in their relative molar abundance over time (Figure 6.6).

A

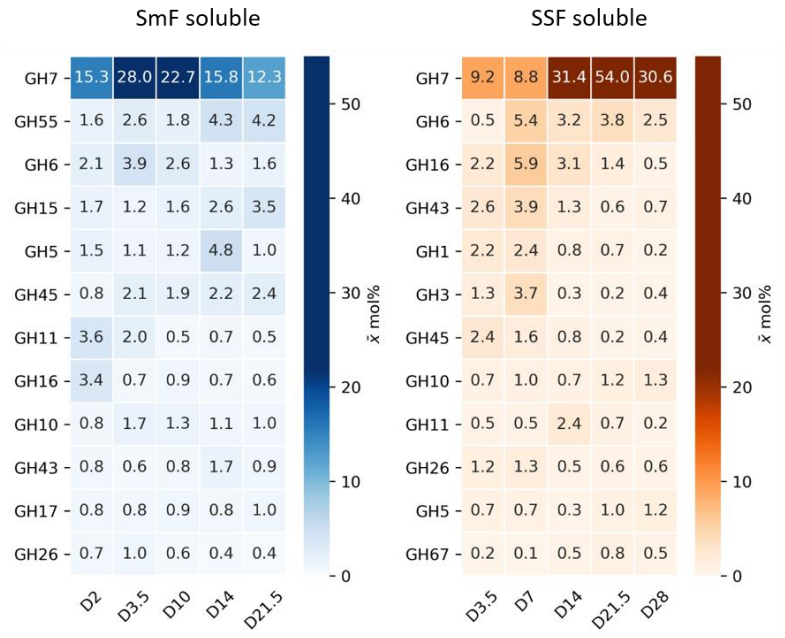

B

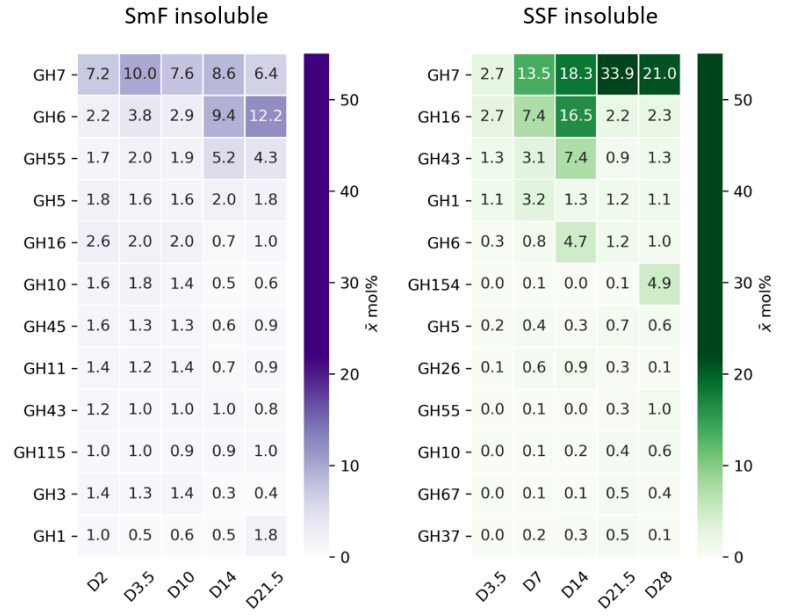

Figure 6.6. Temporal profiles of the 12 most abundant glycoside hydrolase families within SmF and SSF secretomes. Heat maps show relative molar abundance of the top 12 glycoside hydrolase families detected within soluble (**A**) and insoluble (**B**) fractions of SmF and SSF secretomes. Data are means (n = 3).

The GH7 family was the most abundant detected within all secretome fractions and is most associated with reducing end-acting cellobiohydrolase (exoglucanase) activity. Its temporal profiles mirrored those observed for the total GH class, in which its abundance under SmF peaked at day 3.5 (soluble = 28%, insoluble = 10%) and then declined, whereas its abundance under SSF increased gradually over time and peaked at day 21.5; at which point the GH7 family contributed over half of the total soluble secretome (54%) and over a third of the total insoluble secretome (33.9%).

Within the soluble fraction under SSF, the second (GH6), third (GH16), fourth (GH43), fifth (GH1) and sixth (GH3) most abundant families of the GH class showed the same temporal trends; increasing initially to peaks at day 7 (5.4%; 5.9%; 3.9%; 2.4% and 3.7%, respectively), then declining sharply. The GH6 family is associated primarily with non-reducing end-acting cellobiohydrolase (exoglucanase) activity, in contrast to the reducing end-acting activity of the GH7 family, while other activities included β-glucosidase (GH1/GH3), β-xylosidase (GH43/GH3) and non-reducing end α-L-arabinofuranosidase (GH43/GH3). In contrast, under SmF, in equivalent order of abundance within the soluble fraction were the GH55, GH6, GH15, GH5 and GH45 families, whose temporal profiles were more sporadic and peaked at different points throughout the time course (GH55 = day 14, 4.3%; GH6 = day 3.5, 3.9%; GH15 = day 21.5, 3.5%; GH5 = day 14; 4.8%). Interestingly, only the GH6 and GH7 families were shared between the top six most abundant families identified within soluble fractions under SmF and SSF, and both with greater overall abundances under SSF. Other activities identified within the soluble fraction under SmF included exoglucanase (GH55), α-glucosidase (GH15) and endoglucanase (GH5), as well as endoxylanase activity (GH11) whose abundance quickly declined along with the GH16 family after peaking at day 2 (3.6% and 3.4%, respectively).

Within the insoluble fraction under SSF, the second (GH16), third (GH43) and fifth (GH6) most abundant families shared the same temporal trends, increasing sharply during the second week in particular and peaking at day 14 (GH16 = 16.5%, GH43 = 7.4%, GH6 = 4.7%), then quickly declining. The fourth most abundant family (GH1) showed a similar trend though shifted earlier in time, with abundance peaking at day 7 (3.2%). The GH154 family, most associated with β-glucuronidase activity, remained at extremely low abundance (≤ 0.1%) throughout the time course until day 28 at which it rose sharply (4.9%). In comparison, under SmF, abundance of the second most abundant family (GH6) was greater but remained relatively stable for the first ten days, then increased thereafter, peaking at day 21.5 (12.2%). The third most abundant family (GH55) family within the insoluble fraction showed a similar trend but peaked at day 14 (5.2%), while all other families were present at low abundances (≤ 2.6%) throughout the time course.

6.3.8 Auxiliary activity class

To explore the temporal profiles of the six most abundant families within the AA class (the second most abundant CAZyme class detected within all secretome fractions under SmF and SSF), bar charts were plotted to explore the changes in their relative molar abundance over time (Figure 6.7).

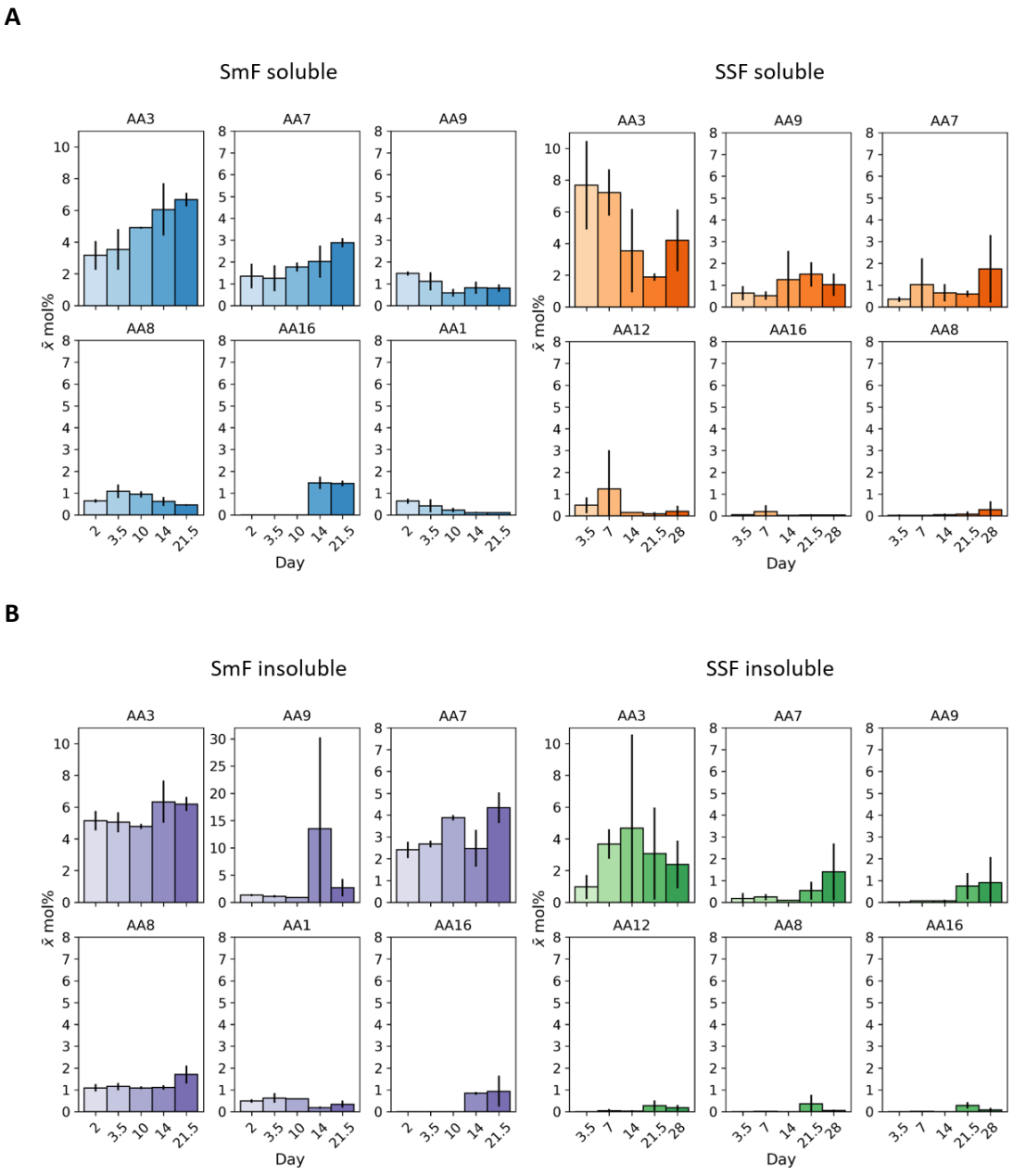

Figure 6.7. Temporal profiles of the six most abundant auxiliary activity families within SmF and SSF secretomes. Bar charts show relative molar abundance of the top six auxiliary activity families detected within soluble (**A**) and insoluble (**B**) fractions of SmF and SSF secretomes. Data are means ± SD (n = 3).

The AA3 family was the most abundant detected within all secretome fractions and comprises glucose-methanol-choline (GMC) oxidoreductases, possessing activities such as cellobiose dehydrogenase (subfamily 1), aryl alcohol and glucose oxidase/dehydrogenase (subfamily 2). They catalyse a wide range of redox reactions during lignocellulose deconstruction and form metabolites, such as hydrogen peroxide, required by other AA families (e.g. AA9). Under SSF, abundance of the AA3 family within the soluble fraction showed a general decline, with a temporal maximum of 7.7% (day 3.5) and minimum of 1.9% (day 21.5). In contrast, under SmF, the reverse trend was observed in which its abundance increased over time, with a temporal minimum of 3.2% (day 2) and maximum of 6.7% (day 21.5). Temporal profiles within the insoluble fraction also differed, in which under SSF, abundance of the AA3 family increased during the first half of the time course (peak at day 14; 4.7%) and declined during the second half, while under SmF its abundance remained relatively stable during the first ten days (4.8-5.1%), then increased (day 14 = 6.3%, day 21 = 6.2%).

Within the soluble fraction under SmF, the AA7 family was the second most abundant detected, and like enzymes within the AA3 family, its members also produce hydrogen peroxide. Its abundance profile mirrored that of the AA3 family only at lower abundance, with a temporal minimum of 1.3% (day 3.5) and maximum of 2.9% (day 21.5). The third most abundant family detected within the soluble fraction under SmF was the AA9 family, most associated with copper-dependent lytic polysaccharide monooxygenase (LPMO) activity, though its abundance declined over time (day 2 = 1.5%, day 21.5 = 0.8%). In contrast, under SSF, abundance of the AA9 family within the soluble fraction increased over time and peaked at day 21.5 (1.5%), and instead was the second most abundant family detected. The AA7 family was the third most abundant family detected within the soluble fraction under SSF and of lower abundance throughout in comparison to that observed under SmF.

Similarly, within the insoluble fractions, under SmF and SSF, the second and third most abundant families detected were either AA7 or AA9, though were present at greater abundance under SmF. The fifth most abundant family under SmF was the AA1 family, most associated with laccase activity towards phenolic substrates (e.g. lignin). Although detected at low abundance, its profile remained relatively stable over time with a temporal minimum of 0.2% (day 14). The AA1 family was also detected within the soluble fraction under SmF and showed a gradually declining trend (maximum at day 2 = 0.6%, minimum day 21.5 = 0.1%), though it did not feature within the top six most abundant families of the AA class under SSF within either fraction.

6.3.9 Carbohydrate esterase class

To explore the temporal profiles of the six most abundant families within the CE class, bar charts were plotted to explore the changes in their relative molar abundance over time (Figure 6.8).

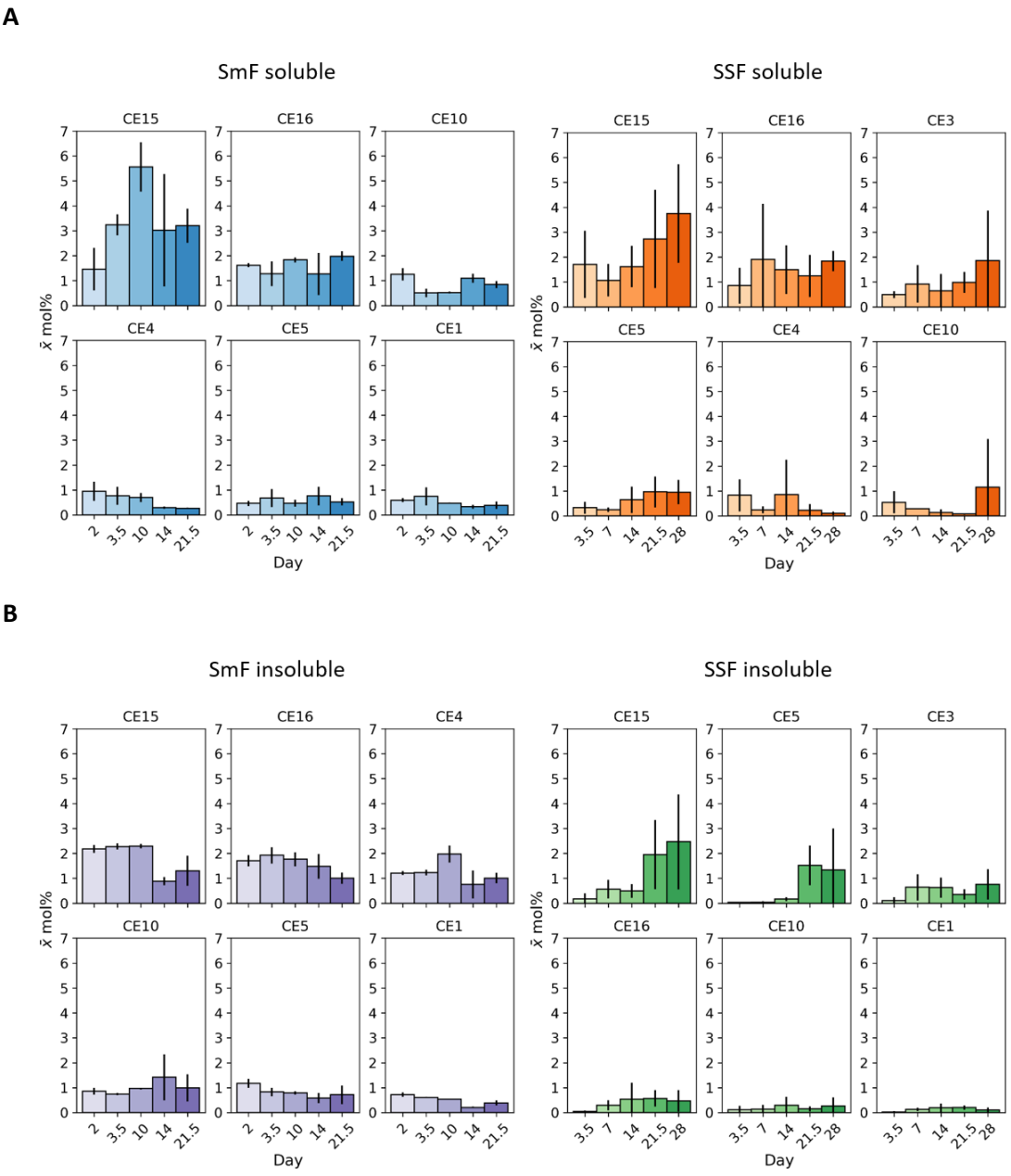

Figure 6.8. Temporal profiles of the six most abundant carbohydrate esterase families within SmF and SSF secretomes. Bar charts show relative molar abundance of the top six carbohydrate esterase families detected within soluble (**A**) and insoluble (**B**) fractions of SmF and SSF secretomes. Data are means ± SD (n = 3).

The CE15 family was the most abundant detected within all secretome fractions and is most associated with glucuronoyl esterase activity. Its temporal profiles under SSF were similar within soluble and insoluble fractions, in which its abundance increased over time and peaked at day 28 (soluble = 3.7%, insoluble = 2.5%). Under SmF, similar trends were observed within both fractions (though different to those observed under SSF), in which the abundance of the CE15 family increased initially with a peak at day 10 (soluble = 5.6%, insoluble = 2.3%), then declined.

Within the soluble fraction under SmF and SSF, the second most abundant family detected was the CE16, most associated with acetylesterase activity, whose temporal profiles fluctuated over time at a relatively low level throughout (0.9-2%). The third (CE3) and fourth (CE5) most abundant families detected under SSF showed similar temporal profiles to the CE15 family, peaking at day 28 (1.9%) and day 21.5 (1%), respectively; both most associated with acetyl xylan esterase activity. In contrast, under SmF, the CE3 family did not feature within the top six most abundant families detected within the soluble fraction, while the CE5 family fluctuated in its abundance over time (0.5-0.8%). Instead, the third and fourth most abundant families detected under SmF were the CE10 and CE4 families; the latter of which is also associated with acetyl xylan esterase activity and showed a declining trend over time (day 2 = 0.9%, day 21.5 = 0.3%). The CE1 family was the sixth most abundant family detected, not observed within the top six most abundant under SSF, which peaked at day 3.5 (0.7%) and is associated with both feruloyl esterase and acetyl xylan esterase activities.

In accordance with the soluble fraction, the second most abundant family detected within the insoluble fraction under SmF was the CE16. However, its temporal profile differed, in which its abundance peaked at day 3.5 (1.9%) and declined gradually thereafter. The third most abundant family was the CE4, whose abundance increased relatively sharply between day 3.5 (1.2%) and day 10 (2%), then declined. In contrast, under SSF, the second and third most abundant families were the CE5 and CE3, respectively. After an initial lag phase (day 3.5 = 0.1%), abundance of the CE3 family showed a relatively stable temporal profile (0.4-0.8%) while abundance of the CE5 family remained at negligible abundance during the first week (≤ 0.04%), then increased dramatically at day 21.5 (1.5%) and remained at a relatively high level at day 28 (1.3%).

6.3.10 Polysaccharide lyase class

To explore the temporal profiles of the four families detected within the PL class, bar charts were plotted to explore the changes in their relative molar abundance over time (Figure 6.9).

A

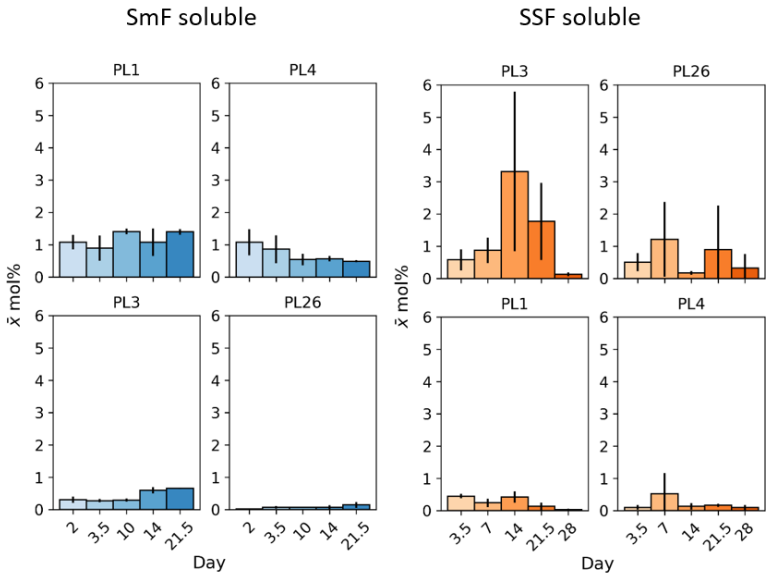

B

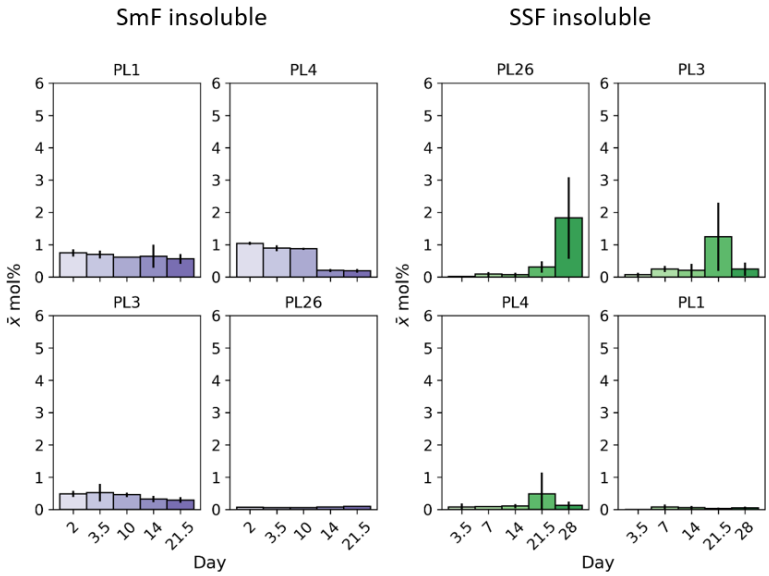

Figure 6.9. Temporal profiles of the polysaccharide lyase families within SmF and SSF secretomes. Bar charts show relative molar abundance of the four polysaccharide lyase families detected within soluble (**A**) and insoluble (**B**) fractions of SmF and SSF secretomes. Data are means ± SD (n = 3).

The same four PL families were detected within all secretome fractions though their order of relative abundance under SmF and SSF differed starkly. Activities included pectate lyase (PL1/PL3), rhamnogalacturonan endolyase (PL4) and rhamnogalacturonan exolyase (PL26). Within the soluble and insoluble fractions, under SmF, the first and second most abundant families were the PL1 and PL4 families, respectively.

The PL1 family showed a relatively constant profile that fluctuated over time (soluble = 0.9-1.4%, insoluble = 0.6-0.7%), while abundance of the PL4 family declined, with maxima at day 2 of 1.1% (soluble) and 1% (insoluble), and minima at day 21.5 of 0.5% (soluble) and 0.2% (insoluble). In contrast, under SSF, the PL3 and PL26 families were the two most abundant families detected within both the soluble and insoluble fractions, while abundance of the PL1 and PL4 families remained ≤ 0.5%. Abundance of the PL3 family within the soluble fraction increased particularly during the second week and peaked at day 14 (3.3%), then declined, while the PL26 family showed a more sporadic profile over time (0.3-1.2%). Within the insoluble fraction, abundance of the PL3 and PL26 families remained at low abundance (≤ 0.3%) until increasing sharply towards the end of the time course, peaking at day 28 (1.8%) and day 21.5 (1.2%), respectively.

6.3.11 Hierarchical clustering by Euclidean distance

Having explored the temporal trends of the most abundant families detected within individual CAZyme classes (GH, AA, CE, PL) under SmF and SSF, their profiles were hierarchically clustered using Euclidean distances to identify family-level clusters across all CAZyme classes (Figure 6.10).

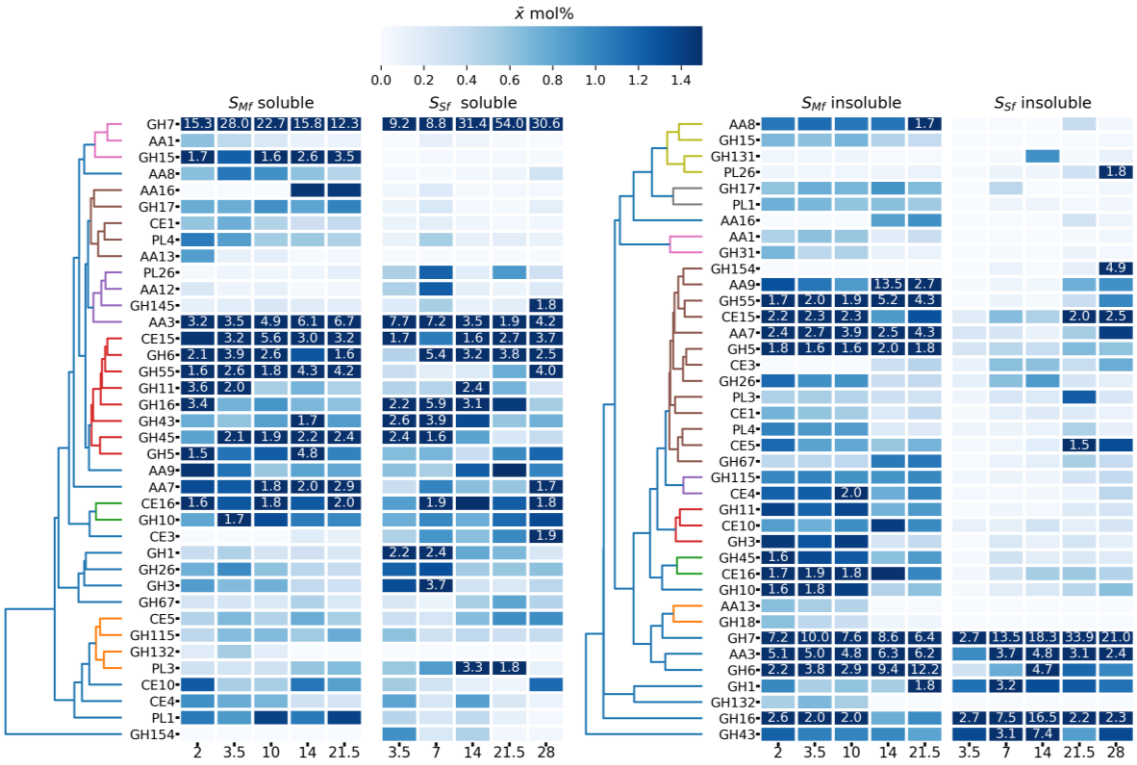

Figure 6.10. Hierarchical clustering of carbohydrate-active enzyme domains within SmF and SSF secretomes. Hierarchical clustering (Euclidean distance) was conducted on CAZyme family relative molar abundances ($\log_2$ $\bar{x}$ mol %; ≤ $1e^5$) with a change of ≥ 0.5% in at least one time point. Families exceeding the colour map limit (≥ 1.5%) are annotated with their relative molar abundance. Cluster colour threshold distance = 4.75. Data are means (n = 3).

Hierarchical clustering by Euclidean distance provided a holistic overview of the temporal abundance profiles of the major CAZyme families detected within SmF and SSF secretomes, with dominance by the GH7 family corroborated across all fractions, as well as high abundance of the AA3 family. Common to both secretomes within the soluble fractions, a core cluster containing CE15, GH6, GH55, GH11, GH16, GH43, GH45 and GH5 families was revealed, with CE15 and GH6 families highly abundant under SmF and SSF. Under SmF, the GH55 and GH5 families were more abundant, while under SSF, the GH16 and GH43 families were more abundant. In addition, a common cluster containing AA9, AA7, CE16 and GH10 families was revealed which captured the second and third most abundant AA families across soluble and insoluble fractions, as well as the second most abundant CE family (except for within the insoluble fraction under SSF). Most notably, within the insoluble fraction, a greater diversity of CAZyme domains were detected at higher abundances under SmF (e.g. cluster containing AA9, GH55, CE15, AA7 and GH5 families).

An additional cluster containing GH45, CE16 and GH10 families was also revealed, of higher abundance under SmF, as well as a cluster containing GH16 and GH43 families which were comparatively more abundant under SSF (particularly at day 14; 16.5% and 7.4%, respectively).

6.3.12 Protein abundance distribution

Having investigated CAZyme class and family-level temporal profiles, the abundance distribution of proteins detected within SmF and SSF secretomes was explored (Figure 6.11).

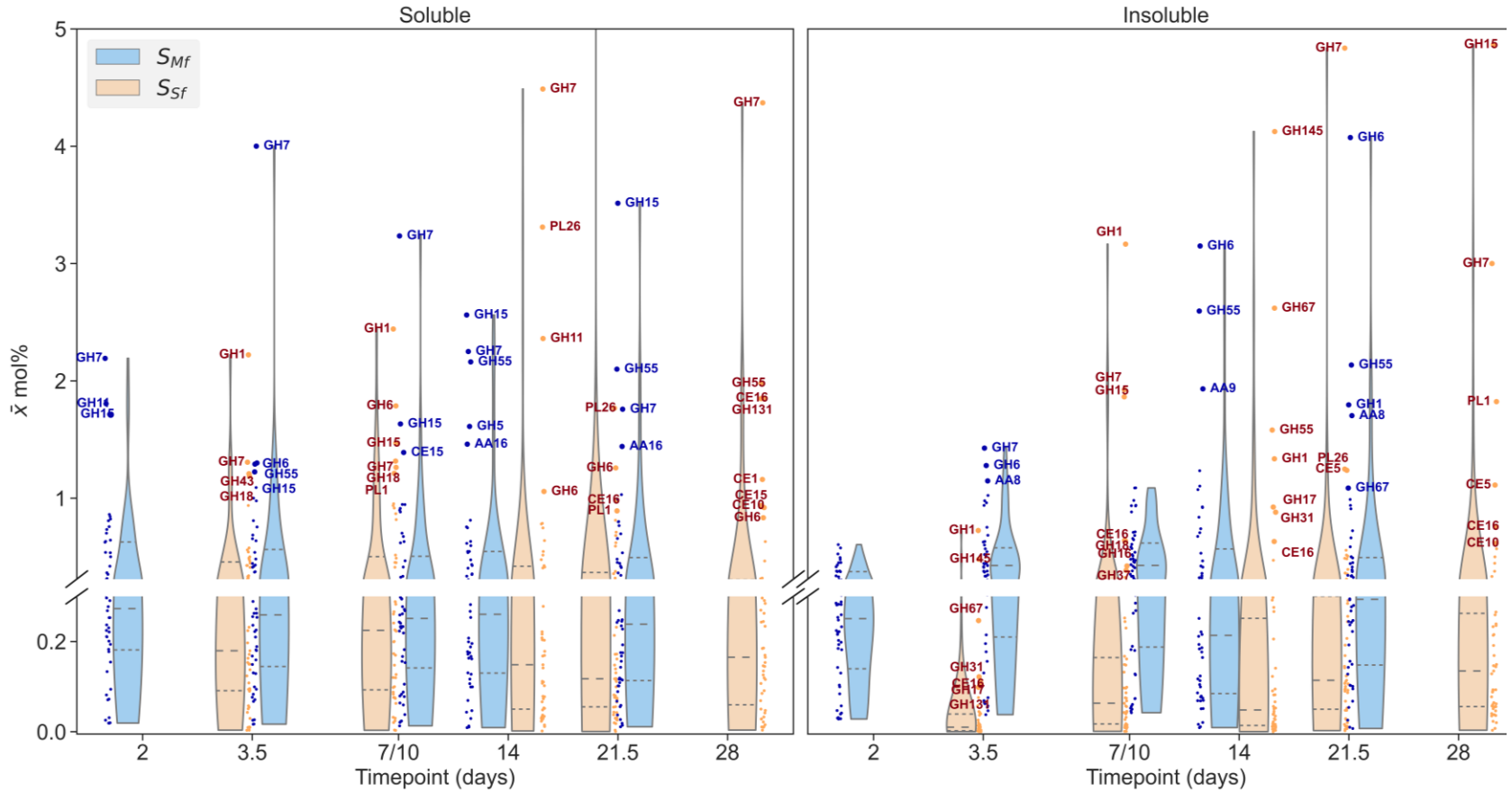

Figure 6.11. Protein abundance distribution within SmF and SSF secretomes. Violin plot of protein abundance distribution within soluble and insoluble fractions of SmF and SSF secretomes. Dashed horizontal lines within violins represent the relative (mean) molar abundance of all proteins within a given fraction ($\bar{x}$ mol %), while dotted horizontal lines represent lower (first) and upper (third) quartiles (interquartile range; IQR). Data points with CAZyme annotation (outliers, defined as third quartile + 1.5 IQR) represent the relative (mean) molar abundance of proteins within a given CAZyme family ($\bar{x}$ mol %). Proteins with no CAZyme annotation (≤ $1e^5$) were filtered. One data point was omitted for clarity (GH7, SSF soluble fraction, day 21.5; $\bar{x}$ mol % = 7.7).

Protein abundance distribution was dissimilar within SmF and SSF secretomes over time. Within soluble and insoluble fractions, SSF secretomes contained comparatively greater numbers of disproportionately abundant proteins (outliers); most notably those of the CE5, CE16, GH16, GH43 and PL26 CAZyme families. Although fewer in number, notable outliers detected within SmF secretomes included proteins of the AA8, AA16 (LPMO) and GH5 families, while outliers common to both SmF and SSF secretomes included those of the CE15, GH6 and GH7 families. Protein abundance distribution was further investigated using an alpha diversity measure (*d*; dominance, defined as 1 - Simpson's index). Within both fractions and at all time points (except for day 3.5, soluble fraction), the SSF secretomes possessed greater dominance values in comparison to the SmF secretomes. For instance, within the soluble fraction at day 21.5, the SSF secretome possessed a dominance value five-fold higher than the SmF secretome (SSF: $d = 0.45 \pm 0.06$, SmF: $d = 0.09 \pm 0.01$), at which point GH7 family proteins showed a mean molar abundance of 7.7% (the highest observed within all secretome fractions). This was driven primarily by the disproportionate abundance of two proteins (FUN_006103-T1 and FUN_006454-T1), both of which were found in high abundance across all fractions. In addition to containing comparatively greater numbers of disproportionally abundant proteins, SSF secretomes also showed comparatively greater densities of less abundant proteins at all time points within both fractions (particularly within the insoluble fraction at day 3.5).

6.3.13 GH7 family proteins

The GH7 family was the most abundant detected within all secretome fractions, with mean molar abundance peaking at day 3.5 (SmF) and day 21.5 (SSF) (Figure 6.6). To investigate the temporal profiles of individual proteins within the GH7 family, heat maps were plotted to explore the changes in their relative molar abundance over time (Figure 6.12).

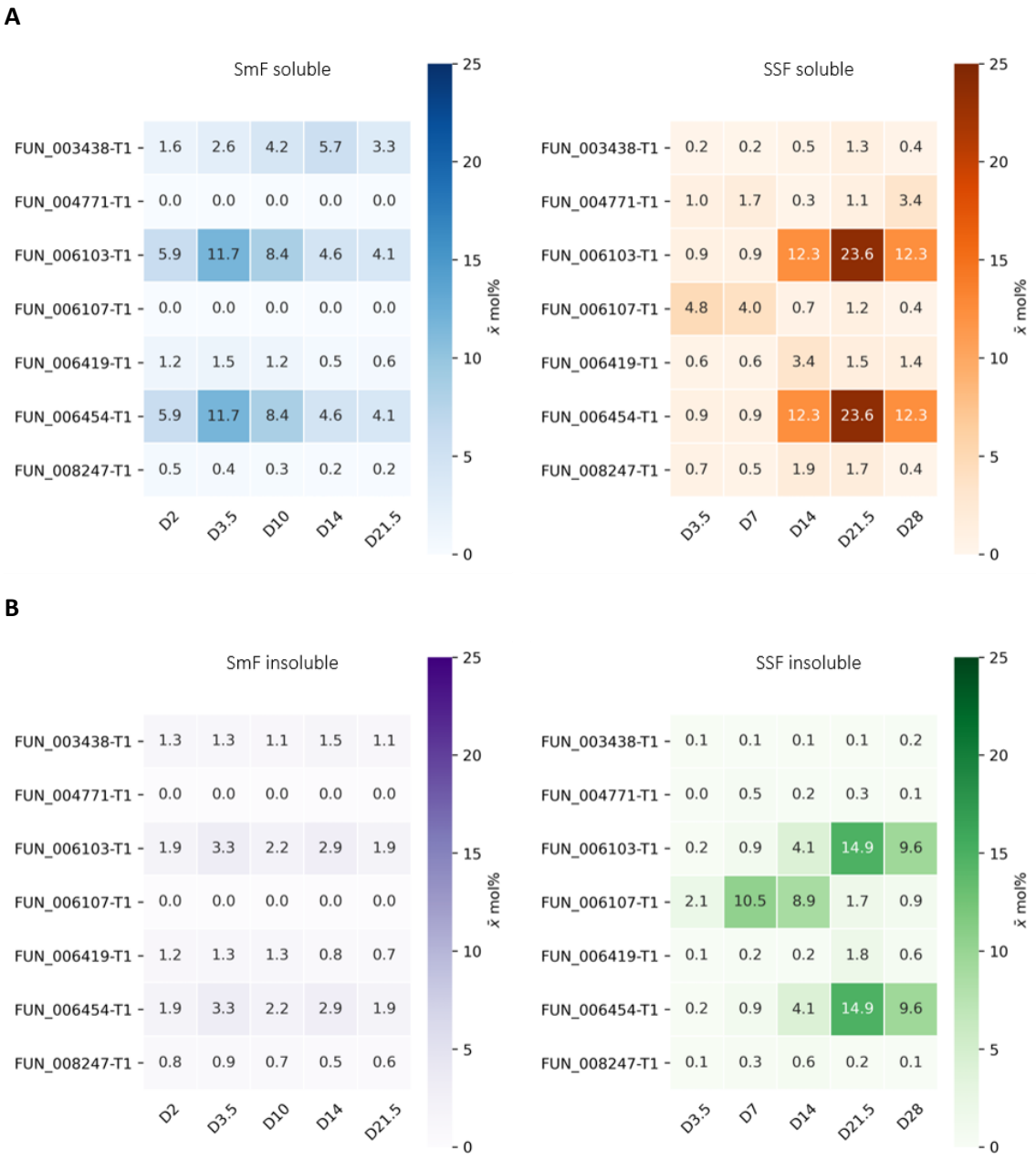

Figure 6.12. Temporal profiles of GH7 proteins within SmF and SSF secretomes. Heat maps show relative molar abundance of all GH7 family proteins detected within soluble (**A**) and insoluble (**B**) fractions of SmF and SSF secretomes. Data are means (n = 3).

All GH7 proteins detected showed homology to known reducing end-acting cellobiohydrolases within the dbCAN CAZyme database. FUN_006103-T1 and FUN_006454-T1 were the most abundant proteins detected within all secretome fractions, though showed different temporal trends under SmF and SSF. Under SmF, their abundance increased rapidly and peaked early in the time course at day 3.5 (soluble = 11.7%; insoluble = 3.3%), then declined slowly. In contrast, under SSF, their abundance increased gradually and peaked later in the time course at day 21.5 (soluble = 23.6%; insoluble = 14.9%).

FUN_004771-T1 and FUN_006107-T1 were detected only within the SSF secretome, with FUN_006107-T1 the third most abundant GH7 protein observed, peaking at day 3.5 within the soluble fraction (4.8%) and day 7 in the insoluble fraction (10.5%). In contrast, under SmF, FUN_003438-T1 was the third most abundant protein detected, showing an increasing temporal trend with a peak at day 14 (soluble = 5.7%; insoluble = 1.5%), though detected at relatively low abundance under SSF. Interestingly, the third most abundant GH7 proteins detected under SmF (FUN_003438-T1) and SSF (FUN_006107-T1) showed the reverse temporal trends to those most abundant (FUN_006103-T1 and FUN_006454-T1), while FUN_006419-T1 and FUN_008247-T1 were detected at low abundance within all fractions.

6.4 Discussion

6.4.1 *P. putredinis* NO1 secretomes are dissimilar under submerged and solid-state fermentation

Comparative exo-proteomic analysis revealed *P. putredinis* NO1 proteomes during growth on wheat straw under SmF and SSF, containing all proteins detected within soluble and insoluble bound fractions. Within the proteomes, *P. putredinis* NO1 secretomes (containing proteins predicted to be extracellular) represented similar proportions under both SmF and SSF (approximately 27%), and within these, similar proportions of proteins with at least one identifiable CAZyme or CBM domain were detected (approximately 46%). Interestingly, Bray-Curtis metrics explored within PCoA showed that the CAZyme abundance profiles within *P. putredinis* NO1 secretomes were significantly dissimilar under SmF and SSF over time, with changes observed in all protein fractions (soluble and insoluble). These temporal changes were comparatively greater and showed a more unidirectional shift under SSF, indicating that the CAZyme profiles within both fractions changed to a greater extent. This was particularly evident within the soluble fractions between days 7 and 14, following an initial phase during the first week in which CAZyme profiles remained relatively similar.

Quantification of total soluble protein production corroborated this, in which the amount of soluble protein produced by *P. putredinis* NO1 remained relatively low and stable during the first week under SSF, then increased sharply by over two-fold during the second week. These observations are in accordance with the short lag phase demonstrated in chapters 4 and 5, in which no biomass degradation was observed during the first three days under SSF, likely due to slow spore germination while the culture established under low moisture conditions (Hassouni et al., 2007). However, once the culture was established, soluble protein production increased rapidly, likely the result of enhanced cell-substrate interaction elicited by a branching hyphal network (mycelium) and accompanied by significantly dissimilar CAZyme profiles (secreted at the hyphal tips) as the culture progressed (Cunha et al., 2012).

In comparison, CAZyme profiles within the SmF secretomes showed less divergence over time, with directional temporal shifts less apparent. Instead, secretome fractions clustered together, indicating their relative similarity over time, while distantly from the SSF fractions. In contrast to growth under SSF, scanning electron microscopy (chapter section 5.3.3) revealed fungal morphology under SmF to present as compact pellets. These were sparse by the end of the time course and likely restricted cell-substrate interaction for enzyme induction and, thus, overall metabolic efficiency (Cunha et al., 2012; Gomes et al., 2018).

Quantification of total soluble protein production corroborated this, showing a plateauing temporal trend with protein content significantly lower at all time points in comparison to that measured under SSF. This is in accordance with previous work showing the growth of *Aspergillus brasiliensis* and *Neurospora sitophila* (filamentous ascomycetes) under SSF to enhance their secreted protein concentration (Salgado-Bautista et al., 2020; Li, Peng and Chen, 2013). As such, these observations indicate SmF to be a system of inferior productivity which by day 21.5 showed hallmarks of autolysis, such as biomass decline and increased extracellular glucanase activity, likely in response to carbon limitation (Nitsche et al., 2012). For instance, within the soluble secretome fractions, abundance of the GH55 family increased sharply during the final week, whose exo-β-1,3 glucanase activity may have led to cleavage of glucan within the fungal cell wall (its most abundant structural polysaccharide) (Garcia-Rubio et al., 2020). In accordance with this, autolysis in the filamentous fungus *Penicillium chrysogenum* is also associated with increased β-1,3 glucanase activity (McNeil et al., 1998). In addition, the decline of *P. putredinis* NO1 culture under SmF may have been exacerbated by an accumulation of toxic breakdown products within the culture supernatant, such as fragments of β-glucans (e.g. derived from the xylan backbone or fungal cell wall) and lignin derived phenolic compounds (e.g. ferulic and p-coumaric acids) (Kont et al., 2013; Arora et al., 2013).

6.4.2 Carbohydrate-active enzyme profiles differ under submerged and solid-state fermentation

Annotation of soluble and insoluble secretomes during growth on wheat straw revealed significantly greater CAZyme family diversity under SmF, indicating that *P. putredinis* NO1 secreted extracellular proteins belonging to a wider range of CAZyme families in comparison to growth under SSF. This is in accordance with previous proteomic research in which enzymes produced by *T. reesei* during growth on sugarcane bagasse showed greater diversity under SmF, in comparison to that observed under sequential fermentation (SSF followed by SmF) (Florencio et al., 2016). However, the reverse was observed for *A. niger* and *A. brasiliensis*, which showed greater protein diversity during growth under sequential fermentation on sugarcane bagasse and during growth under SSF on glucose, respectively (Salgado-Bautista et al., 2020; Florencio et al., 2016). This suggests that secretome responses are likely species-specific, as well as influenced by fermentation state. Interestingly, interrogation of *P. putredinis* NO1 protein abundance distribution within the secretomes showed greater CAZyme family dominance under SSF, with CAZyme profiles within soluble and insoluble fractions containing comparatively greater numbers of disproportionally abundant proteins. Greater densities of less abundant proteins were also detected under SSF, corroborating the dominance weighting towards proteins of disproportionate abundance.

These observations indicate that *P. putredinis* NO1 secretomes on wheat straw are more targeted under SSF, comprising a disproportionally abundant suite of CAZymes with the most appropriate catalytic function to deconstruct the substrates encountered via its expansive mycelium. In line with this, proteins belonging to the GH class (containing a range of cellulolytic and hemicellulolytic activities) reached a significantly higher peak abundance under SSF and showed a progressive increase over time, in comparison to the early initial increase and subsequent decline in abundance observed under SmF. Similarly, enzymes produced by *T. reesei* during growth under sequential fermentation (SSF followed by SmF) on sugarcane bagasse possessed higher levels of cellulolytic and hemicellulolytic activity compared to those produced under SmF (Florencio et al., 2016). In contrast, the greater CAZyme family diversity observed under SmF combined with a lesser dominance effect indicates a system of greater volatility, whose comparatively untargeted CAZyme profiles likely reflect the diversity of substrates experienced by individual fungal pellets during continuous agitation.

Under SmF and SSF, cellulases were of greatest abundance within the CAZyme profiles of *P. putredinis* NO1 secretomes, reflecting the fact that cellulose is the most abundant carbon source within wheat straw. Cellulases were of wide-ranging activities and detected primarily at greater abundances under SSF, in accordance with previous research showing increased cellulase production under SSF by *A. niger* during growth on coir waste and *Eupenicillium javanicum* (filamentous ascomycete) during growth on pineapple crown leaves (Mrudula and Murugammal, 2011; Evelyn et al., 2020). Proteins belonging to the GH7 family were of highest relative abundance within all fractions under both SmF and SSF; all of which showed homology to known reducing end-acting cellobiohydrolases within the dbCAN CAZyme database. As such, these proteins were most likely involved in the cleavage of cellobiose (two linked glucose monomers) from the reducing end of the cellulose chain during *P. putredinis* NO1 growth on wheat straw (Glass et al., 2013). The GH7 family showed markedly greater abundance under SSF with peak abundances of nearly two and 3.5 fold higher within soluble and insoluble fractions, respectively. Temporal abundance profiles mirrored those of the total GH class, while the dominance in protein abundance distribution appeared largely driven by two proteins – FUN_006103-T1 and FUN_006454-T1 (the most abundant detected under both SmF and SSF). In accordance with this, a transcriptional study showed notably high expression of a GH7 family cellobiohydrolase during growth of *T. reesei* on wheat straw, as well as a GH3 family β-xylosidase and GH6 family cellobiohydrolase at comparatively lower (yet still high) expression levels (Ries et al., 2013). Similarly, during growth of *P. putredinis* NO1 on wheat straw, proteins belonging to the GH6 and GH3 families were abundant under both SmF and SSF, encompassing non-reducing end-acting cellobiohydrolase activity (GH6) as well as β-glucosidase, β-xylosidase and non-reducing end α-L-arabinofuranosidase activities (GH3).

Within the soluble fraction, the GH6 family showed similar temporal trends under both fermentation states, though peak relative abundance was greater under SSF despite an initial delay in secretion, as observed for the GH7 family.

Also, within the soluble fraction, under SSF, β-glucosidase activity was bolstered by the GH1 family and β-xylosidase activity by the GH43 family, whose temporal abundance profiles followed the same trend as the GH6 family, peaking at day 7 and at higher relative abundances in comparison to those observed under SmF, following a short initial lag phase. These coordinated temporal CAZyme profiles, therefore, corroborate the targeted degradative behaviour observed by *P. putredinis* NO1 towards wheat straw under SSF, by which cellulases (particularly exoglucanase and β-glucosidase activities) and xylanases (particularly β-xylosidase activities) work in concert to target the most abundant cell wall polysaccharides within wheat straw (cellulose and xylan). Under SmF, despite significant abundance of the GH7 and GH6 families within both fractions, CAZyme profiles were different to those observed under SSF, with exoglucanase activity bolstered further by the GH55 family. In addition, GH15, GH5 and GH11 families were highly abundant under SmF, conferring α-glucosidase, endoglucanase and endoxylanase activities, respectively. Furthermore, abundances of GH1, GH3 and GH43 families (conferring β-glucosidase and β-xylosidase activities) were much lower, in accordance with previous research in which the β-glucosidase activity of *N. sitophila* was significantly higher during growth on steam exploded wheat straw under SSF (Li, Peng and Chen, 2013). Particularly within the soluble fraction, temporal abundance profiles of the five most abundant GH families detected (GH7, GH55, GH6, GH15 and GH5) showed markedly different temporal trends under SmF, in stark contrast to the coordinated secretion of the most abundant cellulases and xylanases under SSF. This indicates that the secretion of CAZymes by *P. putredinis* NO1 under SmF was more sporadic over time, supporting the greater diversity (and lesser dominance) of CAZyme families detected. This likely reflects the highly dynamic conditions experienced by the formation of compact pellets during culture which offered less cell-substrate interaction in comparison to the expansive mycelium formed under SSF.

Euclidean clustering of temporal CAZyme profiles within the soluble fractions of *P. putredinis* NO1 secretomes revealed a core cluster containing highly abundant members of the GH class (e.g. GH6, GH43 and GH55), accompanied by the CE15 family (glucuronoyl esterase). Activity of the CE15 family is most associated with the cleavage of ester bonds within lignin-carbohydrate complexes, such as the complex between 4-O-methyl-D-glucuronic acid (within glucuronoxylan and glucuronoarabinoxylan) and lignin whose presence enhances the recalcitrance of the cell wall to deconstruction (Ernst et al., 2020; Dilokpimol et al., 2018).

The CE15 family was the most abundant of the CE class detected during *P. putredinis* NO1 growth on wheat straw, though its temporal abundance profiles differed under SmF and SSF. Within the soluble fraction under SSF, the CE15 family showed an increasing temporal trend which mirrored those of key cellulase and xylanase activities conferred by GH family members. This further supports the progressive nature of *P. putredinis* NO1 growth observed on wheat straw under SSF, whereby its mycelial network expanded over time, enabling greater secretion of enzymes with appropriate catalytic function. In contrast, under SmF, abundance of the CE15 family showed a more explosive temporal profile which peaked at day 10, then declined. Interestingly, activity of the CE15 family was bolstered by the CE16 family (acetylxylan esterase) under both SmF and SSF, though its abundance within the insoluble fraction was significantly greater under SmF throughout the time course. In addition, abundances of the CE4, CE10, CE5 and CE1 families within the insoluble fractions were generally greater across the time course under SmF, indicating that proteins of acetylxylan and feruloyl esterase activities were bound in greater abundance. These findings support the greater degradation of the matrix polysaccharide fraction observed under SmF by composition analyses, particularly of xylan (chapter 5).

Within all fractions under SmF and SSF, the AA3 family was the most abundant of all AA class members within *P. putredinis* NO1 secretomes during growth on wheat straw. Interestingly, the vast majority of proteins with homology to AA3 domains were of subfamily 2, comprising aryl alcohol and glucose oxidase/dehydrogenase activities whose common feature is the formation of key metabolites, such as hydrogen peroxide, required by the action of other AA families (e.g. AA9) (Sützl et al., 2018). The AA3 family was bolstered further by proteins belonging to the AA7 family, of greater abundance under SmF within both fractions, and whose activity also generates hydrogen peroxide. The combined action of these hydrogen peroxide producing families likely supports the activity of AA9 family proteins (LPMOs) which open up the architecture of cellulose fibres by creating 'nicking' points via oxidation reactions, and as such, create new initiation sites for hydrolytic cellulases (e.g. GH family proteins) (Villares et al., 2017). Despite presence within all fractions, the AA9 family was generally detected at relatively low abundance during *P. putredinis* NO1 growth on wheat straw, in accordance with previous work (Oates, 2016).

Pectate and rhamnogalacturonan lyase activities were also observed during *P. putredinis* NO1 growth on wheat straw, though conferred most abundantly by different PL families under SmF and SSF. Within soluble and insoluble fractions, pectate lyase activity was conferred predominantly by the PL1 family under SmF, while the equivalent activity was conferred by the PL3 family under SSF. Similarly, under SmF, rhamnogalacturonan endolyase activity was conferred most abundantly by the PL4 family, while under SSF, rhamnogalacturonan exolyase activity was conferred instead by the PL26 family.

This supports the greater abundance of endo-acting activities observed under SmF, alongside endoglucanase (e.g. GH5) and endoxylanase (e.g. GH11) activities.

6.4.3 Solid-state fermentation as a superior system for Black Soldier Fly larvae feed production

This chapter presented a functional protein-level characterisation of *P. putredinis* NO1 growth on wheat straw under SmF and SSF; building upon composition analyses (chapter 5) which elucidated the changes to cell wall composition. Results revealed the CAZymes employed by *P. putredinis* NO1 most likely responsible for the improvements observed in wheat straw digestibility by BSFL (chapters 3 and 4). Total soluble protein production was significantly higher under SSF, leading to generation of BSFL feed with a much greater protein content. Temporal CAZyme profiles under SSF appeared more coordinated and targeted in comparison to those observed under SmF. Cellulases were more abundant under SSF (particularly proteins of the GH7 family). As discussed, these observations likely reflect the culture conditions experienced by *P. putredinis* NO1 during growth on wheat straw and indicate that SSF may be a more reproducible pretreatment system, which is vital for the production of BSFL feed at scale. In contrast, pretreatment under SmF appeared a more sporadic process with a more temporally diverse CAZyme profile, which, therefore, would likely be more difficult to control at scale and offer less reproducibility for BSFL feed production in comparison to SSF (Gupta, Lee and Chen, 2018).

7) Final discussion

This thesis describes the development and characterisation of an innovative fungal pretreatment process to convert wheat straw into feed for Black Soldier Fly larvae (BSFL). Wheat straw, as well other agricultural crop residues produced worldwide, is abundant, underutilised, homogenous and of low value. Crop residues, therefore, are excellent candidates as BSFL feed, though are indigestible by larvae due to their lignocellulose composition. In this thesis, the lignocellulolytic ability of *P. putredinis* NO1 was exploited to improve the digestibility of the plant cell wall by BSFL, enabling their growth. This was fundamentally characterised by various techniques to reveal the changes in cell wall composition and the enzymatic mechanisms underpinning the improvements in its digestibility.

Chapter 3 showed proof of concept, demonstrating that BSFL can survive and grow on wheat straw pretreated with *P. putredinis* NO1 under submerged fermentation (SmF). In contrast, untreated wheat straw supported negligible growth during a 28-day feeding trial. Neonate BSFL performed better than four-day-old larvae, with higher growth rates and yields on pretreated wheat straw, while their growth was influenced by feeding rate and limited by feed nitrogen content. The results also indicated that there is an optimum fermentation duration which likely balances the accessibility of plant cell wall sugars (e.g. cellulose and xylose) with the quantity of fungal biomass produced.

Chapter 4 demonstrated the ability of *P. putredinis* NO1 to degrade wheat straw and oil palm empty fruit bunch under solid-state fermentation (SSF), forming the basis for a more scalable, cost-effective pretreatment system requiring lower resource and energy inputs in comparison to SmF. Wheat straw pretreated with *P. putredinis* NO1 under SSF supported BSFL growth and possessed an improved (lower) carbon to nitrogen ratio in comparison to untreated wheat straw. Larval growth remained limited by feed nitrogen content, improved by supplementation with brewers' spent grain, while the concentration of fungal inoculum (spores) used to pretreat wheat straw showed little effect upon BSFL growth. An optimal fermentation duration was indicated in line with the observations of chapter 3, though this duration was longer under SSF due to a short initial lag phase in fungal growth. The results within chapter 4 also confirmed the feed safety of fungal pretreated wheat straw using mycotoxin and multi-elemental testing. Pretreated wheat straw contained low levels of mycotoxins, with deoxynivalenol detected at levels significantly below permitted EU limits, while the levels of toxic heavy metals (arsenic, cadmium and lead) were detected at trace levels and similarly below EU limits.

Elemental analysis also showed pretreated wheat straw to be low in calcium and phosphorus, in comparison to chick starter crumb (positive control diet), indicating that BSFL growth was likely limited by the quantities of various elements within pretreated wheat straw that are fundamental to larval growth, in addition to nitrogen.

Chapter 5 revealed the changes in cell wall composition elicited by *P. putredinis* NO1 growth on wheat straw using a range of techniques. Results demonstrated the compositional changes most likely responsible for the improvements observed in wheat straw digestibility by BSFL (chapters 3 and 4), in which *P. putredinis* NO1 growth improved the availability of cell wall sugars (e.g. cellulose and xylose) and provided a protein source for larval consumption. Under both SmF and SSF, *P. putredinis* NO1 preferentially degraded the crystalline cellulose fraction in line with the classical action of soft rot ascomycetes (Langer et al., 2021). While there was no evidence for the degradation of lignin, solid-state nuclear magnetic resonance revealed a reduction in the frequency of β-O-4 linkages during *P. putredinis* NO1 growth under SSF, indicating their cleavage and possible remodelling of lignin. The matrix polysaccharide fraction showed greater degradation under SmF, with a wide variety of monosaccharides degraded sporadically over time, while under SSF, gradual degradation of the most abundant sugars predominated (xylose, arabinose and glucose). Scanning electron microscopy (SEM) showed the presence of a hyphal network (mycelium) under SSF, while under SmF, morphology presented as compact 'pellets'.

Chapter 6 built upon the results of chapter 5, presenting an exo-proteomic study of *P. putredinis* NO1 growth on wheat straw (summarised in Figure 7.1). This functional characterisation revealed the carbohydrate-active enzymes (CAZymes) responsible for the changes observed in cell wall composition and, thus, those underpinning the improved digestibility of lignocellulose by BSFL (chapters 3 and 4). Total soluble protein production was significantly higher under SSF, generating a BSFL feed of higher protein value. The relative abundance of cellulases was also greater under SSF, such as those of the glycoside hydrolase (GH) class. Two GH7 proteins of reducing-end acting cellobiohydrolase activity were particularly abundant and dominated *P. putredinis* NO1 secretomes under SSF during the latter growth stages. Temporal CAZyme profiles appeared more coordinated and targeted under SSF in comparison to those observed under SmF, supporting the wheat straw degradation profiles revealed in chapter 5. The results of chapter 6, therefore, indicated that a solid-state biomass pretreatment system would offer improved process control and reproducibility for the production of BSFL feed.

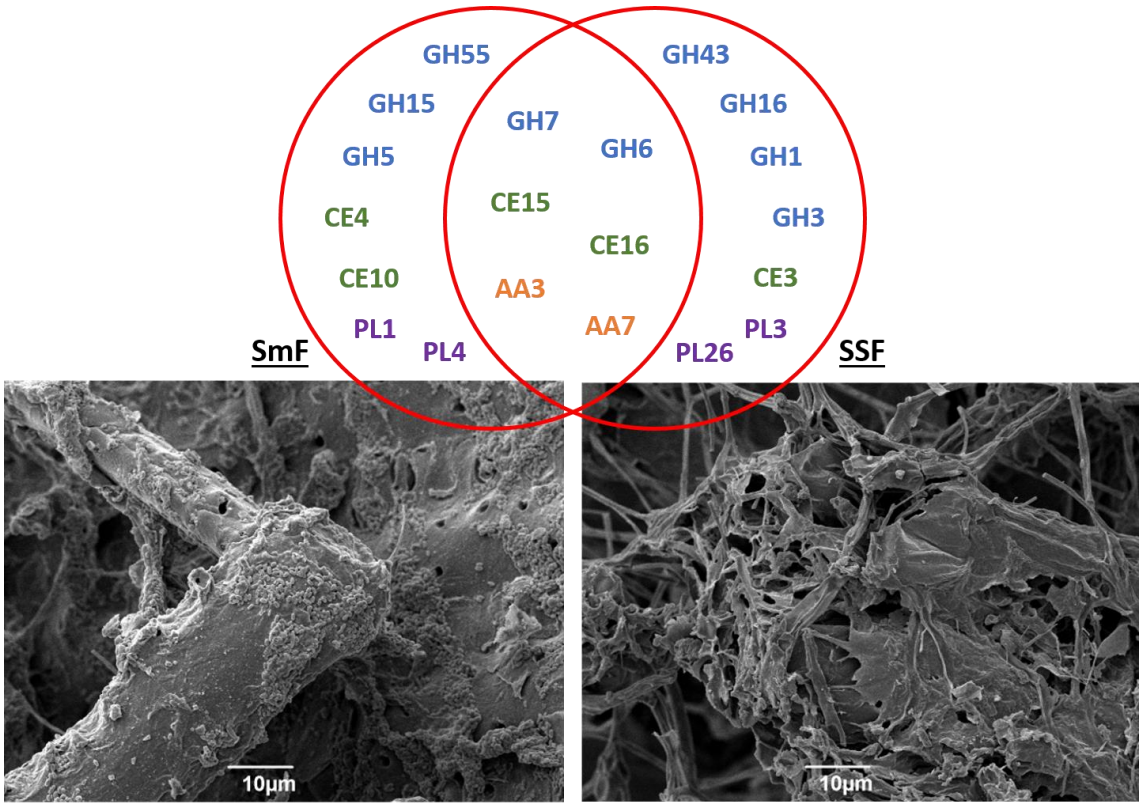

Figure 7.1. Key morphological and proteomic differences between *P. putredinis* NO1 growth on wheat straw under SmF and SSF. SEM images show pellet formation under SmF (left), in comparison to hyphal formation under SSF (right) at day 10. Venn diagram shows the major CAZyme families detected at high abundance within both SmF and SSF secretomes (centre), as well as key families detected at higher abundance under SmF (left) and SSF (right).

7.1 Future directions

The solid-state pretreatment process developed and characterised in this thesis holds industrial potential to enable the transformation of lignocellulosic biomass into feed for BSFL. This approach has various advantages over the use of current insect feeds (e.g. pre-consumer food waste), as discussed in chapter 3. However, to enable translation, the pretreatment process must be optimised, demonstrated at commensurate scale and shown to be economically viable.

7.1.1 Process optimisation

The BSFL feeding trials within chapter 4 demonstrated that larvae can grow on wheat straw pretreated with *P. putredinis* NO1 under SSF. Wheat straw pretreated for 14 days enabled the greatest BSFL growth rates and yields, while wheat straw pretreated with *P. putredinis* NO1 for three and seven days also enabled growth, with larvae reaching similar yields. The results within chapter 5 indicated that the SSF pretreatment duration could be shortened to seven days or less, showing that the abundance of reducing sugars (e.g. xylose and glucose) for larval consumption was highest during the first week of the time course, prior to their likely digestion by *P. putredinis* NO1 during later growth stages. In addition, SEM revealed the formation of intricate mycelial networks under SSF, which expanded over time and likely provided BSFL with a protein source during rearing. Therefore, repeat feeding trials should confirm the optimal pretreatment duration which optimises the balance between cell wall digestion, availability of sugars and the quantity of fungal protein.

Different methods to inoculate the pretreatment should also be explored, such as inoculating the biomass with pre-cultured *P. putredinis* NO1 mycelia instead of spores (as conducted in this thesis). This would likely reduce the length of the early lag phase observed in chapters 4-6 under SSF, as the addition of fungal mycelia would eliminate the spore germination stage most likely responsible for the lag. A shorter pretreatment would also be desirable from a commercial perspective. Additionally, the effects of the growth media components upon BSFL growth should be explored; in particular, the nitrogen rich yeast extract added at 8.55 g/L. If yeast extract is shown to improve larval growth performance in future feeding trials, an alternative (cheaper) nitrogen source should be pursued (e.g. of waste origin) as a culture supplement. In addition to yeast extract, *P. putredinis* NO1 growth media contains a range of elements (e.g. copper, iron and sodium), although calcium is absent. Multi-elemental analysis in chapter 4 showed that pretreated wheat straw was particularly low in calcium and phosphorus, relative to chick starter crumb (positive control diet).

It may be possible to provide BSFL with sufficient sources of key elements (e.g. calcium) during rearing by optimising the components of the fungal growth media and their abundances. Given the large number of variables involved, a 'Design of Experiment' approach would be appropriate for this, which reveals the relationship between multiple input variables (e.g. media components) and key output variables (e.g. fungal protein content measured by ergosterol content, BSFL yield). In addition, the particle size of the biomass should be considered, as this affects larval growth and yield during rearing (Palma et al., 2019), and likely the availability of nutrients to *P. putredinis* NO1 during the pretreatment process. It is also likely that the fermentation duration required, culture composition and processing parameters (e.g. temperature, pH and agitation) will differ across substrates due to variability in their cell wall composition. Therefore, individual substrates may require independent optimisation.

Unfortunately, due to various COVID-19 related issues, it was not possible to measure the nutritional profiles of BSFL fed on pretreated wheat straw (e.g. protein content, amino acid and lipid profiles), or conduct feed safety testing on the larvae (e.g. mycotoxin and heavy metal analysis). However, given its importance to the application of this work, larval nutritional profiling and feed safety testing should be conducted alongside future optimisation of the pretreatment to ensure a product that meets regulatory standards, and that contains desirable nutritional value.

7.1.2 Scale-up

A solid-state pretreatment system holds strong economic feasibility at scale. As such, alongside the process optimisation described above, methods by which to scale-up should be explored. For instance, the size, shape and layout of pretreatment vessels should be established, as well as the thickness of the biomass layer pretreated by *P. putredinis* NO1. In addition, with increased production scale, it may become more difficult to maintain aeration of the culture. Although SSF does not require constant shaking, the culture must still be agitated periodically to maintain aerobic conditions for fungal growth, which, therefore, should also be considered. One potential method to scale the pretreatment would be to use rotating or stirred drum bioreactors (Figure 7.2). These rely on passive aeration and enable frequent intermittent mixing at low energy input (Prabhu et al., 2022). Alternatively, tray bioreactors could be used (Figure 7.2), which similarly rely on passive aeration though have a more limited capacity for mixing (Prabhu et al., 2022).

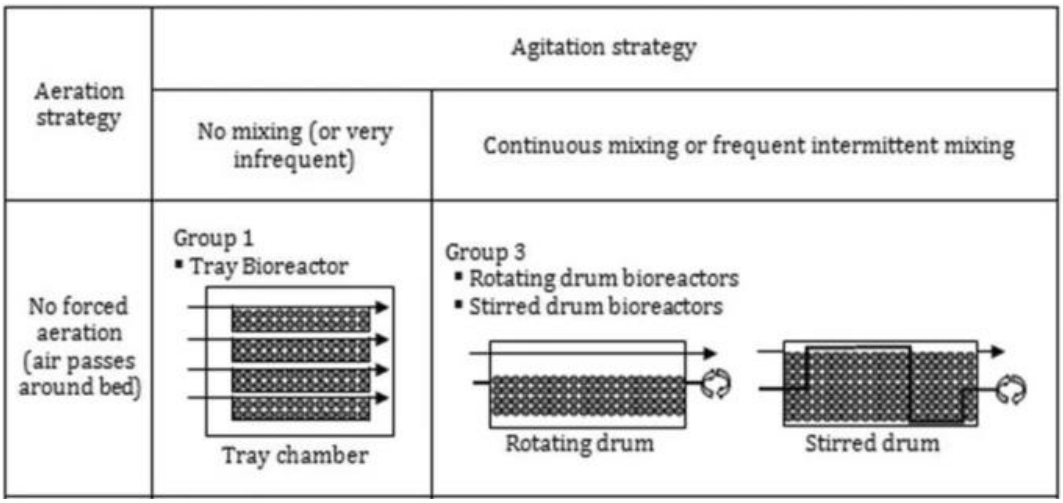

Figure 7.2. Bioreactor design for SSF technologies. Adapted from (Prabhu et al., 2022).

If tray bioreactors were employed, it would be possible to adopt a vertical farming approach in which trays (each containing a single culture) are stacked on top of each other to achieve increased scale. This approach would reduce the required size of an individual culture (within a single tray), which is beneficial for process optimisation, and uses space efficiently. Furthermore, multiple, independent pretreatments contained within individual trays would provide greater process control (e.g. over fungal growth and contamination), as well as process redundancy in which feed output is shared across multiple pretreatment cultures. At present, a range of BSFL production companies employ vertical farming systems to rear larvae, which typically consist of trays (containing feeding BSFL) stacked vertically in storage units maintained at around 30°C (Filou, 2022). Therefore, if the *P. putredinis* NO1 based pretreatment system described in this thesis could be developed using tray bioreactors and demonstrated at increased scale using a vertical farming approach, it may be well suited for implementation in a commercial setting.

Abbreviations

AA	auxiliary activity
ABSL	acetyl bromide soluble lignin
ANOSIM	analysis of similarities
ANOVA	analysis of variance
BSF	Black Soldier Fly
BSFL	Black Soldier Fly larvae
BSG	brewers' spent grain
BUSCA	Bologna unified subcellular component annotator
CAZyme	carbohydrate-active enzyme
CBM	carbohydrate-binding module
CE	carbohydrate esterase
CMF	chelator-mediated Fenton
CSC	chick starter crumb
dbCAN	database for automated carbohydrate-active enzyme annotation
DMSO	dimethyl sulfoxide
DP	degree of polymerisation
EFB	empty fruit bunch
EU	European Union
G	guaiacyl
GH	glycoside hydrolase
GMC	glucose-methanol-choline
GT	glycosyl transferase
H	p-hydroxyphenyl
H_0	null hypothesis
HTE	Hutner's trace elements
IDE	integrated development environment
IQR	interquartile range
LC-MS/MS	liquid chromatography and tandem mass spectrometry

LPMO	lytic polysaccharide monooxygenase
MWCO	molecular weight cut-off
NA	not applicable
NCBI	National Centre for Biotechnology Information
PAPs	processed animal proteins
PBS	phosphate buffered saline
PES	polyethersulfone
PCA	principal component analysis
PCoA	principal coordinate analysis
PL	polysaccharide lyase
PTFE	polytetrafluoroethylene
S	syringyl
SD	standard deviation
SE	standard error
SDS	sodium dodecyl sulfate
SDS-PAGE	sodium dodecyl sulfate-polyacrylamide electrophoresis
SmF	submerged fermentation
SSF	solid-state fermentation
TEMED	tetramethylethylenediamine
TFA	trifluoroacetic acid
TMHMM	transmembrane helix hidden Markov model
UoY	University of York
v/v	volume to volume ratio
w/v	weight to volume ratio
WS	wheat straw
$\bar{x}$	sample mean

References

Abd-Elsalam, I. S. (2009). Role of the biomass and pelleted forms of Aspergillus ochraceus ATCC 3150 on the 11α-hydroxylation of progesterone. *Malaysian Journal of Microbiology*, 5 (2).

Abu Yazid, N. et al. (2017). Solid-state fermentation as a novel paradigm for organic waste valorization: a review. *Sustainability*, 9 (2).

Adav, S. S. et al. (2012). Quantitative proteomic analysis of secretome of microbial consortium during saw dust utilization. *Journal of Proteomics*, 75 (18).

Adu, M. O. et al. (2022). The use of oil palm empty fruit bunches as a soil amendment to improve growth and yield of crops. A meta-analysis. *Agronomy for Sustainable Development*, 42 (2).

Agrios, G. N. (2005). Parasitism and disease development. In: *Plant Pathology*. Academic Press.

AHDB. (2022). *Hay and straw prices*. [Online]. Available at: https://ahdb.org.uk/dairy/hay-and-straw-prices.

Alessi, A. M. et al. (2017). Revealing the insoluble metasecretome of lignocellulose-degrading microbial communities. *Scientific Reports*, 7 (1).

Almagro Armenteros, J. J. et al. (2017). DeepLoc: prediction of protein subcellular localization using deep learning. *Bioinformatics*, 33 (21).

Almagro Armenteros, J. J. et al. (2019a). Detecting sequence signals in targeting peptides using deep learning. *Life Science Alliance*, 2 (5).

Almagro Armenteros, J. J. et al. (2019b). SignalP 5.0 improves signal peptide predictions using deep neural networks. *Nature Biotechnology*, 37 (4).

Al-Mobarak, T., Gafur, M. A. and Mina, M. F. (2012). Material properties of acetylated jute-mat composites. *Journal of Scientific Research*, 5 (1).

Arora, A. et al. (2013). Effect of formic acid and furfural on the enzymatic hydrolysis of cellulose powder and dilute acid-pretreated poplar hydrolysates. *ACS Sustainable Chemistry and Engineering*, 1 (1).

Azadfar, M., Graham, M. R. and Wolcott, M. P. (2019). Effect of cellulose reducing ends on the reinforcing capacity of powdered cellulose in polypropylene composites. *Journal of Composites Science*, 3 (4).

Bari, E. et al. (2020). Comparison of the decay behavior of two white-rot fungi in relation to wood type and exposure conditions. *Microorganisms*, 8 (12).

Barragan-Fonseca, K. B., Dicke, M. and van Loon, J. J. A. (2018). Influence of larval density and dietary nutrient concentration on performance, body protein, and fat contents of Black Soldier Fly larvae (Hermetia illucens). *Entomologia Experimentalis et Applicata*, 166 (9).

Barros-Cordeiro, K. B., Báo, S. N. and Pujol-Luz, J. R. (2014). Intra-puparial development of the Black Soldier Fly, Hermetia illucens. *Journal of Insect Science*, 14 (1).

Bava, L. et al. (2019). Rearing of Hermetia illucens on different organic by-products: influence on growth, waste reduction, and environmental impact. *Animals*, 9 (6).

Beesigamukama, D. et al. (2021). Low-cost technology for recycling agro-industrial waste into nutrient-rich organic fertilizer using Black Soldier Fly. *Waste Management*, 119.

Bendtsen, J. D. et al. (2004). Feature-based prediction of non-classical and leaderless protein secretion. *Protein Engineering, Design and Selection*, 17 (4).

Bernardes, A. et al. (2019). Carbohydrate binding modules enhance cellulose enzymatic hydrolysis by increasing access of cellulases to the substrate. *Carbohydrate Polymers*, 211.

Bernard, J. K. (2022). Oilseed and oilseed meals. *Encyclopedia of Dairy Sciences*, 1 (3).

Bjone, H. and Fitches, E. C. (2021). Which insect species and why? In: *Insects as Animal Feed: Novel Ingredients for Use in Pet, Aquaculture and Livestock Diets*. CABI.

Bloukounon-Goubalan, A. Y. et al. (2021). By-products of insect rearing: insect residues as biofertilizers. In: *Insects as Animal Feed: Novel Ingredients for Use in Pet, Aquaculture and Livestock Diets*. CABI.

Boakye-Yiadom, K. A., Ilari, A. and Duca, D. (2022). Greenhouse gas emissions and life cycle assessment on the Black Soldier Fly (Hermetia illucens). *Sustainability*, 14 (16).

Boerjan, W., Ralph, J. and Baucher, M. (2003). Lignin biosynthesis. *Annual Review of Plant Biology*, 54.

Bohorquez, J. et al. (2021). Spore viability and germination of some ectomycorrhizal fungi from New Zealand and implications for forest restoration. *New Zealand Journal of Botany*, 59 (2).

Booth, A., O'Neill, H. M. and Quigley, L. (2021). The challenges facing the feed industry. In: *Insects as Animal Feed: Novel Ingredients for Use in Pet, Aquaculture and Livestock Diets*. CABI.

Borin, G. P. et al. (2015). Comparative secretome analysis of Trichoderma reesei and Aspergillus niger during growth on sugarcane biomass. *PLoS ONE*, 10 (6).

Bosch, G. et al. (2017). Aflatoxin B1 tolerance and accumulation in Black Soldier Fly larvae (Hermetia illucens) and yellow mealworms (Tenebrio molitor). *Toxins*, 9 (6).

Brandt, S. C. et al. (2021). Insights into the genome and secretome of Fusarium metavorans DSM105788 by cultivation on agro-residual biomass and synthetic nutrient sources. *Biotechnology for Biofuels*, 14 (1).

Challacombe, J. F. et al. (2019). Genomes and secretomes of Ascomycota fungi reveal diverse functions in plant biomass decomposition and pathogenesis. *BMC Genomics*, 20 (1).

Charlton, A. J. et al. (2015). Exploring the chemical safety of fly larvae as a source of protein for animal feed. *Journal of Insects as Food and Feed*, 1 (1).

Chatel, G. and Rogers, R. D. (2014). Review: oxidation of lignin using ionic liquids-an innovative strategy to produce renewable chemicals. *ACS Sustainable Chemistry and Engineering*, 2 (3).

Chia, S. Y. et al. (2020). Nutritional composition of Black Soldier Fly larvae feeding on agro-industrial by-products. *Entomologia Experimentalis et Applicata*, 168 (6–7).

Chorozian, K. et al. (2022). Characterization of a dual cellulolytic/xylanolytic AA9 lytic polysaccharide monooxygenase from Thermothelomyces thermophilus and its utilization toward nanocellulose production in a multi-step bioprocess. *ACS Sustainable Chemistry and Engineering*, 10 (27).

Clemmensen, K. E. et al. (2013). Roots and associated fungi drive long-term carbon sequestration in boreal forest. *Science*, 339 (6127).

Cocero, M. J. et al. (2018). Understanding biomass fractionation in subcritical & supercritical water. *The Journal of Supercritical Fluids*, 133.

Collins, S. R. et al. (2014). Variation in the chemical composition of wheat straw: The role of tissue ratio and composition. *Biotechnology for Biofuels*, 7 (1), pp.1–14. [Online]. Available at: doi:10.1186/S13068-014-0121-Y/TABLES/3 [Accessed 25 July 2022].

Commer, B. and Shaw, B. D. (2021). Current views on endocytosis in filamentous fungi. *Mycology*, 12 (1).

Copeland, D. and Turley, J. (2008). *National and regional supply/demand balance for agricultural straw in Great Britain*. [Online]. Available at: https://www.researchgate.net/publication/265823113_National_and_regional_supplydemand_balance_for_agricultural_straw_in_Great_Britain.

Coral Medina, J. D. et al. (2018). Energetic and economic analysis of ethanol, xylitol and lignin production using oil palm empty fruit bunches from a Brazilian factory. *Journal of Cleaner Production*, 195.

Cosgrove, D. J. and Jarvis, M. C. (2012). Comparative structure and biomechanics of plant primary and secondary cell walls. *Frontiers in Plant Science*, 3.

Cragg, S. M. et al. (2015). Lignocellulose degradation mechanisms across the Tree of Life. *Current Opinion in Chemical Biology*, 29, pp.108–119. [Online]. Available at: doi:10.1016/J.CBPA.2015.10.018 [Accessed 8 November 2022].

Cunha, F. M. et al. (2012). Sequential solid-state and submerged cultivation of Aspergillus niger on sugarcane bagasse for the production of cellulase. *Bioresource Technology*, 112.

Dicko, M. et al. (2020). Lignin degradation and its use in signaling development by the coprophilous ascomycete Podospora anserina. *Journal of Fungi*, 6 (4).

Diener, S. et al. (2011). Biological treatment of municipal organic waste using Black Soldier Fly larvae. *Waste and Biomass Valorization*, 2 (4).

Diener, S., Zurbrügg, C. and Tockner, K. (2009). Conversion of organic material by Black Soldier Fly larvae: establishing optimal feeding rates. *Waste Management and Research*, 27 (6).

Diener, S., Zurbrügg, C. and Tockner, K. (2015). Bioaccumulation of heavy metals in the Black Soldier Fly, Hermetia illucens, and effects on its life cycle. *Journal of Insects as Food and Feed*, 1 (4).

Dilokpimol, A. et al. (2018). Fungal glucuronoyl esterases: genome mining based enzyme discovery and biochemical characterization. *New Biotechnology*, 40.

Dinis, M. J. et al. (2009). Modification of wheat straw lignin by solid state fermentation with white-rot fungi. *Bioresource Technology*, 100 (20).

Doriya, K. et al. (2016). Solid-state fermentation vs submerged fermentation for the production of l-asparaginase. *Advances in Food and Nutrition Research*, 78.

Dzepe, D. et al. (2021). Feeding strategies for small-scale rearing Black Soldier Fly larvae (Hermetia illucens) as organic waste recycler. *SN Applied Sciences*, 3 (2).

Egerton, S. et al. (2020). Replacing fishmeal with plant protein in Atlantic salmon (Salmo salar) diets by supplementation with fish protein hydrolysate. *Scientific Reports*, 10 (1).

El-Metwally, M. M., El-Hersh, M. S. and Saber, W. I. A. (2017). A dual microbial culture for improving C/N ratio and multi-response optimization of rice straw fermentation for bioethanol production. *Research Journal of Microbiology*, 12 (3).

Ernst, H. A. et al. (2020). The structural basis of fungal glucuronoyl esterase activity on natural substrates. *Nature Communications*, 11 (1).

van Erven, G. et al. (2018). Mechanistic insight in the selective delignification of wheat straw by three white-rot fungal species through quantitative 13C-IS py-GC–MS and whole cell wall HSQC NMR. *Biotechnology for Biofuels*, 11 (1).

van Erven, G. et al. (2020). Evidence for ligninolytic activity of the ascomycete fungus Podospora anserina. *Biotechnology for Biofuels*, 13 (75).

Evelyn et al. (2020). Production of cellulase and xylanase from Eupenicillium javanicum by solid-state fermentation utilizing pineapple crown leaves waste as the substrate. *Journal of Physics: Conference Series*, 1655 (1).

Farkhoy, M. et al. (2012). Evaluation of protein concentration and limiting amino acids including lysine and met + cys in prestarter diet on performance of broilers. *Veterinary Medicine International*, 2012.

Filou, E. (2022). *Look inside a high-tech farm growing fly larvae for protein*. [Online]. Available at: https://www.businessinsider.com/inside-fly-farm-sustainable-protein-agriculture-industry-protex-2022-1?r=US&IR=T.

Finke, M. D. (2007). Estimate of chitin in raw whole insects. *Zoo Biology*, 26 (2).

Finke, M. D. (2013). Complete nutrient content of four species of feeder insects. *Zoo Biology*, 32 (1).

Fischer, H. et al. (2022). Comparing Black Soldier Fly (Hermetia illucens) larvae versus prepupae in the diets of largemouth bass, Micropterus salmoides: effects on their growth, biochemical composition, histopathology, and gene expression. *Aquaculture*, 546.

Florencio, C. et al. (2016). Secretome analysis of Trichoderma reesei and Aspergillus niger cultivated by submerged and sequential fermentation processes: enzyme production for sugarcane bagasse hydrolysis. *Enzyme and Microbial Technology*, 90.

Floudas, D. et al. (2012). The paleozoic origin of enzymatic lignin decomposition reconstructed from 31 fungal genomes. *Science*, 336 (6089).

Foster, C. E., Martin, T. M. and Pauly, M. (2010). Comprehensive compositional analysis of plant cell walls (lignocellulosic biomass) part I: lignin. *Journal of Visualized Experiments*, (37).

Fraanje, W. and Garnett, T. (2020). *Soy: food, feed, and land use change*. [Online]. Available at: https://www.academia.edu/41842107/Soy_food_feed_and_land_use_change.

Fricke, W. (2017). Turgor pressure. In: *eLS*. John Wiley & Sons, Ltd.

Gaitán-Cremaschi, D. et al. (2015). Benchmarking the sustainability performance of the Brazilian non-GM and GM soybean meal chains: an indicator-based approach. *Food Policy*, 55.

Gao, Z. et al. (2019). Bioconversion performance and life table of Black Soldier Fly (Hermetia illucens) on fermented maize straw. *Journal of Cleaner Production*, 230.

Garcia-Rubio, R. et al. (2020). The fungal cell wall: Candida, Cryptococcus, and Aspergillus species. *Frontiers in Microbiology*, 10.

Gassara, F. et al. (2013). Influence of aeration and agitation modes on solid-state fermentation of apple pomace waste by Phanerochaete chrysosporium to produce ligninolytic enzymes and co-extract polyphenols. *International Journal of Food Science & Technology*, 48 (10).

Georgescu, B. et al. (2020). Body weight loss of Black Soldier Fly Hermetia illucens (Diptera: Stratiomyidae) during development in non-feeding stages: implications for egg clutch parameters. *European Journal of Entomology*, 117.

Gillman, S. (2017). *Wheat straw waste could be basis for greener chemicals*. [Online]. Available at: https://ec.europa.eu/research-and-innovation/en/horizon-magazine/wheat-straw-waste-could-be-basis-greener-chemicals.

Giummarella, N. et al. (2019). A critical review on the analysis of lignin carbohydrate bonds. *Green Chemistry*, 21 (7).

Glass, N. L. et al. (2013). Plant cell wall deconstruction by ascomycete fungi. *Annual Review of Microbiology*, 67 (1).

Global Food Security. (2022). *The food security challenge*. [Online]. Available at: https://www.foodsecurity.ac.uk/challenge/.

Gomes, E. et al. (2018). Fungal growth on solid substrates: a physiological overview. In: *Current Developments in Biotechnology and Bioengineering*. Elsevier.

Grandmontagne, D. et al. (2021). The secretomes of Aspergillus japonicus and Aspergillus terreus supplement the Rovabio enzyme cocktail for the degradation of soybean meal for animal feed. *Journal of Fungi*, 7 (4).

Gu, H. et al. (2019). Physiological mechanism of improved tolerance of Saccharomyces cerevisiae to lignin-derived phenolic acids in lignocellulosic ethanol fermentation by short-term adaptation. *Biotechnology for Biofuels*, 12 (1).

Gu, H., Zhang, J. and Bao, J. (2014). Inhibitor analysis and adaptive evolution of Saccharomyces cerevisiae for simultaneous saccharification and ethanol fermentation from industrial waste corncob residues. *Bioresource Technology*, 157.

Gupta, S., Lee, J. J. L. and Chen, W. N. (2018). Analysis of improved nutritional composition of potential functional food (okara) after probiotic solid-state fermentation. *Journal of Agricultural and Food Chemistry*, 66 (21).

Habte-Tsion, H. M. et al. (2022). The effects of fish meal substitution by clam meal on the growth and health of Florida pompano (Trachinotus carolinus). *Scientific Reports*, 12 (1).

Hall, H., Fitches, E. and Smith, R. (2021). *Insects as animal feed: novel ingredients for use in pet, aquaculture and livestock diets*. Hall, H., Fitches, E. and Smith, R. (Eds). CABI.

Harris, D. and DeBolt, S. (2010). Synthesis, regulation and utilization of lignocellulosic biomass. *Plant Biotechnology Journal*, 8 (3).

Harris, S. D. (2019). Hyphal branching in filamentous fungi. *Developmental Biology*, 451 (1).

Hasan, M. S., Crenshaw, M. A. and Liao, S. F. (2020). Dietary lysine affects amino acid metabolism and growth performance, which may not involve the GH/IGF-1 axis, in young growing pigs. *Journal of Animal Science*, 98 (1).

Hassouni, H. et al. (2007). Comparative spore germination of filamentous fungi on solid state fermentation under different culture conditions. *Micología Aplicada Internacional*, 19.

Hawkey, K. et al. (2021). Suitability of insects for animal feeding. In: *Insects as Animal Feed: Novel Ingredients for Use in Pet, Aquaculture and Livestock Diets*. CABI.

Henchion, M. et al. (2017). Future protein supply and demand: strategies and factors influencing a sustainable equilibrium. *Foods*, 6 (7).

Henrissat, B. (1991). A classification of glycosyl hydrolases based on amino acid sequence similarities. *Biochemical Journal*, 280 (2).

Herbaut, M. et al. (2018). Multimodal analysis of pretreated biomass species highlights generic markers of lignocellulose recalcitrance. *Biotechnology for Biofuels*, 11 (1).

Himmel, M. E. et al. (2007). Biomass recalcitrance: engineering plants and enzymes for biofuels production. *Science*, 315.

Hocid, B. et al. (2019). Optimization of Black Soldier Fly (Hermetia illucens) artificial reproduction. *PLoS ONE*, 14 (4).

Hong, L. et al. (2012). Enhancement of reducing sugar production by A. niger USM AI1 on oil palm frond in tray system via solid state fermentation. *Proceedings of The Annual International Conference Syiah Kuala University*, 2 (1).

Huang, L. et al. (2018). dbCAN-seq: a database of carbohydrate-active enzyme (CAZyme) sequence and annotation. *Nucleic Acids Research*, 46.

van Huis, A. et al. (2013). *Edible insects: future prospects for food and feed security*. FAO.

Ibáñez, M. A. et al. (2020). Chemical composition, protein quality and nutritive value of commercial soybean meals produced from beans from different countries: a meta-analytical study. *Animal Feed Science and Technology*, 267.

Ibarruri, J., Cebrián, M. and Hernández, I. (2021). Valorisation of fruit and vegetable discards by fungal submerged and solid-state fermentation for alternative feed ingredients production. *Journal of Environmental Management*, 281.

Ibrahim, D., Weloosamy, H. and Lim, S. H. (2015). Effect of agitation speed on the morphology of Aspergillus niger HFD5A-1 hyphae and its pectinase production in submerged fermentation. *World Journal of Biological Chemistry*, 6 (3).

IFFO. (2022). *Increased fishmeal production by 3.6%, year on year, while fish oil production dropped by 6% (January-December 2021)*. [Online]. Available at: https://www.iffo.com/increased-fishmeal-production-36-while-fish-oil-production-dropped-6-january-december-2021.

IFPRI. (2016). *Global nutrition report 2016: from promise to impact - ending malnutrition by 2030*. [Online]. Available at: https://ebrary.ifpri.org/digital/collection/p15738coll2/id/130354.

IPIFF. (2022a). *Building bridges between the insect production chain, research and policymakers*. [Online]. Available at: https://ipiff.org/wp-content/uploads/2019/12/IPIFF-researchpriorities-HorizonEurope.pdf.

IPIFF. (2022b). *Insects as feed EU legislation – aquaculture, poultry & pig Species*. [Online]. Available at: https://ipiff.org/insects-eu-legislation/.

Isibika, A. et al. (2019). Pre-treatment of banana peel to improve composting by Black Soldier Fly (Hermetia illucens (L.), Diptera: Stratiomyidae) larvae. *Waste Management*, 100.

Jain, M. S., Daga, M. and Kalamdhad, A. S. (2019). Variation in the key indicators during composting of municipal solid organic wastes. *Sustainable Environment Research*, 1 (1).

Jucker, C. et al. (2020). Brewery's waste streams as a valuable substrate for Black Soldier Fly Hermetia illucens (Diptera: Stratiomyidae). *Journal of Entomological and Acarological Research*, 51 (3).

Karunakaran, V., Abd-Talib, N. and Kelly Yong, T. L. (2020). Lignin from oil palm empty fruit bunches (EFB) under subcritical phenol conditions as a precursor for carbon fiber production. *Materials Today: Proceedings*, 31.

Katongole, C. B. et al. (2017). Effect of solid-state fermentation with Arxula adeninivorans or Hypocrea jecorina (anamorph Trichoderma reesei) on hygienic quality and in-vitro digestibility of banana peels by mono-gastric animals. *Livestock Science*, 199.

Kaya, C. et al. (2021). Global population genetic structure and demographic trajectories of the Black Soldier Fly, Hermetia illucens. *BMC Biology*, 19 (1).

Kerr, B. J. and Shurson, G. C. (2013). Strategies to improve fiber utilization in swine. *Journal of Animal Science and Biotechnology*, 4 (1).

Kim, H. and Ralph, J. (2010). Solution-state 2D NMR of ball-milled plant cell wall gels in DMSO-d 6/pyridine-d5. *Organic and Biomolecular Chemistry*, 8 (3).

Kongruang, S. et al. (2004). Quantitative analysis of cellulose-reducing ends. *Applied Biochemistry and Biotechnology*, 1 (3).

Kont, R. et al. (2013). Strong cellulase inhibitors from the hydrothermal pretreatment of wheat straw. *Biotechnology for Biofuels*, 6 (1).

Kövilein, A., Umpfenbach, J. and Ochsenreither, K. (2021). Acetate as substrate for l-malic acid production with Aspergillus oryzae DSM 1863. *Biotechnology for Biofuels*, 14 (1).

Kretschmer, M. et al. (2018). Acetate provokes mitochondrial stress and cell death in Ustilago maydis. *Molecular Microbiology*, 107 (4).

Krogh, A. et al. (2001). Predicting transmembrane protein topology with a hidden Markov model: application to complete genomes. *Journal of Molecular Biology*, 305 (3).

Lalander, C. et al. (2019). Effects of feedstock on larval development and process efficiency in waste treatment with Black Soldier Fly (Hermetia illucens). *Journal of Cleaner Production*, 208.

Lam, P. Y. et al. (2017). Disrupting flavone synthase II alters lignin and improves biomass digestibility. *Plant Physiology*, 174 (2).

Lam, P. Y. et al. (2019). OsCAldOMT1 is a bifunctional O-methyltransferase involved in the biosynthesis of tricin-lignins in rice cell walls. *Scientific Reports*, 9 (1).

Langer, G. J. et al. (2021). Fungi inhabiting woody tree tissues. In: *Forest Microbiology*. 1. Academic Press.

Liland, N. S. et al. (2017). Modulation of nutrient composition of Black Soldier Fly (Hermetia illucens) larvae by feeding seaweed-enriched media. *PLoS ONE*, 12 (8).

Liu, X. et al. (2017). Dynamic changes of nutrient composition throughout the entire life cycle of Black Soldier Fly. *PLoS ONE*, 12 (8).

Li, Y., Peng, X. and Chen, H. (2013). Comparative characterization of proteins secreted by Neurospora sitophila in solid-state and submerged fermentation. *Journal of Bioscience and Bioengineering*, 116 (4).

Lizardi-Jiménez, M. A. and Hernández-Martínez, R. (2017). Solid state fermentation (SSF): diversity of applications to valorize waste and biomass. *3 Biotech*, 7 (1).

Lombard, V. et al. (2014). The carbohydrate-active enzymes database (CAZy) in 2013. 2013/11/21. *Nucleic Acids Research*, 42.

Lübeck, M. and Lübeck, P. S. (2022). Fungal cell factories for efficient and sustainable production of proteins and peptides. *Microorganisms*, 10 (4).

Lu, Y. et al. (2021). Effects of different nitrogen sources and ratios to carbon on larval development and bioconversion efficiency in food waste treatment by Black Soldier Fly larvae (Hermetia illucens). *Insects*, 12 (6).

Makkar, H. P. S. et al. (2014). State-of-the-art on use of insects as animal feed. *Animal Feed Science and Technology*, 197.

Mansfield, S. D. et al. (2012). Whole plant cell wall characterization using solution-state 2D NMR. *Nature Protocols*, 7 (9).

de Maria, M. et al. (2020). *Global soybean trade: the geopolitics of a bean*. [Online]. Available at: https://tradehub.earth/wp-content/uploads/2020/10/Global-Soybean-Trade-The-Geopolitcs-of-a-Bean-1.pdf.

Masey O'Neill, H. et al. (2014). Influence of the in vivo method and basal dietary ingredients employed in the determination of the amino acid digestibility of wheat distillers dried grains with solubles in broilers. *Poultry Science*, 93 (5).

McCulloch, J. and Nelson, J. (2021). Legislation, policy and quality assurance. In: *Insects as Animal Feed: Novel Ingredients for Use in Pet, Aquaculture and Livestock Diets*. CABI.

McKendry, P. (2002). Energy production from biomass (part 1): overview of biomass. *Bioresource Technology*, 83 (1).

McNeil, B. et al. (1998). Measurement of autolysis in submerged batch cultures of Penicillium chrysogenum. *Biotechnology and Bioengineering*.

Meijer, N. et al. (2019). Aflatoxin B(1) conversion by Black Soldier Fly (Hermetia illucens) larval enzyme extracts. *Toxins*, 11 (9).

Meng, S., Yin, Y. and Yu, L. (2019). Exploration of a high-efficiency and low-cost technique for maximizing the glucoamylase production from food waste. *RSC Advances*, 9 (40).

Min, D. Y. et al. (2014). The influence of lignin–carbohydrate complexes on the cellulase-mediated saccharification II: transgenic hybrid poplars (Populus nigra L. and Populus maximowiczii A.). *Fuel*, 116.

Miner, L. P. et al. (2022). Predicting Black Soldier Fly larvae biomass and methionine accumulation using a kinetic model for batch cultivation and improving system performance using semi-batch cultivation. *Bioprocess and Biosystems Engineering*, 45 (2).

Miyauchi, S. et al. (2020). Conserved white-rot enzymatic mechanism for wood decay in the basidiomycota genus Pycnoporus. *DNA Research*, 27 (2).

Moreira-Vilar, F. C. et al. (2014). The acetyl bromide method is faster, simpler and presents best recovery of lignin in different herbaceous tissues than klason and thioglycolic acid methods. *PLoS ONE*, 9 (10).

Mota, T. R. et al. (2018). Plant cell wall composition and enzymatic deconstruction. *AIMS Bioengineering*, 5 (1).

Mrudula, S. and Murugammal, R. (2011). Production of cellulose by Aspergillus niger under submerged and solid state fermentation using coir waste as a substrate. *Brazilian Journal of Microbiology*, 42 (3).

Myers, H. M. et al. (2008). Development of Black Soldier Fly (Diptera: Stratiomyidae) larvae fed dairy manure. *Environmental Entomology*, 37 (1).

Nations, U. (2022). *World population prospects 2022: summary of results*. [Online]. Available at: https://www.un.org/development/desa/pd/sites/www.un.org.development.desa.pd/files/wpp2022_summary_of_results.pdf.

Naylor, R. L. et al. (2021). Blue food demand across geographic and temporal scales. *Nature Communications*, 12 (1).

Newton, L. et al. (2005). *Using the Black Soldier Fly, Hermetia illucens, as a value-added tool for the management of swine manure*. [Online]. Available at: https://www.researchgate.net/publication/267377822_Using_the_Black_Soldier_Fly_Hermetia_Illucens_as_a_Value-Added_Tool_for_the_Management_of_Swine_Manure.

Niermans, K. et al. (2021). A systematic literature review on the effects of mycotoxin exposure on insects and on mycotoxin accumulation and biotransformation. *Mycotoxin Research*, 37 (4).

Nishiyama, Y., Langan, P. and Chanzy, H. (2002). Crystal structure and hydrogen-bonding system in cellulose Iβ from synchrotron X-ray and neutron fiber diffraction. *Journal of the American Chemical Society*, 124 (31).

Nitsche, B. M. et al. (2012). The carbon starvation response of Aspergillus niger during submerged cultivation: Insights from the transcriptome and secretome. *BMC Genomics*, 13.

NNFCC. (2019). *Straw production and value chains*. [Online]. Available at: https://www.nnfcc.co.uk/files/mydocs/Straw%20factsheet.pdf.

Nol, L. and Henis, Y. (1987). Effect of spore concentration on germination and autotropism in Trichoderma hamatum. *Plant and Soil*, 100 (1).

Novy, V. et al. (2021). The characteristics of insoluble softwood substrates affect fungal morphology, secretome composition, and hydrolytic efficiency of enzymes produced by Trichoderma reesei. *Biotechnology for Biofuels*, 14 (1).

Nurika, I. et al. (2018). A comparison of ergosterol and PLFA methods for monitoring the growth of ligninolytic fungi during wheat straw solid state cultivation. *Journal of Microbiological Methods*.

Oates, N. C. (2016). Mining microbial compost communities for lignocellulose degrading proteins. *Department of Biology*, University of York.

Oates, N. C. et al. (2021). A multi-omics approach to lignocellulolytic enzyme discovery reveals a new ligninase activity from Parascedosporium putredinis NO1. *PNAS*, 118 (18).

de O. Buanafina, M. M. (2009). Feruloylation in grasses: current and future perspectives. *Molecular Plant*, 2 (5).

de Oliveira, D. M. et al. (2015). Ferulic acid: a key component in grass lignocellulose recalcitrance to hydrolysis. *Plant Biotechnology Journal*, 13 (9).

Oonincx, D. G. A. B. et al. (2015). Feed conversion, survival and development, and composition of four insect species on diets composed of food by-products. *PLoS ONE*, 10 (12).

Oonincx, D. G. A. B. (2021). Environmental impact of insect rearing. In: *Insects as Animal Feed: Novel Ingredients for Use in Pet, Aquaculture and Livestock Diets*. CABI.

Padzil, F. N. M. et al. (2020). Potential of oil palm empty fruit bunch resources in nanocellulose hydrogel production for versatile applications: a review. *Materials*, 13 (5).

Pallín, M. Á. et al. (2022). Towards industrial application of fungal pretreatment in 2G biorefinery: scale-up of solid-state fermentation of wheat straw. *Biomass Conversion and Biorefinery*, 1.

Palma, L. et al. (2019). Managing high fiber food waste for the cultivation of Black Soldier Fly larvae. *NPJ Science of Food*, 3 (1).

Pandey, A., Larroche, C. and Soccol, C. R. (2017). Current advances in solid-state fermentation. In: *Current Developments in Biotechnology and Bioengineering*. Elsevier.

Pang, W. et al. (2020). The influence on carbon, nitrogen recycling, and greenhouse gas emissions under different C/N ratios by Black Soldier Fly. *Environmental Science and Pollution Research International*, 27 (34).

Pan, G. X., Bolton, J. L. and Leary, G. J. (1998). Determination of ferulic and p-coumaric acids in wheat straw and the amounts released by mild acid and alkaline peroxide treatment. *Journal of Agricultural and Food Chemistry*, 46 (12).

Pan, X., Gilkes, N. and Saddler, J. N. (2006). Effect of acetyl groups on enzymatic hydrolysis of cellulosic substrates. *Holzforschung*, 60 (4).

Parkes, G. M. and Niranjan, M. (2019). Uncovering extensive post-translation regulation during human cell cycle progression by integrative multi-'omics analysis. *BMC Bioinformatics*, 20 (1).

Parkinson, D. R., Warren, J. M. and Pawliszyn, J. (2010). Analysis of ergosterol for the detection of mold in soils by automated on-fiber derivatization headspace extraction-SPME-GC/MS. *Analytica Chimica Acta*, 661 (2).

Pazouki, M. and Panda, T. (2000). Understanding the morphology of fungi. *Bioprocess Engineering*, 22 (2).

Peguero, D. A. et al. (2022). A review of pretreatment methods to improve agri-food waste bioconversion by Black Soldier Fly larvae. *Frontiers in Sustainable Food Systems*, 5.

Pielou, E. C. (1984). *The interpretation of ecological data: a primer on classification and ordination*. Wiley.

Prabhu, G. et al. (2022). A critical look at bioproducts co-cultured under solid state fermentation and their challenges and industrial applications. *Waste and Biomass Valorization*, 13 (7).

Prescott, M. P. et al. (2019). Resources, barriers, and tradeoffs: A mixed methods analysis of school pre-consumer food waste. *Journal of the Academy of Nutrition and Dietetics*, 119 (8).

Purschke, B. et al. (2017). Impact of substrate contamination with mycotoxins, heavy metals and pesticides on the growth performance and composition of Black Soldier Fly larvae (Hermetia illucens) for use in the feed and food value chain. *Food Additives & Contaminants*, 34 (8).

Rahman, M. A. and Hopke, P. K. (2017). Assessment of methods for the measurement of wood fuel compositions. *Energy & Fuels*, 31 (5).

Read, N. D. (2011). Exocytosis and growth do not occur only at hyphal tips. *Molecular Microbiology*, 81 (1).

Reichel, R. et al. (2018). Potential of wheat straw, spruce sawdust, and lignin as high organic carbon soil amendments to improve agricultural nitrogen retention capacity: an incubation study. *Frontiers in Plant Science*, 9.

Revell, B. (2015). Meat and milk consumption 2050: the potential for demand-side solutions to greenhouse gas emissions reduction. *EuroChoices*, 14 (3).

Ries, L. et al. (2013). Genome-wide transcriptional response of Trichoderma reesei to lignocellulose using RNA sequencing and comparison with Aspergillus niger. *BMC Genomics*, 14.

Riquelme, M. et al. (2018). Fungal morphogenesis, from the polarized growth of hyphae to complex reproduction and infection structures. *Microbiology and Molecular Biology Reviews*, 82 (2).

Rocha, T. et al. (2014). Solid wastes in brewing process: a review. *Journal of Brewing and Distilling*, 5 (1).

Rodríguez-Sanz, A. et al. (2022). Extraction of the wheat straw hemicellulose fraction assisted by commercial endo-xylanases. Role of the accessory enzyme activities. *Industrial Crops and Products*, 179.

Rojo, S. (2021). Insect production and utilization of insect products in Europe. In: *Insects as Animal Feed: Novel Ingredients for Use in Pet, Aquaculture and Livestock Diets*. CABI.

Ruel, K., Nishiyama, Y. and Joseleau, J. P. (2012). Crystalline and amorphous cellulose in the secondary walls of Arabidopsis. *Plant Science*, 193–194.

Saeman, J. F. (1945). Kinetics of wood saccharification - hydrolysis of cellulose and decomposition of sugars in dilute acid at high temperature. *Industrial and Engineering Chemistry*, 37 (1).

Salgado-Bautista, D. et al. (2020). Solid-state fermentation increases secretome complexity in Aspergillus brasiliensis. *Fungal Biology*, 124 (8).

Samayoa, A. C., Chen, W. T. and Hwang, S. Y. (2016). Survival and development of Hermetia illucens (Diptera: Stratiomyidae): a biodegradation agent of organic waste. *Journal of Economic Entomology*, 109 (6).

Sangha, A. K. et al. (2012). Molecular simulation as a tool for studying lignin. *Environmental Progress and Sustainable Energy*, 31 (1).

Savojardo, C. et al. (2018). BUSCA: an integrative web server to predict subcellular localization of proteins. *Nucleic Acids Research*, 46.

Schmidt, C. G. et al. (2014). Antioxidant activity and enzyme inhibition of phenolic acids from fermented rice bran with fungus Rizhopus oryzae. *Food Chemistry*, 146.

Schmieder, S. S. et al. (2019). Bidirectional propagation of signals and nutrients in fungal networks via specialized hyphae. *Current Biology*, 29 (2), pp.217-228.e4. [Online]. Available at: doi:10.1016/J.CUB.2018.11.058 [Accessed 30 July 2022].

Schmitt, E. et al. (2019). Growth and safety assessment of feed streams for Black Soldier Fly larvae: a case study with aquaculture sludge. *Animals*, 9 (4).

Sephton-Clark, P. C. S. et al. (2018). Pathways of pathogenicity: transcriptional stages of germination in the fatal fungal pathogen Rhizopus delemar. *mSphere*, 3 (5).

Seyedalmoosavi, M. M. et al. (2022). Growth efficiency, intestinal biology, and nutrient utilization and requirements of Black Soldier Fly (Hermetia illucens) larvae compared to monogastric livestock species: a review. *Journal of Animal Science and Biotechnology 2022 13:1*, 13 (1).

Shi, Z. et al. (2020). Novel synergistic mechanism for lignocellulose degradation by a thermophilic filamentous fungus and a thermophilic actinobacterium based on functional proteomics. *Frontiers in Microbiology*, 11.

Shrivastava, B. et al. (2012). Solid state bioconversion of wheat straw into digestible and nutritive ruminant feed by Ganoderma sp. rckk02. *Bioresource Technology*, 107.

Shrivastava, B. et al. (2014). Bioprocessing of wheat straw into nutritionally rich and digested cattle feed. *Scientific Reports*, 4 (1).

Shumo, M. et al. (2019). The nutritive value of Black Soldier Fly larvae reared on common organic waste streams in Kenya. *Scientific Reports*, 9 (1).

Sidar, A. et al. (2020). Carbohydrate binding modules: diversity of domain architecture in amylases and cellulases from filamentous microorganisms. *Frontiers in Bioengineering and Biotechnology*, 8.

Singh, G. et al. (2021). Rice straw burning: a review on its global prevalence and the sustainable alternatives for its effective mitigation. *Environmental Science and Pollution Research*, 28 (25).

Sista Kameshwar, A. K. and Qin, W. (2018). Comparative study of genome-wide plant biomass-degrading CAZymes in white rot, brown rot and soft rot fungi. *Mycology*, 9 (2), p.93. [Online]. Available at: doi:10.1080/21501203.2017.1419296 [Accessed 12 September 2022].

de Smet, J. et al. (2018). Microbial community dynamics during rearing of Black Soldier Fly larvae (Hermetia illucens) and impact on exploitation potential. Drake, H. L. (Ed). *Applied and Environmental Microbiology*, 84 (9).

Soccol, C. R. et al. (2017). Recent developments and innovations in solid state fermentation. *Biotechnology Research and Innovation*, 1 (1).

Sogari, G. et al. (2019). The potential role of insects as feed: a multi-perspective review. *Animals*, 9 (4).

Song, B. et al. (2020). Direct measurement of plant cellulose microfibril and bundles in native cell walls. *Frontiers in Plant Science*, 11.

Spranghers, T. et al. (2017). Nutritional composition of Black Soldier Fly (Hermetia illucens) prepupae reared on different organic waste substrates. *Journal of the Science of Food and Agriculture*, 97.

Streffer, F. (2014). Lignocellulose to biogas and other products. *JSM Biotechnology and Biomedical Engineering*, 2.

Stuart, E. K. and Plett, K. L. (2020). Digging deeper: in search of the mechanisms of carbon and nitrogen exchange in ectomycorrhizal symbioses. *Frontiers in Plant Science*, 10.

Sützl, L. et al. (2018). Multiplicity of enzymatic functions in the CAZy AA3 family. *Applied Microbiology and Biotechnology*, 102 (6).

Tabuchi, A., Li, L. C. and Cosgrove, D. J. (2011). Matrix solubilization and cell wall weakening by β-expansin (group-1 allergen) from maize pollen. *The Plant Journal*, 68 (3).

Takeda, Y. et al. (2019). Comparative evaluations of lignocellulose reactivity and usability in transgenic rice plants with altered lignin composition. *Journal of Wood Science*, 65 (1).

Tannenbaum, J. and Bennett, B. T. (2015). Russell and Burch's 3Rs then and now: the need for clarity in definition and purpose. *Journal of the American Association for Laboratory Animal Science*, 54 (2).

Tarasov, D., Leitch, M. and Fatehi, P. (2018). Lignin–carbohydrate complexes: properties, applications, analyses, and methods of extraction: a review. *Biotechnology for Biofuels* , 11 (1).

Tengerdy, R. P. and Szakacs, G. (2003). Bioconversion of lignocellulose in solid substrate fermentation. *Biochemical Engineering Journal*, 13.

Terrett, O. M. and Dupree, P. (2019). Covalent interactions between lignin and hemicelluloses in plant secondary cell walls. *Current Opinion in Biotechnology*, 56.

Thanapimmetha, A. et al. (2012). Optimization of solid state fermentation for reducing sugar production from agricultural residues of sweet sorghum by Trichoderma harzianum. *Chiang Mai Journal of Science*, 39 (2).

Tian, S. Q., Zhao, R. Y. and Chen, Z. C. (2018). Review of the pretreatment and bioconversion of lignocellulosic biomass from wheat straw materials. *Renewable and Sustainable Energy Reviews*, 91.

Tomberlin, J. K., Adler, P. H. and Myers, H. M. (2009). Development of the Black Soldier Fly (Diptera: Stratiomyidae) in relation to temperature. *Environmental Entomology*, 38 (3).

Tomberlin, J. K., Sheppard, D. C. and Joyce, J. A. (2002). Selected life-history traits of Black Soldier Flies (Diptera: Stratiomyidae) reared on three artificial diets. *Annals of the Entomological Society of America*.

Troell, M. et al. (2014). Does aquaculture add resilience to the global food system? *PNAS*, 111 (37).

Tufail, T. et al. (2018). Biochemical characterization of wheat straw cell wall with special reference to bioactive profile. *International Journal of Food Properties*.

Turgeman, T. et al. (2016). The role of aquaporins in pH-dependent germination of Rhizopus delemar spores. *PLoS ONE*, 11 (3).

USDA. (2011). *Carbon to nitrogen ratios in cropping systems*. [Online]. Available at: http://www.nm.nrcs.usda.gov/Technical/tech-notes/agro/.

Valkonen, M. et al. (2007). Spatially segregated SNARE protein interactions in living fungal cells. *Journal of Biological Chemistry*, 282 (31).

Veiter, L., Rajamanickam, V. and Herwig, C. (2018). The filamentous fungal pellet—relationship between morphology and productivity. *Applied Microbiology and Biotechnology*, 102 (7).

Veldkamp, T. et al. (2012). *Insects as a sustainable feed ingredient in pig and poultry diets : a feasibility study*. [Online]. Available at: http://www.livestockresearch.wur.nl [Accessed 2 November 2022].

Verduzco-Oliva, R. and Gutierrez-Uribe, J. A. (2020). Beyond enzyme production: solid state fermentation (SSF) as an alternative approach to produce antioxidant polysaccharides. *Sustainability*, 12 (2).

Villares, A. et al. (2017). Lytic polysaccharide monooxygenases disrupt the cellulose fibers structure. *Scientific Reports*, 7.

Viniegra-González, G. et al. (2003). Advantages of fungal enzyme production in solid state over liquid fermentation systems. *Biochemical Engineering Journal*, 13 (2–3).

Virtanen, P. et al. (2020). SciPy 1.0: fundamental algorithms for scientific computing in Python. *Nature Methods*, 17 (3).

Wang, H. et al. (2018). Carbon dots enhance the nitrogen fixation activity of Azotobacter Chroococcum. *ACS Applied Materials and Interfaces*, 10 (19).

Waskom, M. (2021). seaborn: statistical data visualization. *Journal of Open Source Software*, 6 (60).

Ween, O. et al. (2017). Nutritional and functional properties of fishmeal produced from fresh by-products of cod (Gadus morhua L.) and saithe (Pollachius virens). *Heliyon*, 3 (7).

Wesenberg, D., Kyriakides, I. and Agathos, S. N. (2003). White-rot fungi and their enzymes for the treatment of industrial dye effluents. *Biotechnology Advances*, 22 (1–2).

WRAP. (2017). *Estimates of food surplus and waste arisings in the UK*. [Online]. Available at: https://www.givergy.com/wp-content/uploads/2020/03/Estimates_20in_the_UK_Jan17.pdf.

Wu, N. et al. (2020). Effects of heavy metals on the bioaccumulation, excretion and gut microbiome of Black Soldier Fly larvae (Hermetia illucens). *Ecotoxicology and Environmental Safety*, 192.

WWF. (2022). *Aquaculture*. [Online]. Available at: https://www.wwf.org.uk/what-we-do/aquaculture.

Yang, Q. and Pan, X. (2016). Correlation between lignin physicochemical properties and inhibition to enzymatic hydrolysis of cellulose. *Biotechnology and Bioengineering*, 113 (6).

Yoo, C. G. et al. (2017). Effects of organosolv and ammonia pretreatments on lignin properties and its inhibition for enzymatic hydrolysis. *Green Chemistry*, 19 (8).

Yuan, Y. et al. (2021). Recent advances in understanding the effects of lignin structural characteristics on enzymatic hydrolysis. *Biotechnology for Biofuels*, 14 (1).

Yu, B. et al. (2021). Simultaneous isolation of cellulose and lignin from wheat straw and catalytic conversion to valuable chemical products. *Applied Biological Chemistry*, 64 (1).

Zhang, L. et al. (2022). Comparison of lignin distribution, structure, and morphology in wheat straw and wood. *Industrial Crops and Products*, 187.

Zhang, Y., Ghaly, A. E. and Li, B. (2012). Physical properties of wheat straw varieties cultivated under different climatic and soil conditions in three continents. *American Journal of Engineering and Applied Sciences*, 5 (2).

Zhao, S. et al. (2019). Differential transcriptomic profiling of filamentous fungus during solid-state and submerged fermentation and identification of an essential regulatory gene PoxMBF1 that directly regulated cellulase and xylanase gene expression. *Biotechnology for Biofuels*, 12 (1).

Zheng, L. et al. (2013). Bacteria mediate oviposition by the Black Soldier Fly, Hermetia illucens (L.), (Diptera: Stratiomyidae). *Scientific Reports*, 3.

Zhou, S. et al. (2017). Biological wheat straw valorization: multicriteria optimization of Polyporus brumalis pretreatment in packed bed bioreactor. *Microbiology Open*, 7 (1).

Zhuang, J. et al. (2007). Economic analysis of cellulase production methods for bio-ethanol. *Applied Engineering in Agriculture*, 23 (5).

Zhu, L. et al. (2008). Structural features affecting biomass enzymatic digestibility. *Bioresource Technology*, 99 (9).

Zhu, Y. et al. (2020). Nanostructural analysis of enzymatic and non-enzymatic brown rot fungal deconstruction of the lignocellulose cell wall. *Frontiers in Microbiology*, 11.

Zoghlami, A. and Paës, G. (2019). Lignocellulosic biomass: understanding recalcitrance and predicting hydrolysis. *Frontiers in Chemistry*, 7.